Stimuli-responsive Turn-on Fluorogenic Donors of Hydrogen Sulfide (H_2S) and the Prodrugs of Anti-cancer Compounds

A Thesis

Submitted in Partial Fulfilment of the

Requirements for the Degree of

Doctor of Philosophy

by

Sulendar K. Mahato

Department of Chemistry

Indian Institute of Technology Guwahati

Guwahati – 781039, Assam, India

February 2023

Stimuli-responsive Turn-on Fluorogenic Donors of Hydrogen Sulfide (H_2S) and the Prodrugs of Anti-cancer Compounds

A Thesis

Submitted in Partial Fulfilment of the

Requirements for the Degree of

Doctor of Philosophy

by

Sulendar K. Mahato

Roll no. - 166122106

Department of Chemistry

Indian Institute of Technology Guwahati

Guwahati – 781039, Assam, India

February 2023

Dedicated To

My Parents and Family Members

Indian Institute of Technology Guwahati

Department of Chemistry

Guwahati

Assam – 781039

STATEMENT

I hereby declare that the research work described in the thesis entitled "***Stimuli-responsive Turn-on Fluorogenic Donors of Hydrogen Sulfide (H_2S) and the Prodrugs of Anti-cancer Compounds***" is the outcome of investigations carried out by me under the supervision of **Dr. Krishna P. Bhabak** at Department of Chemistry, Indian Institute of Technology Guwahati, India, for the award of degree of Doctor of Philosophy.

In keeping with the general practice of reporting scientific observations, due acknowledgements have been made wherever the work described in this thesis is based on the findings of other investigators. Any omission that might have occurred by oversight or mistake is unintentional and gravely regretted.

Sulendar K. Mahato

Sulendar K. Mahato

Roll No: 166122106

Indian Intitute of Technology Guwahati
Department of Chemistry
Guwahati
Assam – 781039

CERTIFICATE

This is to certify that the research work presented in the thesis entitled "***Stimuli-responsive Turn-on Fluorogenic Donors of Hydrogen Sulfide (H_2S) and the Prodrugs of Anti-cancer Compounds***" by **Mr. Sulendar K. Mahato** (Roll no: 166122106) for the award of the degree of Doctor of Philosophy is an authentic record of the results obtained from the research work carried out under my supervision at Department of Chemistry, Indian Institute of Technology Guwahati, India. The research work reported in his thesis is original and the same has not been submitted elsewhere for a degree.

Dr. Krishna P. Bhabak

(Supervisor)
Associate Professor
Department of Chemistry
Indian Institute of Technology Guwahati
Assam – 781039

Acknowledgements

I would like to take this opportunity to appreciate the kind help and support of all the people around me to make the journey, a very memorable one. Without their help, it would not have been possible to achieve this goal.

First and foremost, I would like to express my deepest gratitude towards my thesis supervisor **Dr. Krishna P. Bhabak** for his constant and persistent support, motivation and guidance throughout the entire tenure of my research work. His perseverant support, unparalleled efforts and never-ending patience, even in the midst of COVID-19 pandemic, proved to be extremely important for fulfilling this goal. Under his close supervision, the ideals of a true researcher have been inculcated within me. It has been, indeed, a very nice and pleasant experience in working with him.

I would like to extend my acknowledgement to my doctoral committee members **Prof. Bhubaneswar Mandal** (Chairman), **Prof. A. S. Achalkumar** (Member), and **Dr. Pavan K. Kancharla** (Member) for taking the time out of their busy schedules to review my progress and also to share their knowledge, provide invaluable suggestions to overall improve my research.

I am thankful to the **Indian Institute of Technology Guwahati** for providing my fellowship, and to the Department of Chemistry, **Central Instruments Facility** (**CIF**) and the **North East Centre for Biological Sciences and Healthcare Engineering** (**NECBH**) for providing me with instrumental facilities for nuclear magnetic resonance (NMR). Additionally, I would like to acknowledge all the instrument operators and non-teaching staff of the Department of Chemistry and Administrative building, IIT Guwahati for extending their kind help in whichever ways applicable.

I am forever grateful and thankful to other lab members **Mr. Debojit Bhattacherjee**, **Mr. Abu Sufian**, **Ms. Shivani Marandi**, **Ms. Pallavi Barman**, **Mr. Rahul Kesarwani**, **Mr. Roopjyoti Misra**, **Mr. MD. Badirujjaman**, **Ms. Nikita Pal** for bearing with me throughout the entirety of my research journey.

I would specially like to thank **Mr. Debojit Bhattacherjee** and **Ms. Pallavi Barman** for performing the cellular works of my synthesized compounds.

Next, most importantly I would like to thank my family for their constant support throughout my life. I would like to mention my father **Mr. Shankar Mahato** and my mother **Mrs. Lalita Devi** for making me the better person as I am today.

Last but not the least, I must acknowledge the unparalleled motivation and constant encouragement I received from **Mr. Adit Shah** and **Mr. Umesh Kumar Bagha** during my difficult times. Finally, I would like to thank the Almighty God for making this possible and giving me the strength, perseverance, and determination to work.

Sd/- Sulendar K. Mahato

Sulendar K. Mahato

Table of Contents

Abbreviations

Ala	L-Alanine
anhyd.	Anhydrous
Arg	L-Arginine
Asn	L-Asparagine
Asp	L-Aspartic acid
BSA	Bovine Serum Albumin
°C	Degree Celsius
Calcd.	Calculated
CAT	Cysteine aminotransferase
CBS	Cystathionine-β-synthase
$CDCl_3$	Chloroform-*d*
CO_2	Carbon dioxide
COS	Carbonyl sulfide
CSE	Cystathionine-γ-lyase
Cys	L-Cysteine
DADS	Diallyl disulfide
DAO	D-amino acid oxidase
DAS	Diallyl sulfide
DATS	Diallyl trisulfide
DCM	Dichloromethane
DMEM	Dulbecco's Modified Eagle Medium
DMF	N, N-dimethylformamide
DMSO	Dimethyl sulfoxide
DNCB	2,4-Dinitrochlorobenzene
DPBS	Dulbecco's phosphate buffered saline
DTT	1,4-Dithiothreitol
ESI-MS	Electrospray ionization mass spectroscopy
FBS	Fetal bovine serum
g	Gram
Gln	L-Glutamine
Glu	L-Glutamic acid
Gly	Glycine
GPx	Glutathione peroxidase
GR	Glutathione reductase
GSH	Glutathione reduced
GSSH	Glutathione persulfide
h	Hour(s)
H_2O_2	Hydrogen peroxide
H_2S	Hydrogen sulfide
H_2SO_4	Sulfuric acid
HCl	Hydrochloric acid
Hcy	*D,L*-Homocysteine
HEK-293	Human embryonic kidney normal cell
HeLa	Human cervical cancer cell
His	L-Histidine
HPLC	High performance liquid chromatography
Hz	Hertz
KCl	Potassium chloride

M	Molar
MB	Methylene Blue
mBBr	Monobromobimane
MDA-MB-231	Triple-negative breast cancer cell
ME	2-Mercaptoethanol
Met	L-Methionine
MHz	Megahertz
mM	Millimolar
mmol	Millimoles
M.P.	Melting Point
MST	3-Mercaptopyruvate sulfurtransferase
Na_2S	Sodium sulfide
NAC	N-acetyl cysteine
NaCl	Sodium chloride
NADPH	Nicotinamide adenine dinucleotide phosphate reduced
NaHS	Sodium Hydrosulfide
NEM	N-ethyl maleimide
NMR	Nuclear Magnetic Resonance
Obs.	Observed
PAG	*D,L*-Propargyl glycine
PBS	Phosphate Buffer Saline
Pet. Ether	Petroleum Ether (60 – 80)
Ph_3PAuCl	Triphenylphosphinegold(I) chloride
PhSH	Thiophenol
PhSSPh	Diphenyl disulfide
PI	Propidium iodide
Pro	L-Proline
PSO	Persulfide dioxygenase
Q-TOF	Quadrupole time-of-flight
ROS	Reactive oxygen species
rt/RT	Room temperature
$S_2O_3^{2-}$	Thiosulfate
S_8	Sulfur powder
Ser	L-Serine
SO	Sulfite oxidase
SO_4^{2-}	Sulfate
SQR	Sulfide quinone reductase
TBHP	Tert-butyl hydroperoxide
TCEP	Tris(2-carboxyethyl) phosphine
TLC	Thin layer chromatography
Trp	L-Tryptophan
Trx	Thioredoxin
TrxR	Thioredoxin reductase
TST	Thiosulfate transferase
Tyr	L-Tyrosine
UV-Vis	Ultra-violet visible
δ	Chemical shift (ppm)
μM	Micromolar

Synopsis Report

Hydrogen sulfide (H_2S), was first coined by Swedish German chemist Carl Wilhelm Scheele in the year 1777.[1] It was considered as a foul-smelling substance having the characteristic smell of rotten eggs until 1996 when Abe and Kimura proved that H_2S acts as a neuromodulator by improving the response of NMDA receptors in the brain.[2] Because of the significance of H_2S in the biological system, there has been a lot of research into its pharmacological roles. In mammals, three H_2S-producing enzymes such as cystathionine-γ-lyase (CSE), cystathionine-β-synthase (CBS), and 3-mercaptopyruvate sulfurtransferase (3-MST) work together along with cysteine aminotransferase (CAT) for the biosynthesis of H_2S.[3,4]A recent report showed that H_2S can also be biosynthesized from D-cysteine involving 3-mercaptopyruvate and D-amino acid oxidase (DAO).[5] The involvement of H_2S has been shown in several pathological conditions and diseases such as diabetes, atherosclerosis and Parkinson's disease etc.[6,7] It also provides protection against several other processes such as neurotransmission, vasodilation and cytoprotection against reactive oxygen species (ROS).[8-10] In order to avoid direct administration of H_2S gas, several research groups have employed sodium hydrosulfide (NaHS) and sodium sulfide (Na_2S) as exogenous sources of H_2S.[11] However, when these inorganic sulfide salts were added to buffered aqueous solutions, the concentration of H_2S increases rapidly and then gradually decreases as a result of the volatilization of H_2S gas into the atmosphere. This rapid release of H_2S from inorganic sources contradicts the rate of H_2S release by the endogenous H_2S generating enzymes such as CBS and CSE. Due to these reasons, it is essential to create alternative H_2S sources that more closely resemble the rate of endogenous H_2S generation. Naturally occurring allium species such as garlic and onion have shown beneficial effects in several disease conditions such as cardiovascular disease, diabetes and thrombosis.[12,13] The beneficial effects of garlic is attributed to the generation of H_2S in the presence of thiols. The main component present in garlic is allicin, a thiosulfinate species that decomposes to diallyl sulfide (DAS), diallyl disulfide (DADS) and diallyl trisulfide (DATS).[14] As DATS showed beneficial properties in the biological system several synthetic mimics of H_2S have been developed in order to mimic the slow endogenous production of H_2S.

The present thesis, entitled "***Stimuli-responsive Turn-on Fluorogenic Donors of Hydrogen Sulfide (H_2S) and the Prodrugs of Anti-cancer compounds***" consists of four

chapters based on the results of experimental works performed during the complete course of PhD research tenure.

Chapter 1: Introduction

The first chapter discusses the general introduction to H_2S and the different types of donors being developed in the literature. The introduction section is divided into several sub-sections. Firstly, a brief introduction about the different sources (plant, dietary) of H_2S was discussed (Figure 1). Secondly, the detailed endogenous production of H_2S and its metabolism in the biological system have been discussed. Thirdly, owing to the importance of H_2S in the biological system, different tools for the quantitative detection of H_2S have been discussed. Fourthly, a brief discussion about the different types of inhibitors that are used for the quenching of endogenous enzymes present in the biological system. Finally, a brief discussion about the role of H_2S in different disease conditions is highlighted. Moreover, the rate of release of H_2S (fast or sustained) from the H_2S releasing compounds (inorganic and organic donors) has been associated with either beneficial or toxic effects in the cellular system. The synthetic donors of H_2S are widely developed to mimic the slow and sustained endogenous production of H_2S in the biological system. A thorough discussion has been made on the development of different stimuli-responsive organic donors of H_2S such as- (i) hydrolysis-based H_2S donors, (ii) biothiol-triggered H_2S donors, (iii) light-triggered H_2S donors, (iv) enzyme-triggered H_2S donors etc. To quantify the release of H_2S from these donors, several detection techniques has been developed and improved over the years. The most widely used technique is the methylene blue (MB) assay wherein the sulfide species react in the presence of acidic solutions of *N*,*N*-dimethyl-*p*-phenylene diamine sulfate, ferric chloride ($FeCl_3$), and zinc acetate dihydrate $Zn(OAc)_2{\cdot}2H_2O$ to generate methylene blue (MB) with a characteristic absorbance maxima at 670 nm in the UV-Vis spectrum. The concentrations of H_2S can be determined by using a calibration curve obtained using samples of known concentrations of Na_2S. However, the limit of detection of this method is relatively lower (about 1 μM) due to the formation of dimer and trimer species in solutions. Additionally, the quantification of intracellular H_2S release is not possible due to the highly acidic conditions used in the measurement of H_2S. Notably, other detection techniques such as lead acetate has also been used to detect H_2S by measuring the formation of insoluble compound lead sulfide, which showed turbidity at 390 nm in the UV-Vis spectrum. Electrochemical methods such as the ion-selective electrode method and polarographic

sensors have also been used for the quantification of H_2S. The ion-selective electrodes use a silver sulfide membrane that specifically interacts with S^{2-} creating a change in potential across the membrane. The electrodes are not expensive, easy to operate and showed high selectivity towards H_2S. However, the main drawback of the electrochemical method is that frequent reconditioning of the electrode is necessary to remove the impurities of the previous experiments. Furthermore, these electrodes operate under highly basic conditions that are not suitable for monitoring intracellular H_2S release. Another method for the quantification of H_2S release is the monobromobimane method (MBB) that reacts with H_2S at basic pH (9.5) to generate a highly fluorescent sulfide dibimane (SDB) product. The formation of SDB can be detected using HPLC equipped with a fluorescence detector as a high fluorescence intensity band is generated that can be easily observed. The detection limit for the MBB method is 2 nM. However, the major drawback of this technique is that MBB showed side reactions with thiols. Although, several turn-on fluorogenic sensors of H_2S such as azide-based, nitro-based, disulfide-based and metal-based sensors have been developed for monitoring the intracellular level of H_2S, some of these sensors are also reactive towards the cellular abundant thiols. Moreover, these sensors also consume some amount of the intracellular H_2S for its sensing process and thereby reduces the intracellular level of H_2S further. Therefore, with the state-of-art knowledge on this topic, the real-time and convenient monitoring of the exogenous H_2S donation process is not feasible.

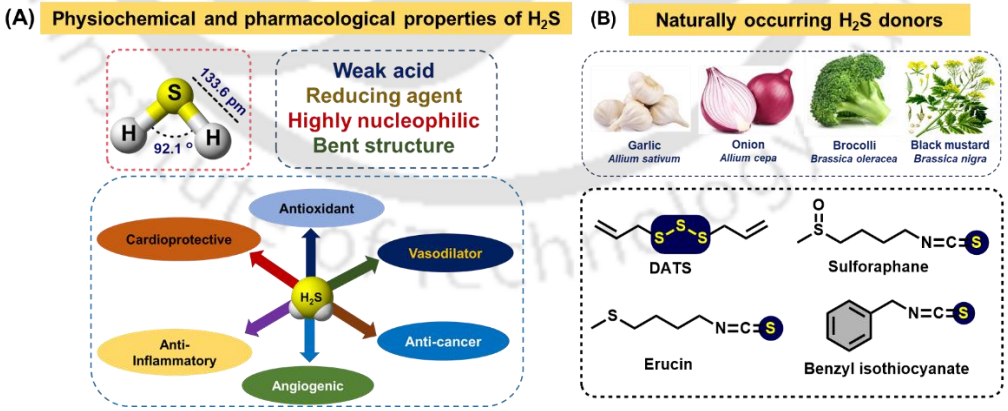

Figure 1. (A) Physiochemical and pharmacological properties of H_2S. (B) Pictorial representation and chemical structures of some naturally occurring H_2S donors.

Inspired by the previous reports on H_2S donors, we took the initiatives in developing bioanalyte-triggered turn-on fluorogenic donors of H_2S for the real-time monitoring of

intracellular H_2S release. The bioanalyte-triggered fluorogenic H_2S donors would be of wide importance as they are overexpressed in certain disease conditions. The strategy could be extended further for the bioanalyte-triggered uncaging of a prodrug that releases an anti-cancer compound along with the release of H_2S.

Chapter 2: The biothiol-triggered organotrisulfide-based self-immolative fluorogenic donors of hydrogen sulfide enable lysosomal trafficking

As discussed in the previous section, a number of H_2S donors have been reported in the literature that are activated by different stimuli. However, these H_2S donors require another molecule (H_2S sensors) to detect the released H_2S from the donors in the cellular medium. Moreover, the H_2S sensors consume some amount of the released H_2S during the course of sensing process. It is observed that a controlled and sustained release of H_2S is associated with several benefits such as anti-inflammatory, cardioprotective, vasodilatory, neurotransmission etc. Therefore, the dysregulation of intracellular H_2S level leads to several pathological conditions and disease states. These observations are indicative of proper regulation of endogenous H_2S or administration of exogenous H_2S during its deficiency for therapeutic benefits. Several non-fluorescent organic donors of H_2S have been developed over the last few years for sustained release of H_2S in aqueous and cellular media as the inorganic salts such as Na_2S or NaHS (instantaneous sources) are not suitable in the cellular medium. However, real-time monitoring of H_2S release in living cells is a big challenge using the currently available detection techniques. While the conventional methylene blue (MB) assay for estimating H_2S utilizes highly acidic conditions, the commonly used ion-sensitive electrodes (ISEs) and amperometric microsensors work in alkaline and acidic/neutral media, respectively. These are therefore not feasible in cellular medium. Although, recent reports highlight numerous fluorescent sensors of H_2S suitable in the cellular medium, many of them interfere with cell-abundant biothiols with false fluorescent signals for H_2S. Therefore, at present, the real-time detection of the intracellular release of H_2S is not feasible with both non-fluorescent organic donors as well as with turn-on fluorescent sensors of H_2S.

In this chapter, we report the design and synthesis of thiol-reactive symmetrical organotrisulfide-based self-immolative fluorogenic donors of H_2S (**UTS-1** and **UTS-2**) compatible in aqueous and cellular media. Upon activation by thiols, H_2S is released in a controlled manner with a concomitant release of the free fluorophore for the real-time monitoring of H_2S release profile (Figure 2). The probe **UTS-2** was designed for a targeted

delivery of H_2S to an important intracellular organelle such as lysosome (acidic pH) that contains many bio-molecules and hydrolytic enzymes.

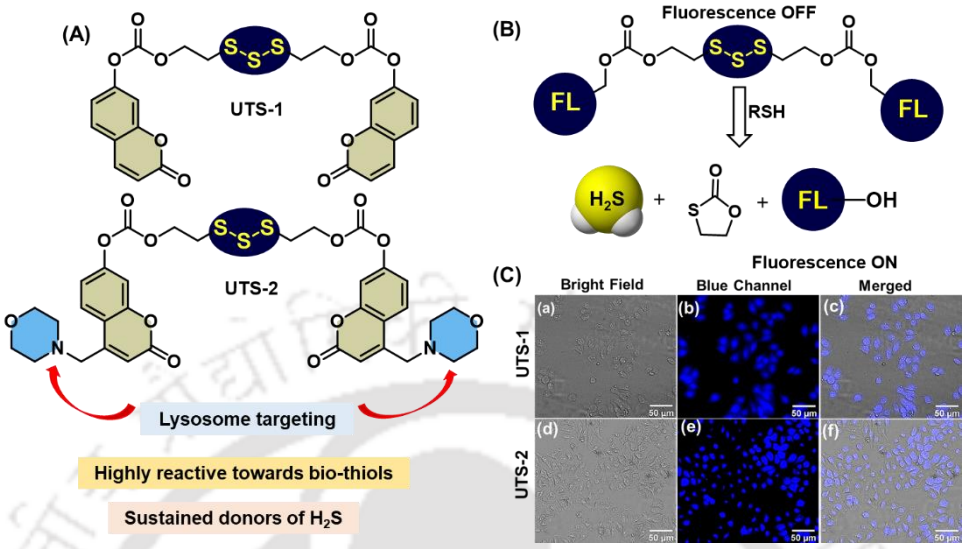

Figure 2. (A) Chemical structures of the trisulfide-based H_2S donors **UTS-1** and **UTS-2** synthesized herein. (B) Thiol-induced concomitant release of H_2S and fluorophore unit from the probes. (C) Fluorescence microscopy images (bright field, blue channel and merged) of HeLa cells incubated with **UTS-1** and **UTS-2** (5.0 µM; images a–f). Scale bar represents 50 µm.

The probes were synthesized from the commercially available starting materials. Initially, 2-chloroethanol reacts in the presence of sodium polysulfide (Na_2S_n, n = 2-5) to form symmetrical polysulfide alcohol. The symmetrical polysulfide alcohol obtained was reacted with 4-nitrophenyl chloroformate to give the carbonate intermediate. The carbonate intermediate further reacts with umbelliferone derivatives to form **UTS-1** and **UTS-2** as a polysulfide mixture of trisulfide, tetrasulfide and pentasulfide. **UTS-1** and **UTS-2** were purified by reverse-phase HPLC to obtain the pure trisulfides. All the probes as well as intermediate compounds were characterized by NMR (^1H, ^{13}C) and ESI-MS analysis. After synthesizing the probes, their spectroscopic properties were evaluated from UV-Vis absorption and fluorescence emission studies.

The release of fluorophore from the synthesized probes **UTS-1** and **UTS-2** were confirmed by UV-Vis and fluorescence emission studies (Figures 3A-3B). After that the H_2S releasing ability of the probes were evaluated by UV-Vis spectrophotometric methylene blue and fluorescence assay (Figure 3C). After performing spectroscopic studies, lysosomal selectivity of **UTS-2** was studied using fluorescence and confocal

microscopy upon co-treatment with standard lysosomal probes (Lyso-Tracker Red, **DND-99**). Interestingly, the blue emission of **UTS-2** merged well with the red emission of **DND-99**, indicating the effective lysosomal selectivity of **UTS-2**. Furthermore, the lysosomal selectivity of the synthesized probes was confirmed using confocal microscopic studies and also intensity plot showed a good overlap between the blue and red channels (Figure 3D). With the confirmation of cellular internalization and localization of the probes, the H_2S release was studied by co-treatment of the probes with the literature-reported H_2S-sensitive probes **NAP-1** and **NAP-2**. Interestingly, emission of umbelliferone derivatives **2.1a** or **2.1b** under the blue channel and H_2S-induced turn-on fluorescence due to **NAP-1P** and **NAP-2P** under the green channel with the excellent overlay is indicative of a concomitant release of H_2S from **UTS-1** and **UTS-2** (Figure 3E).

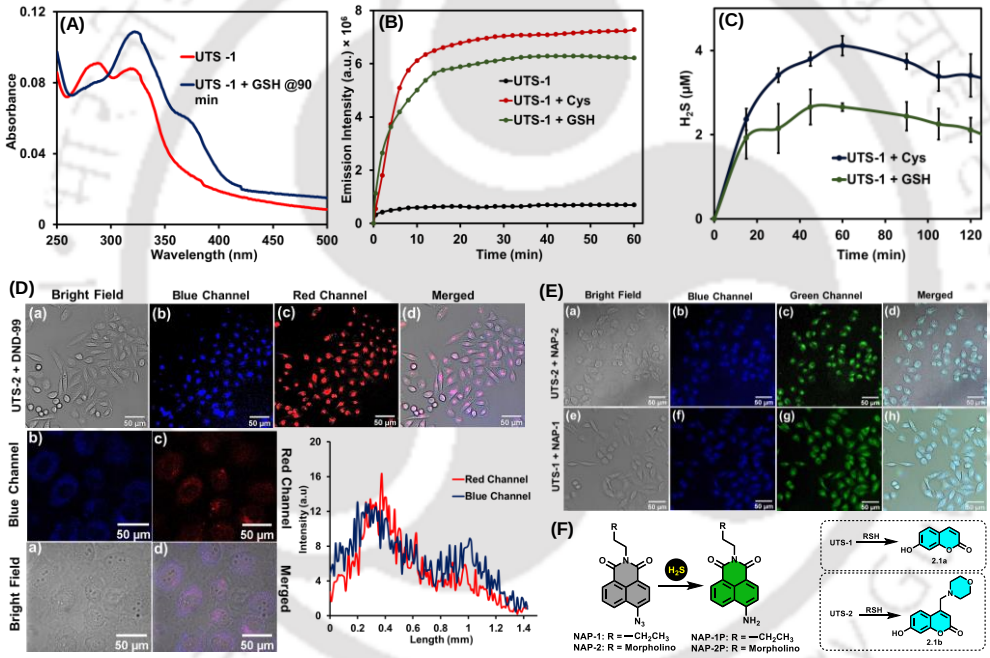

Figure 3. (A) UV-Vis spectra of **UTS-1** and its reaction with GSH. (B) Kinetics of the reaction of **UTS-1** in the absence/presence of biothiols such as Cys and GSH. (C) Estimation of the released H_2S from **UTS-1** in the presence of Cys and GSH using the MB assay. (D) Fluorescence and confocal microscopy images (bright field, fluorescence and merged) of HeLa cells after the co-treatment of **UTS-2** and lyso-tracker red dye **DND-99**, Intensity profiles for the region of interest (ROI) across HeLa cells for red (**DND-99**) and blue (**UTS-2**) channels; (E) Fluorescence microscopy images (bright field, fluorescence and merged) for detecting the released H_2S from **UTS-1** and **UTS-2** using the azide-based probes in HeLa cells; (F) Chemical structures and reaction schemes for the turn-on fluorescence response from **NAP-1**, **NAP-2**, **UTS-1** and **UTS-2**.

Chapter 3: **Thioredoxin reductase-triggered fluorogenic donor of hydrogen sulfide: a model study with a symmetrical organopolysulfide probe with turn-on near-infrared fluorescent emission**

In chapter 1, we have observed that biothiols such as cysteine and glutathione react with trisulfide-based fluorogenic H_2S donors to release H_2S as well as fluorophore with concomitant turn-on fluorescence via self-immolative process. Apart from biothiols (Cys, GSH), there are certain antioxidant enzymes such as thioredoxin reductase (TrxR), glutathione reductase (GR) and glutathione peroxidase (GPx) that are reported to be overexpressed in certain disease conditions particularly cancer. These enzymes contain a highly reactive cysteine/selenocysteine moieties at the active sites. The contribution of these enzymes to trigger a molecular process cannot be completely ignored. However, due to the abundance of thiols in the biological system, the specific reporter for these probes are quite limited in the literature. The thioredoxin reductase system consists of NADPH, thioredoxin reductase (TrxR) and thioredoxin (Trx). Initially, NADPH supplies electrons to TrxR thereby activating the enzyme, which can reduce the disulfide bond of Trx to thiol and that supplies electrons to many other proteins.

In the present study, we describe the rational development of an organopolysulfide-based fluorogenic donor of H_2S (**DCI-PS**) that can be activated by the antioxidant selenoenzyme TrxR with the concomitant release of dicyanoisophorone-based near-infrared (NIR) fluorophore **DCI-OH** (Figures 4A and 4B). Along with the polysulfide probe **DCI-PS** capable of releasing the NIR fluorophore and H_2S, the corresponding disulfide-probe **DCI-DS** was also rationally designed and synthesized, which releases the fluorophore without releasing any H_2S.

After synthesis of the probes, spectroscopic studies for **DCI-PS** were performed in the presence of DTT and GSH to confirm the release fluorophore as well as H_2S. **DCI-PS** reacts in the presence of thiol to release H_2S with the concomitant turn-on the fluorescence. The majority of spectroscopic studies for **DCI-PS** were performed with DTT as it has similar nucleophilic properties and its arrangement can be correlated with the active site of TrxR (Figures 4C and 4D).

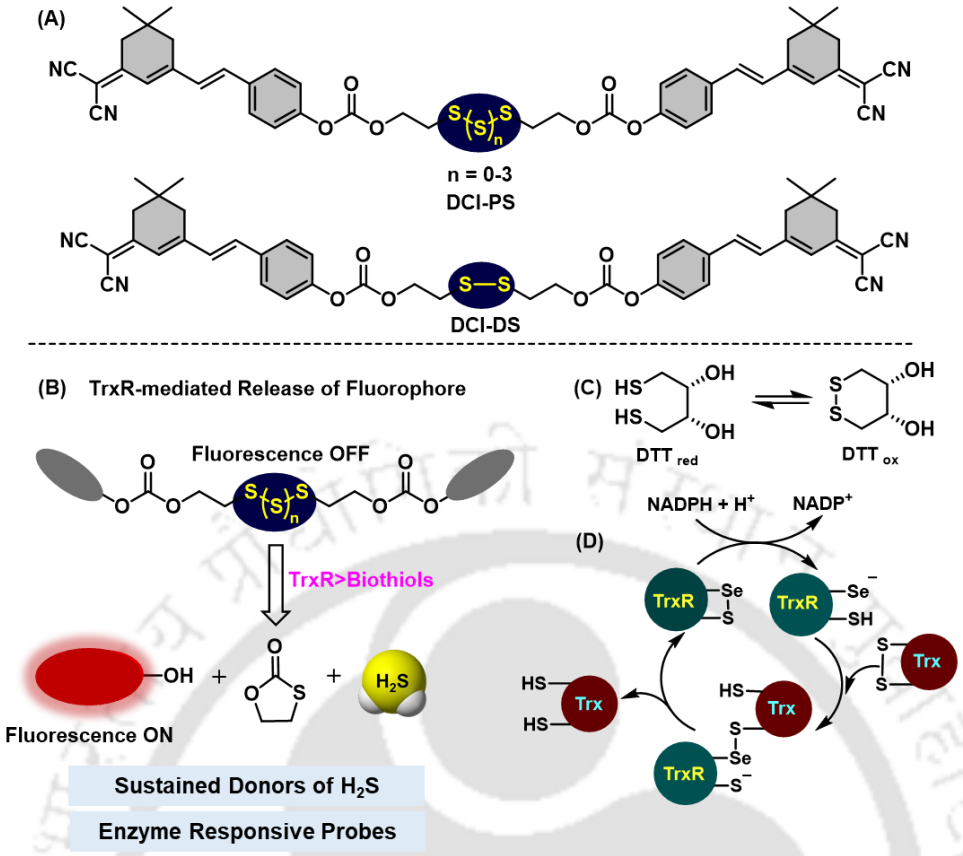

Figure 4. (A) Chemical structures of **DCI-PS** and **DCI-DS**. (B) Schematic representation of antioxidant enzyme thioredoxin reductase (TrxR)-responsive fluorogenic donation of H_2S, along with the simultaneous release of red-emitting NIR fluorophore. (C) Redox process of DTT and oxidized DTT (DTT_{ox}). (D) Catalytic cycle of TrxR for the reduction of Trx in the presence of NADPH.

UV-Vis Spectroscopic and fluorescence emission studies revealed significantly higher reactivity of the **DCI-PS** towards DTT (for TrxR activity) over the well-known cellular abundant biothiol GSH. Furthermore, to confirm the release of fluorophore intracellularly, both **DCI-PS** and **DCI-DS** were incubated in MDA-MB231 cells and the results were analyzed by fluorescence microscopy. The emission under the red channel indicates the bioanalyte-triggered release of fluorophore and the results are shown in Figure 5A. Mechanistic studies indicate that the nucleophilic attack at the polysulfide linkage by the thiol/selenol group of the bio-analytes leads to the self-immolative cyclization process with the release of the turn-on fluorophore and H_2S (Figure 5B). The release of H_2S was confirmed intracellularly by a nucleophilic-substitution cyclization-based fluorogenic probe **WSP2** (Figure 5C).

The selectivity towards TrxR-triggered fluorescence turn-on process from **DCI-PS** was further supported by performing the emission studies using cell lysate of MDA-MB-231

cells (breast cancer adenocarcinoma) as it is estimated to have higher expression of TrxR. As shown in Figure 5D, maximum fluorescence emission was observed from the cell lysate as compared to other pure proteins as well as enzymes such as bovine serum albumin (BSA), glutathione reductase (GR) and glutathione peroxidase (GPx). The active participation of TrxR was further confirmed by the inhibition studies performed using selective small-molecule inhibitors of TrxR such as ebselen, DNCB and triphenylphosphine gold (I) chloride (Figure 5E).

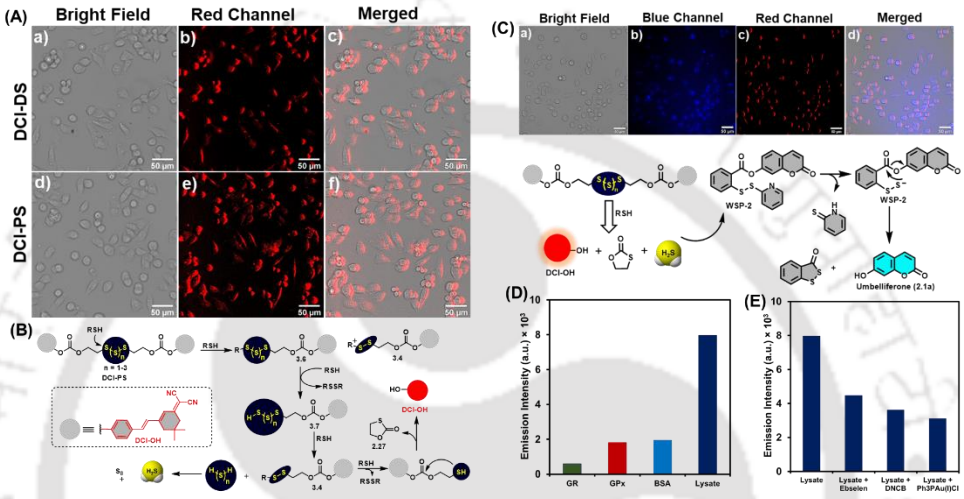

Figure 5. (A) Fluorescence microscopy images (bright field, red channel and merged) of MDA-MB-231 cells for the bio-analyte-triggered release of **DCI-OH** from **DCI-PS** (a–c) and **DIC-DS** (d-f); (B) Proposed mechanism for the release of **DCI-OH** and H_2S upon reaction of **DCI-PS** with thiols; (C) Schematic representation and fluorescence microscopy images (bright field, blue channel, red channel and merged) for the detection of released H_2S from **DCI-PS** in MDA-MB-231 cells using the H_2S-selective turn-on fluorogenic probe **WSP2**; (D) Relative reactivity of **DCI-PS** with cysteine/selenocysteine containing proteins such as BSA, GR, GPx; (E) Inhibition of cell lysate-mediated emission from **DCI-PS** using TrxR selective inhibitors such as ebselen, DNCB and PPh_3AuCl.

Chapter 4: Cysteine-triggered fluorogenic prodrugs for the adjuvant delivery of hydrogen sulfide and the anti-cancer compounds

In the previous chapter, we reported thioredoxin-reductase enzyme-triggered organopolysulfide-based fluorogenic donors of H_2S that is compatible both in aqueous as well cellular medium. However, it would be highly desirable to develop organosulfur compounds as prodrugs that are activated in the presence of bio-analytes to release the active drug molecules and hydrogen sulfide. Real-time monitoring of the drug release

process could be monitored using spectroscopic methods and the activity of these drugs can be checked using the suitable activity assay.

In this chapter, we have synthesized two isothiocyanate-based prodrugs such as **AM-ITC** and **NB-ITC** that are responsive towards cysteine (Figure 6A). The prodrug **AM-ITC** reacts with cysteine and releases H_2S and the anti-cancer compound amonafide. Owing to the inherent fluorescence of amonafide, the uncaging of the prodrug could be monitored by the turn-on fluorogenic processes. Both **AM-ITC** and **NB-ITC** were synthesized from the commercially available starting materials. Initially, 3-nitro-1,8-naphthalic anhydride is reduced to 3-amino-1,8-naphthalic anhydride using stannous chloride dihydrate and hydrochloric acid in absolute ethanol under reflux. Then 3-amino-1,8-naphthalic anhydride was treated with *n*-butyl amine/*N*-*N*-dimethyl ethylene diamine in absolute ethanol under reflux to give the corresponding imide compounds. The amide compounds obtained react with thiocarbonyldiimidazole and triethylamine in dry DMF to give the final compounds **NB-ITC** and **AM-ITC** in moderate yields.

After synthesis of the prodrugs, spectroscopic studies were performed to confirm the release of fluorophore in the presence of cysteine under physiological conditions. UV-Vis and fluorescence emission studies of **AM-ITC** in the presence of cysteine showed selectivity towards cysteine as compared to other thiols such as GSH, DTT and Hcy in phosphate buffer saline (PBS 20 mM, pH 7.4). The release of H_2S was confirmed by methylene blue assay as well as fluorescence assay.

Initially, the molecule is weakly fluorescent due to perturbation of fluorescence by the PET process, but upon reaction with cysteine, there is an enhancement of fluorescence as shown in Figure 6B. From spectroscopic and cellular studies, the release of fluorophore and H_2S was confirmed. The mechanistic details for the reaction of **NB-ITC** with cysteine is shown in Figure 6C. Furthermore, the cytotoxicity profile of **NB-ITC** and **AM-ITC** along with the released amine compounds were performed in MDA-MB-231 cells and the results showed dose-dependent toxicity for **AM-ITC** as well as the released compound amonafide while no toxicity was observed for **NB-ITC** and the released fluorophore **NAB** (Figures 6D and 6E). The cytotoxicity of **AM-ITC** may be due to its reaction with the endogenous cysteine to form amonafide inside the cellular medium.

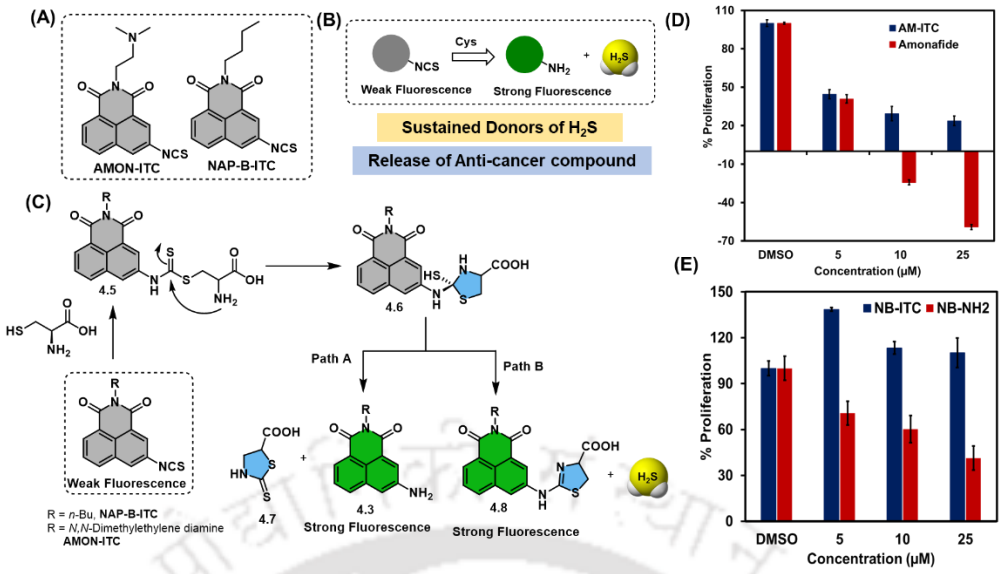

Figure 6. (A) Chemical structures of **AM-ITC** and **NB-ITC**; (B) Schematic representation for the cysteine-triggered release of H_2S with turn-on fluorescence from the isothiocyanate-based prodrugs; (C) Plausible mechanistic pathways for the reaction of **NB-ITC**/**AM-ITC** with cysteine for the release of free anti-cancer compounds and H_2S; Anti-proliferative activity of (D) **AM-ITC** and released product amonafide and (E) **NB-ITC** and the released product NAB in HeLa cells.

Conclusions

In chapter 2, a biothiol-triggered organotrisulfide-linked fluorogenic donors of H_2S such as **UTS-1** and **UTS-2** were developed that are compatible in both aqueous and cellular environments. The release of H_2S and fluorophore enables proper monitoring of the intracellular H_2S release and its further trafficking towards a specific intracellular organelle such as lysosome. The release of fluorophore from **UTS-1** and **UTS-2** was confirmed by spectroscopic studies. The H_2S releasing ability of **UTS-1** and **UTS-2** was measured by methylene blue assay. Both the probes release H_2S in the presence of cysteine and glutathione. Both the synthesized trisulfide donors are non-toxic in cancer (HeLa) and normal cell (HEK-293). In chapter 3, TrxR responsive organopolysulfide-based fluorogenic donor of H_2S (**DCI-PS**) with concomitant release of NIR fluorophore are described. All the spectroscopic and kinetic studies with **DCI-PS**/**DCI-DS** revealed its much higher reactivity towards DTT (for TrxR activity) as compared to the cellular abundant biothiol GSH. The turn-on fluorogenic H_2S donation process from the cellular non-toxic **DCI-PS** was studied in a representative breast cancer cell line (MDA-MB-231) for the sustained donation of H_2S with concomitant release of red-emitting NIR

fluorophore. The participation of TrxR was supported by significant inhibition of the fluorogenic processes in the presence of TrxR selective small-molecule inhibitors. In chapter 4, cysteine responsive isothiocyanate-based fluorogenic donors of H_2S **AM-ITC** and **NB-ITC** were developed. The spectroscopic studies for **AM-ITC** reveal that the probe is only reactive towards cysteine over other thiols such as GSH, DTT and Hcy. Mechanistic investigations reveal that isothiocyanates react with cysteine to release H_2S and the naphthalimide amine-based fluorogenic anti-cancer compounds. The higher anti-cancer activity of the released anti-cancer compound amonafide as compared to the prodrug **AM-ITC** was evidenced by the MTT assay in a representative breast cancer cells.

Reference

1. Filipovic, M. R.; Zivanovic, J.; Alvarez, B.; Banerjee, R., *Chem. Rev.* **2018**, *118*, 1253-1337.
2. Abe, K.; Kimura, H., *J. Neurosci.* **1996**, *16*, 1066-1071.
3. Hartle, M. D.; Pluth, M. D., *Chem. Soc. Rev.* **2016**, *45*, 6108-6117.
4. Powell, C. R.; Dillon, K. M.; Matson, J. B., *Biochem. Pharmacol.* **2018**, *149*, 110-123.
5. Shibuya, N.; Koike, S.; Tanaka, M.; Ishigami-Yuasa, M.; Kimura, Y.; Ogasawara, Y.; Fukui, K.; Nagahara, N.; Kimura, H., *Nat. Commun.* **2013**, *4*, 1-7.
6. Cao, L.; Cao, X.; Zhou, Y.; Nagpure, B. V.; Wu, Z.-Y.; Hu, L. F.; Yang, Y.; Sethi, G.; Moore, P. K.; Bian, J.-S., *Brain Behav. Immun.* **2018**, *73*, 603-614.
7. Vandiver, M. S.; Snyder, S. H., *J. Mol. Med.* **2012**, *90*, 255-263.
8. Kimura, H., *Neurochem. Int.* **2013**, *63*, 492-497.
9. Bhatia, M., *IUBMB life* **2005**, *57*, 603-606.
10. Carballal, S.; Trujillo, M.; Cuevasanta, E.; Bartesaghi, S.; Möller, M. N.; Folkes, L. K.; García-Bereguiaín, M. A.; Gutiérrez-Merino, C.; Wardman, P.; Denicola, A., *Free Radic. Biol. Med.* **2011**, *50*, 196-205.
11. DeLeon, E. R.; Stoy, G. F.; Olson, K. R., *Anal. Biochem.* **2012**, *421*, 203-207.
12. Wu, L.; Yang, W.; Jia, X.; Yang, G.; Duridanova, D.; Cao, K.; Wang, R., *Lab. Invest.* **2009**, *89*, 59-67.
13. Bayan, L.; Koulivand, P. H.; Gorji, A., *Avicenna J. Phytomed.* **2014**, *4*, 1.
14. Brodnitz, M. H.; Pascale, J. V.; Van Derslice, L., *J. Agric. Food. Chem.* **1971**, *19*, 273-275.

Chapter 1

Introduction

1.1. Organochalcogen compounds

The chalcogens belong to a family of group 16 elements of the periodic table. Chalcogens contain five elements such as oxygen, sulfur, selenium, tellurium and polonium. Among all these elements, oxygen is not a member of the organochalcogen family because it behaves chemically differently from the other elements. The coordination number of its compounds are generally lower and oxygen is the only member of the group to exist as a diatomic molecule under normal conditions.

1.1.1. Organosulfur compounds

Organosulfur compounds are widely present in our body and in the natural environment. They are widely found in allium species such as garlic and onion. Garlic contains the organosulfur compound allicin, which further decomposes to other organosulfur compounds such as diallyl sulfide (DAS), diallyl disulfide (DADS) and diallyl trisulfide (DATS). DATS exhibits biological activities including anti-inflammatory, anti-carcinogenic, and anti-angiogenic effects. Organosulfur compounds are also found in cruciferous vegetables such as broccoli and cabbage.

1.1.2. Organoselenium compounds

Organoselenium compounds are chemical compounds that contain carbon to selenium chemical bonds. Elemental selenium is readily available, cheap, bench-stable, and easy to handle as compared to organoselenium compounds. Selenium is also an essential micronutrient that protects us against oxidative damage and is required for the correct functioning of the immune system. Organoselenium compounds have found such wide utility because of their effects on many reactions, including many carbon-carbon bond formations, under relatively mild reaction conditions. Several proteins in the human body contains selenocysteine The selenium atom can be incorporated in an organic substrate via both nucleophilic and electrophilic reagents and organoselenium anions are powerful nucleophiles and usually, they are prepared in situ because of their sensitivity to oxidations in air.

1.1.3. Organotellurium compounds

Organotellurium compounds contain a carbon-tellurium bond. The property of organotellurium compounds is believed to be similar to that of an organoselenium, organosulfur, organotin, and organophosphorus. Organotellurium compounds are readily oxidized from the divalent to tetravalent state and because of this property, tellurides act as scavengers of reactive oxidizing agents, such as hydrogen peroxide, hypochloride, and peroxyl radicals.

1.2. Background of hydrogen sulfide (H_2S)

Early life forms on earth may have thrived in an environment with a lot of H_2S. H_2S may have served as an energy source for the body's metabolism as well as for synthetic purposes. One of the oldest examples of lithography or the ability to utilize inorganic substrates for energy production is the H_2S-oxidizing bacterium *Beggiatoa*, which was discovered in the year 1887 by Winogradsky.[1] In medicine, the discovery of H_2S was made in 1713 when an Italian physicist carefully observed that the workers were experiencing eye inflammation and agony after inhaling an acidic vapour (H_2S).[2] Carl Wilhelm Scheele, a Swedish chemist, accidentally generated H_2S while working with iron pyrite (FeS_2) and mineral acid, which he referred to as "sulfur air".[3] Previously believed to be a nasty substance with the characteristic odour of rotten eggs, is now recognized as the third member of the gasotransmitter family, along with nitric oxide (NO) and carbon monoxide (CO), with a wide range of biological applications. The beneficial effect of H_2S was not recognized until Kimura and co-workers showed that the H_2S-releasing chemical NaHS functions as a neuromodulator in the brain by long-term potentiation.[4] The same group also showed that H_2S in coordination with nitric oxide (NO) acts as a vasodilator by relaxation of smooth muscle cells.[5] In mammals, H_2S is produced by a combination of the enzymes cystathionine-β-synthase (CBS), cystathionine-γ-lyase (CSE), and 3-mercaptopyruvate sulfurtransferase (3-MST).[6] All of these enzymes can be found inside the human body in various organelles. The central nervous system and liver are the two organs where CBS is most widely expressed. While CSE causes H_2S to be produced in the circulatory system, MST is mostly expressed in the mitochondria.[7,8] The cytosolic enzymes CBS and CSE are found in several tissues in humans. L-cysteine (Cys) and L-homocysteine (Hcy) react with pyruvate and α-ketoglutarate to produce ammonia and H_2S, in a reaction catalyzed by cysteine aminotransferase (CAT). The CAT enzyme collaborates with 3-MST in producing H_2S. Before the 3-MST conversion of 3-mercaptopyruvate to pyruvate and H_2S, CAT catalyzes the conversion of Cys to 3-mercaptopyruvate.[9] H_2S also exerts a variety of physiological effects on animals, including cardioprotection,[10] protection against ischemic-reperfusion damage,[11] vasodilation,[12] anti-inflammation,[13] and defense against oxidative stress (Figure 1.1).[14] H_2S also exerts protective effects in the liver by suppressing inflammatory mediators such as TNF-α, and interleukin-10 (IL-10).[15] H_2S exerts cardioprotective effects against high glucose (HG) induced injury by activation of p38 MAPK and ERK1 pathways in myocardial cells (H9C2) cells.[16]

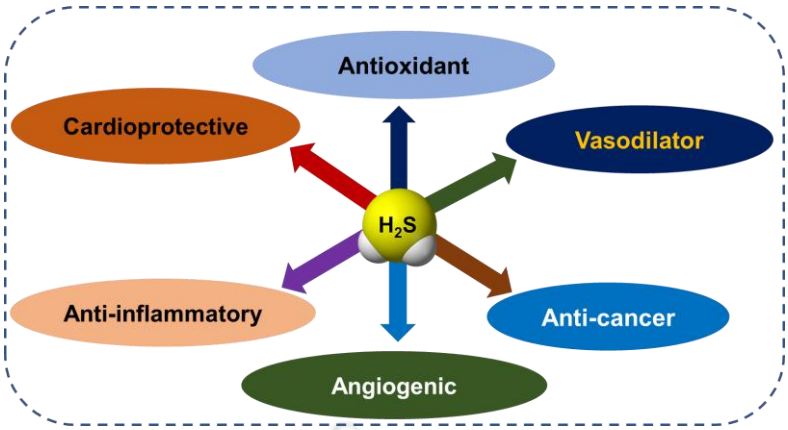

Figure 1.1. Schematic representation of some of the pharmacological effects of H_2S.

1.3. Physiochemical properties of H_2S

H_2S is a corrosive and combustible gas with a characteristic odour of rotten eggs. Under normal physiological conditions, the density of H_2S is higher than air at 15 °C. H_2S is a weak acid with first pK_{a1} of 6.99 and second pK_{a2} of >17. It exists in equilibrium with hydrosulfide ion (HS^-, 80%), molecular H_2S (20%) and anionic sulfide ions (S^{2-}, <1%).[17] Both HS^- and S^{2-} are present in 1:3 ratio at physiological conditions. However, ionization to S^{2-} requires alkaline condition. H_2S can freely diffuse through membranes because it is lipophilic in nature.[18] The electronic configurations of sulfur and oxygen are similar, although, they have quite different physiochemical properties. The electronegativity of sulfur is less compared to oxygen. In comparison to water at physiological pH, H_2S has a more diffuse orbital system and a more polarized electron cloud, making it a better nucleophile. Sulfur can expand its valence shell to take on additional electrons when it has six valence electrons and a vacant 3d orbital, leading to oxidation states ranging from -2 to + 6. Sulfane sulfur has an oxidation state of S^0.[19]

1.4. Different sources of H_2S

1.4.1. Dietary sources

Garlic (*Allium sativum*) is one of the most significant and ancient authenticated herbs that have been used in traditional medicine since ancient times.[20] Allium species and their active ingredients have been shown to exhibit antibacterial, antifungal, anti-aging, and anti-cancer effects, as well as to reduce the incidence of diabetes and cardiovascular disease.[21] These claims have been supported by epidemiological data from human clinical research.[22] People have been using garlic as a spice in cooking since ancient times realizing that it prevents cardiovascular diseases and treats ailments including whooping

cough, gastrointestinal problems, colds, and earaches.[23] Aged garlic extract (AGE), a traditional herbal remedy, has been shown to support the immune system and prevent cancer and heart diseases. Raw garlic and its processed derivatives, which are employed in a number of applications, are said to contain various organosulfur compounds.[24] The dietary sources of H_2S include allium species such as garlic, shallots, and other vegetables which are used in our daily life. Organosulfur compounds (OSCs) are found to be one of the major components present in all of these species and the bioactivity of garlic and its health benefits have been known for several years and is attributed to the production of H_2S in the presence of thiols.[25] The active component present in garlic for demonstrating the biological activity was discovered to be alliin and further it is converted to allicin by the enzyme alliinase.[26] This unstable compound (allicin) readily decomposes in an aqueous solution to different polysulfide compounds such as diallyl sulfide (DAS), diallyl disulfide (DADS) and diallyl trisulfide (DATS) (Figure 1.2).

1.4.2. Natural sources of H_2S

In addition to the garlic derived allium species there are also other organosulfur compounds such as diisopropyl trisulfide **1.1** have been reported in the literature and are found to exhibit anti-inflammatory and antioxidant properties.[27] Apart from allium species, polysulfides such as dimethyl trisulfide **1.2** and dimethyl tetrasulfide **1.3** are found in the family of cacti.[28] Other branched polysulfides commonly found in the spices of the middle east and Asia are *sec*-butyl trisulfide **1.4** and the corresponding tetrasulfide **1.5**. In addition to the symmetrical polysulfides, unsymmetrical polysulfides such as **1.6** and **1.7** are also found in the bark of *Scorodophloeus Zenkeri* and these polysulfides have been found to exhibit potent anti-bacterial and anti-fungal properties.[29] The chemical structures of naturally occurring organosulfur compounds is shown in Figure 1.2.

Other than polysulfides, organosulfur compounds such as isothiocyanates also releases H_2S. These compounds are present in vegetables like broccoli (SFN, **1.8**), black mustard (AITC, **1.9**), garden cress (BITC, **1.10**), and white mustard (HBITC, present in **1.11**) and rocket (ERU, **1.12** and phenyl isothiocyanate (PITC, **1.13**).[30]

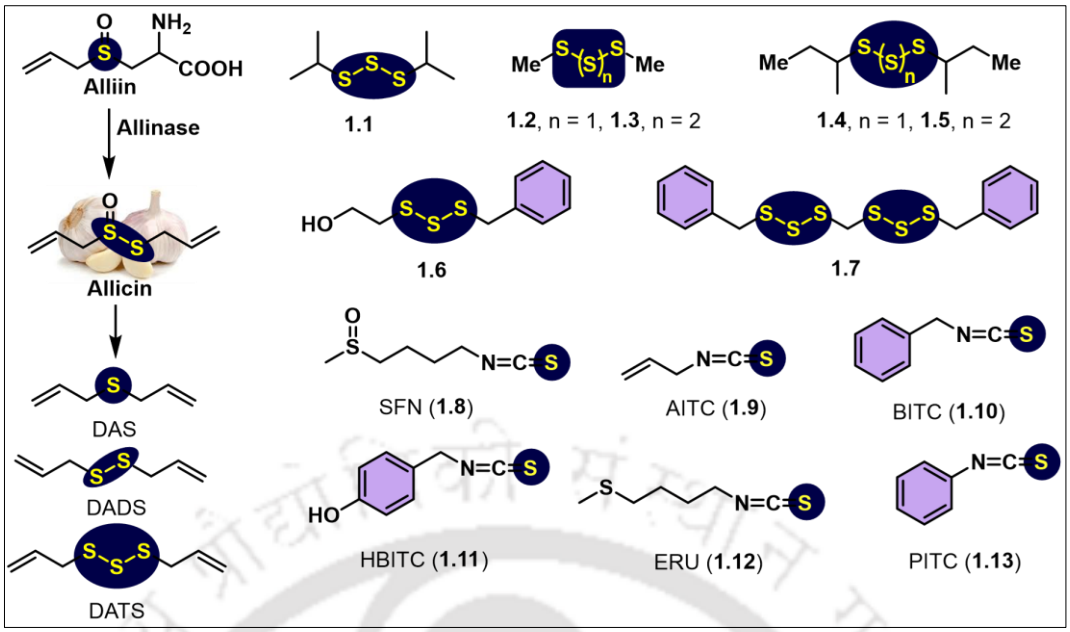

Figure 1.2. Some representative naturally-occurring OSCs as potent sources of H_2S.

1.4.3. Bacterial sources of H_2S

The diverse bacterial and archaeal species that make up the bacteria and create H_2S using different sulfur-containing materials as a source of energy. H_2S is produced by sulfur-reducing bacteria during a process called anaerobiosis. These sulfate-reducing bacteria are one of the oldest bacterial life formed on Earth. As a by-product of anaerobic respiration, these bacteria used inorganic sulfur salts as substrates to generate H_2S.[31] H_2S generating enzymes such as 3-MST, CBS and CSE have been found in numerous bacterial species.[32]

1.4.4. Environmental sources of H_2S

Majority of the sources that release H_2S into the atmosphere are natural. H_2S is generally produced when a dead plant and animal matter decomposes in moist and low environmental oxygen conditions such as swamps and further released it into the atmosphere.[33] H_2S is also released by hot springs, volcanoes, and other geothermal sources.[34] Industrial operations, particularly those related to the extraction and refinement of oil and natural gas as well as the production of paper and pulp, the presence of the gas at sewage treatment facilities, are the main sources of anthropogenic emissions of H_2S into the atmosphere.[35] Intriguingly, multiple mass extinctions on Earth's history have been linked with higher amounts of H_2S in the atmosphere, which are probably the result of volcanic eruptions.[36]

1.4.5. Endogenous production of H_2S

Three different enzymes are majorly responsible for the production of H_2S in the biological system such as CSE, CBS), and 3-MST in co-ordination with CAT. The transsulfuration route includes the enzymes cystathionine-β-synthase (CBS) and cystathionine-γ-lyase (CSE). The transsulfuration pathway enzymes are primarily found in the cytoplasm, though under some circumstances they may also be found in the nucleus or the mitochondrion. Any alteration in them can lead to a variety of disorders. In addition to being produced endogenously by means of these enzymes, H_2S is also stored in the form of sulfane sulfur.[37] The enzyme CSE catalyzes the reaction of Cys to give Ser and H_2S. Cys can also combine with Hcy in the presence of CBS to give cystathionine and H_2S. In another pathway, the enzyme CAT catalyzes the reaction of Cys in the presence of α-ketoglutarate to give 3-mercaptopyruvate, that in turn is converted to pyruvate, ammonia and H_2S in a reaction catalyzed by enzyme 3-MST.[38] Recently it was discovered that D-Cys can also produce H_2S in the presence of an enzyme DAO to give to give 3-mercaptopyruvate, that in turn is converted to pyruvate, ammonia and H_2S in a reaction catalyzed by enzyme 3-MST.[39] The details of the enzymatic processes is shown in Figure 1.3.

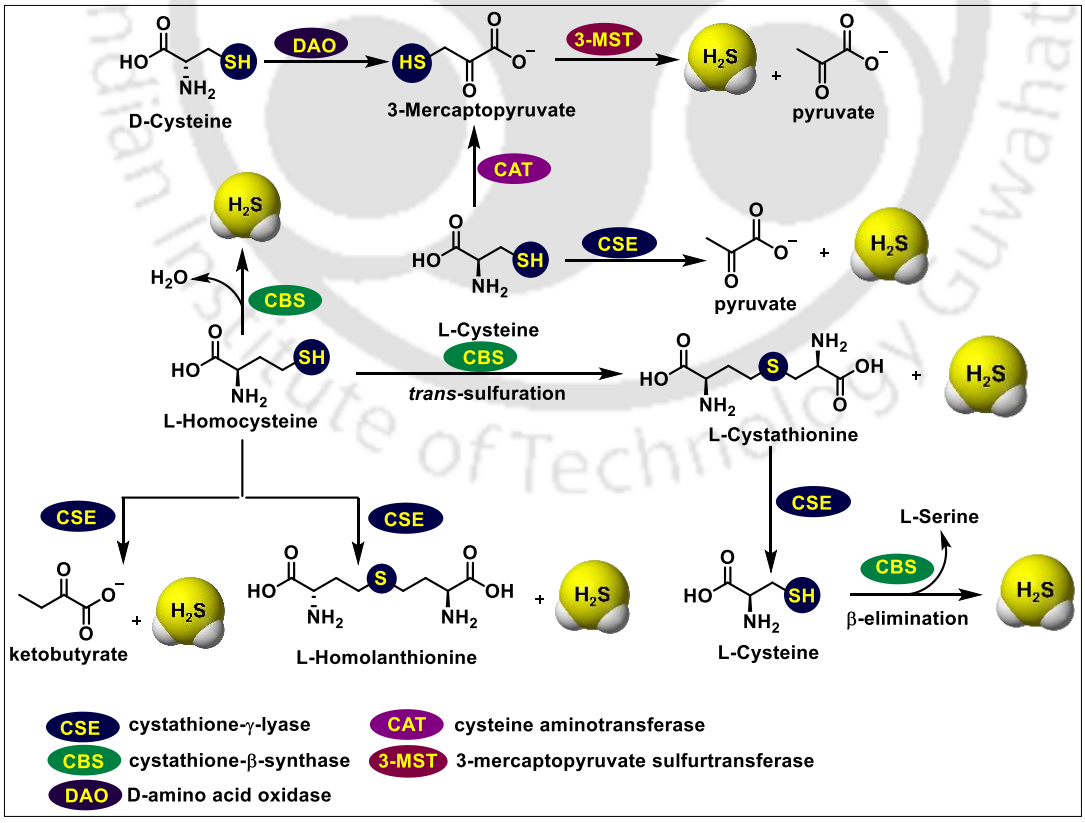

Figure 1.3. Schematic representation of endogenous production of H_2S.

1.5. Different types of H_2S donors

1.5.1. Hydrolysis-based H_2S donors

1.5.1.1. Sulfide salts

The majority of H_2S research involved either direct H_2S inhalation or the use of sulfide salts like sodium hydrosulfide (NaHS) or sodium sulfide (Na_2S). These sulfide salts give quick access to the physiologically significant forms of sulfide (H_2S and HS^-), as they are merely solid analogs of gaseous H_2S. Due to their therapeutic potential for exerting protective effects in a variety of illness models, these sulfide salts have been frequently exploited as an exogenous sources of H_2S for example treating rat aortic rings with NaHS, Wang and co-workers first described the vascular effects of exogenous H_2S administration and found that the relaxation rate was significantly increased (by about 60%).[40] In a different investigation, Du and co-workers demonstrated how NaHS protected against acute liver damage and decreased cytotoxicity, lipid peroxidation, and protein oxidation.[16]

In another report, Lefer and co-workers showed that Na_2S protects against ischemia-induced heart failure. The anti-inflammatory effects of NaHS were further shown by Kloesch and co-workers by down-regulating the IL-6 and IL-8 cytokines.[41] But the anti-inflammatory effects were reversed after 1 h probably due to the volatilization of H_2S in the atmosphere. Although, these sulfide salts showed protective effects, the rate of H_2S release from these salts was very spontaneous. Olson and co-workers conducted an experiment regarding the existence of H_2S in the tissue interestingly no H_2S release was observed in the experimental samples after 5 min due to the volatilization of H_2S in the atmosphere.[42] Even while some studies have shown that these salts are effective at donating H_2S, the instantaneous release of H_2S via quick hydrolysis in an aqueous solution has negative side effects. These results inspired the development of slow and persistent release of H_2S similar to the endogenous production of H_2S.

1.5.1.2. Lawesson's reagent and analogues

In several organic reactions, Lawesson's reagent (LR, **1.14**) is employed to transform amides, ketones, and esters to the corresponding thiol counterparts.[43]. Interestingly, it has been observed that LR is capable of donating H_2S upon the hydrolysis and the rate can be enhanced in the acidic medium. LR hydrolyzes in an aqueous solution and produces H_2S over a substantially longer duration than the equivalent sulfide salts. It can be prepared by the reaction between anisole and phosphorus pentasulfide.[44] Cunha and co-workers further assessed the positive effects of the H_2S generated by the LR, revealing that LR

showed protective benefits during a condition called sepsis.[45] Despite the fact that LR showed protective effects in the diseased models, its uses are limited due to the lack of solubility in aqueous solution. In order to overcome the solubility problem, a water-soluble derivative of LR has been developed and widely used that is termed as GYY4137 (Morpholin-4-ium-4-methoxyphenyl(morpholino) phosphonodithioate, **1.15**). It can be prepared by the reaction of LR and morpholine in dichloromethane at room temperature. The compound GYY4137 releases H_2S upon the hydrolysis in aqueous solution. As compared to LR, GYY4137 was shown to release H_2S in a sustained manner up to 180 min after it was administered intravenously or intraperitonially.[46] The release of H_2S from GYY4137 reached a maxima within 10 min of its administration. Upon incubation in phosphate buffer, GYY4137 releases lesser amount of H_2S over a sustained period of time with higher release rates observed upto 15 min and then reached saturation after 75 min. The release of H_2S from GYY4137 was pH- and temperature-dependent particularly requiring lower temperature (<4 °C) and acidic pH for a faster release.[47] In an interesting study, Moore and co-workers have further compared the anti-inflammatory properties of H_2S using NaHS and GYY4137 in LPS-treated macrophage cell line. The main objective of the study was to understand the impact of H_2S release rate on anti-inflammation. Their results indicated that GYY4137 significantly reduced the LPS-mediated release of pro-inflammatory mediators such as IL-6, TNF-α, whereas such effects were not observed for NaHS.[48-50] Further development of H_2S donor was reported by Xian and co-workers utilizing o-aryl and -alkyl substituted phosphorodithioate (**1.16**).[51] A series of compounds were synthesized and compared with GYY4137 for their H_2S donating capacities. For example, in the year 2016, Xian and co-workers have synthesized another derivative of GYY4137 by modifying the morpholine unit with C-protected amino acids such as glycine, alanine, valine, proline and phenylalanine. The derivatives were named as JK donors (**1.17**) that released H_2S slowly in neutral and basic medium (Figure 1.4). However, in the acidic pH the H_2S release was more facile and there is an intramolecular cyclization that facilitated the release of H_2S by breaking of P-S bond. The JK derivatives released H_2S at a faster rate under acidic conditions and showed significant reduction in cardiac troponin I levels, that is a biomarker for a healthy heart.[52] JK donors also provided protection against H_2O_2-induced cellular damage.[53]

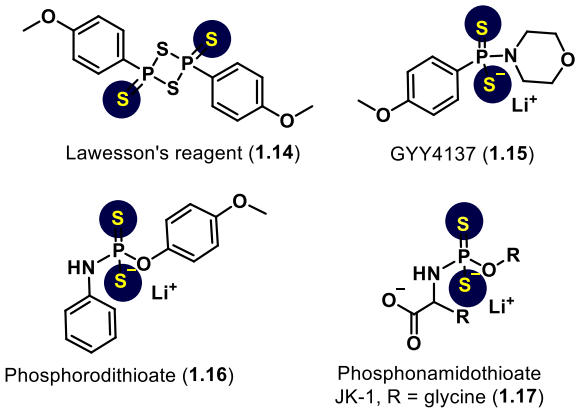

Figure 1.4. Chemical structures of some hydrolysis-based H_2S donors.

1.5.1.3. 1,2-Dithiole-3-thiones

Another class of H_2S donors reported in the literature that work via the hydrolysis mechanism are 1,2-dithiole-3-thiones (DTTs). These can be synthesized by the reaction of elemental sulfur with anethole.[54-57] The mechanism of H_2S release from DTTs is not well understood. Many research groups believe that 1,2-dithiole-3-thiones are converted to 1,2-dithiole-3-ones upon hydrolysis.[58] DTTs showed much pharmacological significance upon conjugation with anethole trithiane (ADT-OH, **1.18**), because it helps in the restoration of salivation of dry mouth caused by administration of chemotherapeutic drugs in a diseased condition called xerostomia.[59] DTTs have been extensively studied when combined with NSAIDs. The regular administration of these NSAID's causes damage in the gastrointestinal track.[60] However, these damages are minimized upon administration of ADT-NSAID hybrids as compared to the native NSAIDs.[61,62] Moore and co-workers reported the first example of DTT-NSAID hybrid named S-Diclofenac.[63] In another report, Wallace and co-workers compared the anti-inflammatory effects of ADT-OH (**1.19**) with ATB-337 (**1.20**) in vitro using rat liver homogenate and observed that the rate of H_2S release was lesser for ADT-OH .[64] Results suggested that the rate of H_2S release from ATB-337 was 3-times higher than ADT-OH. The authors further investigated the efficacy of ATB-337 moiety by incubating ADT-OH and diclofenac against gastric ulcers and observed that ADT-OH induces the same level of gastric damage to that of diclofenac. These results indicated that ADT-OH did not show any protective effect against gastric ulcers. However, interesting results of gastric protection was observed when treated with ATB-337 hybrid probably as the rate of H_2S release that was three times higher than ADT-OH. The authors compared the effects of diclofenac and ATB-337 for gastrointestinal damage. Oral administration of diclofenac resulted in

haemorrhagic damage in the rat stomach, while a similar dose of ATB-337 did not produce such damage. It is still unclear how ATB-337 releases higher amount of H_2S as compared to free ADT-OH. One hypothesis for the higher H_2S release could be due to increased solubility of ATB-337. In addition to the protective effects of NSAID against gastrointestinal damage, Kashfi and workers have evaluated these H_2S-NSAID hybrids for chemopreventive activities and observed that HS-SUL (**1.21**), HS-NAP (ATB-345, **1.22**) HS-ASA (**1.23**), and HS-IBU (**1.24**) could inhibit the growth of several organ-specific cancer cells such as breast, lung and colon cancers (Figure 1.5). The chemopreventive activity of these donors might be due to the released H_2S via the hydrolysis of dithiolenes.[65]

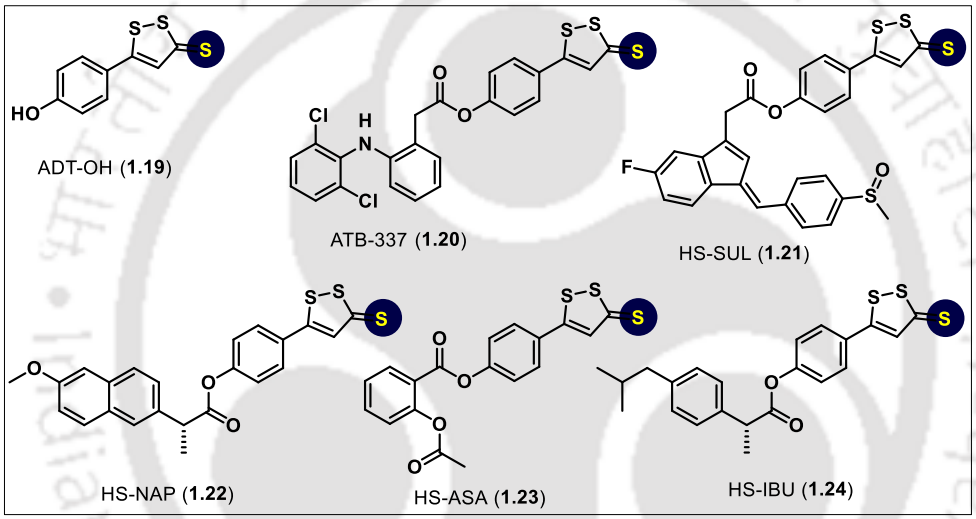

Figure 1.5. Chemical structures of some representative H_2S-NSAID hybrids.

1.5.1.4. Thiol-triggered H_2S donors

Thiol-triggered H_2S donors are very useful as thiols are abundant in the biological system. Xian and co-workers provided the first example of thiol-triggered H_2S donors in 2011.[53] The authors have synthesized a series of N-(Benzoylthio)benzamide (**1.25**) in two steps from substituted thiobenzoic acids and evaluated their H_2S donating capability in the presence of Cys and GSH (Figure 1.6). In the presence of Cys, a sharp increase in H_2S concentration was observed upto 18 min and then slight decrease was observed upto 80 min. Additionally, this donor provided a cardioprotective effect against myocardial I/R injury, by decreasing infarct size as compared to the controls in mouse models. The reaction mechanism involves a thiol-exchange reaction between Cys and the donors and generate S-acylcysteine and *N*-mercaptobenzamide intermediate. The S-acylcysteine undergoes native chemical ligation approach to form a stable *N*-acylcysteine. The *N*-

mercaptobenzamide intermediate reacts with Cys to give benzamide and cysteine perthiol intermediates and the perthiol intermediate reacts with Cys to release H_2S. The perthiol-based donors are another class of thiol-triggered donors that eventually need disulfide exchange to promote the release of H_2S. As many of the processes in the biological system proceed through persulfide chemistry, Xian and co-workers created the first acyl perthiol donors (**1.26**).[66] The donors were synthesized in two steps using N-benzoyl cysteine methyl ester and derivatives of thiobenzoic acid. By changing the aromatic R substituent, these donors demonstrated variable rate of H_2S release. Both steric and electronic variables affected the amount of H_2S released while electron-withdrawing substituents accelerated release rates whereas bulky aromatic ring substituents led to a relatively slower rate of H_2S release. Furthermore, the authors have also observed the protective effects of these donors against myocardial reperfusion injury. The rate of H_2S release from these acyl perthiols were higher in the presence of Cys as compared to GSH. Since H_2S provides protection against myocardial-ischemic reperfusion injury (MI), the authors have tested the effect of these synthesized acyl perthiols in a MI/R murine model. After administrating the H_2S donors to mice, a notable decrease in myocardial infarct size per area and cardiac troponin I levels were observed indicating that perthiol (-SSH) groups may have H_2S-mediate cardiac defence against MI/R.

The dithioperoxy anhydride-based H_2S donors **1.27-1.28** reported by Galardon and co-workers in 2013.[67] The authors reported both aromatic and aliphatic dithioperoxyanhydrides and was prepared by the reaction of thiobenzoic acid with methoxycarbonylsulfenyl chloride. The authors observed a similar rate of H_2S release when treated with Cys and GSH as measured by amperometric measurements. The compounds were found to be non-toxic in nature upto a concentration of 200 μM in human fibroblasts and exert vasorelaxation in rat aortic rings. The release of H_2S from these donors were confirmed from cell lysate experiments as well as in buffer solutions.

Arylthiooximes (SATOs, **1.29**) are another class of H_2S donors developed by Matson and co-workers.[68] They were synthesized by the condensation reaction of an aryl aldehyde or ketone and an S-aroylthiohydroxylamine in the presence of a catalytic amount of acid. A library of SATOs were synthesized, varying the substituents at the aldehyde/ketone as well as the SATHA ring. The arylthioximes release H_2S in the presence of thiols. The H_2S release from these donors was measured by amperometry as well as the methylene blue method (Figure 1.6).

Another class of thiol activated H_2S donors developed by Calderone and co-workers are arylthioamides.[69] Arylthioamides (**1.30-1.31**) are prepared from indirect route by the reaction of benzonitrile with phosphorus pentasulfide (P_4S_{10}) or direct thionation of arylamides using Lawesson's reagent. The authors have synthesized a series of arylthioamide using different substituents in the aromatic ring. The H_2S releasing ability of aryl thioamides were check by adding excessive amount of Cys (4 mM) in PBS buffer (10 mM, pH 7.4). The rate of H_2S release from these donors were similar to DADS and GYY4137 under identical experimental conditions. However, many of the synthesized arylthioamides released H_2S without adding any Cys suggesting hydrolysis mechanism for H_2S release. Among all the donors, *p*-hydroxybenzothioamide was evaluated for their vasoconstriction effects in rat aortic rings. Initially, the authors induce vasoconstrictive effects in rat aortic rings by using noradrenaline (NA) and then treated the aortic rings with NaHS and arylthioamide compound. Interestingly, arylthioamide reduces vasoconstriction without adding any external Cys, suggesting endogenous biomolecule triggered H_2S release at higher donor concentration. The arylthioamide donor showed its ability to hyperpolarize vascular smooth muscle cells at a much lower concentration of 300 µM as compared to the higher concentration of NaHS. This data suggests that slow and sustained release of H_2S from thioamides might be one reason for its activity at such a lower concentration. The mechanism of H_2S donation from these thioamides still remains unclear.

In the year 2017, Pluth and co-workers reported the H_2S donating capabilities of bis(alkyl) **1.32** and bis(aryl) tetrasulfides **1.33** upon treatment with cellular abundant thiol glutathione (GSH) and observed a higher H_2S releasing capacity for these synthesized tetrasulfides as compared to DATS. The same group have reported the anti-proliferative activity of different sulfane sulfur compounds such as benzyl trisulfide **1.34** and tetrasulfide **1.35** in bEnd.3 cells and observed a higher anti-proliferative activity for trisulfide and tetrasulfide as compared to DATS. The authors report that the anti-proliferative activity of tetrasulfides is due to higher build-up S^0 content in tetrasulfides as compared to trisulfides (Figure 1.6) [70]. In another work, Quinn and co-workers in the same year have reported a self-assembling compound **1.36** having PEG-cholesterol conjugate connected via a trisulfide linkage.

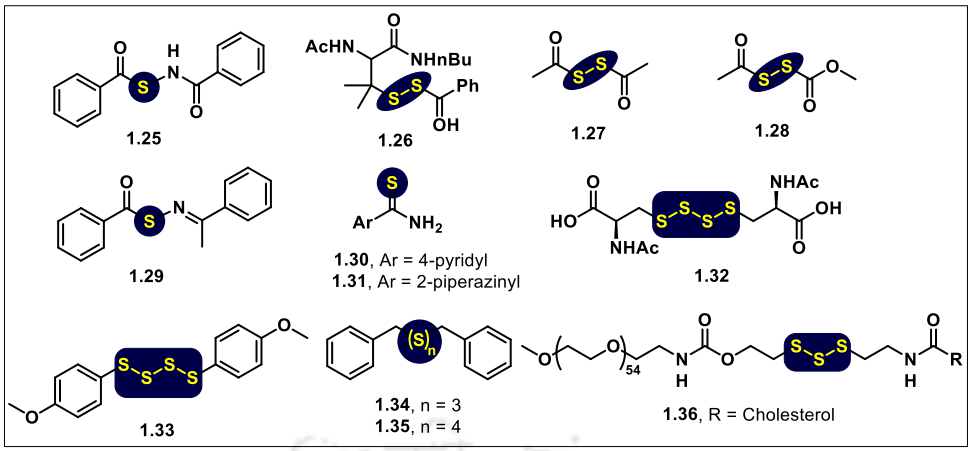

Figure 1.6. Schematic representation of thiol-triggered H_2S donors.

1.5.2. Light-triggered H_2S donors

The activation of H_2S donors that are triggered by light allows for the precise control of H_2S release at a specific wavelength of light. This method allowed the delivery of H_2S to a particular tissue within the body. Researchers have developed a number of light-triggered donors over the last decade employing various photoactive groups, including o-nitrobenzyl, ketoprofenate, xanthone and phenacyl. In the year 2013, Xian and co-workers reported the first photoactivated H_2S donor photo-gem-dithiol in which a geminal-dithiol is protected by bis(orthonitrobenzyl) group. The compound undergoes a Norrish type II rearrangement upon its exposure to light ($\lambda = 365$ nm) to reveal an unstable gem-dithiol intermediate that is subsequently hydrolyzed to release H_2S. [71] In this work, the authors have synthesized geminal dithiol using titanium (IV)-catalyzed coupling of o-nitrobenzyl mercaptan and acetone producing the geminal dithiol **1.37.** Upon irradiation of compound **1.37** to light ($\lambda = 365$ nm), a time-dependent H_2S generation was observed. Mechanistically, the reaction proceeds via a radical transfer pathway. The release of H_2S was not observed in the absence of light, indicating the reasonable stability of the donor under physiological conditions.

In the year 2013, Nakagawa and co-workers have reported an alternative photo controllable H_2S donor **1.38** that relies on a functionalized thioether and releases H_2S immediately following photocleavage of the protective groups.[72] Upon the exposure of donor **1.38**, it emitted one molecule of H_2S, the donor emitted one molecule of H_2S, two molecules of 2-propenylbenzophenone, and a carbon dioxide (CO_2). This donor was employed in a fetal bovine serum (FBS) solution to ascertain the H_2S release behaviour in a biological system. Without UV irradiation, no H_2S was released. However, after 10

min of UV irradiation, the methylene blue assay revealed the presence of 30 μM H_2S from 500 μM donor.

The light-triggered H_2S donors were revisited by Connal and co-workers with the development of thioether ketones such as compound **1.39**.[73] The thioether ketone **1.39** decomposes in the presence of UV-light releasing thioaldehyde and benzophenone. The generated thioaldehyde releases H_2S upon the reaction with amines. Furthermore, the authors also applied this donor in 3T3 cells to visualize the H_2S release using H_2S selective nucleophilic substitution cyclization-based fluorescent probe **WSP1**. In another report, Chakrapani and co-workers have developed a BODIPY-based thiocarbamate probe **1.40** that can be excited by the visible light (≥410 nm). Upon irradiation with visible light, the B-O bond of the donor undergoes cleavage to release COS/H_2S. The probe was found to be non-toxic in HeLa cell line upto 50 μM concentration.[74] The H_2S release from the donor was measured using methylene blue assay and a sustained release of H_2S was observed upto 2 h. Expanding the research of light-triggered H_2S donors further, You and co-workers have developed visible light-triggered H_2S donors using 1,3-diarylisobenzothiophene **1.41** moiety and singlet oxygen as a photosensitizer.[75] Mechanistic insights reveal that the photosensitizer converts molecular oxygen to singlet oxygen and the singlet oxygen reacts with the diarylisobenzothiophene to endoperoxide, which undergoes fragmentation to give 2-benzoylbenzophenone and H_2S. All the donors developed above are non-fluorogenic and hence the real-time monitoring of H_2S release could not be achieved. Moreover, most of them require a two-step process for the release of H_2S. Contributing to the development of visible light-triggered H_2S donor Singh and co-workers have developed a colorimetric probe **1.42** that releases H_2S in a single step upon the irradiation with visible light (λ ≥410 nm). The chemical structures of each of the light-triggered donors is shown in Figure 1.7.[76]

In another work, Wilson and co-workers described a hybrid system that includes the ruthenium photo-caged GYY4137 (**1.43**), which emits H_2S upon the reaction with red light (λ_{ex} = 626 nm). It is significant to note that, despite the fact that GYY4137 is known to hydrolyse spontaneously in aqueous conditions, complexation with the Ru (II) center prevents the spontaneous release of H_2S.[77] The researchers have tuned the release of H_2S from the donor and it was found to protect cardiac myoblast cells from an ischemia-reperfusion injury upon irradiation with red light. Light-triggered H_2S donors enable a more precise triggering mechanism than nucleophiles generally do, offering practical possibilities for H_2S release under specific circumstances. It is also possible to control the

release of H_2S spatiotemporally by using light as a trigger. Due to the limited penetration depth of UV and visible light in mammalian tissue, this donor class is most likely to be useful as chemical instruments for researching H_2S biology *in vitro*. However, because of the capacity of near-infrared light to penetrate tissue at a higher depth than UV and visible light with little damage to surrounding tissue, the development of donors that are triggered by NIR light may enable applications *in vivo*.

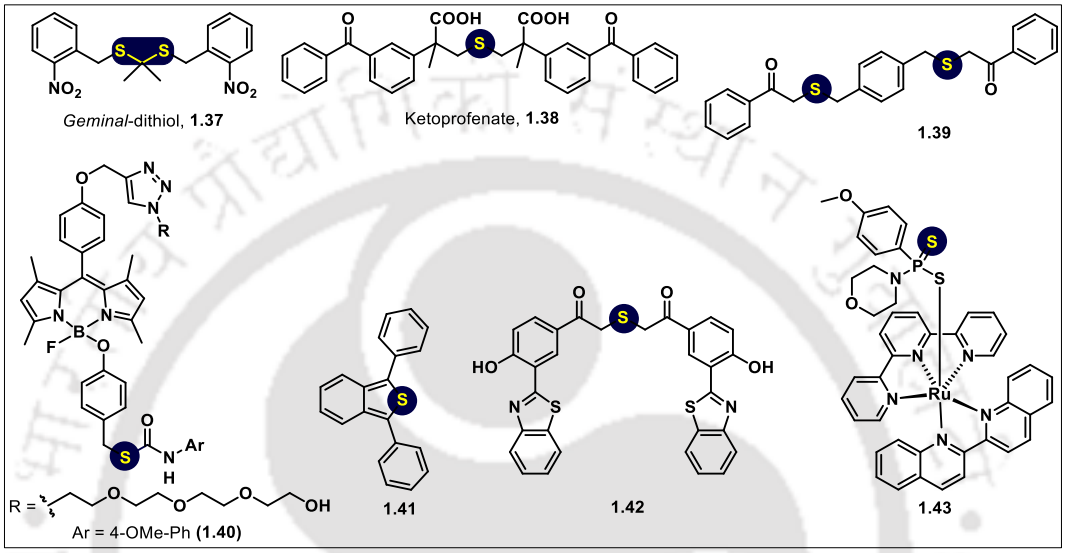

Figure 1.7. Chemical structures of some representative light-triggered H_2S donors.

1.5.3. Amino acid-based H_2S donors

Giannis and co-workers in the year 2012 have reported the first example of amino acid-based H_2S donors such as thioglycine **1.44** and thiovaline **1.45**.[78] However, the release of H_2S from these amino acids were observed only in bicarbonate buffer. The H_2S release from these amino acids was measured by monobromobimane method to form a sulfide dibimane product that is highly fluorescent (Figure 1.8). Moreover, it was also observed that these donors reached saturation within 1 hour of reaction when compared to known H_2S donors such as sodium sulfide NaHS and Na_2S. These amino acids were further evaluated for their dilatation effects on intracellular cyclic guanosine monophosphate levels and observed in a concentration-dependent manner in cGMP levels.

Figure 1.8. Chemical structures of the representative amino acid-based H_2S donors.

1.5.4. Enzyme-triggered H_2S donors

The use of enzymes as the triggers for the H_2S release offers a number of advantages over the small molecule bio-analytes as they are endogenous to living beings and they showed tissue and substrate-specific localizations in the biological system. However, excessive enzyme expression is a common cause of numerous diseases. The use of enzyme-triggered strategies offers interesting targets as a therapy to treat certain disorders. Nevertheless, only a small number of enzyme-triggered H_2S donors have been identified so far and these donors are anticipated to have a significant impact in the future. The first enzyme-triggered H_2S donors were a series of esterase-responsive compounds developed by Wang and co-workers in 2016.[79] The donors of this category such as HP-101 (**1.46**) rely on the esterase-triggered cleavage of the aromatic ester group followed by the lactonization process popularly termed ‘‘trimethyl lock” (TML), which has been used to promote the release of a variety of drugs. Upon the cleavage by porcine liver esterase (PLE) enzyme, the alkoxide generated attacks the carbonyl carbon of thioacid to release H_2S along with the formation of a five-membered lactone ring. The authors have confirmed the H_2S release by using an H_2S selective microelectrode. However, the rate of H_2S release was found to be slower for donors lacking the dimethyl groups on the aliphatic side chain. All the synthesized H_2S donors exhibited anti-inflammatory properties but some also showed protection against myocardial-infarction injury. Additionally, NSAID-TML hybrids such as (HP-105, **1.47**) were successfully developed for their effectiveness as anti-inflammatory drugs (Figure 1.9).

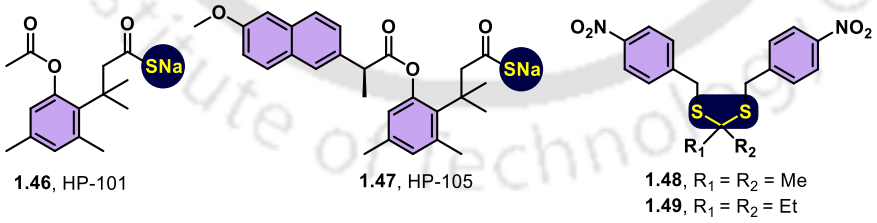

1.46, HP-101 **1.47**, HP-105 **1.48**, $R_1 = R_2$ = Me
1.49, $R_1 = R_2$ = Et

Figure 1.9. Chemical structures of enzyme triggered H_2S donors.

In the year 2017, Chakrapani and co-workers combined the concept of enzyme-specific cleavable functionalities with the protected geminal dithiol as an H_2S releasing moiety in another class of enzyme-triggered H_2S donors.[80] The work of Chakrapani and co-workers on enzyme-triggered donor platforms was extended in order to develop donors that were triggered by bacterial nitroreductase (NTR) **1.48-1.49** as bacteria commonly contain NTRs, which are also increased in a variety of cell types under hypoxic environments. In

the presence of NTR, the nitro groups undergo reduction to the corresponding amino group. The amino group facilitate the self-immolative process with the release of geminal dithiols and quinone methide intermediates. The nitrogen lone pair was then free to resonate through to liberate the iminoquinone methide. The released H_2S was measured by the monobromobimane method. The use of these donors allowed researchers to better understand how H_2S affects intracellular redox balance and the existence of antibiotic resistance in bacteria, particularly *E. coli*.

1.6. Carbonyl sulfide-based H_2S donors

Another class of compounds releasing H_2S is the self-immolative thiocarbamates that can be connected to specific triggering groups. In the year 2016, Pluth and co-workers have reported the first example of analyte replacement probe by the conjugation of azide moiety to rhodamine fluorophore via thiocarbamate linkage, **1.50**. Upon the reaction with NaHS, the azide moiety is reduced to amine and that leads to the self-immolative process with the release of COS and the free fluorophore (Rhodamine).[81] The release of H_2S from the COS took place in the presence of carbonic anhydrase (CA).

In another work Pluth and co-workers, have developed donors **1.51-1.52** in which boronate ester was incorporated as a triggering unit, which was linked to the thiocarbamate unit via a benzyl group. The authors observed that these donors were non-toxic and reactive towards cellular nucleophiles such as H_2O_2, O_2^- and $ONOO^-$. The donors also exhibited cytoprotective effects in a dose-dependent manner (10-50 µM) in HeLa cells, against H_2O_2-induced toxicity. These results showed the ability of boronate esters to react with intracellular ROS and to protect cells from oxidative damage with the released H_2S.[82]

The concept of COS-based donors was extended further to several other stimuli present in the biological system. The first report of enzyme-triggered self-immolative COS/H_2S donor was reported by Pluth and co-workers. In this work, the authors have conjugated pivaloyl and methyl ester groups to the COS donors that were preferentially hydrolyzed in the presence of the porcine liver esterase (PLE). Interestingly, as compared to Na_2S and GYY4137, these thiocarbamate donors exhibited higher level of cytotoxicity in BEAS 2B (human lung epithelial cells) and in HeLa cells. The observed cytotoxicity was due to decrease in the cellular respiration and ATP generation which is consistent with well-known capacity of H_2S to inhibit cytochrome c oxidase (Cco).[83]

In the year 2017, Pluth and co-workers have reported the first example of self-immolative H_2S donors **TCO-1** (**1.53**) and **TCO-2** (**1.54**) using bio-orthogonal chemistry. In order to

release H_2S from both the donors, click reaction between tetrazine and cyclooctene takes place. The release of H_2S from these donors were measured by amperometry.[84] In another study, Pluth and co-workers have synthesized three sets of compounds (i) Photo TCM-1 (**1.55**) and Photo TCM-2 (**1.56**) (*o*-nitrobenzyl group with and without methoxy substituents) (ii) Photo CM-1 (**1.57**) (*o*-nitrogroup with CO_2/H_2O donors) and (iii) TCM **1.58**, lacking the o-nitrobenzyl group as the phototrigger). The *o*-nitrobenzyl group undergoes photocleavage in the presence of UV-light (λ = 365 nm). Among all the synthesized photocleavable donors, the 4,5-dimethoxy substituent exhibited two times faster H_2S release as compared to the unsubstituted ones probably as a result of higher light absorption by the dimethoxy group.[85] However, the authors did not provide any data regarding the applicability of these donors under cellular conditions as these wavelengths of light might be harmful to the cells. The chemical structures of all the COS-based donors is shown together in Figure 1.10.

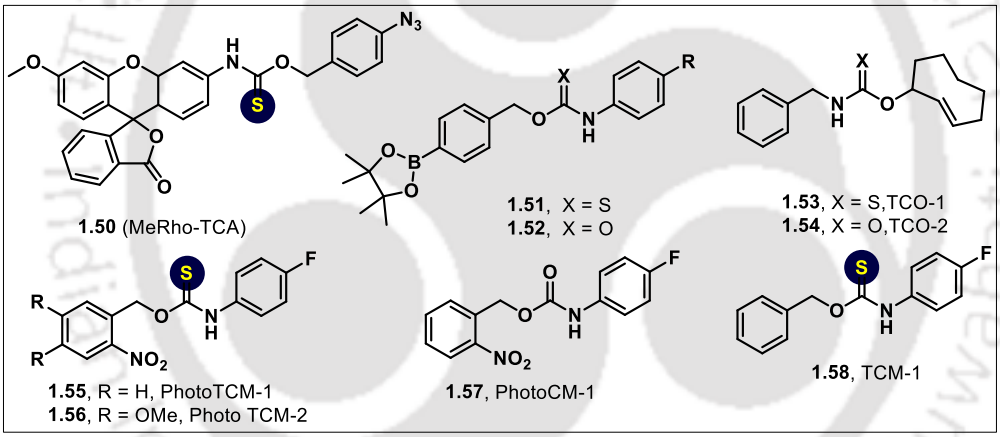

Figure 1.10. Chemical structures of some bio-analyte triggered self-immolative COS/H_2S donors.

1.7. Different methods for H_2S measurement

1.7.1. Electrochemical methods

Two types of sensors are generally used for the quantification of H_2S using electrochemical methods: ion-selective electrodes and amperometric (polarographic) sensors.

Ion-selective electrode (ISE) is an analytical method used to determine the activity of ions in an aqueous solution. These electrodes typically use an ion-selective membrane (Ag/Ag_2S) that utilizes H_2S permeability for the measurements in solutions and oxidizes H_2S to S^0 and release two electrons. The electrons generated during this process are

proportional to the amount of current produced. H_2S levels in biological samples have also been detected using ISEs, with a detection range of 1–100 µM.[86,87]

Another method to measure H_2S concentration is by using polarography. According to Kraus and co-workers and the Olson laboratory, detection and estimation of H_2S using the polarographic method is a well-documented and accurate way to quantify H_2S levels.[50] H_2S gas from biological samples can be measured in real-time using polarographic H_2S detection technique with a lower detection limit (nM range under anoxic conditions). The working cell requires a strongly basic environment in the electrode's solution phase enabling the dianionic sulfide ion to reduce $[Fe(CN)_6]^{3-}$ to $[Fe(CN)_6]^{4-}$, which is then reoxidized at the platinum electrode to provide a current proportional to the concentration of H_2S. Experimental results showed that endogenous rat blood and aorta contains sulfide levels in the µM range (<5 µM).[88] The main advantage of polarographic measurements is that it allows for real-time measurement of free gas without disturbing the sample. However, the electrode requires frequent reconditioning to minimize the interference from other species and also the electrodes operate under highly basic condition. The schematic diagram of an ISE is shown in Figure 1.11.

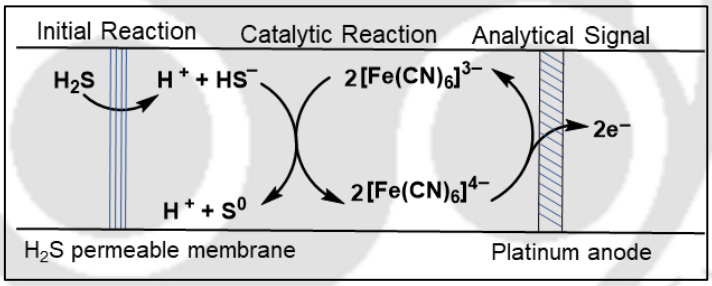

Figure 1.11. Schematic representation of amperometric methods for H_2S detection.

1.7.2. Gas chromatography

The analysis of H_2S by gas chromatography involves its derivatization to bis(pentafluorobenzyl)sulfide, extraction into ethyl acetate as the solvent and tetradecyldimethyl benzyl ammonium chloride as the phase-transfer catalyst then analysis by gas chromatography. The sample to be analyzed was mixed with extraction reagents under alkaline conditions and allowed to centrifuge at room temperature. After centrifugation the organic phase was analysed by gas chromatography Very low sulfide concentrations can be measured by this technique.[89]

1.7.3. Methylene blue (MB) method

This method is one of the oldest techniques used for the determination of H_2S concentration in samples. The methylene blue (MB) method was described by Fischer in 1883 and later introduced by Siegel in 1965.[90] It involves the formation of methylene blue (**1.59**) having a characteristic absorbance at 670 nm spectrophotometrically. The H_2S generated by experimental samples react with N, N-dimethyl-*p*-phenylenediamine, in the presence of anhydrous ferric chloride and zinc acetate (Scheme 1.1). The concentration of H_2S is determined by using H_2S calibration curves obtained by measuring known concentrations of H_2S using $Na_2S.9H_2O$.

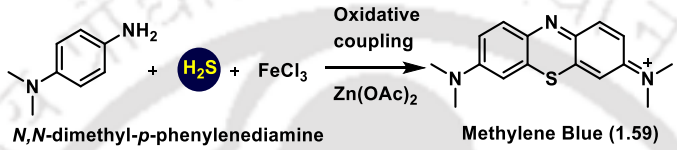

Scheme 1.1. Schematic representation of methylene blue formation.

There are several drawbacks associated with this assay as it does not obey the Beer-Lambert law at concentrations greater than 1 µM due to the formation of dimer and trimer species.[91] Another disadvantage of using this method is that it operates under highly acidic condition and such environments are not suitable for measurement of H_2S in cellular condition.

1.7.4. Monobromobimane method

The monobromobimane (mBB) method is used for the detection of very low concentration of H_2S (nanomolar range) using fluorogenic detection technique. Nucleophilic substitution reactions of sulfide with two equivalents of monobromobimane mBB leads to the formation of stable and highly fluorescent sulfide dibimane (sDB) **1.60** as shown in Figure 1.12.[92] One of the drawbacks of this process is that both thiols and H_2S react with monobromobimane via a nucleophilic substitution reaction leading to the formation of the associated sulfide products. The products are generally separated and quantified using reverse phase HPLC method with fluorescence detector.

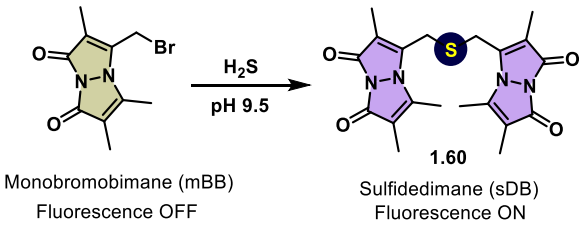

Figure 1.12. Chemical structures of monobromobimane-based H_2S donors.

1.7.5. Reaction-based fluorogenic sensors of H_2S

Most of the reported probes for H_2S detection work either in strongly acidic condition or basic conditions, which limit their application in cellular mediums. However, in this regard fluorescence methods are widely useful because of its simplicity, high sensitivity and non-invasiveness. Azide-based fluorescent probes **1.61**-**1.63** are weakly fluorescent due to energy transfer processes (ICT, PET), but in the presence of H_2S, it is reduced to highly fluorescent amines (R-NH_2). Several azide-based probes are reported in the literature having different fluorophores connected. Apart from azide probes, researchers have come up with nitro reduction-based probes **1.64** that are weakly fluorescent, but upon reduction with H_2S, a highly fluorescent amine is formed.[93]

The higher affinity of metals towards sulfur has also been utilized in addition to the strong nucleophilicity of HS^- for sensing. As shown in the probe **1.65**, fluorescence quenching, for instance, happens when a fluorescent molecule is bound to a paramagnetic metal ion like Cu^{2+}. The fluorophore is released and a turn-on response is generated as a result of the subsequent reaction with H_2S, which causes CuS production and precipitation.[94] The chemical structures of all the fluorogenic H_2S sensors are shown in Figure 1.13.

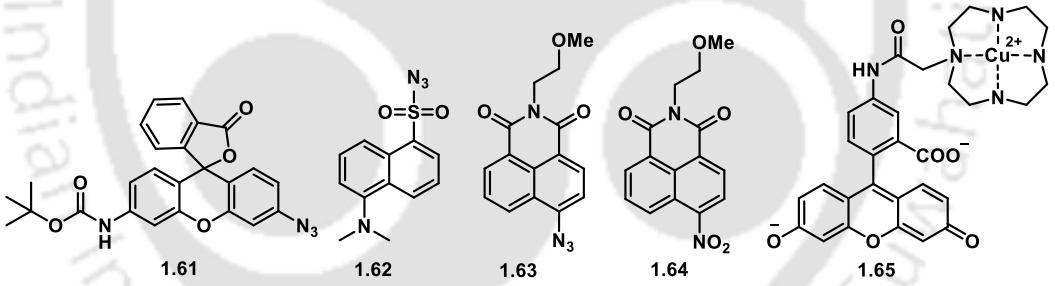

Figure 1.13. Chemical structures of some representative reaction-based turn-on fluorogenic probes for the detection of H_2S.

The azide-based probes developed so far suffer from a lack of selectivity towards H_2S and generates false signals due to the reaction with bio-thiols such as Cys and GSH that are present in the biological system. In another report, Xian and co-workers have developed a series of nucleophilic substitution-based probes (**WSP 1-5**) for H_2S **1.66-1.70**). One of the advantages associated with nucleophilic substitution-based probes for providing selectivity towards H_2S than thiols are because H_2S can participate in nucleophilic substitution followed by the cyclization process leading to the release of free fluorophore. The authors have used a wide range of fluorescent dyes such as coumarin, fluorescein, resorufin, etc (Figure 1.14). Moreover, no reaction was observed in the

absence of H_2S, indicating the stability of the probes under physiological conditions. These probes rely on the ability of H_2S to participate in dual nucleophilic substitution reactions to release the protecting group.[95]

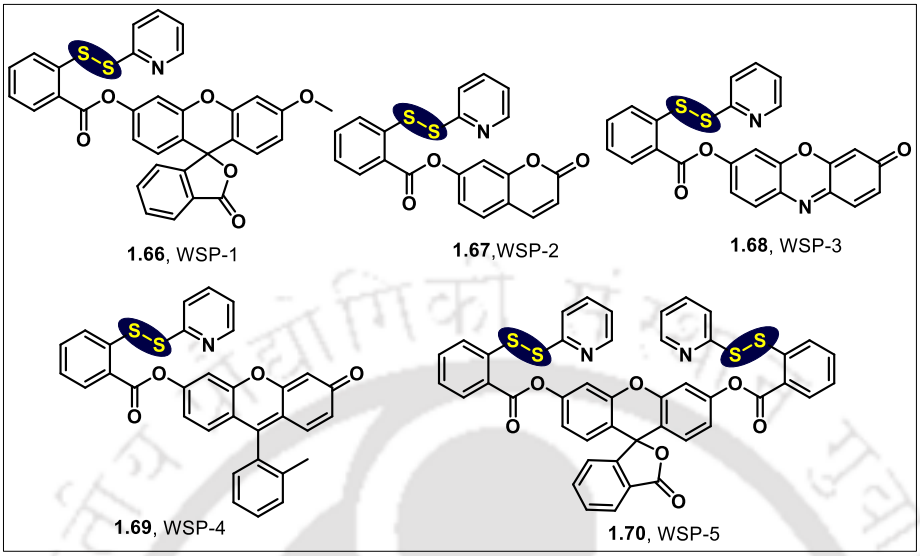

Figure 1.14. Chemical structures of some representative nucleophilic-substitution-based H_2S selective probes.

1.8. Different inhibitors of H_2S

Inhibitors of H_2S are used to decrease the concentration of H_2S generated by the enzymatic pathway inside the cells. Using small-molecule inhibitors of H_2S-producing enzymes, the production of H_2S is frequently reduced in research using cell culture models or isolated enzymes. Due to its extensive use, a lot of effort has been made to discover or produce efficient enzymatic inhibitors for CBS, CSE, and 3-MST. It is still highly challenging to develop inhibitors that are specific for one enzyme over another and have low inhibitory constants (K_i) values, despite the fact that these investigations have yielded a useful collection of compounds for the partial inhibition of H_2S-producing enzymes. Till date, only inhibitors for enzymes such as CBS and CSE are available commercially. The most commonly used CSE inhibitors are L-aminoethoxyvinyl glycine **1.71** (AVG, 1 μM), β-cyano-L-alanine **1.72** (BCA, 14 μM), and propargyl glycine **1.73** (PAG, 40 μM,).[96-98] From structural investigations of CSE enzyme it was found that PAG binds with Tyr114 in the active site of the CSE enzyme. However, it still challenging to inhibit CBS enzyme selectively. In addition to these, inhibitors for CBS includes aminooxyacetic acid **1.74** (AOAA, 8.52 μM,) trifluoroalanine **1.75** (289 μM) and

hydroxylamine (HA, 4.8 µM, **1.76**).[99-101] The chemical structures of all the enzyme inhibitors are shown in Figure 1.15.

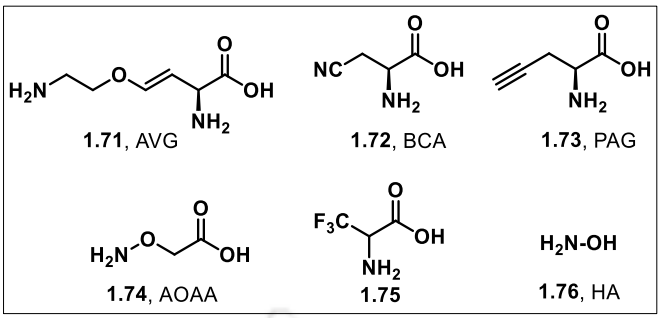

Figure 1.15. Chemical structures of commonly used inhibitors of **CSE** and **CBS**.

1.9. Metabolism of H_2S in mammals

There are three enzymes responsible for the metabolism of H_2S. The main mechanism for H_2S catabolism occurs in mitochondria. Several enzymes, including quinone oxidoreductase, persulfide dioxygenase, and S-transferase participate in the oxidative alteration of H_2S in the mitochondria to produce sulfite (SO_3^{2-}). The sulfite generated is further transformed into sulfate (SO_4^{2-}) by the enzyme sulfite oxidase. The sulfite can also be transformed into thiosulfate ($S_2O_3^{2-}$) by thiosulfate sulfurtransferase. Sulfate is therefore a key end-product of H_2S metabolism in physiological contexts.[102-104] The secondary process of H_2S catabolism is the methylation of methanethiol and dimethyl sulfide by thiol S-methyltransferase in the cytosol.[105,106] The third phase of H_2S metabolism, which results in the production of sulfhemoglobin, is regarded to be a possible biomarker of plasma H_2S (Figure 1.16).[107]

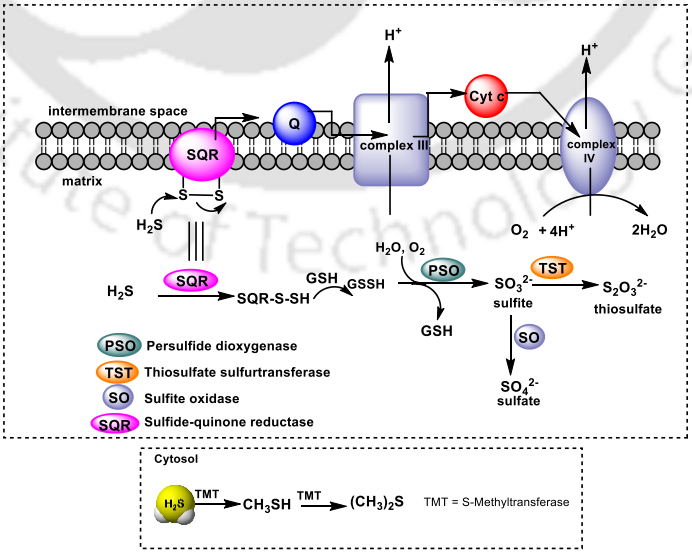

Figure 1.16. Metabolism of H_2S in biological system inside the mitochondrial matrix and cytosol.

1.10. Pharmacological properties of H_2S

1.10.1. Role of H_2S as neuromodulator

The hippocampus and cerebellum of brain cells are known to contain CBS which helps in producing H_2S in the brain.[108] In the year 1991, Kimura and co-workers first identified the neuromodulatory effects of H_2S and observed the long-term potentiation (LTP) in neuronal cells by acting on N-methyl-D-aspartate (NMDA) receptors and which are responsible for learning and memory. Later on, they found that H_2S increases the production of cAMP/PKC in primary cultured neuronal cells. H_2S was also found to reduce the pH in rat microglia and astrocyte primary cultures in a dose-dependent manner via controlling the activity of Cl^-/HCO_3^-.[4] The authors also observed that H_2S stimulates Ca^{2+} permeability, which was suppressed by broad-spectrum transient receptor potential (TRP) channels.[5] Bian and co-workers showed that H_2S exerts a neuroprotective effect by boosting glutamate uptake in neurons that had been damaged by H_2O_2 in primary cultured rat astrocytes.[109] It is also hypothesized that the activity of NMDA receptors in the brain is due to the persulfidation of Cys residues.

1.10.2. Cardioprotective effects of H_2S

H_2S affects the cardiovascular system in a variety of ways by providing protection against cardiac ischemia-reperfusion injury, relaxing smooth muscle cells, and lowering of blood pressure. Wang and co-workers showed that H_2S induces relaxation of rat aortic ring precontracted by phyenylepinepherine.[110] It has also been observed that boosting the endogenous production of H_2S protects the body against myocardial infarction injury (MI/R). H_2S has been shown to cause contraction, relaxation, or multiphasic responses in vascular smooth muscle of the aorta by stimulation of ATP-sensitive K^+ channels. Hyperpolarization and relaxation are caused by K_{ATP} activation in smooth muscle cells, and cardioprotection is caused by K_{ATP} activation in the heart.[40]

1.10.3. Role of H_2S in inflammation

It has been reported that H_2S causes pro- and anti-inflammatory actions in various types of inflammation. In mouse models, CSE expression was knocked down and the proinflammatory activity of H_2S was reduced. H_2S donors can also lessen inflammation by preserving the expression of the pro-inflammatory cytokine IL-10 while reducing the expression of other pro-inflammatory cytokines, such as interleukin (IL-1, IL-8), and TNF-α.[111] The reduction of nuclear factor-β (NFκB) activity by H_2S prevents the generation of pro-inflammatory cytokines. Another example of the anti-inflammatory effects of H_2S is provided by H_2S-NSAID hybrids and long-term administration of these

non-steroidal anti-inflammatory drugs causes gastric ulceration and bleeding by inhibition of COX-1 in the gastrointestinal track thereby leading to a reduction of prostaglandin secretion and inhibiting its cytoprotective effects in the gastric mucuosa. [112]

1.10.4. Role of H_2S in liver disease

The liver is the main organ that produces endogenous H_2S under physiological conditions. The regulation of glucose metabolism, lipoprotein synthesis, hepatic circulation, liver bioenergetics and oxidative stress are all affected by endogenous production of H_2S. The hepatic problems caused by insufficient production of H_2S include cirrhosis and hepatic fibrosis, but excessive endogenous H_2S may also contribute to insulin resistance and the development of diabetes.[113] High concentrations of H_2S can have hepatotoxic effects, while low concentrations of H_2S provides cytoprotection. Modulating H_2S generation and the expression of the enzymes that produce it may prove to be a successful technique for treating hepatic diseases and liver physiology. [114]

1.10.5. Role of H_2S in cancer

The role of H_2S is varied in the biological system while lower concentrations of it showed cytoprotective effects and at higher concentrations it shows cytotoxicity. It has been found that many of the enzymes responsible for the endogenous production of H_2S are highly expressed in cancer cells. The enzyme CSE is overexpressed at both the mRNA and protein levels in human colon cancer HCT 116 cells. Moore and co-workers showed that GYY4137, a slow-releasing H_2S donor exhibited anti-cancer activities in a variety of cancer cells. It has been observed that incubation of 400 μM of GYY4137 showed anti-cancer activities in MCF-7 cells, while similar dose of NaHS failed to show such activities. In another report, Szabo and co-workers observed that CBS is overexpressed in many organ-specific forms of cancer (HCT-116, HT-29 and LoVo) as compared to non-cancerous tissues and showed cellular migratory properties. The authors observed that inhibition of CBS using selective inhibitors such as AOAA reduced the proliferation of HCT-116 cells.[115]. Apart from colon cancer cells, the CBS enzyme is found to be overexpressed in primary epithelial ovarian cancer cells.[116]

1.11. Thesis objectives

H_2S is considered a gasotransmitter along with NO and CO. It is produced endogenously in the body by enzymatic and non-enzymatic pathways. The slow release of H_2S is beneficial for several pathological conditions in the body. To understand the role of H_2S in biological systems, several researchers have used sulfide salts such as NaHS and Na_2S as exogenous sources of H_2S. These inorganic salts do not perform well in cellular media

as the rate of H_2S release is very fast. To overcome these, several non-fluorescent organic donors of H_2S have been developed in recent years for the prolonged release of H_2S in aqueous and cellular media. The real-time monitoring of H_2S release in living cells is quite difficult with the currently available non-fluorogenic donors. The previously used techniques for measurement of H_2S release such as ion-sensitive electrodes (ISEs) and amperometric microsensors work in alkaline medium, respectively, whereas the traditional methylene blue (MB) assay uses strongly acidic conditions to estimate H_2S. These techniques led to the destruction of the sample being used for the measurement of H_2S release in the intracellular medium.

Although, several reaction-based fluorescent H_2S sensors of H_2S are adequate for cellular environments, many of them interfere with the cellular abundant biothiols by sending out false fluorescence signals for H_2S. Therefore, using both organic donors that are not fluorescent and the turn-on fluorogenic H_2S sensors, real-time detection of the intracellular release of H_2S is not possible. Therefore, development of the fluorogenic H_2S donors that are suitable for the donation of H_2S in aqueous and cellular medium with simultaneous turn-on fluorescence could be a beneficial strategy. This thesis focuses on the following unanswered questions that are unexplored in the literature-

(a) The development of bioanalyte-triggered fluorogenic H_2S donor for the real-time monitoring of intracellular H_2S release; (b) The use of a specific bioanalyte that is overexpressed in the cancer cells under certain diseased conditions; (c) The development of bioanalyte-triggered fluorogenic prodrugs for the adjuvant delivery of H_2S and the anti-cancer compounds.

1.12. Thesis overview

Recently, H_2S has been recognized as a significant biological signaling molecule that plays a role in several crucial physiological processes in the body. These findings have raised interest in using H_2S as a possible therapeutic agent to treat chronic diseases linked to H_2S-based signaling. H_2S and other reactive sulfur species, such as sulfane sulfur and persulfides, are frequently present in various physiological activities, according to a mechanistic examination of them. Chemical tools for measuring the H_2S release under controlled reaction conditions are required for better understanding of the biological characteristics of these reactive sulfur species. This thesis consists of four chapters. In chapter 1, we have discussed a brief introduction about the different sources of H_2S donors (endogenous, dietary, natural and synthetic mimics) developed over the years by several researchers. In chapter 2, a biothiol-triggered organotrisulfide-linked fluorogenic donors

of H_2S such as **UTS-1** and **UTS-2** were developed that are compatible in both aqueous and cellular environments. The release of H_2S and fluorophore enables proper monitoring of the intracellular H_2S release and its further trafficking towards a specific intracellular organelle such as lysosome. The release of fluorophore from **UTS-1** and **UTS-2** was confirmed by spectroscopic studies. The H_2S releasing ability of **UTS-1** and **UTS-2** was measured by methylene blue assay. Both the probes release H_2S in the presence of Cys and GSH. Both the synthesized trisulfide donors are non-toxic in cancer (HeLa) and normal cell (HEK-293). In chapter 3, TrxR responsive organopolysulfide-based fluorogenic donor of H_2S (**DCI-PS**) with concomitant release of NIR fluorophore are described. All the spectroscopic and kinetic studies with **DCI-PS**/**DCI-DS** revealed its much higher reactivity towards DTT (for TrxR activity) as compared to the cellular abundant biothiol GSH. The turn-on fluorogenic H_2S donation process from the cellular non-toxic **DCI-PS** was studied in a representative breast cancer cell line (MDA-MB-231) for the sustained donation of H_2S with concomitant release of red-emitting NIR fluorophore. The participation of TrxR was supported by significant inhibition of the fluorogenic processes in the presence of TrxR selective small-molecule inhibitors. In chapter 4, Cys responsive isothiocyanate-based fluorogenic donors of H_2S **AM-ITC** and **NB-ITC** were developed. The spectroscopic studies for **AM-ITC** reveal that the probe is only reactive towards Cys over other thiols such as GSH, DTT and Hcy. Mechanistic investigations reveal that isothiocyanates react with Cys to release H_2S and the naphthalimide amine-based fluorogenic anti-cancer compounds. The higher anti-cancer activity of the released anti-cancer compound amonafide as compared to the prodrug **AM-ITC** was evidenced by the MTT assay in a representative breast cancer cells.

1.13. References

1. Filipovic, M. R.; Zivanovic, J.; Alvarez, B.; Banerjee, R., *Chem. Rev.* **2018**, *118*, 1253-1337.
2. Ramazzini, B., *Am. J. Public Health* **2001**, *91*, 1380-1382.
3. Szabo, C., *Biochem. Pharmacol.* **2018**, *149*, 5-19.
4. Abe, K.; Kimura, H., *J. Neurosci.* **1996**, *16*, 1066-1071.
5. Hosoki, R.; Matsuki, N.; Kimura, H., *Biochem. Biophys. Res. Commun.* **1997**, *237*, 527-531.
6. Akagi, R., *Acta. Med. Okayama* **1982**, *36*, 187-197.
7. Eto, K.; Kimura, H., *J. Biol. Chem.* **2002**, *277*, 42680-42685.

8. Awata, S.; Nakayama, K.; Suzuki, I.; Sugahara, K.; Kodama, H., *Biochem. Mol. Biol. Int.* **1995**, *35*, 1331-1338.
9. Wu, D.; Wang, J.; Li, H.; Xue, M.; Ji, A.; Li, Y., *Oxid. Med. and Cell. Longev.* **2015**, *2015*, 186908.
10. Shen, Y.; Shen, Z.; Luo, S.; Guo, W.; Zhu, Y. Z., *Oxid. Med. Cell. Longev.* **2015**, *2015*, 925167.
11. Nicholson, C. K.; Calvert, J. W., *Pharmacol. Res.* **2010**, *62*, 289-297.
12. Yang, G.; Wang, R., *Handb. Exp. Pharmacol.* **2015**, *230*, 85-110.
13. Gemici, B.; Wallace, J. L., *Methods Enzymol.* **2015**, *555*, 169-193.
14. Xiao, Q.; Ying, J.; Xiang, L.; Zhang, C., *Medicine* **2018**, *97*, e13065.
15. Lin, J.; Chen, M.; Liu, D.; Guo, R.; Lin, K.; Deng, H.; Zhi, X.; Zhang, W.; Feng, J.; Wu, W., *Int. J. Mol. Med.* **2018**, *41*, 1477-1486.
16. Li, T.; Zhao, B.; Wang, C.; Wang, H.; Liu, Z.; Li, W.; Jin, H.; Tang, C.; Du, J., *Exp. Biol. Med.* **2008**, *233*, 1081-1087.
17. Wang, R., *Physiol. Rev.* **2012**, *92*, 791-896.
18. Mathai, J. C.; Missner, A.; Kügler, P.; Saparov, S. M.; Zeidel, M. L.; Lee, J. K.; Pohl, P., *Proc. Natl. Acad. Sci.* **2009**, *106*, 16633-16638.
19. Mishanina, T. V.; Libiad, M.; Banerjee, R., *Nat. Chem. Biol.* **2015**, *11*, 457-464.
20. Badal, D. S.; Dwivedi, A.; Kumar, V.; Singh, S.; Prakash, A.; Verma, S.; Kumar, J., *J. Pharmacogn. Phytochem.* **2019**, *8*, 587-590.
21. Banerjee, S. K.; Maulik, S. K., *Nutr. J.* **2002**, *1*, 4.
22. Boonpeng, S.; Siripongvutikorn, S.; Sae-Wong, C.; Sutthirak, P., *Food Sci. Nutr.* **2014**, *2*, 792-801.
23. Amagase, H., *J. Nutr.* **2006**, *136*, 716S-725S.
24. Bayan, L.; Koulivand, P. H.; Gorji, A., *Avicenna J. Phytomed.* **2014**, *4*, 1-14.
25. Rajanikanth, B.; Ravindranath, B.; Shankaranarayana, M., *Phytochemistry* **1984**, *23*, 899-900.
26. De Sousa, J. R.; Demuner, A. J.; Pinheiro, J. A.; Breitmaier, E.; Cassels, B. K., *Phytochemistry* **1990**, *29*, 3653-3655.
27. Boelens, M.; De Valois, P. J.; Wobben, H. J.; Van der Gen, A., *J. Agric. Food Chem.* **1971**, *19*, 984-991.
28. Knudsen, J. T.; Tollsten, L., *Bot. J. Linn. Soc.* **1995**, *119*, 45-57.
29. Kouokam, J. C.; Jahns, T.; Becker, H., *Planta Med.* **2002**, *68*, 1082-1087.

30. Citi, V.; Martelli, A.; Testai, L.; Marino, A.; Breschi, M. C.; Calderone, V., *Planta Med.* **2014**, *80*, 610-613.
31. Crowe, S. A.; Døssing, L. N.; Beukes, N. J.; Bau, M.; Kruger, S. J.; Frei, R.; Canfield, D. E., *Nature* **2013**, *501*, 535-538.
32. Myers, J. T., *J. Bacteriol.* **1920**, *5*, 231-252.
33. Malone Rubright, S. L.; Pearce, L. L.; Peterson, J., *Nitric Oxide*, **2017**, *71*, 1-13.
34. Tobler, M.; Passow, C. N.; Greenway, R.; Kelley, J. L.; Shaw, J. H., *Annu. Rev. Ecol. Evol. Syst.* **2016**, *47*, 239-262.
35. Shinohara, H.; Kazahaya, K.; Saito, G.; Matsushima, N.; Kawanabe, Y., *Earth Planets Space* **2002**, *54*, 175-185.
36. Sievert, S. M.; Kiene, R. P.; Schulz-Vogt, H. N., *Oceanography* **2007**, *20*, 117-123.
37. Knoll, A. H.; Bambach, R. K.; Payne, J. L.; Pruss, S.; Fischer, W. W., *Earth Planet. Sci. Lett.* **2007**, *256*, 295-313.
38. Kabil, O.; Banerjee, R., *J. Biol Chem.* **2010**, *285*, 21903-21907.
39. Shibuya, N.; Koike, S.; Tanaka, M.; Ishigami-Yuasa, M.; Kimura, Y.; Ogasawara, Y.; Fukui, K.; Nagahara, N.; Kimura, H., *Nat. Commun.* **2013**, *4*, 1-7.
40. Zhao, W.; Zhang, J.; Lu, Y.; Wang, R., *EMBO J.* **2001**, *20*, 6008-6016.
41. Lin, S. J.; Ford, E.; Haigis, M.; Liszt, G.; Guarente, L., *Genes Dev.* **2004**, *18*, 12-16.
42. DeLeon, E. R.; Stoy, G. F.; Olson, K. R., *Anal. Biochem.* **2012**, *421*, 203-207.
43. Ozturk, T.; Ertas, E.; Mert, O., *Chem. Rev.* **2007**, *107*, 5210-5278.
44. Lecher, H.; Greenwood, R.; Whitehouse, K.; Chao, T., *J. Am. Chem. Soc.* **1956**, *78*, 5018-5022.
45. Spiller, F.; Orrico, M. I.; Nascimento, D. C.; Czaikoski, P. G.; Souto, F. O.; Alves-Filho, J. C.; Freitas, A.; Carlos, D.; Montenegro, M. F.; Neto, A. F., *Am. J. Respir. Crit. Care Med.* **2010**, *182*, 360-368.
46. Li, L.; Whiteman, M.; Guan, Y. Y.; Neo, K. L.; Cheng, Y.; Lee, S. W.; Zhao, Y.; Baskar, R.; Tan, C. H.; Moore, P. K., *Circulation* **2008**, *117*, 2351-2360.
47. Cao, X.; Ding, L.; Xie, Z. Z.; Yang, Y.; Whiteman, M.; Moore, P. K.; Bian, J. S., *Antioxid. Redox Signaling* **2019**, *31*, 1-38.
48. Lee, Z. W.; Zhou, J.; Chen, C.-S.; Zhao, Y.; Tan, C.-H.; Li, L.; Moore, P. K.; Deng, L.-W., *PLOS ONE* **2011**, *6*, e21077.

49. Li, L.; Bhatia, M.; Zhu, Y. Z.; Zhu, Y. C.; Ramnath, R. D.; Wang, Z. J.; Anuar, F. B.; Whiteman, M.; Salto-Tellez, M.; Moore, P. K., *FASEB J.* **2005**, *19*, 1196-1198.
50. Doeller, J. E.; Isbell, T. S.; Benavides, G.; Koenitzer, J.; Patel, H.; Patel, R. P.; Lancaster Jr, J. R.; Darley-Usmar, V. M.; Kraus, D. W., *Anal. Biochem.* **2005**, *341*, 40-51.
51. Park, C.-M.; Zhao, Y.; Zhu, Z.; Pacheco, A.; Peng, B.; Devarie-Baez, N. O.; Bagdon, P.; Zhang, H.; Xian, M., *Mol. Biosyst.* **2013**, *9*, 2430-2434.
52. Kang, J.; Li, Z.; Organ, C. L.; Park, C.-M.; Yang, C.-t.; Pacheco, A.; Wang, D.; Lefer, D. J.; Xian, M., *J. Am. Chem. Soc.* **2016**, *138*, 6336-6339.
53. Zhao, Y.; Wang, H.; Xian, M., *J. Am. Chem. Soc.* **2011**, *133*, 15-17.
54. Medvedeva, S. M.; Shikhaliev, K. S., *Molecules (Basel, Switzerland)* **2022**, *27*, 4033.
55. Landis, P. S., *Chem. Rev.* **1965**, *65*, 237-245.
56. Landis, P. S.; HAMILTON, L. A., *J. Org. Chem.* **1960**, *25*, 1742-1744.
57. Spindt, R. S.; Stevens, D. R.; Baldwin, W., *J. Am. Chem. Soc.* **1951**, *73*, 3693-3697.
58. Caliendo, G.; Cirino, G.; Santagada, V.; Wallace, J. L., *J. Med. Chem.* **2010**, *53*, 6275-6286.
59. Hamada, T.; Nakane, T.; Kimura, T.; Arisawa, K.; Yoneda, K.; Yamamoto, T.; Osaki, T., *Am. J. Med. Sci.* **1999**, *318*, 146-151.
60. Kurahara, K.; Matsumoto, T.; Iida, M.; Honda, K.; Yao, T.; Fujishima, M., *Am. J. Gastroenterol.* **2001**, *96*, 473-480.
61. Chan, M. V.; Wallace, J. L., *Am. J. Physiol. Gastrointest. Liver. Physiol.* **2013**, *305*, G467-G473.
62. Singh, G.; Fort, J. G.; Goldstein, J. L.; Levy, R. A.; Hanrahan, P. S.; Bello, A. E.; Andrade-Ortega, L.; Wallemark, C.; Agrawal, N. M.; Eisen, G. M., *Am. J. Med.* **2006**, *119*, 255-266.
63. Mancardi, D.; Penna, C.; Merlino, A.; Del Soldato, P.; Wink, D. A.; Pagliaro, P., *Biochim. Biophysic. Acta Bioenerg.* **2009**, *1787*, 864-872.
64. Wallace, J. L.; Caliendo, G.; Santagada, V.; Cirino, G.; Fiorucci, S., *Gastroenterology* **2007**, *132*, 261-271.
65. Ianaro, A.; Cirino, G., Hydrogen sulfide pathway and cancer. In *Brain Metastases from Primary Tumors, Volume 3*, Elsevier: 2016; pp 133-144.

66. Zhao, Y.; Bhushan, S.; Yang, C.; Otsuka, H.; Stein, J. D.; Pacheco, A.; Peng, B.; Devarie-Baez, N. O.; Aguilar, H. C.; Lefer, D. J., *ACS Chem. Biol.* **2013**, *8*, 1283-1290.

67. Roger, T.; Raynaud, F.; Bouillaud, F.; Ransy, C.; Simonet, S.; Crespo, C.; Bourguignon, M. P.; Villeneuve, N.; Vilaine, J. P.; Artaud, I., *ChemBioChem* **2013**, *14*, 2268-2271.

68. Foster, J. C.; Powell, C. R.; Radzinski, S. C.; Matson, J. B., *Org. Lett.* **2014**, *16*, 1558-1561.

69. Martelli, A.; Testai, L.; Citi, V.; Marino, A.; Pugliesi, I.; Barresi, E.; Nesi, G.; Rapposelli, S.; Taliani, S.; Da Settimo, F., *ACS Med. Chem. Lett.* **2013**, *4*, 904-908.

70. Cerda, M. M.; Hammers, M. D.; Earp, M. S.; Zakharov, L. N.; Pluth, M. D., *Org. Lett.* **2017**, *19*, 2314-2317.

71. Ercole, F.; Whittaker, M. R.; Halls, M. L.; Boyd, B. J.; Davis, T. P.; Quinn, J. F., *Chem. Commun.* **2017**, *53*, 8030-8033.

72. Fukushima, N.; Ieda, N.; Sasakura, K.; Nagano, T.; Hanaoka, K.; Suzuki, T.; Miyata, N.; Nakagawa, H., *Chem. Commun.* **2013**, *50*, 587-589.

73. Xiao, Z.; Bonnard, T.; Shakouri-Motlagh, A.; Wylie, R. A.; Collins, J.; White, J.; Heath, D. E.; Hagemeyer, C. E.; Connal, L. A., *Chem. Eur. J.* **2017**, *23*, 11294-11300.

74. Sharma, A. K.; Nair, M.; Chauhan, P.; Gupta, K.; Saini, D. K.; Chakrapani, H., *Org. Lett.* **2017**, *19*, 4822-4825.

75. Yi, S. Y.; Moon, Y. K.; Kim, S.; Kim, S.; Park, G.; Kim, J. J.; You, Y., *Chem. Commun.* **2017**, *53*, 11830-11833.

76. Venkatesh, Y.; Das, J.; Chaudhuri, A.; Karmakar, A.; Maiti, T. K.; Singh, N. D. P., *Chem. Commun.* **2018**, *54*, 3106-3109.

77. Woods, J. J.; Cao, J.; Lippert, A. R.; Wilson, J. J., *J. Am. Chem. Soc.* **2018**, *140*, 12383-12387.

78. Zhou, Z.; von Wantoch Rekowski, M.; Coletta, C.; Szabo, C.; Bucci, M.; Cirino, G.; Topouzis, S.; Papapetropoulos, A.; Giannis, A., *Biorg. Med. Chem.* **2012**, *20*, 2675-2678.

79. Zheng, Y.; Yu, B.; Ji, K.; Pan, Z.; Chittavong, V.; Wang, B., *Angew. Chem. Int. Ed.* **2016**, *55*, 4514-4518.

80. Shukla, P.; Khodade, V. S.; SharathChandra, M.; Chauhan, P.; Mishra, S.; Siddaramappa, S.; Pradeep, B. E.; Singh, A.; Chakrapani, H., *Chem. Sci.* **2017**, *8*, 4967-4972.

81. Steiger, A. K.; Pardue, S.; Kevil, C. G.; Pluth, M. D., *J. Am. Chem. Soc.* **2016**, *138*, 7256-7259.

82. Zhao, Y.; Pluth, M. D., *Angew. Chem., Int. Ed.* **2016**, *55*, 14638.

83. Steiger, A. K.; Marcatti, M.; Szabo, C.; Szczesny, B.; Pluth, M. D., *ACS Chem. Biol.* **2017**, *12*, 2117-2123.

84. Steiger, A. K.; Yang, Y.; Royzen, M.; Pluth, M. D., *Chem. Commun.* **2017**, *53*, 1378-1380.

85. Zhao, Y.; Bolton, S. G.; Pluth, M. D., *Org. Lett.* **2017**, *19*, 2278-2281.

86. Xu, T.; Scafa, N.; Xu, L. P.; Zhou, S.; Abdullah Al-Ghanem, K.; Mahboob, S.; Fugetsu, B.; Zhang, X., *Analyst* **2016**, *141*, 1185-1195.

87. Li, G.; Polk, B. J.; Meazell, L. A.; Hatchett, D. W., *J. Chem. Edu.* **2000**, *77*, 1049.

88. Koenitzer, J. R.; Isbell, T. S.; Patel, H. D.; Benavides, G. A.; Dickinson, D. A.; Patel, R. P.; Darley-Usmar, V. M.; Lancaster Jr, J. R.; Doeller, J. E.; Kraus, D. W., *Am. J. Physiol. Heart Circ.* **2007**, *292*, H1953-H1960.

89. Ubuka, T., *J. Chromatogr. B* **2002**, *781*, 227-249.

90. Powell, C. R.; Dillon, K. M.; Matson, J. B., *Biochem. Pharmacol.* **2018**, *149*, 110-123.

91. Zhao, Z.; Malinowski, E. R., *J. Chemom.* **1999**, *13*, 83-94.

92. Shen, X.; Peter, E. A.; Bir, S.; Wang, R.; Kevil, C. G., *Free Radic. Biol. Med.* **2012**, *52*, 2276-2283.

93. Lippert, A. R.; New, E. J.; Chang, C. J., *J. Am. Chem. Soc.* **2011**, *133*, 10078-10080.

94. Sasakura, K.; Hanaoka, K.; Shibuya, N.; Mikami, Y.; Kimura, Y.; Komatsu, T.; Ueno, T.; Terai, T.; Kimura, H.; Nagano, T., *J. Am. Chem. Soc.* **2011**, *133*, 18003-18005.

95. Peng, B.; Chen, W.; Liu, C.; Rosser, E. W.; Pacheco, A.; Zhao, Y.; Aguilar, H. C.; Xian, M., *Chem. Eur. J.* **2014**, *20*, 1010-1016.

96. Steegborn, C.; Clausen, T.; Sondermann, P.; Jacob, U.; Worbs, M.; Marinkovic, S.; Huber, R.; Wahl, M. C., *J. Biol. Chem.* **1999**, *274*, 12675-12684.

97. Asimakopoulou, A.; Panopoulos, P.; Chasapis, C. T.; Coletta, C.; Zhou, Z.; Cirino, G.; Giannis, A.; Szabo, C.; Spyroulias, G. A.; Papapetropoulos, A., *Br. J. Pharmacol.* **2013**, *169*, 922-932.
98. Abeles, R. H.; Walsh, C. T., *J. Am. Chem. Soc.* **1973**, *95*, 6124-6125.
99. Asimakopoulou, A.; Panopoulos, P.; Chasapis, C. T.; Coletta, C.; Zhou, Z.; Cirino, G.; Giannis, A.; Szabo, C.; Spyroulias, G. A.; Papapetropoulos, A., *Br. J. Pharmacol.* **2013**, *169*, 922-932.
100. Cao, X.; Ding, L.; Xie, Z.-z.; Yang, Y.; Whiteman, M.; Moore, P. K.; Bian, J.-S., *Antioxid. Redox signaling* **2019**, *31*, 1-38.
101. Alston, T. A.; Porter, D. J.; Mela, L.; Bright, H. J., *Biochem. Biophys. Res. Commun.* **1980**, *92*, 299-304.
102. Powell, M. A.; Somero, G. N., *Science* **1986**, *233*, 563-566.
103. Goubern, M.; Andriamihaja, M.; Nübel, T.; Blachier, F.; Bouillaud, F., *FASEB J.* **2007**, *21*, 1699-1706.
104. Brito, J. A.; Sousa, F. L.; Stelter, M.; Bandeiras, T. M.; Vonrhein, C.; Teixeira, M.; Pereira, M. M.; Archer, M., *Biochemistry* **2009**, *48*, 5613-5622.
105. Weisiger, R. A.; Pinkus, L. M.; Jakoby, W. B., *Biochem. Pharmacol.* **1980**, *29*, 2885-2887.
106. Maldonato, B. J.; Russell, D. A.; Totah, R. A., *Sci. Rep.* **2021**, *11*, 4857.
107. Hildebrandt, T. M.; Grieshaber, M. K., *FEBS J.* **2008**, *275*, 3352-3361.
108. Chen, X.; Jhee, K.-H.; Kruger, W. D., *J. Biol. Chem.* **2004**, *279*, 52082-52086.
109. Zhang, X.; Bian, J.-S., *ACS Chem. Neurosci.* **2014**, *5*, 876-883.
110. Siegel, L. M., *Anal. Biochem.* **1965**, *11*, 126-132.
111. Bian, J.-S.; Yong, Q. C.; Pan, T.-T.; Feng, Z.-N.; Ali, M. Y.; Zhou, S.; Moore, P. K., *J. Pharmacol. Exp. Ther.* **2006**, *316*, 670-678.
112. Fiorucci, S.; Orlandi, S.; Mencarelli, A.; Caliendo, G.; Santagada, V.; Distrutti, E.; Santucci, L.; Cirino, G.; Wallace, J., *Br. J. Pharmacol.* **2007**, *150*, 996-1002.
113. Mani, S.; Cao, W.; Wu, L.; Wang, R., *Nitric Oxide* **2014**, *41*, 62-71.
114. Wallace, J. L.; Nagy, P.; Feener, T. D.; Allain, T.; Ditrói, T.; Vaughan, D. J.; Muscara, M. N.; De Nucci, G.; Buret, A. G., *Br. J. Pharmacol.* **2020**, *177*, 769-777.
115. Fiorucci, S.; Antonelli, E.; Mencarelli, A.; Orlandi, S.; Renga, B.; Rizzo, G.; Distrutti, E.; Shah, V.; Morelli, A., *Hepatology* **2005**, *42*, 539-548.

116. Hellmich, M. R.; Coletta, C.; Chao, C.; Szabo, C., *Antioxid. Redox Signaling* **2015**, *22*, 424-448.

Chapter 2

The Biothiol-triggered Organotrisulfide-based Self-immolative Fluorogenic Donors of Hydrogen Sulfide Enable Lysosomal Trafficking

2.1. Introduction

Hydrogen sulfide (H_2S) was previously considered as a foul-smelling substance, it is now widely accepted as a gasotransmitter along with NO and CO.[1,2] It is bio-synthesized from Cys and Hcy mainly by three key enzymes namely CSE, CBS and 3-MST in co-ordination with CAT. While CBS is mainly expressed in the hippocampus, nervous system, and liver, cystathionine-γ-lyase is expressed in the cardiovascular system and 3-MST sulfurtransferase is primarily localized in the mitochondria of the cell.[3] The endogenous generation of H_2S has been linked to several biological processes such as anti-inflammation, cardioprotection, vasodilation, neurotransmission, and other functions, a dysregulation of H_2S results in a variety of disease conditions.[4-6] The antioxidant and cardioprotective activity of H_2S mainly arises due to its rapid reactivity towards ROS.[7-9] These observations are indicative of proper regulation of endogenous H_2S or administration of exogenous H_2S during its deficiency for therapeutic benefits. Therefore, several organosulfur compounds were developed over the last two decades as sustained donors of H_2S. Several non-fluorescent organic donors of H_2S have been developed over the last few years for sustained release of H_2S in aqueous and cellular media as the inorganic salts such as Na_2S or NaHS (instantaneous sources) are not suitable for the cellular application.[10-14] However, real-time monitoring of H_2S release in living cells is a big challenge using the currently available detection techniques. While the conventional methylene blue (MB) assay for estimating H_2S utilizes highly acidic condition, the commonly used ion-sensitive electrodes (ISEs) and amperometric microsensors work in alkaline and acidic/neutral media, respectively. These methods are therefore not suitable for cellular medium.[15-17] Although, recent reports highlight numerous fluorescent sensors of H_2S suitable in the cellular medium,[18-20] many of them interfere with the cell-abundant biothiols with false fluorescent signals for H_2S.[21-23] Therefore, at present, the real-time detection of the intracellular release of H_2S is not feasible with both non-fluorescent organic donors as well as with turn-on fluorescent sensors of H_2S. A useful approach could be to develop bioanalyte-triggered fluorogenic H_2S donors, which would be eligible for an intracellular H_2S delivery with concomitant turn-on fluorescence. Interestingly, during the process of our research in this direction, two relevant reports appeared (in 2019). Pluth and co-workers reported the first example of a thiol-sensitive sulfenyl thiocarbonate-based probe (**FLD-1**) with the release of a fluorophore and carbonyl sulfide (Figure 2.1).[24] Subsequently, Ma and co-workers reported a ROS-sensitive thiocarbamate-based probe (**NAB**) for imaging in live cells (Figure 2.1).[25] However, the detection of H_2S from the

ROS-triggered donors may be difficult in aqueous/cellular medium as ROS can interfere with the generated H_2S. Furthermore, both the reported probes require two bio-analytes (RSH/ROS and carbonic anhydrase, CA) for the generation of H_2S. Herein, we report the design of thiol-reactive organotrisulfide-based self-immolative fluorogenic donors of H_2S (**UTS-1** and **UTS-2**) compatible in both aqueous and cellular media. Upon activation by thiols, they would release H_2S in a controlled manner with a concomitant release of the fluorophore for the real-time monitoring of the H_2S release profile. The probe **UTS-2** was designed for the targeted delivery of H_2S to an important intracellular organelle such as lysosome (acidic pH), containing many bio-molecules and hydrolytic enzymes. The development of the lysosomal H_2S donor is of particular research interest due to the impact of H_2S on the destabilization of the lysosomal membrane for neuronal death.[26] To the best of our knowledge, this is the first study with highly reactive organotrisulfide-based thiol-sensitive self-immolative fluorogenic donors of H_2S for the real-time monitoring of intracellular H_2S release profile, particularly with organelle-specificity.

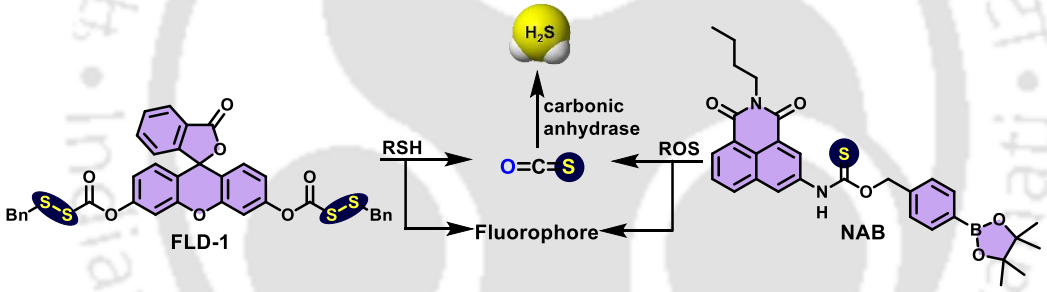

Figure 2.1. Bio-analyte-triggered turn-on fluorogenic H_2S donors reported in 2019.

2.2. Outline of the chapter

In this chapter, we report biothiol-triggered organotrisulfide-based self-immolative fluorogenic donors of H_2S (**UTS-1** and **UTS-2)** compatible in both aqueous as well as cellular medium. The probes contain a trisulfide linker, which is connected to the coumarin fluorophore (OFF-state). The probe **UTS-2** was designed for the targeted delivery of H_2S to a specific intracellular organelle such as lysosome (acidic environment). Upon the single activation with the cellular abundant biothiol GSH self-immolation takes place with the release of H_2S and the free fluorophore (ON-state), enabling the real-time monitoring of the H_2S donation process (Figure 2.2). While **UTS-1** did not contain any targeting group, **UTS-2** was designed to have lysosomal targeting property, which was experimentally validated using fluorescence microscopic experiments in the cellular medium using standard lysosome-targeting dye. In addition to the trisulfide probe, we

have also synthesized the corresponding disulfide probe **UDS-1** as a control compound that releases the free fluorophore without any donation of H_2S. Our experimental results reveal that both the synthesized trisulfide probes release H_2S in a sustained manner that mimics the endogenous biological production of H_2S.

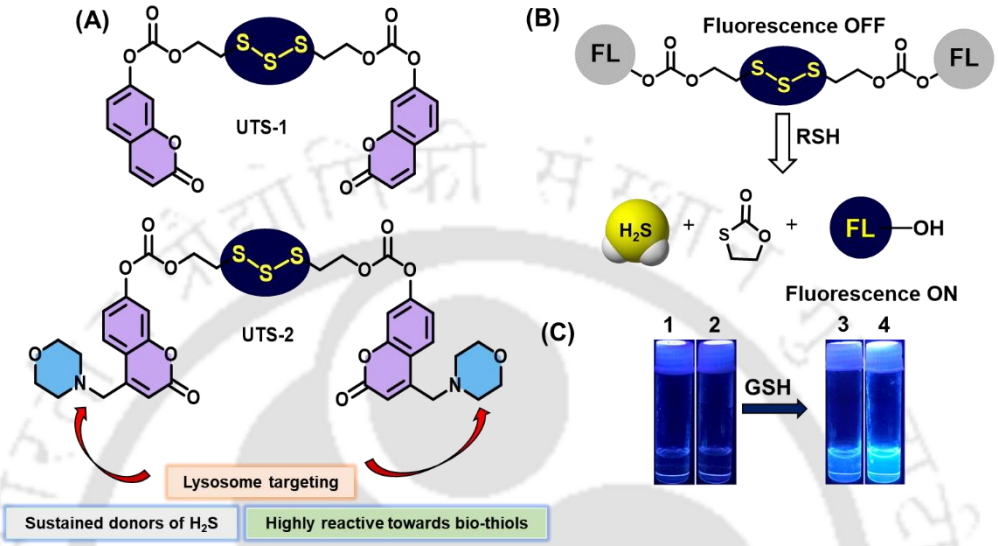

Figure 2.2. (A) Chemical structures of the trisulfide-based H_2S donors **UTS-1** and **UTS-2** synthesized herein. (B) Thiol-induced concomitant release of H_2S and fluorophore unit. (C) Photographic images of **UTS-1** (20 mM, vials 1, and 2) and **UTS-1** (20 mM) + GSH (100 mM, vial 3; 200 mM, vial 4) in DMSO after 15 min.

2.3. Results and Discussion

2.3.1. Synthesis of UTS-1, UTS-2 and UDS-1

We have synthesized symmetrical trisulfide (**UTS-1** and **UTS-2**) disulfide probes (**UDS-1**) at room temperature from disulfide and polysulfide precursors following the literature report with minor modifications.[27,28] The probe **UTS-1** was synthesized in four steps from the commercially available starting materials. For the synthesis of trisulfide probes, we used *in situ* generated sodium polysulfide "Na_2S_n" (n = 2-5) that was prepared by the reaction of elemental sulfur and $Na_2S.9H_2O$. The *in situ* generated Na_2S_n intermediate was then treated with the commercially available 2-chloroethanol **2.3** to obtain the polysulfide alcohols **2.4-2.6** as a pale-yellow oily liquid. The polysulfide alcohols **2.4-2.6** could not be separated due to their very closer polarities and therefore they were used in the next step directly. The polysulfide alcohols obtained were then treated with commercially available 4-nitrophenyl chloroformate in the presence of pyridine as a base in dry DCM to give the symmetrical carbonate intermediate **2.7-2.9** as a sticky white solid. The

carbonate intermediate was treated with umbelliferone **2.1a** in the presence of triethylamine and dry DCM to obtain **UTS-1** as the major product along with the corresponding tetrasulfide and pentasulfide components (Scheme 2.1).

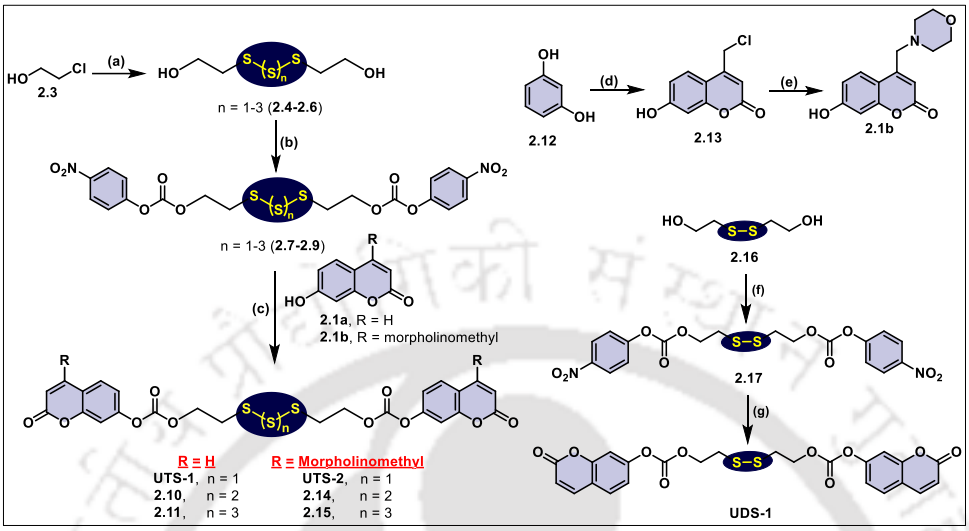

Scheme 2.1. Synthesis of **UTS-1, UTS-2** and **UDS-1**. Reagents and conditions: (a) Na_2S_n (n = 2-5), H_2O, RT, 2 h, (b) 4-Nitrophenyl chloroformate, Pyridine, Dichloromethane, 0 °C- RT, 6 h, (c) **2.1a** / **2.1b**, NEt_3, Dichloromethane, 0 °C-RT, 16 h, (d) Conc. H_2SO_4, 4-chloroethylacetoacetate, 0 °C-RT, 12 h, (e) Morpholine, Acetonitrile, 65 °C, 8 h, (f) 4-Nitrophenyl chloroformate, Pyridine, Dichloromethane, 0 °C-RT, 6 h, (g) **2.1a**, NEt_3, Dichloromethane, 0 °C-RT, 16 h.

For the synthesis of **UTS-2**, initially, compound **2.13** was synthesized from resorcinol **2.12** and 4-chloroethylacetoacetate in conc. H_2SO_4 at 0 °C. Then compound **2.13** was reacted with morpholine in acetonitrile at 85 °C to obtain compound **2.1b** as a white solid. The symmetrical carbonate intermediate **2.7-2.9** was treated with compound **2.1b** in the presence of triethylamine in dry DCM to obtain the **UTS-2** as the major product along with the corresponding tetrasulfide and pentasulfide components. The pure trisulfides **UTS-1** and **UTS-2** was separated using reverse phase HPLC. Unfortunately, the higher polysulfides could not be isolated from the mixture as they decomposed during HPLC separation. The tetrasulfide and pentasulfide products from both **UTS-1** and **UTS-2** could not be separated using normal phase column chromatography and therefore they were separated using reverse-phase column chromatography. Next, for the synthesis of disulfide probe **UDS-1**, the commercially available bis(2-hydroxyethyl disulfide) was coupled with coupling agent 4-nitrophenyl chloroformate in the presence of pyridine in dry DCM to afford the carbonate intermediate **2.17** as a white solid. The carbonate

intermediates were reacted with umbelliferone **2.1a** in the presence of triethylamine in anhydrous dichloromethane to give **UDS-1** as a white solid. All the synthesized probes were purified by reverse phase HPLC and analyzed by NMR (^{1}H and ^{13}C) and ESI-MS analysis before performing the spectroscopic studies.

2.3.2. Absorption and emission studies

After the synthesis of probes, the spectroscopic properties of the probes were evaluated using UV-Vis and fluorescence spectroscopy. Most of the spectroscopic studies were performed using **UTS-1**. The absorption spectra of pure **UTS-1** (5.0 µM) showed two absorption bands at around 285 and 318 nm, respectively in phosphate buffer saline, PBS (20 mM, pH 7.4). Upon treatment of **UTS-1** (5.0 µM) was treated with GSH (200 µM), the intensity of the absorption band at 285 nm decreased and the intensity around 318 nm was increased along with a hump at 380 nm (Figure 2.3A). The resultant absorption pattern resembled the absorption pattern of pure umbelliferone **2.1a**, indicating the release of fluorophore in the presence of GSH.

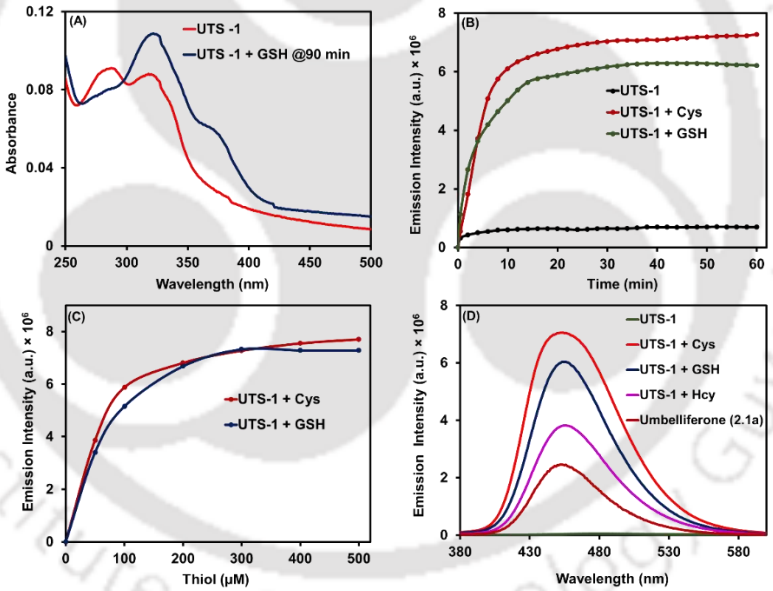

Figure 2.3. (A) Absorption spectra of **UTS-1** (5.0 µM) in the absence (blank) and presence of GSH (200 µM) after 90 min. (B) Fluorescence emission spectra of **UTS-1** (5.0 µM) in the absence (blank) and presence of Cys and GSH (200 µM) over 60 min. (C) Emission spectra of **UTS-1** (5.0 µM) with increasing concentrations of GSH and Cys (0–500 µM, incubation time of 20 min). (D) Emission spectra of **UTS-1** (5.0 µM) in the absence (blank) and presence of Cys, GSH and Hcy (200 µM) after 20 min along with the emission spectrum of pure umbelliferone **2.1a**.

The fluorescence emission studies of **UTS-1** in the presence of Cys and GSH were carried out subsequently. A weak residual fluorescence was observed for **UTS-1** (5.0 µM) in the

absence of any thiol due to the ICT process. However, when time-dependent fluorescence emission studies were performed in the presence of biothiols (Cys and GSH, 200 μM each), a significant enhancement in fluorescence emission was observed over 15-20 min and a saturation pattern was observed up to 60 min with an emission maximum at 446 (Figure 2.3B). A similar reactivity pattern was observed when **UTS-1** was treated with increasing concentrations of GSH and Cys (0-500 μM) (Figures 2.3C). Next, the reactivity of **UTS-1** towards key biothiols such as Cys, GSH and Hcy was studied under identical conditions after incubating for 20 min in phosphate buffer saline, PBS (20 mM, pH 7.4). Interestingly, highly intense fluorescence emission was observed in the presence of key biothiols (GSH, Cys and Hcy) with a maximum at 446 nm. While the enhancement was almost comparable with that of GSH and Cys, it was relatively lower with that of Hcy. The emission profile showed higher reactivity of **UTS-1** towards Cys and GSH, as compared to Hcy Figure 2.3D. Similar studies were performed to understand the reactivity of **UTS-1** and **UDS-1** (5.0 μM) towards key biothiols such as Cys, GSH and Hcy (200 μM each) as shown in Figure 2.4.

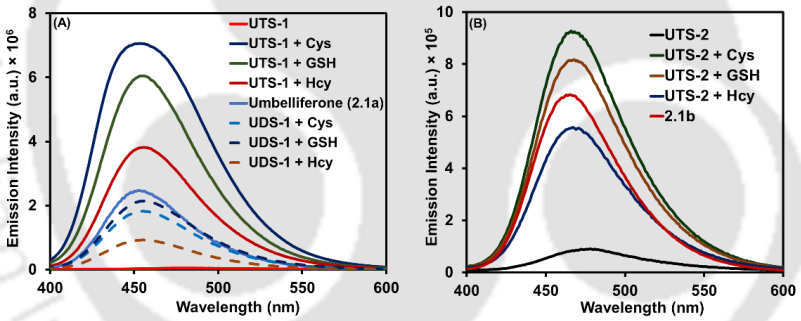

Figure 2.4. (A) Emission spectra of **UTS-1** (5.0 μM) and **UDS-1** (5.0 μM) towards GSH, Cys and Hcy (200 μM) after 20 min along with the emission spectral pattern of the released umbelliferone **2.1a**. (B) Emission spectra of **UTS-2** (5 μM) in the absence and presence of GSH, Cys and Hcy (200 μM) in PBS buffer (20 mM, pH 7.4) after 20 min of incubation. The emission spectrum of the released umbelliferone derivative **2.1b** is plotted for comparison.

For comparison purposes, the emission spectrum of the released fluorophore **2.1a** was plotted under identical conditions. As shown in Figure 2.4A, a higher reactivity of **UTS-1** was observed than **UDS-1** in the presence of biothiols as evident from the higher fluorescence enhancement. Similarly, the reactivity of **UTS-2** towards GSH, Cys and Hcy was studied under identical condition and the fluorescence emission was measured along with the pure released fluorophore **2.1b**. As shown in Figure 2.4B, a similar pattern and

order of reactivity of **UTS-2** as **UTS-1** was observed. The higher reactivity of trisulfides as compared to disulfides is attributed to the higher electrophilic character of trisulfide sulfur (-S-S-S-) than the disulfide ones (-S-S-) in **UTS-1** and **UDS-1** respectively.

2.3.3. Measurement of the released H_2S by MB assay

After confirming the release of fluorophores from **UTS-1**, **UTS-2** and **UDS-1** from UV-Vis and fluorescence emission studies, we studied the H_2S releasing capacity of the synthesized probes using the conventional methylene blue (MB) assay by measuring the absorbance at 671 nm using UV-Vis spectrophotometer.[29] The MB cocktail contains ferric chloride (30 mM in 1.2M HCl), *N*,*N*- dimethyl-p-phenylenediamine sulfate salt (20 mM in 7.2 M HCl) and zinc acetate dihydrate (1% w/v). The release profile of H_2S from **UTS-1** and **UTS-2** (25.0 µM) in the presence of GSH and Cys (500 µM) was monitored over 120 min. As shown in Figure 2.5A and B, the concentration of H_2S increased up to 60 min and remained almost steady up to 120 min. However, the amount of released H_2S from **UTS-1** was relatively higher in the presence of GSH and Cys. Notably, the amount of released H_2S from DATS (25.0 µM) in the presence of Cys (500 µM) was found to be relatively higher under the identical experimental condition Figure 2.5C.

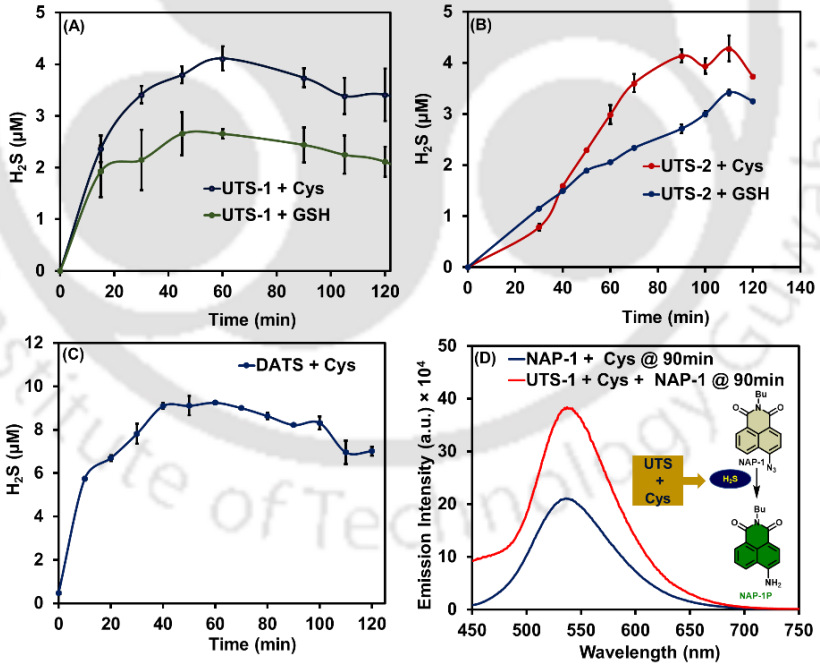

Figure 2.5. (A) H_2S release profile of **UTS-1** (25.0 µM) in the presence of GSH and Cys (500.0 µM) over 120 min; (B) H_2S release profile of **UTS-2** (25.0 µM) in the presence of GSH and Cys (500.0 µM) over 120 min; (C) H_2S release profile from DATS (25.0 µM) in the presence of Cys (500.0 µM); (D) Fluorescence emission after 90 min from **NAP-1** (25.0 µM) in the presence of Cys (500.0 µM) and **UTS-1** (25.0 µM) + Cys (500.0 µM) in PBS (20 mM, pH 7.4).

2.3.4. Measurement of H_2S release by fluorescence assay

In addition to the measurement of H_2S release using MB assay, the release of H_2S from **UTS-1** (25.0 µM) was monitored in the presence of Cys (500 µM) using an azide-based fluorescent probe **NAP-1**. While the pure azide-based fluorescent probe **NAP-1** showed weak fluorescence emission, an enhancement of fluorescence was observed with an emission maximum at 550 nm upon its reaction with the released H_2S from **UTS-1**. The enhancement of emission intensity is due to the reduction of the azide-group in **NAP-1** to the corresponding amino group. In order to exclude the background reaction of **NAP-1** with Cys, **NAP-1** was pre-incubated with Cys for 90 min. An aliquot from the reaction of **UTS-1** and Cys was then added to the previous reaction mixture containing **NAP-1** + Cys and the reaction mixture was incubated for an additional 90 min and finally, the emission spectrum was recorded. After 90 min of incubation, we observed a significant enhancement of fluorescence intensity wherein the released H_2S converts the azide to highly fluorescent amine, thereby enhancing the fluorescence (Figure 2.5D).[30]

2.3.5. Analyte selectivity studies of UTS-1

Before proceeding for cellular studies, the reactivity of **UTS-1** towards biologically relevant analytes as well as thiol and non-thiol analytes, and reactive oxygen species such as H_2O_2 and *t*BuOOH was investigated. As shown in Figure 2.6A, **UTS-1** showed higher fluorescence emission in the presence of thiol-containing analytes as compared to non-thiol analytes. Moreover, among the thiol-containing analytes, the highest reactivity was observed towards Cys and that was slightly higher than GSH. These experimental results demonstrate a greater affinity of **UTS-1** for key biothiols over other biologically relevant nucleophiles present in the biological system.

2.3.6. pH variation studies of UTS-1

It is important to study the stability of the probe at different pH levels to understand its working range. The reactivity of **UTS-1** (5.0 µM) in phosphate buffer saline at various pH ranges between (pH 4-9) was investigated by measuring the fluorescence emission in the absence/presence of GSH (200 µM) in PBS (20 mM). As shown in Figure 2.6B, the fluorescence emission increased gradually after pH 5 and reached almost a saturation pattern up to pH 9. This observation indicated the feasibility of donor activation at physiological pH 7.4. Additionally, there was no emission observed in the absence of thiols, showing that **UTS-1** was stable over the entire pH.

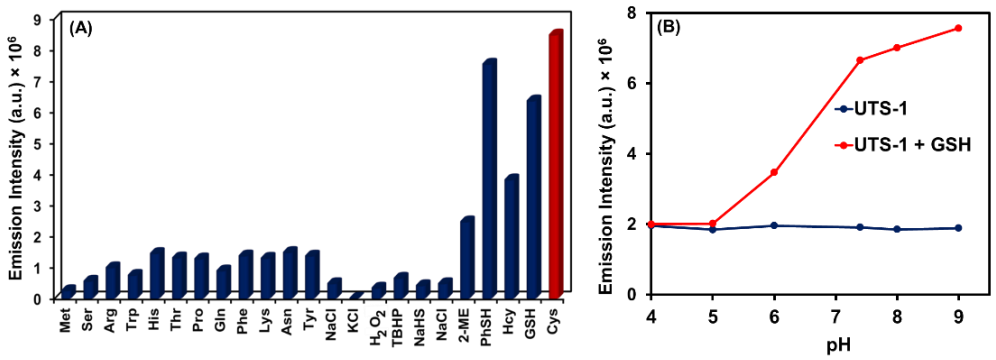

Figure 2.6. (A) The fluorescence emission intensity of **UTS-1** (5.0 μM) upon the addition of bio-analytes (200.0 μM). TBHP, *tert*-butyl hydroperoxide; NaHS, sodium hydrogen sulfide; Na_2S. $9H_2O$ sodium sulfide nonahydrate; 2-ME, 2-mercaptoethanol; (B) Fluorescence emission from **UTS-1** (5.0 μM) with/without GSH (200 μM) at a pH range of 4–9 in PBS (20 mM).

2.3.7. Reaction kinetics of UTS-1 and UDS-1 with PhSH

In order to understand the mechanism of the reaction of **UTS-1** and **UDS-1** with thiols, the reaction of **UTS-1**/**UDS-1**with PhSH was monitored in acetonitrile and the product distribution was analyzed using the reverse phase HPLC method (Scheme 2.2).

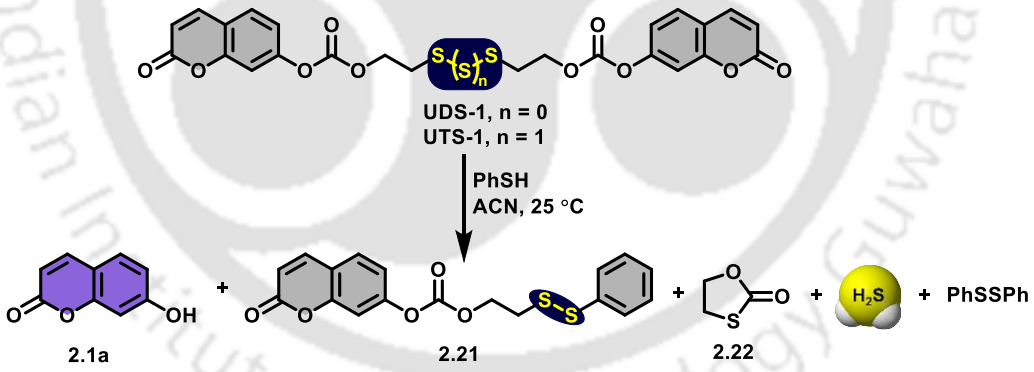

Scheme 2.2. Schematic representation of reaction of **UTS-1** and **UDS-1** with PhSH.

The reaction of **UTS-1**/**UDS-1** with **PhSH** was analyzed after 20 min of incubation. The results showed a small amount of the unreacted **UTS-1/UDS-1**, released fluorophore **2.1a**, mixed disulfide intermediate **2.21**, diphenyl disulfide (PhSSPh) and the cyclic compound **2.22** (not observed in HPLC). The reaction was found to be complete within 1 h and was monitored at two different wavelengths (250 nm and 322 nm), respectively. The retention times for umbelliferone **2.1a** and mixed disulfide intermediate **2.21** was observed at 3.85 and 10.91 min and the retention time of the released umbelliferone is matching with the authentic and pure umbelliferone **2.1a** as shown in Figure 2.7. Although, the cyclic

compound **2.22** could not be detected under the HPLC conditions, the formation of compound **2.21** was evidenced by ESI-MS analysis. The release of umbelliferone (**2.1a**) and mixed disulfide intermediate **2.21** generated from the reaction of **UTS-1** and **UDS-1** with PhSH was further confirmed by NMR (^{1}H and ^{13}C) and ESI-MS analysis.

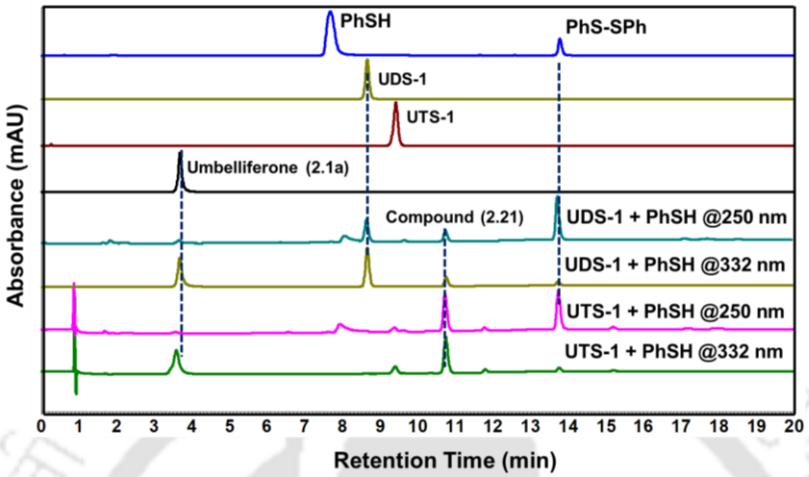

Figure 2.7. Reverse phase HPLC chromatogram (0-20 min) for the reaction of **UTS-1** and **UDS-1** with PhSH. All the chromatograms for **UTS-1**, **UDS-1**, PhSH were extracted at 250 nm except for compound **2.1a**, which was extracted at 332 nm. The chromatograms for the reaction mixtures were recorded after 20 min of reaction.

2.3.8. NMR experiments to confirm the release of compound 2.1a

HPLC analysis of the reaction mixture (**UTS-1** + PhSH) revealed the formation of the released fluorophore **2.1a** from **UTS-1**. The proposed mechanism of H_2S release from **UTS-1**/**UTS-2** was based on analyzing the products/intermediates using analytical HPLC methods and identifying some of those intermediates using ESI-MS studies. In case of HPLC studies, the release of fluorophore **2.1a** was observed after 20 min of reaction in acetonitrile. Next, we performed the NMR scale reactions for **UTS-1** in the presence of PhSH using mesitylene as an internal reference standard. Treatment of **UTS-1** (19.5 mM) with PhSH (100 mM) in a DMSO-d_6 /MeOD-d_4 for 2 h clearly confirmed the release of fluorophore that is observed from stacked plot analysis (^{1}H and ^{13}C) as shown in Figures 2.8 and 2.9. The yields of the products were not calculated using a typical chemical reaction because that would have required a higher amount of the probe (**UTS-1**). We have calculated the product yield (83%) using quantitative ^{1}H NMR experiments with an internal reference standard (Mesitylene, 30 mM).

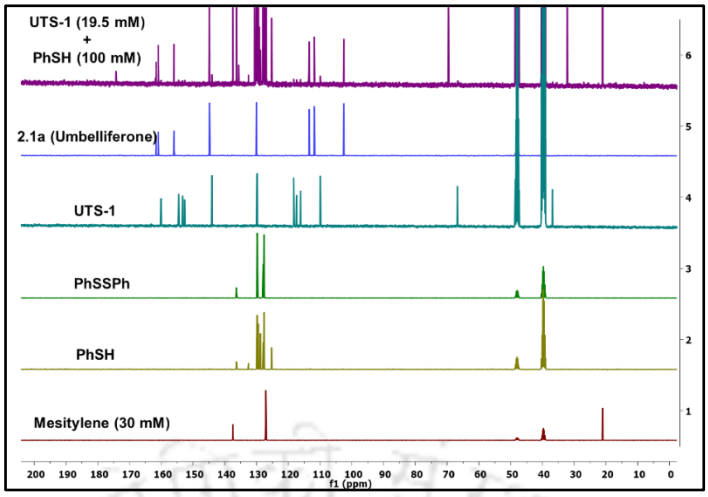

Figure 2.8. ^{13}C {^{1}H} NMR spectra of the reaction mixture of **UTS-1** (19.5 mM) and PhSH (100 mM) in DMSO-d_6/MeOH-d_4 (8:2) mixture at room temperature confirming the release of umbelliferone (**2.1a**).

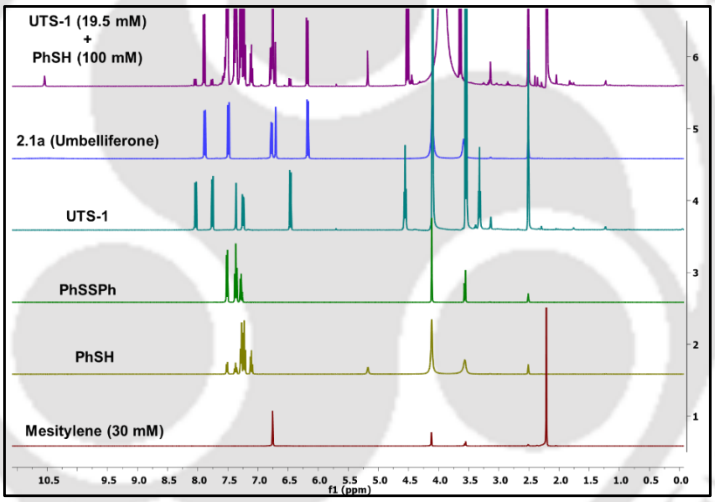

Figure 2.9. ^{1}H NMR spectra of the reaction mixture of **UTS-1** (19.5 mM) and PhSH (100 mM) in DMSO-d_6/MeOH-d_4 (8:2) mixture at room temperature confirming the release of umbelliferone (**2.1a**).

2.3.9. Mechanistic insights

Based on the observations from UV-Vis, fluorescence spectroscopic analysis, HPLC, NMR and ESI-MS analysis, a plausible mechanism is proposed for the release of fluorophore as well as H_2S. There are two pathways proposed for the reaction of **UTS-1** with thiols (RSH) and the incoming thiol can attack via two pathways, either central or terminal sulfur atom (Scheme 2.3). In path A, the incoming thiol attacks the central sulfur atom to give mixed trisulfide intermediate **2.18** and the thiolate intermediate **2.19**

respectively. The thiolate intermediate **2.19** is unstable and undergoes self-immolative cyclization to release the fluorophore **2.1a/2.1b** and the cyclic compound **2.22**. On the contrary, intermediate **2.18** could react with the incoming thiol to generate the perthiol intermediate **2.20** The perthiol species produces the mixed disulfide and releases H_2S upon the nucleophilic attack of the incoming thiol at the internal S-atom of the perthiol species. The mixed disulfide intermediate **2.21** undergoes subsequent attack by the incoming thiol and results in the formation of thiolate intermediate **2.19** and it cyclizes via the self-immolation process to give fluorophore **2.1a/ 2.1b** and cyclic compound **2.22**.

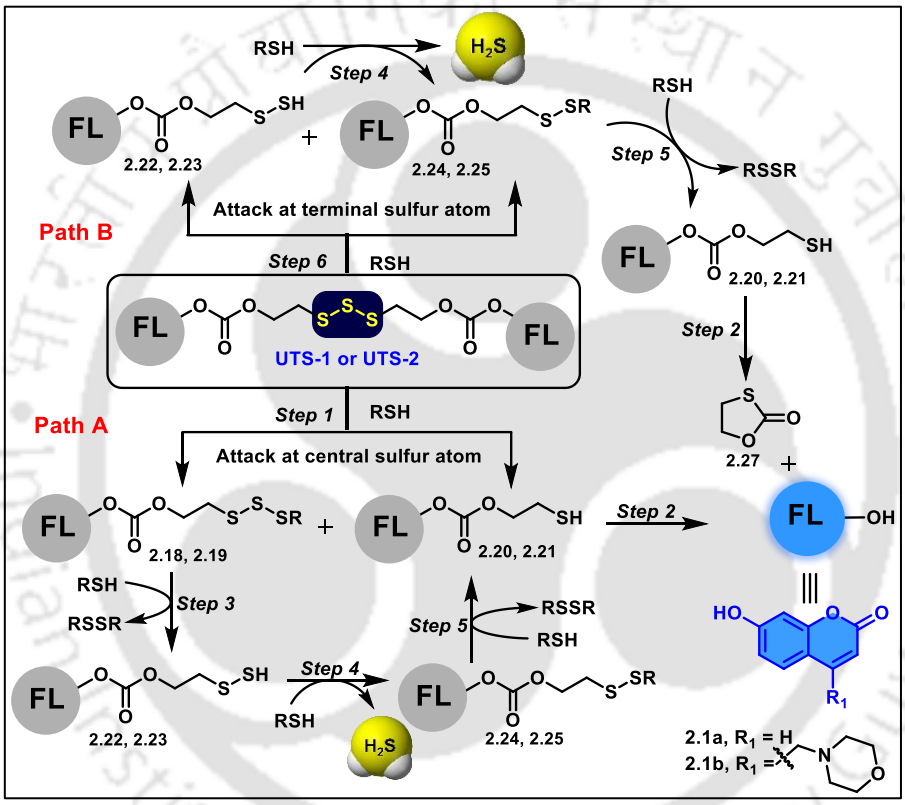

Scheme 2.3. Proposed pathways for the release of fluorophore and H_2S from **UTS-1**/ **UTS-2** in the presence of thiol (RSH).

In path B, attack of the thiol at terminal sulfur atom of either of **UTS-1** or **UTS-2** generates perthiol intermediate **2.20**. The perthiol intermediate **2.20** can react with the thiol and produce the mixed disulfide intermediate **2.21**. The mixed-disulfide intermediate **2.21** reacts with incoming thiol to give thiolate intermediate **2.19** that undergoes self-immolative cyclization to give fluorophore **2.1a/2.1b** and cyclic compound **2.22**. Both of these pathways may work simultaneously for the overall release profile of H_2S and the fluorophore from **UTS-1**/**UTS-2**. However, the literature report suggests that path B is

more favourable in case of diallyl trisulfide (DATS). The details of the mechanistic investigations are depicted in Scheme 2.3.

2.3.10. Anti-proliferative of UTS-1 and UTS-2

To understand the compatibility of the developed fluorogenic H_2S donors **UTS-1** and **UTS-2** in the cellular environment, cytotoxicity profile of the probes was studied. The cellular cytotoxicity of the probes along with the released fluorophore was evaluated in a representative cancer cell line (HeLa) and a non-tumorigenic cell line (HEK 293) using the conventional MTT assay. All the compounds were treated in a dose-dependent manner at five different concentrations (2.5 5.0, 10, 25 and 50 µM) and incubated for 72 h at 37 ºC. Interestingly, as shown in Figure 2.10, all the probes showed >80 % cell viability upto a concentration of 25 µM) in both the cell lines. These results reveal the compatibility of the donors in the cellular medium. Moreover, the released fluorophores and the cyclic by-product were also found to be non-toxic in HeLa cells.

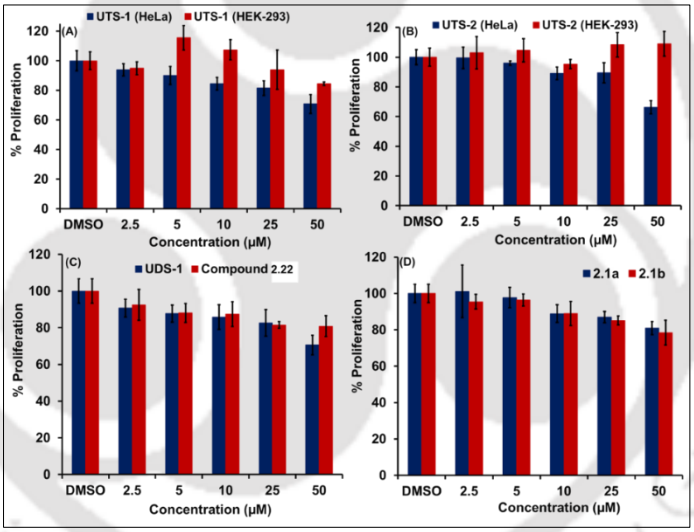

Figure 2.10. (A) and (B) Anti-proliferative activity of **UTS-1** and **UTS-2** in HeLa and HEK-293 cells. (C) Anti-proliferative activity of **UDS-1,** cyclic compound **2.22** and (D) Anti-proliferative activity of umbelliferone **2.1a** and umbelliferone derivative **2.1b** in HeLa cells over 72 h at 37 °C.

2.3.11. Turn-on fluorescence from UTS-1 and UTS-2 in cellular medium

Considering the significantly higher level of endogenous thiol (GSH) in the cancer cells over the normal cells, a representative cervical cancer cell line (HeLa) was chosen in the present study. The cultured HeLa cells were treated with **UTS-1** and **UTS-2** (5.0 µM) and incubated for 1 h at 37 ºC. Interestingly, as shown in Figure 2.11, a significant enhancement of fluorescence was observed under the blue channel which indicates the endogenous thiol-mediated release of the fluorophore **2.1a**/**2.1b** from the probes.

Interestingly, pre-treatment of cells with NEM (2.0 mM) led to the almost complete quenching of the fluorescence emission (Figure 2.11). This is likely due to the non-availability of the endogenous thiols for their reaction with **UTS-1** or **UTS-2**. These observations validate that intracellular biothiols are the active analytes for the fluorogenic H_2S release from the probes.

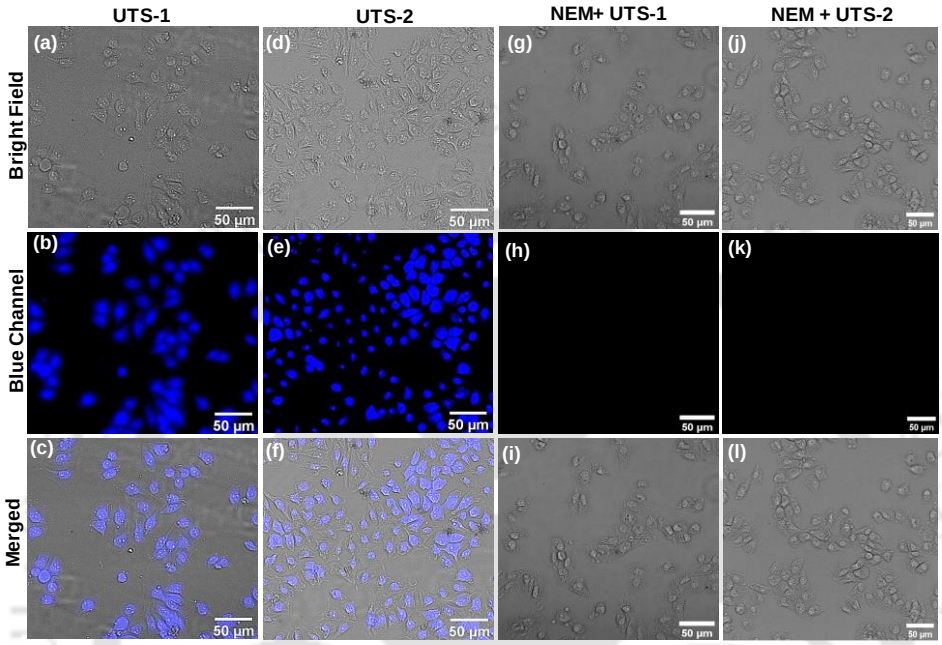

Figure 2.11. Fluorescence microscopic images (bright field, fluorescence and merged) of HeLa cells in the presence of **UTS-1** (a-c) and **UTS-2** (d-f). The quenching of fluorescence upon the pre-treatment of NEM (g-l). The scale bar represents 50 µm.

2.3.12. Intracellular organelle-selectivity of UTS-1 and UTS-2

The lysosomal selectivity of **UTS-2** was studied using fluorescence and confocal microscopy upon co-treatment with standard lysosomal probes (Lyso Tracker Red, **DND-99**). Interestingly, the blue emission of **2.1b** from **UTS-2** merged well with the red emission of **DND-99**, indicating the effective lysosomal selectivity of **UTS-2** (Figure 2.12 (i–l) With the confirmation of cellular internalization and localization of the probes, the H_2S release was studied by co-treatment of the probes with the literature reported H_2S-sensitive probes **NAP-1** and **NAP-2** (lysosomal probe).[30-32] Interestingly, emission of **2.1a** or **2.1b** under the blue channel and H_2S-induced turn-on fluorescence due to **NAP-1P** and **NAP-2P** under the green channel with the excellent overlay is indicative of a concomitant release of H_2S from **UTS-1** and **UTS-2** (Figure 2.12, (a-d) and (e-h)). Furthermore, the lysosomal selectivity of **UTS-2** is evident from the good overlay of the images of **UTS-2** and **NAP-2** and the overlay of **NAP-2** with **DND-99**.

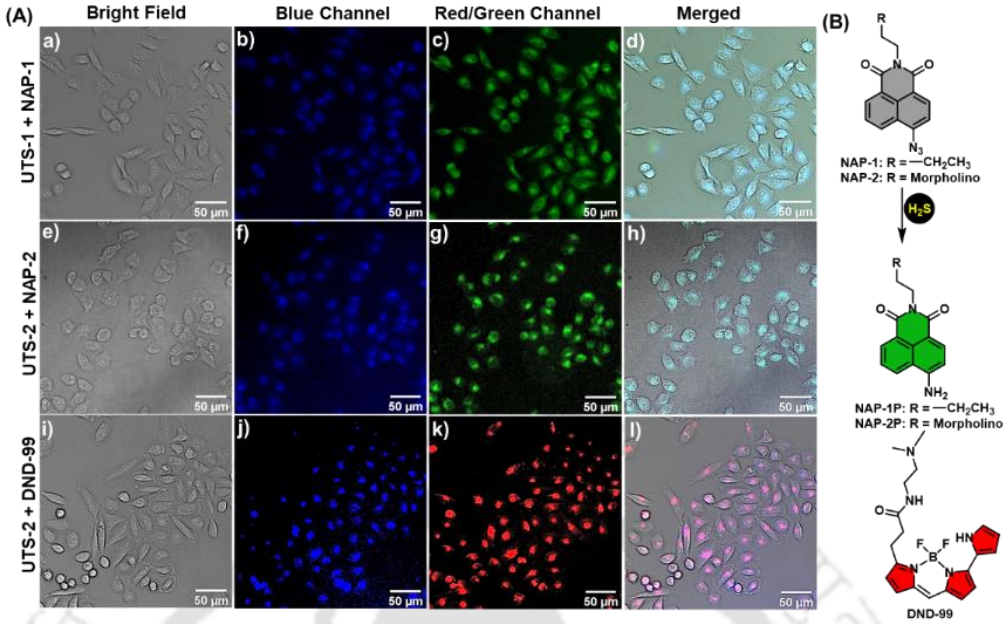

Figure 2.12. (A) Fluorescence microscopic images (bright field, blue, green, red and merged) of HeLa cells after co-treatment of **UTS-1** + **NAP-1** (a-d) and **UTS-2** + **NAP-2** (e-h) and co-treatment of **UTS-2** with **DND-99** (i-l). (B) Chemical structures of **NAP-1**, **NAP-2** and Lysotracker Red (**DND-99**). The scale bar represents 50 µm.

2.3.13. Confirmation of lysosomal targeting of UTS-2 by confocal microscopy

With the fluorescent microscopic evidences about the lysosomal-localization of **UTS-2**, the behaviour was confirmed further using confocal microscopy. Here, the HeLa cells were treated with **UTS-2** and the standard lysosome-selective dye **DND-99** and imaged in blue and red channels to understand the overlapping image. As shown in Figure 2.13A, a significant overlap of blue and red colours was observed outside the nucleus of the cells indicating the lysosomal localization. The co-localization of the released fluorophore **2.1b** and **DND-99** was confirmed further from the intensity plot (Figure 2.13B). A very good overlap of the intensity of blue and red channels further confirms the localization behaviour.

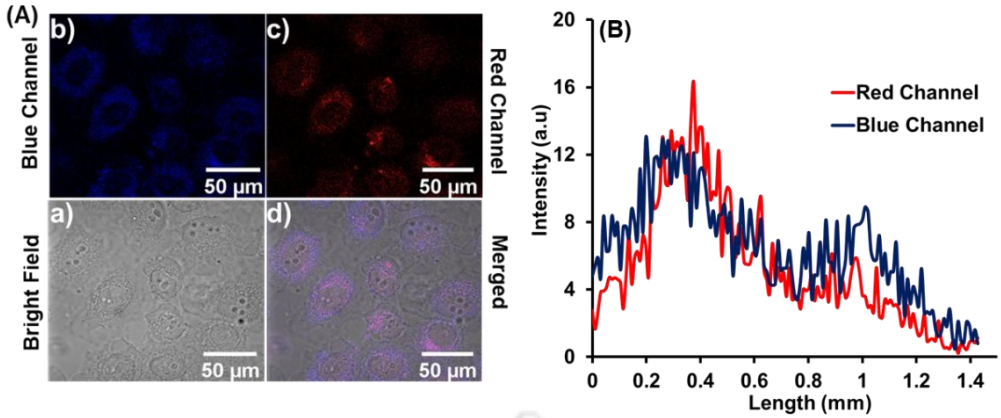

Figure 2.13. (A) Confocal microscopic images (bright field, blue, red and merged) of HeLa cells after the co-treatment of **UTS-2** and **DND-99** (Lysotracker Red, standard lysosomal dye). (B) Intensity profiles for the region of interest (ROI) across HeLa cells for red (**DND-99**) and blue (**UTS-2**) channels indicate significant overlapping profiles. The scale bar represents 50 µm.

2.4. Conclusions

In summary, we report for the first time biothiol-triggered trisulfide-linked fluorogenic donors of H_2S compatible with both aqueous and cellular media. Concomitant release of H_2S and fluorophore enables proper monitoring of the intracellular H_2S release and its further trafficking towards the lysosome. The presence of trisulfide (–S–S–S–) linkers enhanced the sensitivity and reactivity of the probes towards thiols as compared to their disulfide (–S–S–) analogues. Furthermore, the non-toxic nature of the probes in cellular medium (up to 25 µM) could be useful in H_2S-related protective therapies in several disease states.

2.5. Experimental section

2.5.1. Materials and methods

All the chemicals were purchased either from Sigma Aldrich or from reputed local suppliers and used without further purification unless otherwise stated. Thin-layer chromatography (TLC) analyses were carried out on pre-coated silica gel on aluminium sheets and the compounds were visualized with UV or fluorescent light. All the organic solvents used for column chromatography were distilled before use. Melting point of the synthesized compounds was recorded in Büchi melting point apparatus and the values were uncorrected. NMR spectra was recorded on Bruker Ascend^{TM} 400 and 600 MHz NMR spectrometers. All the chemical shift values are reported in ppm using the peak of TMS as an internal standard. High-resolution mass spectra (HRMS) were recorded on Agilent 6520 Accurate-Mass Quadrupole time-of-flight (Q-TOF) LC/MS spectrometer.

UV-Vis spectroscopic measurements were carried out on a Lambda 45 UV-Vis Spectrophotometer and fluorescence emission spectra were recorded on a Fluoromax-4 spectrophotometer (Horiba Jobin Yvon). All the stock solutions of final compounds were prepared in spectroscopic grade DMSO, while stock solutions of thiols were prepared in deionized water.

Synthetic procedure

Synthesis of polysulfides 2.4-2.6[28]

Toa stirred solution of sodium sulfide nonahydrate (0.75 g, 3.12 mmol) in deionized water (10 mL) in 2-neck round bottom flask under inert atmosphere was added sulfur powder (0.20 g, 0.78 mmol) at once. The reaction mixture was stirred at room temperature for 2 h after which the solution turned reddish brown in colour indicating the formation of sodium polysulfide Na_2S_n (n = 2-5) with trisulfide Na_2S_3 being the major species formed in the reaction. To the above solution was added compound **2.3** (0.40 mL, 6.24 mmol) dropwise at room temperature and the reaction was continued for 4 h at room temperature. Progress of the reaction was monitored by TLC analysis. Upon completion of reaction, the aqueous layer was extracted three times with ethyl acetate. The combined organic layer was diluted with brine and dried over anhydrous sodium sulfate. The organic layer was evaporated under reduced pressure to afford the polysulfide mixture (**2.4-2.6**) as faint yellow sticky liquid in almost quantitative yield. The produced disulfide component in the mixture was removed by silica gel column chromatography and the remaining polysulfides (2.4-2.6) were used in the next step directly without further separation. The polysulfide mixture was then used in the next step without further purification. R_f = 0.45 (45% ethyl acetate in pet. ether). ^{1}H NMR (600 MHz, $CDCl_3$): δ (ppm) = 4.00-3.98 (m, overlap of two triplets for O-CH_2- group of trisulfide, tetrasulfide and pentasulfide, 4H), 3.18 (t, *J* = 6.0 Hz, -SCH_2- group of pentasulfide), 3.14 (t, *J* = 6.0 Hz, -SCH_2 group of tetrasulfide) and 3.09 (t, *J* = 6.0 Hz, -S-CH_2- group from trisulfide). ^{13}C NMR (150 MHz, $CDCl_3$): δ (ppm) = 60.2, 59.9, 59.5, 42.3, 41.7,41.6. ESI-MS: *m/z* calcd. for $C_4H_{10}O_2S_3$ (trisulfide) $[M + Na]^+$ = 208.9741, obs. 208.9749, ESI-MS: *m/z* calcd. for $C_4H_{10}O_2S_4$ (tetrasulfide) $[M + Na]^+$ = 240.9461, obs. 240.9468, *m/z* calcd. for $C_4H_{10}O_2S_5$ (pentasulfide) $[M + Na]^+$ = 272.9182, obs. 272.9196.

Synthesis of compound 2.7-2.9

To a stirred solution of polysulfides **2.4-2.6** (0.20 g, 1.07 mmol) in anhydrous dichloromethane (6.0 mL) in 2-neck round bottom flask, was added pyridine (0.43 mL, 5.35 mmol) and the mixture was cooled to 0 ºC under ice-cold mixture. After stirring at 0

ºC for 5-10 min, a solution of 4-nitrophenyl chloroformate (0.54 g, 2.68 mmol) in anhydrous dichloromethane (6.0 mL) was added dropwise manner at 0 ºC. The resulting mixture was allowed to attain room temperature and stirred for 6 h at room temperature. The progress of the reaction was monitored by TLC analysis. Upon completion, the crude mixture was diluted with dichloromethane and subsequently washed with saturated solution of $NaHCO_3$, water and 10% citric acid solution. The organic layer was dried over anhydrous sodium sulfate and the solvent was evaporated under reduced pressure to afford the crude product **2.7-2.9** as white solid in quantitative yield which was used for the next step without further purification. R_f = 0.5 (30 % ethyl acetate in pet. ether 60-80). ^{1}H NMR (600 MHz, $CDCl_3$): δ (ppm) = 8.28 (d, *J* = 9.2 Hz, 4 H), 7.39 (d, *J* = 9.2 Hz, 4H), 4.64-4.62 (m, overlap of two triplets for -OCH_2- group from trisulfide and tetrasulfide, 4H), [3.35-3.30 (m, overlap of two triplets for O-CH_2- from tetrasulfide and pentasulfide) and 3.26 (t, *J* = 6.4 Hz, -OCH_2- group from trisulfide, 4H]. ^{13}C NMR (150 MHz, $CDCl_3$): δ (ppm) = 155.3, 152.3, 145.6, 125.4, 121.8, 66.6, 66.4, 37.0, 36.4. ESI-MS *m/z* calcd. for $C_{18}H_{16}N_2O_{10}S_3$ (trisulfide) $[M + Na]^+$ = 538.9865, obs. 538.9914, ESI-MS *m/z* calcd. for $C_{18}H_{16}N_2O_{10}S_4$ (tetrasulfide) $[M + Na]^+$ = 570.9585, obs. 570.9563, ESI-MS *m/z* calcd. for $C_{18}H_{16}N_2O_{10}S_5$ (pentasulfide) $[M + Na]^+$ = 602.9306, obs. 602.9212.

Synthesis of UTS-1

To a stirred suspension of umbelliferone **2.1a** (0.19 g, 1.17 mmol) in anhydrous dichloromethane in 2-neck round bottom flask at 0 ºC under nitrogen atmosphere triethyl amine (0.27 mL 1.95 mmol) was added and the resulting mixture was stirred for 10 min under ice-cold mixture. To the above mixture was added a solution of compound **2.7-2.9** (0.20 g, 0.39 mmol) in anhydrous dichloromethane in a dropwise manner and the reaction mixture was allowed to attain room temperature and continued for 16 h. The progress of the reaction was monitored by TLC analysis. Upon completion, the reaction mixture was evaporated to dryness and the residue obtained was diluted with ethyl acetate, washed with water and brine solution. The organic layer was dried over anhydrous sodium sulfate and concentrated under reduced pressure to afford the crude product **UTS-1** as white solid. The crude mixture obtained was purified by silica gel column chromatography to afford a polysulfide mixture which was further purified by reverse phase semi-preparative HPLC method. R_f = 0.4 (55% ethyl acetate in pet. ether). White solid, Yield: 50% (0.11 g). From semi-preparative HPLC analysis we observed **UTS-1** as the predominant species along with higher homologues **2.10** (tetrasulfide) and **2.11** (pentasulfide). M.P. 135-137 º C. ^{1}H NMR (400 MHz, $CDCl_3$): δ (ppm) = 7.69 (d, *J* = 9.6 Hz, 2H), 7.50 (d, *J* = 8.5 Hz, 2H),

7.23 (d, J = 2.3 Hz, 2H), 7.16 (dd, J_1 = 8.5 Hz, J_2 = 2.3 Hz, 2H), 6.41 (d, J = 9.6 Hz, 2H), 4.63 (t, J = 6.6 Hz, 4H), 3.26 (t, J = 6.6 Hz, 4H). ^{13}C NMR (400 MHz, $CDCl_3$): δ (ppm) = 160.2, 154.7, 153.2, 152.6, 142.7, 128.8, 117.7, 116.9,116.4, 109.9, 66.4 and 36.6. ESI-MS *m/z* calcd. for $C_{24}H_{18}N_2O_{10}S_3$ (trisulfide) $[M + H]^+$ = 563.0140, obs. 563.0140.

Synthesis of compound 2.13[33]

To an ice-cold solution of conc. H_2SO_4, resorcinol **2.12** (4.0 g, 36.33 mmol) was added followed by the dropwise addition of ethyl 4-chloroacetoacetate (5.4 mL, 40 mmol) at 0 ºC under constant stirring. The reaction was allowed to attain room temperature and continued for 12 h. The progress of the reaction was monitored by TLC analysis. Upon completion, the reaction mixture was poured into ice-cold water and a white precipitate appeared, which was filtered off and washed with deionized water until the pH of the filtrate becomes neutral. The residue was then dried off to give the crude compound **2.13** as white solid. R_f = 0.5 (40% ethyl acetate in pet. ether) Yield: 82% (6.30 g). ^{1}H NMR (400 MHz, DMSO-d_6): δ (ppm) = 10.67 (brs, 1H), 7.66 (d, J = 8.6 Hz, 1H), 6.85 (dd, J_1 = 8.7, J_2 = 2.3 Hz, 1H), 6.76 (d, J = 2.3 Hz, 1H), 6.41 (s, 1H), 4.94 (s, 2H). ^{13}C NMR (100 MHz, DMSO-d_6): δ (ppm) = 161.5, 160.1, 155.3, 151.0, 126.6, 113.1, 111.1, 109.4, 102.6 and 41.4.

Synthesis of compound 2.1b[34]

Compound **2.1b** was synthesized using literature report with minor modifications. To a solution of compound **2.13** (0.20 g, 0.95 mmol) in acetonitrile (3.0 mL), was added morpholine (0.18 mL, 2.10 mmol) and the reaction was allowed to stir for 8 h at 65 ºC. The progress of the reaction was monitored by TLC analysis. Upon completion, the reaction mixture was allowed to cool to room temperature and the solvent was evaporated under reduced pressure to afford the crude compound **2.1b** as white solid. R_f = 0.5 (55% ethyl acetate in pet. ether), Yield = 65% (0.16 g). ^{1}H NMR (400 MHz, DMSO-d_6): δ (ppm) = 10.50 (s, 1H), 7.75 (d, J = 8.8 Hz, 1H), 6.78 (dd, J_1 = 8.7 Hz, J_2 = 2.4 Hz), 6.70 (d, J = 2.3 Hz, 1H), 6.24 (s, 1H), 3.61 (s, 2H), 3.58 (t, J = 4.6 Hz, 4H), 2.46 (t, J = 4.6 Hz, 4 H). ^{13}C NMR (100 MHz, DMSO-d_6): δ (ppm) = 161.0, 160.3, 155.2, 152.3, 126.7, 112.6, 110.8, 110.1, 102.1, 66.2, 58.2 and 53.3.

Synthesis of UTS-2

UTS-2 was prepared using similar method used for **UTS-1**. The polysulfide linker **2.7-2.9** (0.20 g, 0.41 mmol) was added to a solution of compound **2.1b** (0.32 g, 1.23 mmol) in the presence of triethylamine (0.30 mL, 2.05 mmol) in anhydrous dichloromethane (6.0 mL) at 0 ºC. The reaction mixture was allowed to stir for 16 h at room temperature. The

progress of the reaction was monitored by TLC analysis. Upon completion of reaction, the solvent was evaporated under reduced pressure and diluted with ethyl acetate. The organic layer was washed with water, brine and dried over anhydrous sodium sulfate and concentrated under reduced pressure to afford the crude compound as white solid. The crude compound was purified by silica gel column chromatography to remove the unreacted materials to obtain **UTS-2** as a mixture of polysulfide containing trisulfide, **2.15** (tetrasulfide) and **2.16** (pentasulfide) components. The inseparable mixture was then purified by reverse phase HPLC to obtain the pure trisulfide **UTS-2** as white solid. Yield = 29% (0.09 g). M. P. = 64-66 ºC. ^{1}H (400 MHz, $CDCl_3$): δ (ppm) = 7.88 (d, *J* = 8.8 Hz, 2H), 7.22 (d, *J* = 2.3 Hz, 2H), 7.15 (dd, J_1 = 8.7 Hz, J_2 = 2.4 Hz, 2H), 6.50 (s, 2H), 4.63 (t, *J* = 6.5 Hz, 4H), 3.73 (t, *J* = 4.6 Hz, 8H), 3.61 (d, *J* = 1.3 Hz, 4H), 3.26 (t, *J* = 6.5 Hz, 4H), 2.55 (t, *J* = 4.6 Hz, 8H). ^{13}C NMR (100 MHz, $CDCl_3$): δ (ppm) = 160.4, 154.4, 153.0, 152.6, 150.9, 126.0, 117.2, 116.9, 114.8, 109.9, 66.8, 66.3, 59.5, 53.8, 36.5. ESI-MS (+ve) *m/z* calcd. for $[C_{34}H_{36}N_2O_{12}S_3]^+$ $[M + H]^+$: 761.1509, obs. 761.1532.

Synthesis of compound 2.17[35]

In a 25 mL 2-neck round bottom flask, compound **2.16** (0.20 g, 1.30 mmol) was taken and dissolved in anhydrous dichloromethane (6.0 mL), followed by the addition of pyridine (0.5 mL, 6.4 mmol) and the mixture was cooled to 0 ºC. To the above mixture was added a solution of 4-nitrophenyl chloroformate (0.50 g, 3.20 mmol) in anhydrous dichloromethane (6.0 mL) at 0 ºC. The reaction mixture was allowed to attain room temperature and stirred for another 6 h. The progress of the reaction was monitored by TLC analysis. Upon completion, the mixture was evaporated to dryness, and the crude product obtained was diluted with dichloromethane and subsequently washed with saturated $NaHCO_3$, water and 10% citric acid, and brine. The combined organic layer was dried over anhydrous sodium sulfate and evaporated under reduced pressure to afford the crude compound **2.17** as white solid. The crude product was purified by silica gel column chromatography using ethyl acetate and pet. ether as eluents to obtain the product as white solid powder. R_f = 0.5 (30% ethyl acetate in pet. ether), Yield: 62% (0.40 g). ^{1}H NMR (400 MHz, $CDCl_3$): δ (ppm) = 8.28 (d, *J* = 9.1 Hz, 4H), 7.39 (d, *J* = 9.2 Hz, 4H), 4.57 (t, *J* = 6.5 Hz, 4H), 3.08 (t, *J* = 6.5 Hz, 4H). ^{13}C NMR (100 MHz, $CDCl_3$): δ (ppm) = 155.3, 152.3, 145.5, 125.4, 121.8, 66.8 and 36.8. ESI-MS *m/z* calcd. for $C_{14}H_{16}N_2O_{10}S_2$ $[M + K]^+$ = 522.9883, obs. 522.9885.

Synthesis of UDS-1

In a 50 mL 2-neck round bottom flask, compound **2.1a** (0.20 g, 0.41 mmol) was suspended in anhydrous dichloromethane at 0 ºC, followed by addition of triethylamine (0.23 mL, 1.64 mmol). The mixture was stirred for 10 min at this temperature and to the above mixture was added a solution of compound **2.17** (0.20 g, 0.41 mmol) in anhydrous dichloromethane at 0 ºC. The reaction mixture was allowed to attain room temperature and stirred for 16 h. The progress of the reaction was monitored by TLC analysis. Upon completion, the solvent was removed and then diluted with ethyl acetate. The organic layer was washed with water and brine and dried over anhydrous sodium sulfate. The organic layer was evaporated under reduced pressure to afford the crude product as oily liquid. The crude compound was purified by silica gel column chromatography using ethyl acetate and pet. ether as eluents to afford pure **UDS-1** as white solid. R_f = 0.3 (35% ethyl acetate in pet. ether). Yield: 46% (0.10 g), M.P.= 121 - 123 °C. ^{1}H NMR ($CDCl_3$, 400 MHz): δ (ppm) = 7.70 (d, *J* = 9.6 Hz, 2H), 7.51 (d, *J* = 8.5 Hz, 2H), 7.21 (d, *J* = 2.2 Hz, 2H), 7.15 (dd, J_1 = 8.5, J_2 = 2.3 Hz, 2H), 6.41 (d, *J* = 9.6 Hz, 2H), 4.57 (t, *J* = 6.5 Hz, 4H), 3.09 (t, *J* = 6.5 Hz, 4H). ^{13}C NMR (100 MHz, $CDCl_3$): δ (ppm) = 160.2, 154.6, 153.2, 152.6, 142.7, 128.7, 117.6, 116.9, 116.3, 109.9, 66.7, 36.8. ESI-MS *m/z* calcd. for $C_{24}H_{18}O_{10}S_2$ $[M + H]^+$: 531.0420, obs. 531.0431.

2.5.2. UV-Vis absorbance and fluorescence emission studies

Stock solutions of probes were prepared in spectroscopic grade DMSO. All the stock solutions of analytes were prepared in deionized water before doing the experiments. All the spectroscopic measurements were performed under physiological conditions in phosphate buffer saline, PBS (20 mM, pH 7.4). Samples for UV and fluorescence measurements were carried out in quartz cuvettes (1.0 mL). In the fluorescence spectroscopic studies, the optimized incubation time was determined first and then subsequently the concentration of thiol analytes. Fluorescence spectroscopic experiments were carried out with an excitation wavelength (λ_{ex}) of 322 nm with a slit width of 3 nm. UV-Vis studies were done by incubating **UTS-1** (5.0 µM) with GSH and Cys (200.0 µM) for 90 min. For studies with different analytes, emission was measured after incubating **UTS-1** (5.0 µM) with the analyte (200.0 µM) for 15 min in PBS. The resulting mixture was further incubated for 15 min with the addition of equivalent amount of Cys (200.0 µM) to the reaction mixture. The effect of pH on the stability and reactivity of **UTS-1** was studied by the optimized protocol using the PBS (20.0 mM) of different pH (4-9) by fluorescence spectroscopic method.

2.5.3. Release of H_2S from UTS-1 and UTS-2 using MB Assay

The release profile of H_2S from **UTS-1** and **UTS-2** (25.0 µM) was measured in the presence of Cys and GSH (500.0 µM) by MB assay using UV-Vis spectrophotometer. The generation of H_2S was initiated by reacting the probes (25.0 µM) with thiols (500.0 µM) in PBS buffer. Formation of methylene blue was monitored at 670 nm in UV-Vis spectrophotometer every 10 min interval over 180 min after adding 500.0 µL of the above solution to 500.0 µL of methylene blue cocktail (100.0 µL of zinc acetate (1% w/v), 200.0 µL of N, N-dimethyl-1,4-phenylenediamine sulfate (20 mM in 7.2 M HCl), and 200 µL of ferric chloride (30 mM in 1.2 M HCl) in a cuvette. The concentration of the released H_2S from each sample was calculated against a calibration curve, which was obtained using known concentrations of $Na_2S.9H_2O$ solution under identical condition without adding any thiol.

2.5.4. Detection of the released H_2S using turn-on fluorogenic probe

The generated H_2S from **UTS-1** in the presence of Cys was monitored using a H_2S-sensitive turn-on azide-based fluorescent probe **NAP-1** using fluorescence spectrophotometer. Initially probe **NAP-1** (25.0 µM) was pre-incubated with thiol (250.0 µM) for 90 min in PBS (20 mM, pH 7.4) and the emission spectrum was measured to saturate the possible reaction of **NAP-1** with Cys. The aliquot from the experimental solution of **UTS-1** (25.0 µM) + Cys (250.0 µM) was added to the above mixture and measured the emission intensity after an incubation of 90 min to understand the further reaction of **NAP-1** with the generated hydrogen sulfide from **UTS-1** (25.0 µM) in the presence of Cys (500.0 µM).

2.5.5. HPLC studies

Purity of the synthesized probes was analysed by analytical high-performance liquid chromatography (HPLC) Agilent 1220 infinity II LC system using reverse-phase C18 column (Luna®, 150 × 4.6 mm, 5 µm). HPLC grade solvents were used as mobile phase and the HPLC profile of compounds were detected by PDA detector at a wavelength of 250 and 323 nm at room temperature at a flow rate of 1.0 mL/min. The final trisulfide probes UTS-1 and UTS-2 were separated from the polysulfides using a semi-preparative HPLC system (Thermo Scientific Dionex, Ultimate 3000 pump with DAD) using a semi-preparative column (Luna®, polar C18, 250×21.2 mm) using acetonitrile and water as mobile phase with a flow rate of 10 ml/min.

2.5.6. NMR studies

UTS-1 (19.5 mM) was treated with thiophenol (100 mM) in DMSO-d_6/MeOH-d_4 (8:2) mixture at room temperature in the presence of Mesitylene (30 mM) as an internal

standard. The final spectrum was recorded after 2 h to ensure the completion of expected reaction. $^{13}C\{^{1}H\}$ NMR spectra of pure **UTS-1**, released umbelliferone (**2.1a**), diphenyl disulfide (PhSSPh) and thiophenol (PhSH) are included here for spectral comparison. Final spectrum of the reaction mixture clearly demonstrates the formation of umbelliferone (**2.1a**) as the product along with the cyclic compound (or its hydrolysed analogue), PhSSPh and unreacted PhSH. It further indicates that unreacted **UTS-1** is not present in the reaction mixture. Similar NMR experiment has been reported by Pluth and Co-workers in a recent report for the release of hydrogen sulfide from cyclic sulfenyl thiocarbamates.[23]

2.5.7. Cell culture studies

Human cervical cancer cell line (HeLa) was obtained from the National Centre for Cell Science (NCCS), Pune, India. HeLa cells were cultured in DMEM medium (Gibco) supplemented with 10% (v/v) FBS (Gibco) and 1% Pen-Strep (Gibco). Cells were cultured as a monolayer in a humidified incubator at 37 °C in the presence of 5% CO_2 level. Human embryonic kidney cell line (HEK-293) was also cultured in DMEM medium following the similar protocol as used for HeLa cells.

2.5.8. MTT assay

All the synthesized probes **UTS-1**, **UDS-1** and **UTS-2** along with umbelliferone derivatives **2.1a** and **2.1b** and the released cyclic compound **2.22** were evaluated for their anti-proliferative activity using MTT assay. The cells were seeded in 96 well plate at a density of $1x10^4$ cells per 100 µl per well and treated with freshly prepared test compounds (0-50 µM) for 0 to 72 h. At the end of treatment period, 10 µL of 5 mg mL^{-1} of MTT was added to the plate and incubated for 2 h. After 2 h of incubation, the culture medium from the plate was removed and the purple formazan crystals were dissolved using 100 µL of DMSO (Himedia) and the absorbance at 570 nm was measured using microplate reader (Thermo Scientific Multiskan^{TM} GO Microplate Spectrophotometer). In experimental set, similar MTT treatment protocol was followed only after 72 h. The mean ΔOD values were calculated by the subtraction of mean OD values of 0 h plate (control) from the mean OD values of identical wells at 72 h plate (experimental) and the percentage proliferation was calculated keeping the mean ΔOD of untreated control as 100%.

2.5.9. Fluorescence and confocal microscopic studies

HeLa cells were cultured in high glucose DMEM supplemented with 10% fetal bovine serum (FBS) and 1% pen/strep at 37 ° C under 5% CO_2 atmosphere. Cells were then plated (0.7×10^4 cells/plate) in 35 mm cell culture petri dishes containing 2.0 mL of DMEM and

incubated at 37 ºC under 5% CO_2 for 24 h. The confluent cells were washed with DPBS and finally incubated with **UTS-1** or **UTS-2** (5.0 μM) at 37 ºC under 5% CO_2 for 1 h. After washing with DPBS (5 times), cellular morphology was carefully observed and imaged in a Bio-Rad ZOE^{TM} fluorescent cell imager under a bright field and suitable fluorescent-coloured filters. Additionally, the control experiments were designed and performed with the pre-treatment of NEM (2.0 mM) and/or DL-Propargyl glycine (50.0 μM) to affirm the quenching of endogenous biothiols and/or H_2S levels, respectively. Initial treatments with **UTS-1** (5.0 μM) or **UTS-2** (5.0 μM) followed by the H_2S-sensitive azide-based fluorescence turn-on probes such as **NAP-1** (2.0 μM) or **NAP-2** (2.0 μM) were performed and treated cells were incubated at 37 ºC under 5% CO_2 for 1 h. Finally, the treated cells were washed with DPBS (5 times) and imaged in a Bio-Rad ZOE^{TM} fluorescent cell imager to understand the reactivity of the generated H_2S with the fluorescent probes. Similarly, a standard Lyso-Tracker Red dye (**DND-99**, Thermo Fisher Scientific) (75.0 nM) was also used in combination with **UTS-2** using the above protocol to confirm the lysosomal selectivity of **UTS-2**. For the co-localization studies using confocal microscopy (Zeiss LSM 880), HeLa cells were cultured and grown following the above protocol. The confluent cells were washed with DPBS (5 times), cellular morphology was carefully observed. In order to image the localization property of the probe **UTS-2**, the cells were treated with the probe with **UTS-2** (5.0 μM) and kept in the incubator for 1 h at 37 ºC under 5% CO_2. After washing with DPBS (5 times) the standard Lyso Tracker Red dye (**DND-99**, Thermo Fisher Scientific) (75.0 nM) was added and kept for incubation at 37 ºC under 5% CO_2 for another 1 h. Finally, the cells were washed with DPBS (5 times) and fixed with 4% formaldehyde and imaged under confocal microscopy (Zeiss LSM 880) using respective filters for understanding the proper localization behaviour of our compound.

2.6. References

1. Vandiver, M. S.; Snyder, S. H., *J. Mol. Med.* **2012**, *90*, 255-263.
2. Fukuto, J. M.; Carrington, S. J.; Tantillo, D. J.; Harrison, J. G.; Ignarro, L. J.; Freeman, B. A.; Chen, A.; Wink, D. A., *Chem. Res. Toxicol.* **2012**, *25*, 769-793.
3. Predmore, B. L.; Lefer, D. J.; Gojon, G., *Antioxid. Redox Signaling* **2012**, *17*, 119.
4. Bhatia, M., *IUBMB life* **2005**, *57*, 603-606.

5. Eto, K.; Asada, T.; Arima, K.; Makifuchi, T.; Kimura, H., *Biochem. Biophys. Res. Commun.* **2002**, *293*, 1485-1488.
6. Wallace, J. L.; Caliendo, G.; Santagada, V.; Cirino, G.; Fiorucci, S., *Gastroenterology* **2007**, *132*, 261-271.
7. Carballal, S.; Trujillo, M.; Cuevasanta, E.; Bartesaghi, S.; Möller, M. N.; Folkes, L. K.; García-Bereguiaín, M. A.; Gutiérrez-Merino, C.; Wardman, P.; Denicola, A., *Free Radic. Biol. Med.* **2011**, *50*, 196-205.
8. Filipovic, M. R.; Miljkovic, J.; Allgäuer, A.; Chaurio, R.; Shubina, T.; Herrmann, M.; Ivanovic-Burmazovic, I., *Biochem. J.* **2012**, *441*, 609-621.
9. Calvert, J. W.; Jha, S.; Gundewar, S.; Elrod, J. W.; Ramachandran, A.; Pattillo, C. B.; Kevil, C. G.; Lefer, D. J., *Circ. Res.* **2009**, *105*, 365-374.
10. Szabo, C.; Papapetropoulos, A., *Pharmacol. Rev.* **2017**, *69*, 497-564.
11. Hartle, M. D.; Pluth, M. D., *Chem. Soc. Rev.* **2016**, *45*, 6108-6117.
12. Zhao, Y.; Biggs, T. D.; Xian, M., *Chem. Commun.* **2014**, *50*, 11788-11805.
13. Powell, C. R.; Dillon, K. M.; Matson, J. B., *Biochem. Pharmacol.* **2018**, *149*, 110-123.
14. Zheng, Y.; Yu, B.; Ji, K.; Pan, Z.; Chittavong, V.; Wang, B., *Angew. Chem. Int. Ed.* **2016**, *55*, 4514-4518.
15. Moest, R., *Anal. Chem.*, **1975**, *47*, 1204-1205.
16. Kolluru, G. K.; Shen, X.; Bir, S. C.; Kevil, C. G., *Nitric oxide : biology and chemistry* **2013**, *35*, 5-20.
17. Jeroschewski, P.; Steuckart, C.; Kühl, M., *Anal. Chem.* **1996**, *68*, 4351-4357.
18. Peng, H.; Cheng, Y.; Dai, C.; King, A. L.; Predmore, B. L.; Lefer, D. J.; Wang, B., *Angew. Chem. Int. Ed. Engl.* **2011**, *50*, 9672-9675.
19. Shi, D.-T.; Zhou, D.; Zang, Y.; Li, J.; Chen, G.-R.; James, T. D.; He, X.-P.; Tian, H., *Chem. Commun.* **2015**, *51*, 3653-3655.
20. Yu, F.; Han, X.; Chen, L., *Chem. Commun.* **2014**, *50*, 12234-12249.
21. Lin, V. S.; Chen, W.; Xian, M.; Chang, C. J., *Chem. Soc. Rev.* **2015**, *44*, 4596-4618.
22. Wu, L.; Sedgwick, A. C.; Sun, X.; Bull, S. D.; He, X.-P.; James, T. D., *Acc. Chem. Res.* **2019**, *52*, 2582-2597.
23. Zhao, Y.; Steiger, A. K.; Pluth, M. D., *J. Am. Chem. Soc.* **2019**, *141*, 13610-13618.
24. Zhao, Y.; Cerda, M. M.; Pluth, M. D., *Chem. Sci.* **2019**, *10*, 1873-1878.

25. Hu, Y.; Li, X.; Fang, Y.; Shi, W.; Li, X.; Chen, W.; Xian, M.; Ma, H., *Chem. Sci.* **2019**, *10*, 7690-7694.
26. Cheung, N. S.; Peng, Z. F.; Chen, M. J.; Moore, P. K.; Whiteman, M., *Neuropharmacology* **2007**, *53*, 505-514.
27. Fuson, R. C.; Price, C. C.; Burness, D. M.; Hatchard, W. R.; Lipscomb, R. D., *J. Org. Chem.* **1946**, *11*, 469-474.
28. Fuson, R. C.; Price, C. C.; Bauman, R. A.; Bullitt, O. H.; Hatchard, W. R.; Maynert, E. W., *J. Org. Chem.* **1946**, *11*, 487-498.
29. Moest, R., *Anal. Chem.* **1975**, *47*, 1204-1205.
30. Wu, Z.; Liang, D.; Tang, X., *Anal. Chem.* **2016**, *88*, 9213-9218.
31. Qiao, Q.; Zhao, M.; Lang, H.; Mao, D.; Cui, J.; Xu, Z., *RSC Adv.* **2014**, *4*, 25790-25794.
32. Zhang, L.; Li, S.; Hong, M.; Xu, Y.; Wang, S.; Liu, Y.; Qian, Y.; Zhao, J., *Org. Biomol. Chem.* **2014**, *12*, 5115-5125.
33. Chen, Z.; Li, B.; Xie, X.; Zeng, F.; Wu, S., *J. Mater. Chem. B* **2018**, *6*, 2547-2556.
34. Zheng, P.; Somersan-Karakaya, S.; Lu, S.; Roberts, J.; Pingle, M.; Warrier, T.; Little, D.; Guo, X.; Brickner, S. J.; Nathan, C. F., *J. Med. Chem.* **2014**, *57*, 3755-3772.
35. Bhuniya, S.; Lee, M. H.; Jeon, H. M.; Han, J. H.; Lee, J. H.; Park, N.; Maiti, S.; Kang, C.; Kim, J. S., *Chem. Commun.* **2013**, *49*, 7141-7143.

Chapter 3

Thioredoxin Reductase-triggered Fluorogenic Donor of Hydrogen Sulfide: A Model Study with a Symmetrical Organopolysulfide Probe with Turn-on Near-infrared Fluorescent Emission

3.1. Introduction

Hydrogen sulfide (H_2S), a gasotransmitter,[1,2] is produced endogenously from Cys and Hcy by several enzymes belonging to the synthase, lyase, and transferase families.[3,4] A controlled production of H_2S is known to be beneficial to mammals in the regulation of multiple biological processes such as anti-inflammation, cardioprotection, vasodilation, and neurotransmission; however, its dysregulation leads to many disease states.[5-7] Based on these observations, proper regulation of endogenous H_2S or an administration of exogenous H_2S in a sustained manner during its deficiency in different disease states is recommended for cellular homeostasis and therapeutic benefits. In view of this, many organosulfur compounds have been developed over the last two decades as sustained donors of H_2S, while most of them are non-fluorogenic.[8-14] Owing to the added advantages of turn-on fluorogenic H_2S donors over non-fluorogenic donors, a few external stimuli and bio-analyte-triggered fluorogenic H_2S donors have been reported very recently. For example, light-triggered fluorogenic H_2S donors including **Probe 3** have been reported, enabling the real-time monitoring of H_2S release in aqueous and cellular media (Figure 3.1A).[15-17] Additionally, few dual-analyte-triggered (ROS/biothiols and carbonic anhydrase) fluorogenic probes containing thiocarbonate or thiocarbamate moieties such as **FLD-1** have been reported that release H_2S with turn-on fluorescence in aqueous as well as cellular media (Figure 3.1A).[18-20] In 2020, for the first time, we designed and reported single analyte–responsive (biothiol) coumarin-based turn-on fluorogenic probes as H_2S donors with lysosomal selectivity.[21] However, the utilized fluorophore absorbed light in the UV range with high energy blue emission. In 2021, Zhang and co-workers reported the Cys-induced release of H_2S with turn-on fluorescence from a phenyl thiocarbamate-based probe (**Pro-S**) in aqueous and cellular media with further validation in a zebrafish model.[22] This was the first report of fluorogenic H_2S donation with emission in the near-infrared (NIR) region.

Importantly, the enzyme-triggered prodrug strategies offer added advantages over the external stimuli- or small-molecule analyte–responsive processes as enzymes have better substrate specificity and tissue localizations along with overexpression in certain disease models.[11] Additionally, it has been shown that the key antioxidant enzymes such as thioredoxin reductase (TrxR), glutathione peroxidase (GP_x) and glutathione reductase (GR) are overexpressed in cancer cells.[23-25] Therefore, research attention was paid to developing suitable fluorogenic sensors for such enzymes in a broader perspective of enzyme-triggered prodrug strategies. For example, fluorogenic sensors of TrxR are

developed recently by mimicking the structural components of its substrate thioredoxin (Trx).[26] First, a TrxR-responsive fluorogenic probe containing a five-membered dithiolane ring (**TRFS**-green) was reported by Fang and co-workers to conveniently monitor TrxR activity in an aqueous and cellular medium (Figure 3.1B).[27] Subsequently several other dithiolane ring-containing probes were developed and **FAST-TRFS** was reported as the best probe in that category.[28] Very recently (2020), Strongin and co-workers have developed the highly reactive TrxR-selective diselenide-based fluorogenic probe (**Probe 1a**) and the TrxR-triggered fluorescence response was validated in lung cancer cells (Figure 3.1B).[24] These probes can effectively estimate the overexpression level of TrxR in disease conditions such as cancer. Similarly, turn-on fluorogenic probes for other antioxidant enzymes such as GR and GP_x were also developed recently for estimating their cellular expression levels.[29,30] Regarding the release of H_2S from organic compounds, only a few studies with an enzyme–responsive donation of H_2S (non-fluorogenic donors) involving esterase[14,31] and bacterial nitroreductase[32] are reported. However, real-time monitoring of the H_2S release from those non-fluorogenic donors was not feasible due to the lack of a proper monitoring process. Owing to the overexpression of key antioxidant enzymes in cancer cells and the presence of highly nucleophilic thiol/selenol groups at the active sites of most antioxidant enzymes such as TrxR, GP_x, and GR, it would not be surprising that they exhibit superior reactivity towards the probes that are responsive towards biothiols in the cellular medium.

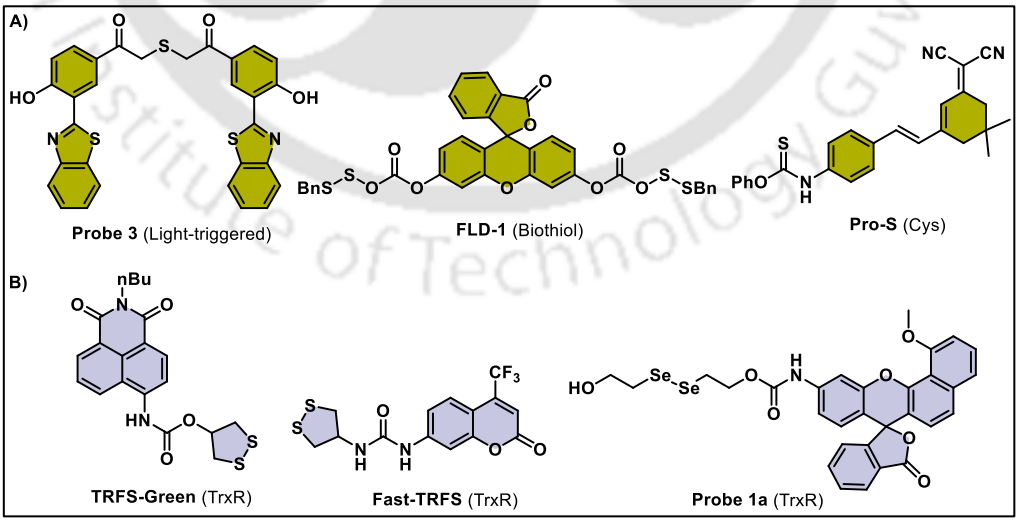

Figure 3.1. (A) Recently developed representative bioanalyte-responsive sustained fluorogenic donors of H_2S. (B) Representative structures of recently reported TrxR-sensitive turn-on fluorogenic probes. The triggering analytes are mentioned in the parentheses.

3.2. Outline of the chapter

In chapter 2, we reported two fluorogenic organotrisulfide probes **UTS-1** and **UTS-2** that are triggered by key biothiols present in the biological system to release an important gasotransmitter H_2S. Both the synthesized trisulfides release H_2S in aqueous as well as in cellular media. In chapter 3, we highlight the design of TrxR-responsive organopolysulfide-based self-immolative turn-on fluorogenic donor of H_2S (**DCI-PS**) compatible in both aqueous and cellular media. The corresponding disulfide analogue (**DCI-DS**) was synthesized for monitoring the turn-on fluorogenic processes without any donation of H_2S (Figure 3.2A). Upon activation, **DCI-PS** releases H_2S in a sustained manner with a concomitant fluorescence emission in the NIR region for real-time monitoring of the H_2S release profile (Figure 3.2B). It should be mentioned here that TrxR, having a selenenyl sulfide linkage, catalytically reduces the disulfide form of Trx to its reduced form (dithiol) using NADPH as a co-factor as proposed in Figure 3.2D. The designed probes in this study resemble the substrate (Trx) of TrxR with disulfide/polysulfide linkers. The reactivity of the synthesized probes towards TrxR in an aqueous medium was studied using a small-molecule dithiol (DTT) and was studied further in representative cancer cells. The choice of DTT, a small-molecule dithiol as a functional mimic of TrxR was based on the structural and nucleophilic functional similarities.[24,33] As the reduction of the selenenyl sulfide (–Se–S–) bond in TrxR generates the highly nucleophilic and adjacent selenolate–thiol moiety, the reduced DTT also exists as highly nucleophilic and adjacent dithiol moieties (Figure 3.2C). The targeted reactivity of the probes with TrxR was validated further with TrxR-selective inhibitors in the cellular medium and with cell lysates. To the best of our knowledge, this is the first report on the antioxidant enzyme (TrxR)-triggered turn-on NIR fluorogenic H_2S donor that is compatible with both aqueous and cellular media. After optimizing the release of fluorophore and H_2S in the aqueous medium, the probe was utilized further in the TrxR-triggered intracellular sustained release of H_2S and fluorophore in a representative cancer cell line.

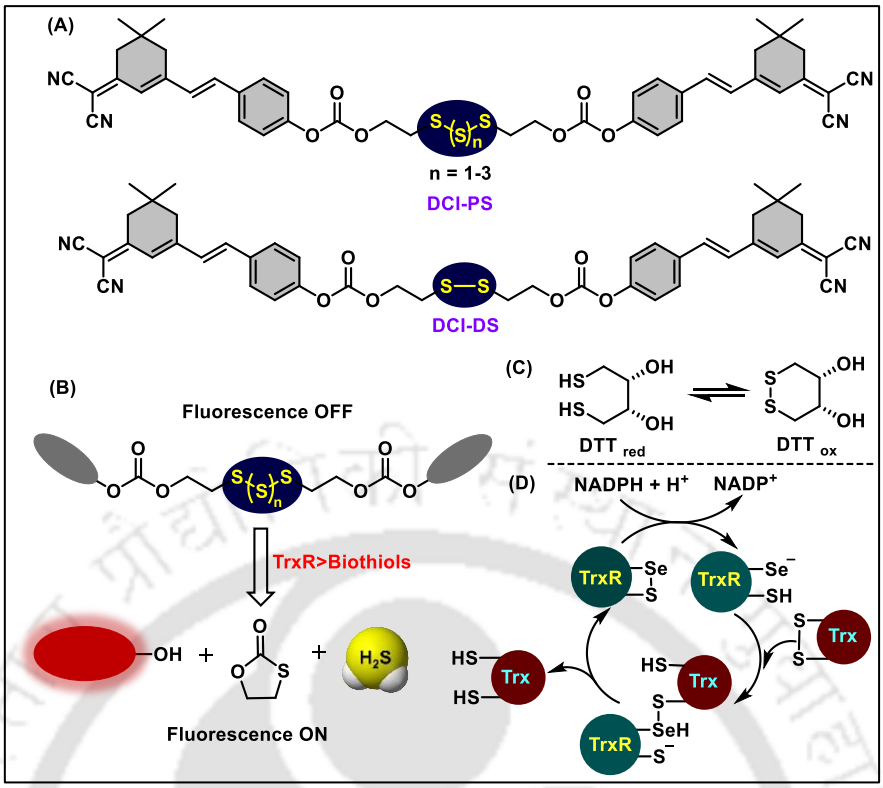

Figure 3.2. (A) Chemical structures of the synthesized self-immolative turn-on fluorogenic probes (**DCI-PS** and **DCI-DS**) emitting in the NIR range. (B) Schematic representation of the bioanalyte–responsive release of the NIR fluorophore along with H_2S from **DCI-PS** (n = 1). (C) Redox process of DTT and oxidized DTT (DTT_{ox}). (D) Proposed catalytic cycle of TrxR for the reduction of Trx in the presence of NADPH.

3.3. Results and discussion

3.3.1. Synthesis of DCI-DS and DCI-PS

The self-immolative NIR probes **DCI-DS** and **DCI-PS** in the present study were synthesized by the coupling of dicyanoisophorone-based fluorophore **DCI-OH** with the alcoholic disulfide **2.16** or polysulfide **2.4-2.6**, respectively, as shown in Scheme 3.1. The NIR fluorogenic dye **DCI-OH** was synthesized from isophorone (**3.1**) in two steps following the literature method.[34] The disulfide probe **DCI-DS** could be prepared in the pure form starting with the pure and commercially available bis(2-hydroxyethyl)disulfide **2.16**. The reaction of disulfide **2.16** with two equiv. of 4-nitrophenyl chloroformate led to the formation of the corresponding carbonate adduct **2.17**. Further reaction of **2.17** with fluorogenic alcohol **DCI-OH** afforded the final disulfide probe **DCI-DS** with the removal of 4-nitrophenol. Unlike the pure disulfide probe **DCI-DS**, the polysulfide analogue **DCI-PS** was prepared from the laboratory-synthesized bis(2-hydroxyethyl) polysulfide **2.4-2.6**. The polysulfide was synthesized from 2-chloroethanol (**2.3**) and disodium polysulfide

(Na_2S_n, n = 2–5). Here, due to the slight difference in polarity of the disulfide with other higher polysulfides, the disulfide component could be purified mostly from the polysulfide alcohol. The reaction of polysulfide **2.4-2.6** with 4-nitrophenyl chloroformate in dry DCM afforded the carbonate intermediate **2.7-2.9**, which upon further reaction with **DCI-OH** led to the formation of the final probe **DCI-PS**. The individual compounds of the final polysulfide probe **DCI-PS** could not be separated due to their very similar polarities. All the intermediates and the final probes were purified and characterized using analytical methods.

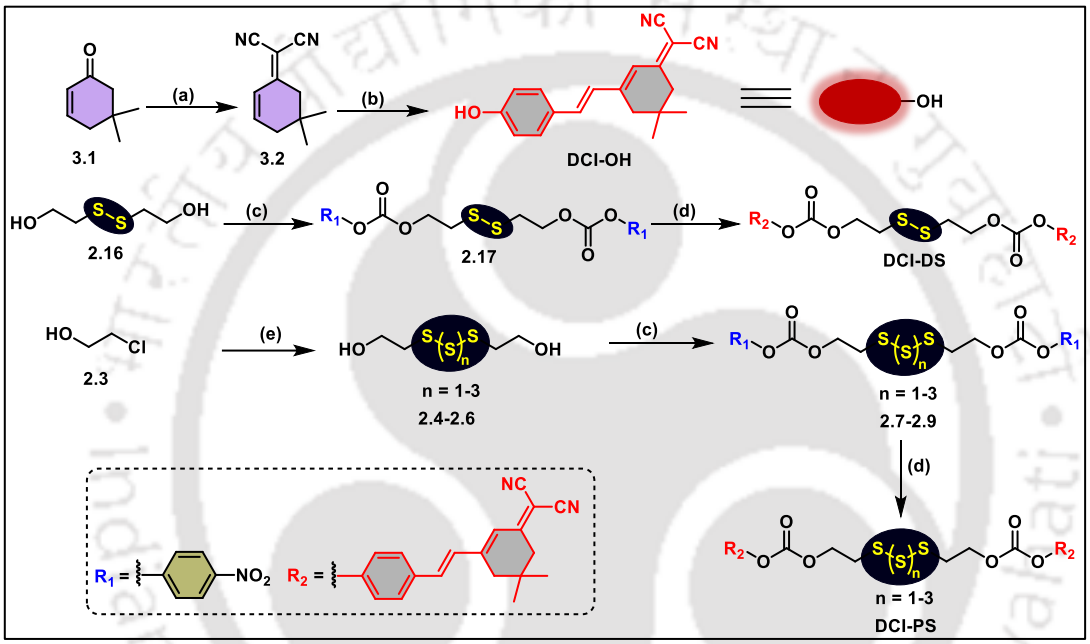

Scheme 3.1. Synthetic strategies to **DCI-OH**, **DCI-DS** and **DCI-PS**. Reagents and conditions: (a) Malononitrile, piperidine, EtOH, 80 °C, 8 h, (b) 4-hydroxybenzaldehyde, piperidine, acetonitrile, 85 °C, 12 h, (c) 4-nitrophenyl chloroformate, pyridine, DCM, 0 °C-RT, 6 h, (d) **DCI-OH**, DIPEA, DCM, 0 °C- RT,16 h, (e) Na_2S_n, (n = 2-5), H_2O, RT, 2 h.

3.3.2. Absorption and emission studies

In general, due to the presence of polysulfide/disulfide linkers, both the probes were expected to be reactive towards thiols. Therefore, the reactivity of the synthesized probes **DCI-DS** and **DCI-PS** towards thiols were studied preliminarily using absorption and emission spectroscopic studies. As shown in Figure 3.3A the polysulfide probe **DCI-PS** showed an absorption band around 414 nm. The absorption pattern after the reaction of **DCI-PS** with reduced glutathione (cellular abundant biothiol) was studied. Interestingly, a slight red shift in the absorbance pattern of the pure **DCI-PS** was observed upon its reaction with GSH with a new hump at around 580 nm. The resultant pattern matched well

with that of the pure released NIR fluorophore (**DCI-OH**). A similar pattern was observed in the presence of other thiols such as Cys and DTT. Interestingly, a more pronounced hump at around 580 nm was observed in the presence of DTT. It should be noted here that the pronounced absorption band at 580 nm and the emission in the NIR range (λ_{em} = 670 nm) was observed in the PBS buffer (20 mM, pH 7.4). in the presence of 50% DMSO.[35] Therefore, the absorption and emission spectra of the released fluorophore **DCI-OH** were collected in PBS with the added DMSO just prior to the measurements. The response of disulfide-based probe **DCI-DS** towards the thiols was also found to be similar (Figure 3.3C).

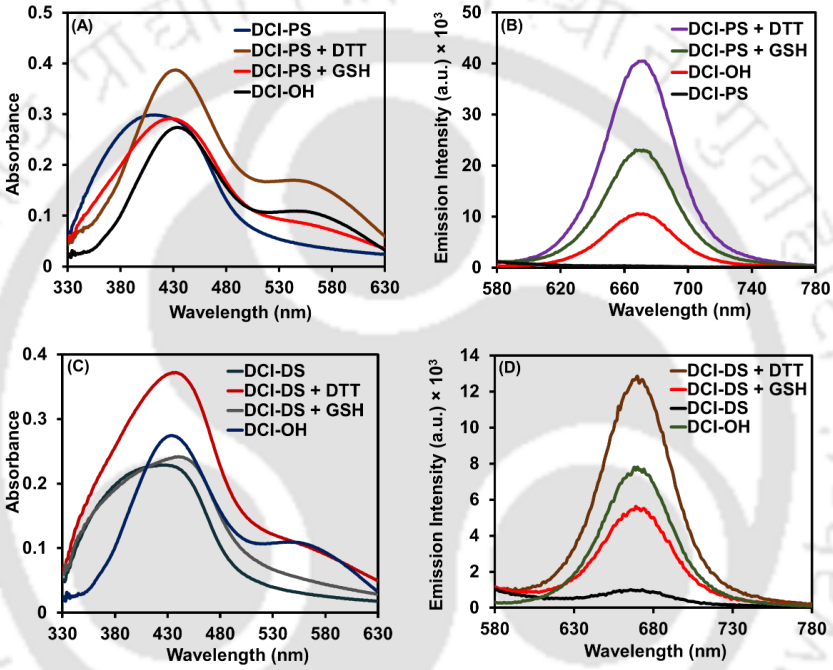

Figure 3.3. (A, C) Absorption and (B, D) emission spectra of **DCI-PS** (5.0 µg/mL) and **DCI-DS** (5.0 µM) in the presence and absence of GSH and DTT (200 µM) in phosphate buffer saline (20 µM) of pH 7.4 in the presence of 50% DMSO. Pure samples of the released fluorophore **DCI-OH** were also analyzed under identical experimental conditions.

With these preliminary results, we have carried out emission experiments with both probes in the presence of biothiols. Considering the absorption band of **DCI-OH** at around 580 nm, the probes were excited at that wavelength for monitoring their reactions with thiols. Interestingly, the reaction of **DCI-PS** (5.0 µg mL^{-1}) and **DCI-DS** (5.0 µM) with different thiols (200 µM) generated new emission bands with the emission maxima at around 670 nm that matched well with the emission spectrum of pure released fluorophore **DCI-OH** (Figures 3.3B and 3.3D). These experiments led to very important preliminary information

that-(a) the emission intensity of **DCI-OH** from the polysulfide probe (**DCI-PS**) was much higher than that of the disulfide probe (**DCI-DS**); (b) both the probes exhibited significantly higher reactivity towards DTT over other thiols such as GSH and Cys. These initial results provided us with the clue for considering TrxR as a superior trigger for the fluorogenic H_2S release from **DCI-PS** than GSH.

3.3.3. Kinetic studies for turn-on fluorescence measurement

With the initial results from UV-Vis and fluorescence spectroscopic studies, the detailed relative reactivity pattern of both the probes towards different thiols was studied with the variation in time and thiol concentration. The comparative emission spectra were monitored over time (60 min) with **DCI-PS** and **DCI-DS** in the presence of DTT and GSH. Interestingly, a significantly higher response for **DCI-PS** over **DCI-DS** was observed for both the thiols used herein over the complete duration (Figure 3.4A). Furthermore, the emission responses of both the probes were found to be significantly higher towards DTT than GSH. To understand the thiol concentration dependency of the probes, the concentration of thiols (0–400 µM) was varied while keeping other parameters constant. Interestingly, a similar trend with exceptionally higher reactivity of **DCI-PS** than **DCI-DS** towards DTT was observed over the entire concentration range of the thiols (Figure 3.4B). The results reveal that, in the presence of DTT, a typical saturation kinetic pattern was observed for the polysulfide probe **DCI-PS** within 15–20 min and at 150 µM concentration of DTT. Furthermore, the results clearly indicated that-(i) the efficiency of the probe can be significantly enhanced by replacing the disulfide unit with the corresponding polysulfide unit; and (ii) the probes could be better responsive towards TrxR compared to the cellular abundant biothiol (GSH).

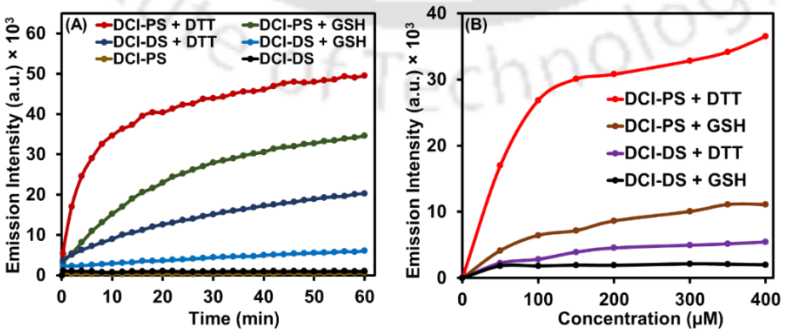

Figure 3.4. (A) Emission spectra of **DCI-PS** (5.0 µg/mL) and **DCI-DS** (5.0 µM) over 60 min in the absence (blank) and presence of DTT and GSH (200 µM). (B) Emission spectra of **DCI-PS** (5.0 µg/mL) and **DCI-DS** (5.0 µM) with increasing concentration of DTT and GSH (0–400 µM) with an incubation time of 20 min in 50% DMSO in PBS at pH 7.4.

3.3.4. Measurement of H_2S release

Based on the higher emission response from **DCI-PS** in the presence of DTT over GSH, the release of H_2S from the probe was measured using conventional methylene blue (MB) assay.[36] Interestingly, a sustained release of H_2S over 120 min was observed with higher intensity in the presence of DTT than in the presence of GSH (Figure 3.5A). The maximum peak intensity was observed after around 30 min and dropped gradually over time.[41] It should be noted here that the H_2S release from **DCI-PS** can be tuned slightly by varying the individual components of the polysulfide during the synthesis of polysulfide alcohol **2.4-2.6**. The evaluation of H_2S release profile of the polysulfide alcohol **2.4-2.6**, prepared from five different synthesized samples, was carried out using MB assay in the presence of DTT. The results showed a similar trend for the H_2S release profile with slight changes in the intensity range (Figure 3.5C).

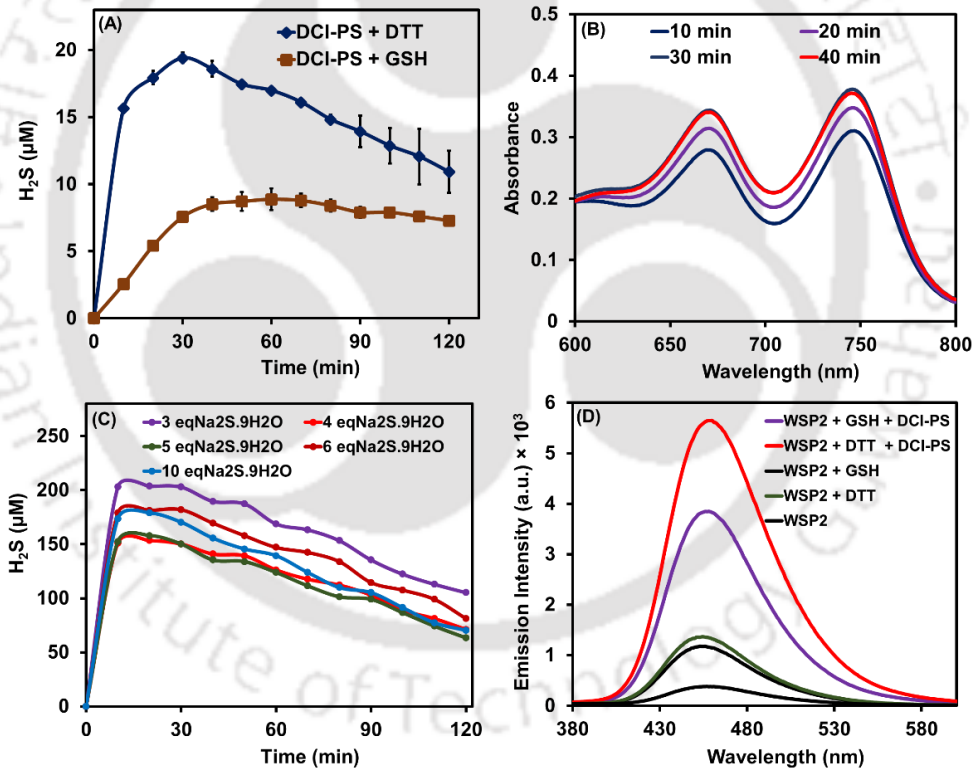

Figure 3.5. (A) The H_2S release profile of **DCI-PS** (25.0 µg/mL) in the presence of DTT and GSH (1.0 mM) over 120 min. (B) Formation of methylene blue for the reaction of **DCI-PS** with DTT. (C) Comparative H_2S release profile of different batches of polysulfide alcohol **2.7-2.9** (25.0 µg/mL) in the presence of DTT (1.0 mM). (D) Fluorescence emission after 60 min from **WSP2** (25.0 µM) in the presence of DTT and GSH (1.0 mM) and **DCI-PS** (25.0 µg/mL) in the presence of DTT/GSH (1.0 mM).

As the H_2S estimation using MB assay is not completely quantitative in nature, H_2S release was further confirmed using the reported nucleophilic substitution–cyclization-based turn-on fluorescent probe **WSP2**.[37] To identify and exclude the background reaction of **WSP2** with thiols (DTT and GSH), **WSP2** was first incubated with the thiols for 60 min and the emission response was measured. Interestingly, a further enhancement of emission intensity in the presence of **DCI-PS** + thiol indicated the desired superior reactivity of **WSP2** with the released H_2S from **DCI-PS** (Figure 3.5D). These observations clearly reveal the nucleophilic biothiol-triggered donation of H_2S from **DCI-PS**.

3.3.5. Reaction of DCI-PS with bio-analytes

With the basic spectroscopic and kinetic results for the fluorogenic H_2S release from **DCI-PS,** we proceeded to identify the best bio-analyte for the triggered fluorogenic process. The turn-on fluorescence emission intensity was measured after the reaction of **DCI-PS** (5.0 μg mL^{-1}) in the presence of different bio-analytes (200 μM) after incubation for 15 min. As shown in Figure 3.6A, very low emission with most of the non-thiol analytes and relatively higher emission with thiol-based analytes such as thiophenol, 2-mercaptoethanol, sodium sulfide, glutathione, Cys, TCEP (tris(2-carboxyethyl) phosphine) and DTT was observed. Interestingly, while the probe was better reactive towards all the thiol-containing analytes, the highest response was observed in the presence of DTT. Furthermore, a significantly higher emission response was observed with DTT at 200 μM compared to the emission intensity with a large excess of GSH (2.0 mM, data not shown). This observation indicated the high possibility of having even more nucleophilic intracellular bio-analytes (mimicked by DTT) than GSH for triggering the fluorophore release from the probe.

3.3.6. Reactivity of DCI-PS with cellular proteins

As **DCI-PS** was highly reactive towards DTT that contains two very nearby thiol groups in a single molecule, this arrangement was correlated in the protein environment (having nearby Cys/Cys or Cys/selenocysteine (Sec) residues) and the examples were GR and TrxR. Therefore, to understand the reactivity of **DCI-PS** towards highly nucleophilic (Cys- and Sec-containing) proteins in addition to the small-molecule biothiols, the turn-on fluorescence emission was studied in the presence of several purified proteins such as GR, GP_x and BSA as well as the cell lysate of MDA-MB-231 cells (for TrxR activity). The proteins such as GR, GP_x and BSA were chosen in this study as they contained highly reactive and nucleophilic thiol/selenol groups. However, as shown in Figure 3.6B, the

emission response was insignificant in the presence of these nucleophilic proteins in the presence of their associated co-factors. Interestingly, a significantly higher emission response was observed in the presence of cell lysate. The lysate of human triple-negative breast cancer cells (MDA-MB-231) was chosen as the antioxidant proteins such as GR, GP_x and TrxR are reported to be overexpressed in this cell line.[38-40] The reactivity of **DCI-PS** with TrxR was explored using the cell lysate in the presence of NADPH that acts as a co-factor of TrxR. As the probe was almost unreactive towards the pure antioxidant proteins (GR and GP_x), TrxR was considered as the possible protein– analyte of the target in the cell lysate. To understand this further, identical experiments were performed and the emission response was measured in the presence of reported and selective small-molecule inhibitors of TrxR such as ebselen, 2,4- dinitrochlorobenzene (DNCB) and triphenylphosphinegold(I) chloride (Figures 3.6C and 3.6D).[41,42-44] Interestingly, as anticipated, the cell lysate-mediated emission intensity from **DCI-PS** was significantly decreased in the presence of the inhibitors (Figure 3.6C). These observations revealed very likely participation of TrxR for the fluorescence turn-on from **DCI-PS** as compared to the basal reactivity towards GSH or other small-molecule biothiols. Indeed, this is not surprising as (a) the structure of **DCI-PS** or **DCI-DS** highly resembles the structures of reported fluorogenic probes of TrxR having cyclic disulfide (**TRFS-green** and **FAST-TRFS**) or acyclic diselenide unit (**Probe 1a**) (Figure 3.1B);[24,28,45] (b) the nucleophilicity of the selenol group of reduced TrxR must be much higher than that of the thiol group of GSH. However, unlike other related antioxidant proteins such as GR and GP_x, the direct reactivity of **DCI-PS** towards purified TrxR could not be explored due to the non-availability of the pure protein from commercial suppliers at reasonable/affordable prices.

3.3.7. pH variation studies of DCI-PS and DCI-DS with DTT

The stability of the probes (**DCI-PS** and **DCI-DS**) and their relative reactivities towards DTT over a range of pH (5 to 9) were studied in a PBS buffer with 20% DMSO to understand the applicability of the probes under physiological conditions. The emission response from the probes in the presence of DTT at the NIR region (670 nm) was found to be very low at a pH range of 5 to 7 and the intensity increased at a higher pH range as shown in Figure 3.6E. Interestingly, while the intensity increased rapidly with the increase in pH up to pH 9 for the polysulfide probe (**DCI-PS**), the increase was found to be nominal for the corresponding disulfide probe (**DCI-DS**). These results further support the significantly higher sensitivity of **DCI-PS** over **DCI-DS**. A significantly higher emission intensity at λ_{max} = 670 nm at higher pH is likely due to the existence of the released

fluorophore **DCI-OH** in the deprotonated phenolate form that emits in the red region Furthermore, in the absence of DTT, emission from the pure probes **DCI-PS** and **DCI-DS** were found to be very low in the entire pH range, indicating high stability of the probes over the complete pH range.

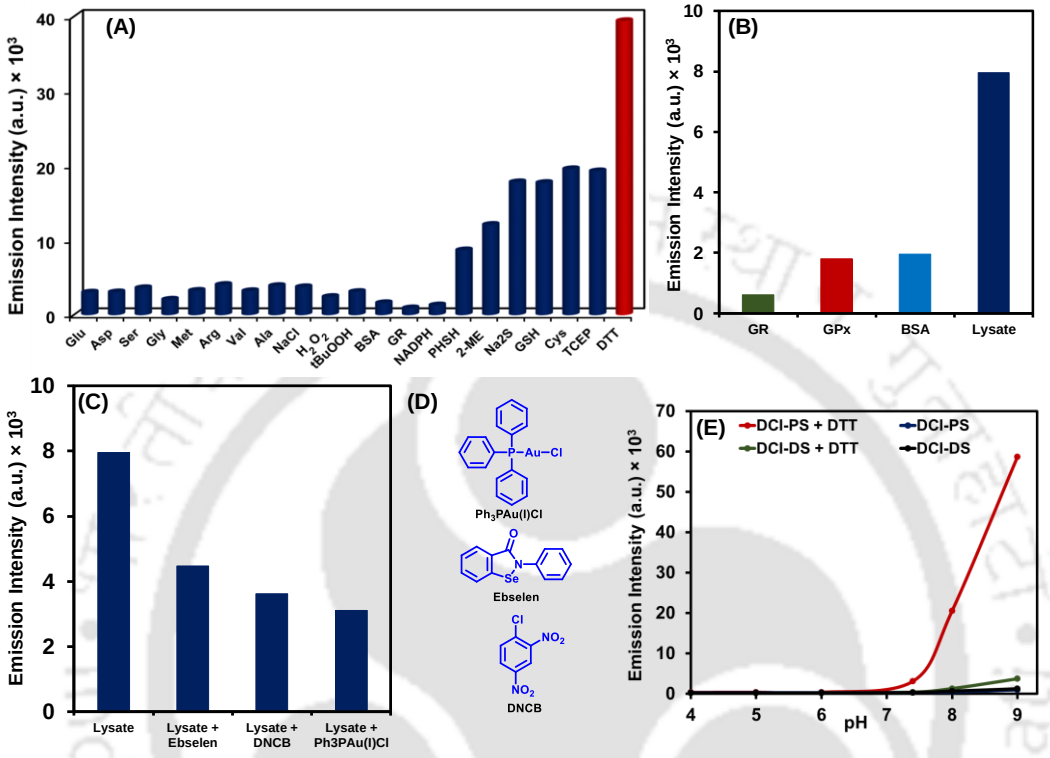

Figure 3.6. (A) Emission intensity of **DCI-PS** (5.0 µg/mL) upon the addition of various small-molecule non-thiol and thiol analytes (200 µM). (B) Cys/ Sec-containing proteins such as GR (2.0 units/mL), GPx (1.0 unit/mL), BSA (3.0 µM) and cell lysate of MDA-MB-231 cells (30 µL). NADPH (200 µM) was used along with GR, GP_x and cell lysate as a co-factor. (C) Inhibition of the cell lysate (30 µL) mediated emission from **DCI-PS** (5.0 µg/mL) using TrxR-selective inhibitors such as Ebselen (5.0 µM), DNCB (20.0 µM) and Ph_3PAuCl (5.0 µM) in the presence of NADPH (200 µM) after an incubation of 15 min. (D) Chemical structures of the potent and selective inhibitors of TrxR. (E) pH-dependent emission response from **DCI-PS** (5.0 µg/mL) and **DCI-DS** (5.0 µM) in the presence and absence of DTT (200 µM) in 20% DMSO in PBS.

3.3.8. HPLC studies

The mechanistic pathways for the release of H_2S from **DCI-PS** and **DCI-DS** were investigated using the reverse phase HPLC method and ESI-MS analysis. Reactions of the pure **DCI-DS** with PhSH was studied initially and the possible intermediates and products were analyzed using the reverse phase HPLC method (Figure 3.7). An equimolar ratio of

DCI-DS (13.2 min) and PhSH (4.7 min) reacted to generate two new peaks (at 12.5 min and 13.4 min) along with the peaks corresponding to PhSSPh (10.3 min) and the released fluorophore **DCI-OH** (5.4 min). The newly generated peaks could be assigned to the intermediates **3.4** and **3.5**, respectively. The peak intensity of the intermediates diminished in the presence of PhSH (5.0 equiv) with the predominant formation of the released fluorophore **DCI-OH**. The formation of unsymmetrical disulfide intermediate **3.4** was further confirmed from the ESI-MS analysis. With this information in hand, the reaction of **DCI-PS** with PhSH was studied. From the chromatogram of only **DCI-PS**, it was understandable that the probe contained four peaks, which could be assigned to the symmetrical disulfide, trisulfide, tetrasulfide and pentasulfide. The reaction of an equimolar amount of **DCI-PS** and PhSH generated the released fluorophore **DCI-OH** along with a series of new peaks of intermediates that did not overlap with the peaks of the polysulfide components of **DCI-PS** (Figure 3.8). The chromatogram became simplified in the presence of higher equiv. (5.0 equiv) of PhSH. Although, the newly generated peaks of the intermediates could not be identified and assigned to the specific unsymmetrical polysulfide analogues with PhSH, their presence could be evidenced in ESI-MS spectra. The reaction of **DCI-PS** and **DCI-DS** with DTT were also studied and analyzed using the HPLC method and, mostly the final released fluorophore was found to be the predominant species with traces of the intermediates (data not shown). The non-existence of unsymmetrical polysulfide intermediates with DTT could be likely due to the feasible intramolecular nucleophilic attack of the free thiol group of DTT to S-center of mixed polysulfide bond with the formation of oxidized DTT (DTT_{ox}).

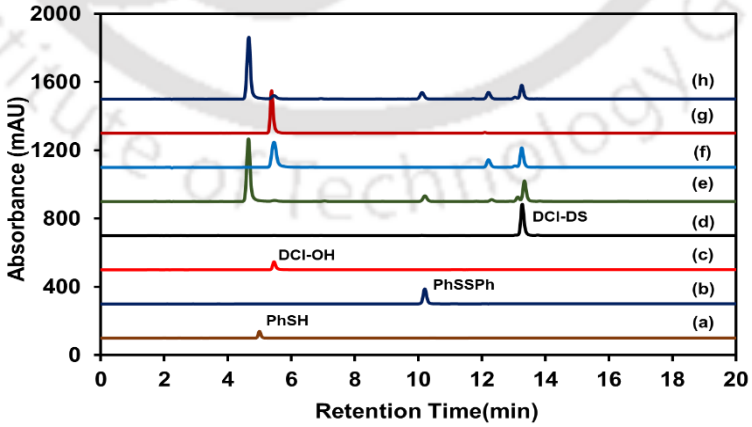

Figure 3.7. HPLC chromatogram (0 - 20 min) for the reaction of **DCI-DS** with PhSH. Lines: (a) PhSH; (b) PhSSPh; (c) **DCI-OH**; (d) **DCI-DS**; (e) **DCI-DS** + PhSH 1:1 @254 nm; (f) **DCI-DS** + PhSH 1:1 @433 nm; (g) **DCI-DS** + PhSH 1:5 @433 nm; (h) **DCI-DS** + PhSH 1:5 @254 nm.

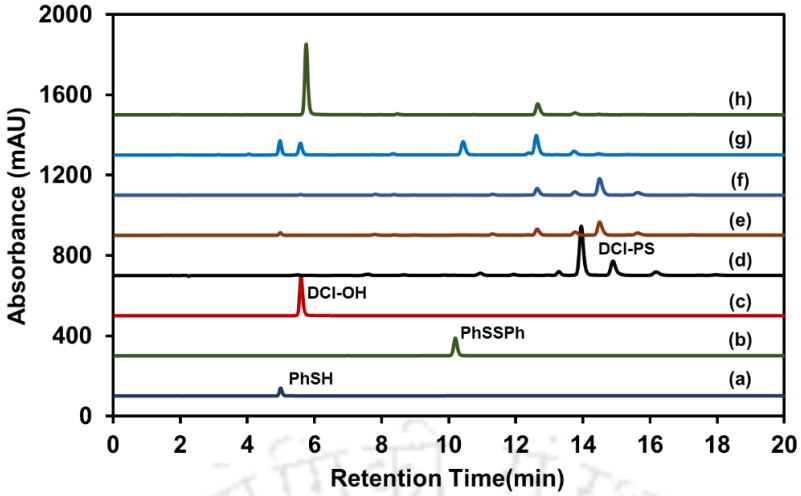

Figure 3.8. (A) Reverse-phase HPLC chromatogram for the reaction of **DCI-PS** with PhSH. Legend: (a) PhSH; (b) PhSSPh; (c) **DCI-OH**; (d) **DCI-PS**; (e) **DCI-PS** + PhSH (1:1) at 254 nm; (f) **DCI-PS** + PhSH (1: 5) at 254 nm; (g) **DCI-PS** + PhSH (1:1) at 433 nm; (h) **DCI-PS** + PhSH (1:5) at 433 nm.

3.3.9. Mechanistic insights

Based on the results from HPLC, plausible mechanistic pathways were proposed for the biothiol-triggered self-immolative turn-on fluorogenic process from **DCI-DS** and **DCI-PS** (Scheme 3.2A and 3.2B). For example, the reaction of **DCI-DS** with RSH would generate intermediates **3.4** and **3.5**. While **3.5** would self-immolate with the release of fluorophore **DCI-OH**, intermediate **3.4** may react with another RSH to generate intermediate **3.5** (Scheme 3.2A). Unlike **DCI-DS**, the polysulfide probe **DCI-PS** would release H_2S with the concomitant release of the fluorophore with the generation of mixed polysulfide (**3.6**) and persulfide (**3.7**) intermediates (Scheme 3.2B). While the reaction pathway with PhSH would resemble the small-molecule biothiol-triggered turn-on fluorogenic processes, the reaction pattern with DTT may fit well with the TrxR-triggered process (Scheme 3.2C). It should be noted that the TrxR-triggered process would be more simplified as the generated unsymmetrical selenopolysulfide intermediate **3.8** may undergo intramolecular cyclization to generate the persulfide intermediate **3.9** with the regeneration of TrxR. A subsequent reaction of **3.9** with the reduced TrxR may release H_2S along with the formation of selenenyl sulfide intermediate **3.10**, which would finally release the fluorophore **DCI-OH**.

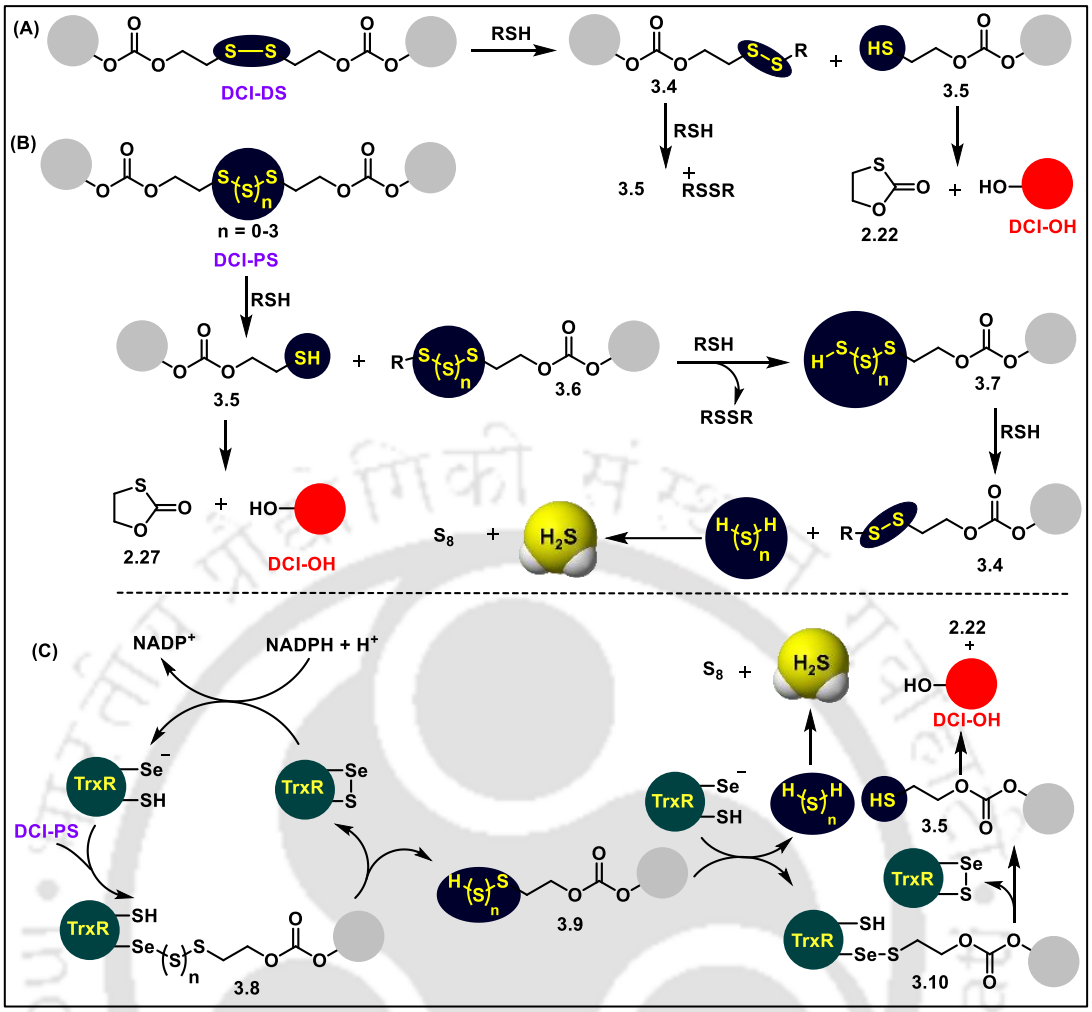

Scheme 3.2. Proposed mechanistic outlines for the biothiol-triggered release of (A) **DCI-OH** from **DCI-DS**, and (B) **DCI-OH** and H_2S from **DCI-PS**, (C) Proposed pathway for the TrxR-triggered release of **DCI-OH** and H_2S from **DCI-PS**.

3.3.10. Anti-proliferative activity of DCI-PS and DCI-DS

After getting all the analytical data from various spectroscopic techniques, we evaluated the toxicity profile of the synthesized probes. The dose-dependent toxicity profile of the probes was studied first to evaluate their compatibility with the cellular medium by incubating over 48 h. Interestingly, both **DCI-PS** (5.0, 10.0, and 25.0 µg/mL) and **DCI-DS** (5.0, 10.0, and 25.0 µM) were found to be non-toxic in MDA-MB-231 cells. Both the probes **DCI-DS** (5.0, 10.0, and 25.0 µM) and **DCI-PS** (5.0, 10.0, and 25.0 µg/mL) were found to be non-toxic in MDA-MB-231 cells as shown in Figure 3.9.

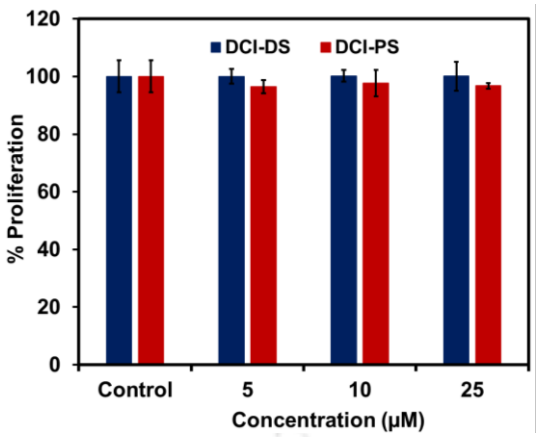

Figure 3.9. Dose-dependent anti-proliferative activities of **DCI-DS** (5.0, 10.0, and 25.0 μM) and **DCI-PS** (5.0, 10.0, and 25.0 μg/mL) in MDA-MB-231 cell line over 48 h.

3.3.11. Fluorescence microscopic studies of DCI-PS and DCI-DS

The fluorescence imaging experiments of the synthesized probes were performed in MDA-MB-231 cells. The cultured cells were incubated with the probes **DCI-PS** (5.0 μg/mL) and **DCI-DS** (5.0 μM) for 2 h and the emission was measured using a fluorescence microscope. Interestingly, red-coloured cells were observed with a good signal-to-noise ratio for both the probes, however, the intensity of the released fluorophore was found to be significantly higher for **DCI-PS** than **DCI-DS** under the identical condition (Figure 3.10). This is expected as the **DCI-PS** having polysulfide linkage is more electrophilic than the disulfide linker in **DCI-DS**, facilitating the nucleophilic attacks from intracellular nucleophilic thiol/selenol analytes.

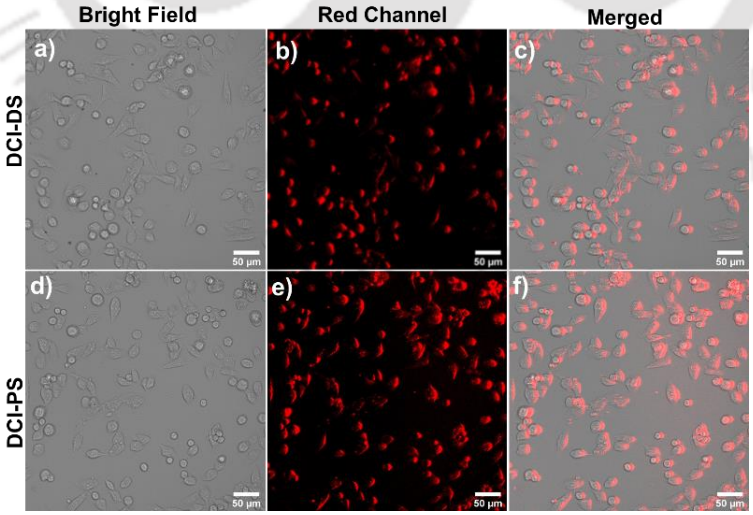

Figure 3.10. Fluorescence microscopy images (bright field, red channel and merged) of MDA-MB-231 cells for the endogenous bio-analyte-triggered release of **DCI-OH** from **DCI-DS** (a–c) and **DCI-PS** (d-f). The scale bar represents 50 μm.

3.3.12. Fluorescence microscopic images of DCI-PS in the presence of inhibitors

The contribution of the cellular protein/non-protein biothiols or selenols for the above process was confirmed by the pre-treatment of cells with a large concentration of N-ethylmaleimide (NEM, 2.0 mM) followed by the incubation with **DCI-PS**. Very negligible emission intensity in the red channel indicates the prior scavenging of intracellular protein and non-protein thiols/selenols by NEM. Similarly, the contribution of TrxR for the turn on fluorogenic process was studied upon the pre-treatment of cells with the reported selective inhibitors of TrxR such as ebselen, 2,4-dinitrochlorobenzene (DNCB) and triphenylphosphinegold(I) chloride (Ph_3PAuCl) followed by the addition of **DCI-PS**.[39,43,46,47] Interestingly, a significantly lower emission intensity from **DCI-PS** was observed when the cells were pre-treated with DNCB (10.0 µM) and Ph_3PAuCl (2.0 µM) as compared to the emission from **DCI-PS** alone (Figure 3.11). These results provide very good support for the TrxR-triggered turn-on fluorogenic processes in the synthesized probes. However, in addition to TrxR, the basal reaction of the probes with cellular abundant GSH should also be considered for the overall fluorogenic H_2S release process in cellular and *in vivo* systems.

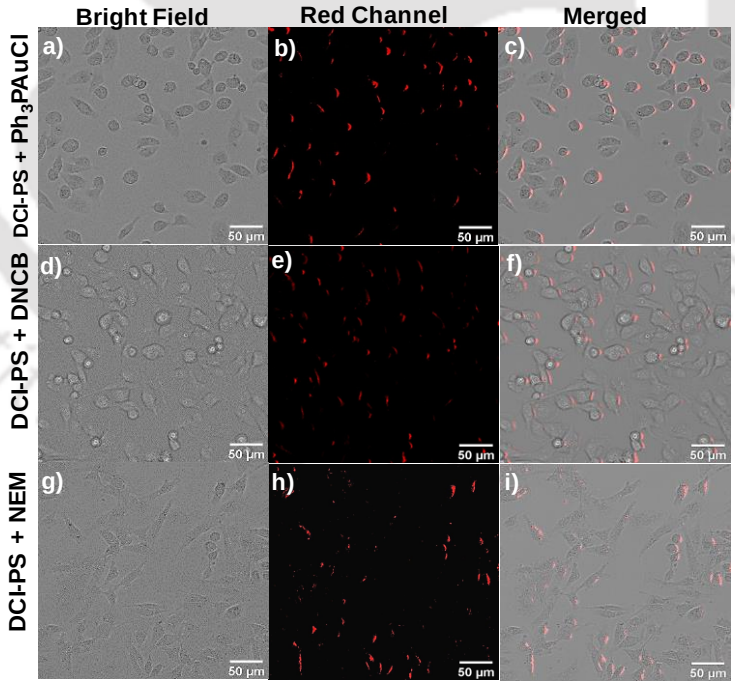

Figure 3.11. (A) Fluorescence microscopy images (bright field, red channel and merged) of MDA-MB-231 cells for the inhibition of TrxR-triggered release of **DCI-OH** from **DCI-PS** using PPh_3AuCl (2.0 µM, a–c) and DNCB (10.0 µM, d–f) and NEM (2.0 mM, g-i). The scale bar represents 50 µm.

3.3.13. Fluorescence microscopic images for H_2S release from DCI-PS

With the confirmation of fluorophore release from the probes in the cellular medium, the intracellular release of H_2S from the polysulfide probe (**DCI-PS**) was studied using the literature reported standard H_2S-sensitive probe **WSP2**.[37] The nucleophilic substitution–cyclization-based fluorescent probe **WSP2** was chosen here as- (i) this is more selective towards H_2S with minimum interference from thiols, and (ii) the emission range from **WSP2** (blue) does not overlap with that of the released fluorophore **DCI-OH** (red) from the probe **DCI-PS**. When the cells were incubated with **WSP2**, weaker fluorescence emission was observed in the blue channel, which could be due to its reaction with the endogenous H_2S (Figure 3.12A). Interestingly, a significant enhancement in the turn-on emission intensity from **WSP2** in the **DCI-PS** pre-treated cells indicates the additional release of H_2S from **DCI-PS** by the intracellular triggers. The released H_2S from **DCI-PS** undertakes nucleophilic attack at the sulfur center in **WSP2** leading to the cyclization and release of free umbelliferone with blue emission (Figure 3.12B).

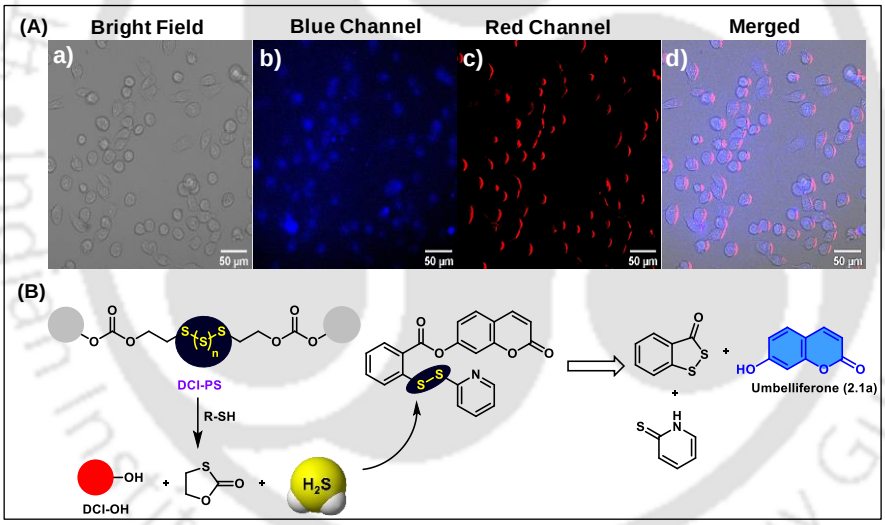

Figure 3.12. (A) Schematic representation and (B) fluorescence microscopy images (bright field, blue channel, red channel and merged) for the detection of released H_2S from **DCI-PS** in MDA-MB-231 cells using the H_2S-selective turn-on fluorogenic probe **WSP2**. The scale bar represents 50 µm.

3.3.14. Binding studies of DCI-PS with TrxR protein

With the positive experimental results of efficient cleavage of **DCI-PS** by the cell lysate and its inhibition in the presence of reported specific inhibitors of TrxR, we have carried out protein-ligand docking studies to understand the binding affinity of the probes towards TrxR1 (PDB: 1H6V). Interestingly, as shown in Figure 3.13, both the probes reached the

active site of TrxR1 and the cleavable disulfide/ polysulfide linkers were in closer proximity (<10 Å) to the active site Sec residue (Sec 498a) of TrxR1. Furthermore, the binding affinity of the synthesized probes towards TrxR1 was found to be strong enough with good binding energy (ΔG_{bind}). The binding energy was relatively higher for polysulfide (**DCI-PS**, n = 3, 4 and 5) as compared to the disulfide analogue (**DCI-DS**) (Table 3.1). Furthermore, the results of this docking study were comparable to the affinity of the recently reported TrxR-sensitive diselenide **Probe 1a** (Figure 3.1B).[24] Interestingly, the observations from all the experimental and theoretical studies collectively provide a sufficient body of evidence for the predominant contribution/participation of TrxR for the turn-on fluorogenic processes for the sustained release of H_2S with concomitant release of NIR fluorophore. The involvement of TrxR is not only beneficial for the sustained donation of H_2S for the H_2S-mediated therapeutics in disease models, but the strategy can also be useful for estimating the relative cellular expression level of TrxR in different organ-specific cancers as well as inflammatory diseases with the highly tissue-penetrating NIR dye. However, our limitation in the present study is the unavailability of a purified TrxR/Trx system for direct reactivity with the developed probes.

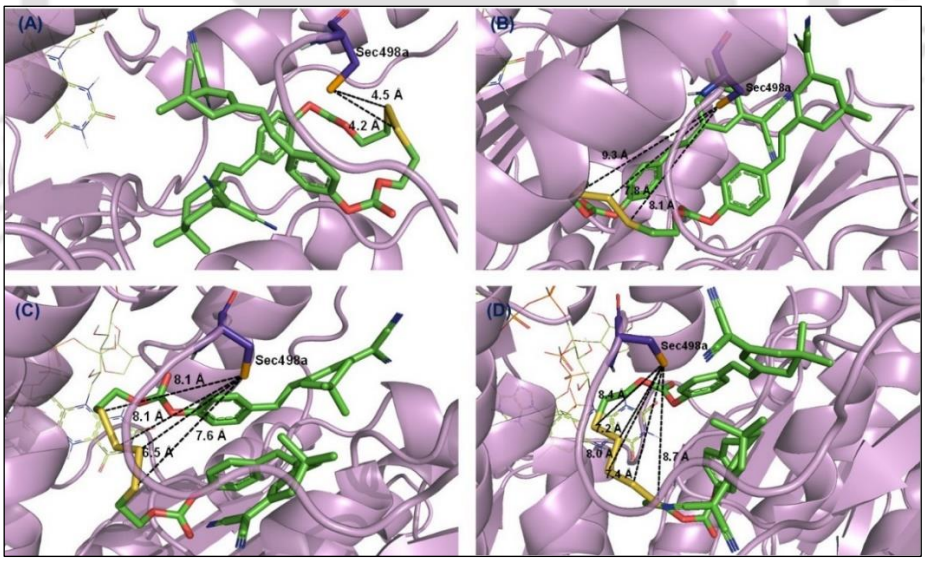

Figure 3.13. Protein-ligand binding interactions of **DCI-DS** and **DCI-PS** (n = 3, 4, 5) at the active site of TrxR1 (PDB: 1H6V). The distances between the Se atom of the Sec 498a residue of TrxR1 and the sulfur atoms of the probes are shown in the images. (A) **DCI-DS**; (B) **DCI-PS** (n = 3, trisulfide); (C) **DCI-PS** (n = 4, tetrasulfide); (D) **DCI-PS** (n = 5, pentasulfide).

Table 3.1. Summary of distances of various sulfur atoms of the ligands with the selenium centre of TrxR1 at the active site and the list of proximal amino acid residues with which the ligands have non-bonding interactions.

Probes	Binding Energy (ΔG_{bind}) (kcal/mol)	Distance of S of ligands from the Se of Sec498 of TrxR (Å)	Amino acids involved in non-bonding interactions
DCI-DS	-8.3	4.2, 4.5	K29, Y116, S404, W407, H472, G496
DCI-PS (trisulfide)	-9.2	7.8, 8.1, 9.3	K33, K123, S404, F406, W407, L409, H472, V474, S483
DCI-PS (tetrasulfide)	-8.7	6.5, 7.6, 8.1, 8.1	K33, Y116, R351, W407, N419, H472, G499
DCI-PS (pentasulfide)	-9.4	7.2, 7.4, 8.0, 8.4, 8.7	S22, K29, Y116, W407, L409, N418, V474, E477, Q494, G496

3.4. Conclusion

In summary, the rational design and synthesis of TrxR responsive organopolysulfide-based fluorogenic donor of H_2S, **DCI-PS** with concomitant release of NIR fluorophore are described. A disulfide-probe **DCI-DS** capable of releasing the NIR fluorophore without H_2S was also rationally designed and synthesized for comparative reactivity. Model spectroscopic and kinetic studies with DTT (for TrxR activity) revealed its much higher reactivity towards **DCI-PS**/**DCI-DS** as compared to the cellular abundant biothiol GSH. Considering the overexpression of mammalian TrxR in different organ-specific cancers, the turn-on fluorogenic H_2S donation process from the cellular non-toxic **DCI-PS** was studied in a representative breast cancer cell line (MDA-MB-231) for the sustained donation of H_2S with concomitant release of red-emitting NIR fluorophore. The participation of TrxR was further supported by the significant inhibition of the fluorogenic process in the presence of TrxR-selective small-molecule inhibitors and by the significant binding affinity of **DCI-PS** with TrxR1 as predicted by the protein–ligand docking study. The antioxidant enzyme (TrxR)-triggered self-immolative cyclization process with the sustained release of H_2S with turn-on NIR fluorophore will certainly find wider biomedical applications in near future, particularly for the H_2S-mediated therapeutics.

3.5. Experimental Section

3.5.1. Materials and methods

All the reagents were purchased either from Sigma Aldrich or from reputed local suppliers and used without further purification unless otherwise stated. Thin layer chromatographic (TLC) analyses were carried out on pre-coated silica gel on aluminium sheets and the compounds were visualized by irradiating with UV or fluorescent light. Organic solvents used for chromatographic separations were distilled before use. The melting point of the synthesized compounds was recorded in a Büchi B540 melting point apparatus and the values are uncorrected. NMR spectra (^{1}H and ^{13}C) were recorded on Bruker (400 or 600 MHz) NMR spectrometers and the chemical shifts are cited with respect to TMS (Me_4Si) as an internal standard. Mass spectra were obtained using an Agilent 6520 Accurate-Mass Quadrupole Time-of-Flight (Q-TOF) LC/MS spectrometer.

Synthesis of compound 3.2: This compound was prepared using a literature report.[34] To a solution of compound **3.1** (0.20 g, 1.47 mmol) and malononitrile (0.11 g, 1.72 mmol) in absolute ethanol was added piperidine (0.01 g, 0.15 mmol) and acetic acid (0.09 g, 0.15 mmol) under argon atmosphere. The reaction mixture was refluxed at 90 °C for 12 h upon which the reaction mixture turned dark black in colour. The progress of the reaction was monitored by TLC analysis. After completion, the mixture was cooled to room temperature, the solvent was evaporated under reduced pressure, and the residue obtained was dissolved in CH_2Cl_2. The organic layer was washed with water, brine and dried over anhydrous sodium sulfate. The solvent was evaporated to afford the crude product as a white solid, which was purified by silica gel column chromatography using pet ether and dichloromethane as eluents to afford the pure product **3.2** as a white solid. R_f = 0.5 (20% dichloromethane in pet ether). Yield: 74% (0.20 g). ^{1}H NMR (600 MHz, $CDCl_3$): δ (ppm) = 6.61 (s, 1H), 2.50 (s, 2H), 2.18 (s, 2H), 2.02 (s, 3H), 1.00 (s, 6H). ^{13}C NMR (150 MHz, $CDCl_3$): δ (ppm) = 170.5, 159.9, 120.6, 113.2, 112.4, 78.2, 45.6, 42.6, 32.4, 27.8, 25.3.

Synthesis of DCI-OH: This compound was prepared using literature report.[34] To a solution of 4-hydroxybenzaldehyde (0.20 g, 1.07 mmol) in acetonitrile (20 mL) was added compound **3.2** (0.14 g, 1.18 mmol) and piperidine (10 µl, 0.10 mmol). The mixture was heated to reflux at 90 °C for 5 h under an inert atmosphere and the reaction mixture turned red in colour. Progress of the reaction was monitored by TLC analysis. Upon completion, the solvent was removed under reduced pressure. The resulting residue was dissolved in dichloromethane, washed with water and dried over anhydrous sodium sulfate. The crude

product was purified by silica gel column chromatography using methanol and dichloromethane as eluents to afford the pure **DCI-OH** as dark orange solid. R_f = 0.5 (30% ethyl acetate in pet ether). Yield: 41% (0.20 g). ^{1}H NMR (600 MHz, $CDCl_3$): δ (ppm) = 7.42 (d, *J* = 8.4 Hz, 2H), 7.01 (d, *J* = 16.2 Hz, 1H), 6.87-6.84 (m, 3H), 6.79 (s, 1H), 2.59 (s, 1H), 2.46 (s, 1H), 1.07 (s, 3H). ^{13}C NMR (150 MHz, $CDCl_3$): δ (ppm) = 169.5, 157.2, 154.4, 136.9, 129.4, 128.6, 127.0, 122.8, 116.1, 113.7, 112.9, 77.7, 43.0, 39.2, 32.0, 28.0.

Compound 2.17:[48] To a solution of compound **2.16** (0.20 g, 1.30 mmol) in anhydrous dichloromethane (6.0 mL) was added pyridine (0.50 mL, 6.40 mmol) and the mixture was cooled to 0 °C. To the above mixture, a solution of 4-nitrophenyl chloroformate (0.60 g, 3.20 mmol) in anhydrous dichloromethane was added dropwise at 0 °C. The reaction mixture was then allowed to attain room temperature and stirred for 6 h. The progress of the reaction was monitored by TLC analysis. Upon completion, the mixture was diluted with dichloromethane and the mixture was sequentially washed with saturated $NaHCO_3$ (10.0 mL), water (10.0 mL), 10% citric acid (10.0 mL), water (10.0 mL) and brine (10.0 mL). The organic layer was dried over anhydrous sodium sulfate and the solvent was evaporated under reduced pressure to afford compound **2.17** as white solid. The crude residue was purified by silica gel column chromatography using ethyl acetate and pet ether as eluents to obtain pure compound **2.17** as white solid. R_f = 0.5 (30% ethyl acetate in pet ether) Yield: 62% (0.40 g). ^{1}H NMR (400 MHz, $CDCl_3$): δ (ppm) = 8.28 (d, *J* = 9.1 Hz, 4H), 7.39 (d, *J* = 9.2 Hz, 4H), 4.57 (t, *J* = 6.5 Hz, 4H), 3.08 (t, *J* = 6.5 Hz, 4H). ^{13}C NMR (100 MHz, $CDCl_3$): δ (ppm) = 155.3, 152.3, 145.5, 125.4, 121.8, 66.7 and 36.8. ESI-MS *m/z* calcd. for $C_{14}H_{16}N_2O_{10}S_2$ $[M + K]^+$ = 522.9883, obs. = 522.9885.

Synthesis of DCI-DS: To a solution of **DCI-OH** (0.25 g, 0.87 mmol) in anhydrous dichloromethane (10.0 mL) at 0 °C under an inert atmosphere was added DIPEA (0.27 g, 2.06 mmol) and the mixture was stirred at 0 °C for 10 min. A solution of compound **2.17** (0.20 g, 0.41 mmol) in anhydrous dichloromethane (5.0 mL) was added to the mixture in a dropwise manner and the reaction mixture was allowed to attain room temperature and stirred for 16 h. The progress of reaction was monitored by TLC analysis. Upon completion, the reaction mixture was poured into water and extracted with dichloromethane. The combined organic layer was washed with brine solution, dried over anhydrous sodium sulfate and concentrated under reduced pressure to afford the crude product as yellow solid. The crude compound was purified by silica gel column chromatography using ethyl acetate and pet ether as eluents to afford the pure **DCI-DS** as

yellow solid. R_f = 0.3 (35% ethyl acetate in pet ether). Yield: 15 % (0.05 g), M.P. = 101-103 °C. ^{1}H NMR (400 MHz, $CDCl_3$): δ (ppm) = δ 7.53 (d, *J* = 8.4 Hz, 4H), 7.23 (d, *J* = 8.4 Hz, 4H), 7.02 (d, *J* = 16.4 Hz, 2H), 6.93 (d, *J* = 16.4 Hz, 2H), 6.83 (s, 2H), 4.54 (t, *J* = 6.4 Hz, 4H), 3.07 (t, *J* = 6.4 Hz, 4H), 2.60 (s, 2H), 2.46 (s, 2H), 1.08 (s, 12H). ^{13}C NMR (100 MHz, $CDCl_3$): δ (ppm) = 169.2, 153.5, 153.1, 151.7, 135.5, 133.7, 129.6, 128.7, 123.9, 121.6, 113.4, 112.6, 79.0, 66.4, 43.0, 39.2, 36.9, 32.0, 28.0. ESI-MS *m/z* calcd. for $C_{44}H_{46}N_5O_6S_2$ $[M + Na]^+$ = 809.2443, obs. 809.2449.

Compound 2.4-2.6:[49] To a solution of sodium sulfide nonahydrate (0.70 g, 3.10 mmol) in deionized water (12.0 mL) was added sulfur powder (0.20 g, 0.80 mmol) and the reaction mixture was stirred for 2.5 h at room temperature during which the solution turned reddish brown indicating the formation of Na_2S_n (n = 2, 3, 4, 5) with Na_2S_3 as the major component. To the above solution, 2-chloroethanol (0.40 mL, 6.20 mmol) was added and the reaction mixture was stirred for 6 h at room temperature. Progress of the reaction was monitored by TLC analysis. Upon completion, the aqueous layer was extracted with ethyl acetate. The combined organic layer was washed with brine solution and dried over anhydrous sodium sulfate. The solvent was evaporated under reduced pressure to afford polysulfide **2.6-2.8** as faint yellow oil with almost quantitative yield. The inseparable polysulfide was used directly for the next step without any further purification. R_f =0.45 (45% ethyl acetate in pet ether). ^{1}H NMR (600 MHz, $CDCl_3$): δ (ppm) = 4.00-3.98 (m, overlap of two triplets for O-CH2- group of trisulfide, tetrasulfide and pentasulfide, 4H), 3.18 (t, *J* = 6.0 Hz-SCH_2- group of pentasulfide), 3.14 (t, *J* = 6.0 Hz, -SCH2 group of tetrasulfide) and 3.09 (t, *J* = 6.0 Hz, -S-CH_2- group from trisulfide). ^{13}C NMR (150 MHz, $CDCl_3$): δ (ppm) = 60.2, 59.9, 59.5, 42.4, 41.8, 41.6. ESI-MS: *m/z* calcd. for $C_4H_{10}O_2S_3$ (trisulfide) $[M + Na]^+$ = 208.9741, obs. 208.9749, ESI-MS: *m/z* calcd. for $C_4H_{10}O_2S_4$ (tetrasulfide) $[M + Na]^+$ = 240.9461, obs. 240.9468, *m/z* calcd. for $C_4H_{10}O_2S_5$ (pentasulfide) $[M + Na]^+$ = 272.9182; obs. 272.9196.

Compound 2.7-2.9:[48] To a solution of polysulfide **2.4-2.6** (0.20 g, 1.0 mmol) in anhydrous dichloromethane (6.0 mL) under inert atmosphere was added pyridine (0.45 mL, 5.30 mmol) and the mixture was cooled to 0 °C with external ice bath. A solution of 4-nitrophenyl chloroformate (0.54 g, 2.60 mmol) in anhydrous dichloromethane (6.0 mL) was added to the above reaction mixture in a dropwise manner at 0 °C. The resulting solution was allowed to attain room temperature and was stirred for another 8 h. The progress of the reaction was monitored by TLC analysis. Upon completion, the mixture was diluted with dichloromethane and sequentially washed with saturated $NaHCO_3$ (15.0

mL), water (15.0 mL), 10% citric acid (15.0 mL) and brine solution (15.0 mL). The organic layer was dried over anhydrous sodium sulfate and the solvent was evaporated under reduced pressure to afford compound **2.7-2.9** as white solid with almost quantitative yield, which was used for the next step without further purification. R_f = 0.5 (30 % ethyl acetate in pet. ether 60-80). ^{1}H NMR (600 MHz, $CDCl_3$): δ (ppm) = 8.28 (d, *J* = 9.2 Hz, 4 Hz), 7.39 (d, *J* = 9.2 Hz, 4H), 4.64-4.62 (m, overlap of two triplets for -OCH_2- group from trisulfide and tetrasulfide, 4H), [3.35-3.30 (m, overlap of two triplets for O-CH_2- from tetrasulfide and pentasulfide) and 3.25 (t, *J* = 6.6 Hz, -OCH_2- group from trisulfide, 4H]. ^{13}C NMR (150 MHz, $CDCl_3$): δ (ppm) = 155.3, 152.3, 145.6, 125.4, 121.8, 66.6, 66.4, 36.9, 36.4. ESI-MS *m/z* calcd. for $C_{18}H_{16}N_2O_{10}S_3$ (trisulfide) $[M + Na]^+$ = 538.9865, obs. 538.9914, ESI-MS *m/z* calcd. for $C_{18}H_{16}N_2O_{10}S_4$ (tetrasulfide) $[M + Na]^+$ = 570.9585, obs. 570.9563, ESI-MS *m/z* calcd. for $C_{18}H_{16}N_2O_{10}S_5$ (pentasulfide) $[M + Na]^+$ = 602.9306, obs. 602.9212.

Synthesis of DCI-PS: To a stirred solution of **3.3** (0.25 g, 0.85 mmol) in anhydrous dichloromethane (10.0 mL) at 0 °C under an inert atmosphere was added DIPEA (0.33 mL, 1.93 mmol) and the mixture was stirred at 0 °C for 10 min. A solution of compound **2.7-2.9** (0.20 g, 0.38 mmol) in anhydrous dichloromethane (5.0 mL) was added to the mixture in a dropwise manner and the reaction mixture was allowed to attain room temperature and stirred for 16 h. The progress of reaction was monitored by TLC analysis. Upon completion, the reaction mixture was poured into water and extracted with ethyl acetate. The combined organic layer was finally washed with brine solution, dried over anhydrous sodium sulfate and concentrated under reduced pressure to afford the crude product as a polysulfide mixture. The crude compound was purified by silica gel column chromatography using ethyl acetate and pet ether as eluents to afford the polysulfide **DCI-PS** as yellow solid. R_f = 0.4 (35% ethyl acetate in pet. ether). Yield: 0.05 g, M.P. = 79 - 81°C. ^{1}H NMR (400 MHz, $CDCl_3$): δ (ppm) = δ 7.53 (d, *J* = 8.4 Hz, 4H), 7.23 (d, *J* = 8.2 Hz, 4H), 7.03 (d, *J* = 16.1 Hz, 2H), 6.93 (d, *J* = 16.1 Hz, 2H), 6.84 (s, 2H), 4.62-4.58 (m, overlap of triplets for –OCH2- group from polysulfide, 4H), [3.33-3.29 (m), 3.26-3.23 (m), overlap of triplets for –SCH2- group from polysulfide, 4H], 2.60 (s, 4H), 2.46 (s, 4H), 1.08 (s, 12H). ^{13}C NMR (100 MHz, $CDCl_3$): δ (ppm) = 169.2, 153.5, 153.1, 151.8, 135.6, 133.8, 129.6, 128.7, 123.9, 121.6, 113.4, 112.6, 79.1, 66.2, 66.1, 43.0, 39.2, 37.1, 36.5, 32.0, 29.7, 28.0. ESI-MS: *m/z* calcd. for $C_{44}H_{46}N_5O_6S_2$ (disulfide) $[M + NH_4]^+$ = 804.2890, obs. = 804.2788, *m/z* calcd. For $C_{44}H_{46}N_5O_6S_3$ (trisulfide) $[M + NH_4]^+$ = 836.2610, obs. 836.2535, *m/z* calcd. for $C_{44}H_{46}N_5O_6S_4$ (tetrasulfide) $[M + NH_4]^+$ = 868.2331, obs.

868.2245, *m/z* calcd. for $C_{44}H_{46}N_5O_6S_5$ (pentasulfide) $[M + NH_4]^+$ = 900.2052, obs. 900.1947.

3.5.2. UV-Vis and fluorescence studies

The stock solutions of the biologically relevant analytes were prepared freshly in Milli-Q/double distilled water and the stock solutions of fluorogenic probes and the organic compounds were prepared freshly in spectroscopy grade DMSO before performing the experiments. All the spectroscopic measurements were carried out at room temperatures (PBS buffer 20 mM, pH 7.4 with 50% DMSO). DMSO was added to the PBS buffer to bring the emission of **DCI-OH** in the NIR region. Samples for absorption and emission spectroscopic measurements were taken in quartz cuvettes (1.0 mL). UV-Vis spectroscopic measurements were carried using an Agilent Carey UV-Vis spectrophotometer and fluorescence emission spectra were recorded on a Fluoromax-4 spectrophotometer (Horiba Jobin Yvon) with an excitation wavelength of 550 nm with a slit width of 5 nm. Time-dependent fluorescence experiments were performed by incubating **DCI-DS** (5.0 µM) or **DCI-PS** (5.0 µg/mL) with suitable analytes (200 µM) over a period of 60 min.

3.5.3. Measurement of H_2S release using MB assay

The release of H_2S from **DCI-PS** (25.0 µg/mL) in the presence of DTT and GSH (1.0 mM) was monitored by methylene blue assay (MB assay) using a UV-Vis spectrophotometer. The H_2S generation was initiated by adding the probe into PBS buffer (pH 7.4, 20 mM) solution containing DTT/GSH and the formation of methylene blue was monitored at 670 nm at different time intervals after adding 500 µL of the above solution to 500 µL of methylene blue cocktail (100 µL of zinc acetate (1% w/v), 200 µL of *N,N* -dimethyl-1,4-phenylenediamine sulfate (20 mM in 7.2 M HCl) and 200 µL of ferric chloride (30 mM in 1.2 M HCl) in a cuvette. The H_2S concentration of each sample was calculated against a calibration curve, which was obtained using the known concentrations of $Na_2S.9H_2O$ solution under identical assay conditions without any thiol.

3.5.4. Measurement of H_2S release using turn-on fluorescence probe

The released H_2S from **DCI-PS** (25.0 µg/mL) in the presence of DTT and GSH (1.0 mM) was monitored using the H_2S-sensitive turn-on fluorogenic probe **WSP2** (25.0 µM) using the fluorescence spectrophotometer. First, the probe **WSP2** (25.0 µM) was pre-incubated with DTT/GSH (1.0 mM) for 60 min in PBS buffer (20 mM, pH 7.4) and the emission spectra were measured to saturate the possible reaction of **WSP2** with thiols.

Subsequently, the aliquot from the experimental solution of **DCI-PS** (25.0 µg/mL) + DTT/GSH (1.0 mM) was added to the above mixture and the emission intensity was measured after an incubation of 60 min to understand the reaction of **WSP2** with the generated H_2S from **DCI-PS** (25.0 µg/mL) in the presence of DTT/GSH (1.0 mM).

3.5.5. Reaction of DCI-PS with bio-analytes

To study the possible reactivity of the polysulfide probe **DCI-PS** with possible nucleophilic proteins, emission profiles were monitored using fluorescence spectroscopic studies. The probe **DCI-PS** (5.0 µg/mL) was pre-incubated with NADPH (200 µM) for 15 min and subsequently, various bio-analytes such as glutathione reductase (GR, 2.0 units per mL), glutathione peroxidase (GP_x, 1.0 unit per mL), bovine serum albumin (BSA, 3.0 µM) and the MDA-MB-231 cell lysate (30 µL) were added and incubated for another 30 min before recording the emission spectra in the PBS buffer with 50% DMSO. Excitation was performed at 550 nm and emission was measured at 570–800 nm with a slit width of 5 nm. The inhibition of TrxR-mediated cleavage of **DCI-PS** was studied using TrxR-selective inhibitors. Inhibition assay was performed by incubating the cell lysate (30 µL) with NADPH (200 µM) for 15 min followed by the treatment of **DCI-PS** (5.0 µg/mL) or by the co-treatment of **DCI-PS** (5.0 µg/mL) + ebselen (5.0 µM), dinitrochlorobenzene (20.0 µM) or Ph_3PAuCl (5.0 µM). The final emission spectra were measured in PBS buffer with 50% DMSO after incubation of the reaction mixture for 30 min.

3.5.6. pH variation studies of DCI-PS and DCI-DS

The emission profiles from **DCI-PS** (5.0 µg/mL) or **DCI-DS** (5.0 µM) in the presence of DTT (200 µM) was carried out at different pH ranges (5 to 9) in PBS buffer with 20% DMSO after an incubation time of 15 min. Control reactions with the probes in the absence of any added thiol were studied under the identical reaction condition to understand the stability of the probes at different pH ranges.

3.5.7. Reaction kinetics analyzed by reverse-phase HPLC

First, the purity of synthesized probes **DCI-DS** and **DCI-PS** were analyzed using analytical high-performance liquid chromatography (HPLC) Agilent 1220 Infinity II LC system using a reverse-phase C18 column (Luna, 150 × 4.6 mm, 5 µm). HPLC grade acetonitrile and water (Finar Ltd.) were used as mobile phase and the absorbance profile of compounds were detected using a PDA detector at a wavelength of 254 and 433 nm. The stock solutions of the samples were prepared in acetonitrile and were injected into the system using the in-built auto sampler at a flow rate of 1.0 mL/min using acetonitrile/water system as a mobile phase (0–10 min: 75% acetonitrile in water; 10–20 min: 95%

acetonitrile in water). The same condition was used for monitoring the reaction kinetics of **DCI-DS** (20 µM) and **DCI-PS** (20 µg/mL) in the presence of DTT/PhSH (20 and100 µM) over 60 min. The peaks due to the analytes, probes, reaction intermediates and the released products were analyzed/ identified at two different wavelengths (254 and 433 nm).

3.5.8. Cell Culture

The triple-negative breast cancer (TNBC) cells (MDA-MB-231) were obtained from the National Centre for Cell Science (NCCS), Pune, India. The cells were cultured in DMEM medium (Gibco) supplemented with 10% (v/v) FBS (Gibco) and 1% Pen-Strep (Gibco). Cells were cultured as a monolayer in a humidified incubator at 37 °C in the presence of a 5% CO_2 level.

3.5.9. MTT assay

The synthesized probes **DCI-DS** and **DCI-PS** were screened for their anti-proliferative activities using the conventional MTT assay. MDA-MB-231 cells were seeded in 96-well culture plates at a density of 2×10^4 cells/100 mL per well and treated with the freshly prepared test compounds **DCI-DS** (5.0, 10.0, and 25.0 µM) and **DCI-PS** (5.0, 10.0, and 25.0 µg/mL) for 0 h (control) and 48 h (experimental), respectively. At the end of the treatment period, 10.0 µL of 5.0 mg/mL of MTT was added to the plate (control) and incubated for 4 h. Following the 4 h incubation, the reagent from the plate was removed and the purple formazan crystals were dissolved using 100 mL of DMSO (Avra Synthesis Pvt Ltd) and the absorbance at 570 nm was measured using a microplate reader (Multiskan Go microplate reader, Thermo Fisher Scientific). In the experimental set, a similar MTT treatment protocol was followed only after 48 h. The mean ΔOD values were calculated by the subtraction of mean OD values of 0 h plate (control) from the mean OD values of identical wells at 48 h plate (experimental) and the percentage proliferation was calculated keeping the mean ΔOD of untreated control as 100%.

3.5.10. Fluorescence microscopic studies

MDA-MB-231 cells were cultured in high glucose Dulbecco's modified Eagle's medium (DMEM) supplemented with 10% fetal bovine serum (FBS) and 1% penicillin/streptomycin at 37 ºC under 5% CO_2 atmosphere. Cells were then plated (2.0×10^4 cells per plate) in 35 mm cell culture Petri dishes containing 2.0 mL of DMEM and incubated at 37 ºC under 5% CO_2 for 24 h. The confluent cells were washed with DPBS and finally incubated with **DCI-DS** (5.0 µM) or **DCI-PS** (5.0 µg/mL) at 37 ºC under 5%

CO_2 for 2 h. After washing with DPBS (3 times), cellular morphology was carefully observed and imaged in a Bio-Rad ZOE^{TM} fluorescent cell imager under a bright field and suitable fluorescent emission filters. The inhibition of the TrxR-mediated fluorescence turn-on process was studied upon the pre-treatment cells with DNCB (10.0 µM) and Ph_3PAuCl (2.0 µM) for 2 h to quench the intracellular TrxR level. The treated cells were washed with DPBS (3 times) and finally treated with **DCI-PS** (5.0 µg/mL) and incubated for an additional 2 h at 37 ºC under a 5% CO_2 atmosphere. Finally, cells were washed with DPBS (3 times) and imaged using Bio-Rad ZOE^{TM} fluorescent cell imager. A negative control experiment was performed upon the pre-treatment of cells with N-ethyl maleimide (NEM, 2.0 mM) to quench the thiols/selenols followed by the treatment of **DCI-PS**. In order to understand the endogenous level of H_2S in MDA-MB-231 cells, H_2S-selective turn-on fluorogenic probe **WSP2** was used. The cells were incubated with **WSP2** (5.0 µM) for 2 h at 37 ºC under 5% CO_2. The treated cells were washed with DPBS (3 times) and imaged in a Bio-Rad ZOE fluorescent cell imager to visualize the endogenous level of H_2S in MDA-MB-231 cells. A similar experiment was carried out upon the pre-treatment of cells with **DCI-PS** (5.0 µg/mL) and **DCI-DS** (5.0 µM) for 2 h followed by washing with DPBS (3 times), treatment of **WSP2** (5.0 µM) and incubation for another 2 h, followed by washing with DPBS (3 times) and final image to sense the released H_2S from **DCI-PS** and **DCI-DS**. Finally, the cells were pre-incubated with DL-propargyl glycine (25.0 µM) and NEM (2.0 mM), incubated at 37 ºC under 5% CO_2 for 2 h. After sequential washing with DPBS, cells were treated with **DCI-PS** (5.0 µg/mL) and incubated at 37 ºC for another 2 h. Finally, cells were washed and imaged under a cell imager to estimate the fluorescence intensity at respective fluorescence channels.[24]

3.5.11. Protein-ligand docking study

Protein Preparation: For the docking studies, the recently published crystal structure of TrxR1 (PDB: 1H6V) was extracted from RCSB (Protein Data Bank).[50] The protein structure was prepared using Auto Dock 4.2 Tools (MGL Tools 1.5.6) and Pymol (Schrodinger LLC) software package.[51] Initially, the protein structure was assembled to the original form having all the important subunits depicted by the crystallographic study. During the protein preparation, addition of missing hydrogens and Gasteiger charges were applied.

Receptor grid generation: The protein TrxR1 was co-crystallized with FAD^+ and NADPH and the crystal structure contained Cys (Cys 498A) residue in its native form. A modified protein was prepared and used in the present study upon the point mutation at the Cys

residue (Cys 498A) with Sec (Sec 498A) using Chimera 1.14 software package.[24,52] In order to locate the binding site, the grid around the Sec sites without altering the entire protein structure was calculated and the grid box was generated by performing the Auto grid. The grid size was set to 40 × 40 × 40 points with grid spacing of 1.000 Å and the grid was centred at Se atom (x = 0.938, y = 8.852, z = 156.484).

Ligand preparation: The 2D structures of **DCI-DS** and **DCI-PS** were drawn carefully and converted to 3D structure using Chem3D Pro (Version: 19.0.1.28). The 3D structures of ligands were subjected to MM2 energy minimization calculations and the correct bond orders were assigned. Finally, for the docking studies, extended PDB format, termed PDBQT, was used for coordinate files, which includes atomic partial charges and atom types. Torsion angles were calculated to assign the fixable and non-bonded rotation of molecules.[53]

Docking Study: Docking simulations were performed using Auto Dock Vina software package by using Perl programming for handling multiple ligands at a time. The number of runs is set by exhaustiveness parameter. Since the individual runs were executed in parallel, proper exhaustiveness parameter is essential. The exhaustiveness parameter of 8 was considered throughout the study. Additionally, we have mentioned 20 binding modes and energy difference of 5 in the conformation file.

3.6. References

1. Vandiver, M. S.; Snyder, S. H., *J. Mol. Med.* **2012**, *90*, 255-263.
2. Fukuto, J. M.; Carrington, S. J.; Tantillo, D. J.; Harrison, J. G.; Ignarro, L. J.; Freeman, B. A.; Chen, A.; Wink, D. A., *Chem. Res. Toxicol.* **2012**, *25*, 769-793.
3. Predmore, B. L.; Lefer, D. J.; Gojon, G., *Antioxid. Redox Signaling* **2012**, *17*, 119.
4. Stipanuk, M. H.; Ueki, I., *Inherited Metab. Dis.* **2011**, *34*, 17-32.
5. Li, L.; Bhatia, M.; Zhu, Y. Z.; Zhu, Y. C.; Ramnath, R. D.; Wang, Z. J.; Anuar, F. B.; Whiteman, M.; Salto-Tellez, M.; Moore, P. K., *FASEB J.* **2005**, *19*, 1196-1198.
6. Eto, K.; Kimura, H., *J. Biol. Chem.* **2002**, *277*, 42680-42685.
7. Wallace, J. L.; Vong, L.; McKnight, W.; Dicay, M.; Martin, G. R., *Gastroenterology* **2009**, *137*, 569-578.e561.
8. Szabo, C.; Papapetropoulos, A., *Pharmacol. Rev.* **2017**, *69*, 497-564.
9. Hartle, M. D.; Pluth, M. D., *Chem. Soc. Rev.* **2016**, *45*, 6108-6117.
10. Zhao, Y.; Biggs, T. D.; Xian, M., *Chem. Commun.* **2014**, *50*, 11788.

11. Powell, C. R.; Dillon, K. M.; Matson, J. B., *Biochem. Pharmacol.* **2018**, *149*, 110-123.
12. Powell, C. R.; Kaur, K.; Dillon, K. M.; Zhou, M.; Alaboalirat, M.; Matson, J. B., *ACS Chem. Biol.* **2019**, *14*, 1129-1134.
13. Zhou, M.; Qian, Y.; Zhu, Y.; Matson, J., *Chem. Commun.* **2020**, *56*, 1085-1088.
14. Zheng, Y.; Yu, B.; Ji, K.; Pan, Z.; Chittavong, V.; Wang, B., *Angew. Chem. Int. Ed.* **2016**, *55*, 4514-4518.
15. Sharma, A. K.; Nair, M.; Chauhan, P.; Gupta, K.; Saini, D. K.; Chakrapani, H., *Org. Lett.* **2017**, *19*, 4822-4825.
16. Venkatesh, Y.; Das, J.; Chaudhuri, A.; Karmakar, A.; Maiti, T. K.; Singh, N. D. P., *Chem. Commun.* **2018**, *54*, 3106-3109.
17. Hua, W.; Zhao, J.; Gou, S., *The Analyst* **2020**, *145*, 3878-3884.
18. Zhao, Y.; Cerda, M. M.; Pluth, M. D., *Chem. Sci.* **2019**, *10*, 1873-1878.
19. Hu, Y.; Li, X.; Fang, Y.; Shi, W.; Li, X.; Chen, W.; Xian, M.; Ma, H., *Chem. Sci.***2019**, *10*, 7690-7694.
20. Zhang, N.; Hu, P.; Wang, Y.; Tang, Q.; Zheng, Q.; Wang, Z.; He, Y., *ACS Sens.* **2020**, *5*, 319-326.
21. Mahato, S. K.; Bhattacherjee, D.; Bhabak, K. P., *Chem. Commun.* **2020**, *56*, 7769-7772.
22. Zhao, X.; Ning, L.; Zhou, X.; Song, Z.; Zhang, J.; Guan, F.; Yang, X.-F., *Anal. Chem.* **2021**, *93*, 4894-4901.
23. Baliga, M. S.; Wang, H.; Zhuo, P.; Schwartz, J. L.; Diamond, A. M., *Biol. Trace Elem. Res.* **2007**, *115*, 227-241.
24. Mafireyi, T. J.; Laws, M.; Bassett, J. W.; Cassidy, P. B.; Escobedo, J. O.; Strongin, R. M., *Angew. Chem. Int. Ed.* **2020**, *59*, 15147-15151.
25. Oh, B. M.; Lee, S.-J.; Cho, H. J.; Park, Y. S.; Kim, J.-T.; Yoon, S. R.; Lee, S. C.; Lim, J.-S.; Kim, B.-Y.; Choe, Y.-K., *Cell Death Dis.* **2017**, *8*, e2682-e2682.
26. Mafireyi, T. J.; Escobedo, J. O.; Strongin, R. M., *Results in Chemistry* **2021**, *3*, 100127.
27. Zhang, L.; Duan, D.; Liu, Y.; Ge, C.; Cui, X.; Sun, J.; Fang, J., *J. Am. Chem. Soc.* **2014**, *136*, 226-233.
28. Li, X.; Zhang, B.; Yan, C.; Li, J.; Wang, S.; Wei, X.; Jiang, X.; Zhou, P.; Fang, J., *Nat. Commun.* **2019**, *10*, 2745.

29. Yi, L.; Li, H.; Sun, L.; Liu, L.; Zhang, C.; Xi, Z., *Angew. Chem. Int. Ed.* **2009**, *48*, 4034-4037.
30. Wang, Y.; Zhang, L.; Chen, L., *Anal. Chem.* **2020**, *92*, 1997-2004.
31. Shyaka, C.; Xian, M.; Park, C.-M., *Org. Biomol. Chem.* **2019**, *17*, 9999-10003.
32. Shukla, P.; Khodade, V. S.; SharathChandra, M.; Chauhan, P.; Mishra, S.; Siddaramappa, S.; Pradeep, B. E.; Singh, A.; Chakrapani, H., *Chem. Sci.* **2017**, *8*, 4967-4972.
33. Arai, K.; Matsunaga, T.; Ueno, H.; Akahoshi, N.; Sato, Y.; Chakrabarty, G.; Mugesh, G.; Iwaoka, M., *Chem. Eur. J.* **2019**, *25*, 12751-12760.
34. Yang, M.; Fan, J.; Sun, W.; Du, J.; Long, S.; Shao, K.; Peng, X., *Chem. Commun.* **2019**, *55*, 8583-8586.
35. Wang, K.; Zhao, C.-X.; Leng, T.-H.; Wang, C.-Y.; Lu, Y.-X.; Shen, Y.-J.; Zhu, W.-H., *Dyes Pigm.* **2018**, *151*, 194-201.
36. Moest, R., *Anal. Chem.* **1975**, *47*, 1204-1205.
37. Peng, B.; Chen, W.; Liu, C.; Rosser, E. W.; Pacheco, A.; Zhao, Y.; Aguilar, H. C.; Xian, M., *Chem. Eur. J.* **2014**, *20*, 1010-1016.
38. Lu, J.; Holmgren, A., *Antioxid. Redox Signaling* **2012**, *17*, 1738-1747.
39. Cai, W.; Zhang, L.; Song, Y.; Wang, B.; Zhang, B.; Cui, X.; Hu, G.; Liu, Y.; Wu, J.; Fang, J., *Free Radic. Biol. Med.* **2012**, *52*, 257-265.
40. Holmgren, A.; Lu, J., *Biochem. Biophys. Res. Commun.* **2010**, *396*, 120-124.
41. Cai, W.; Zhang, L.; Song, Y.; Wang, B.; Zhang, B.; Cui, X.; Hu, G.; Liu, Y.; Wu, J.; Fang, J., *Free Radic. Biol. Med.* **2012**, *52*, 257-265.
42. Leoni, S. G.; Kimura, E. T.; Santisteban, P.; De la Vieja, A., *Mol. Endocrinol.* **2011**, *25*, 1924-1935.
43. Ishikawa, A.; Kubota, Y.; Murayama, T.; Nomura, Y., *Neurosci. Lett.* **1999**, *277*, 99-102.
44. Zhong, L.; Arnér, E. S.; Holmgren, A., *Proc. Natl. Acad. Sci. U S A* **2000**, *97*, 5854-5859.
45. Zhang, L.; Duan, D.; Liu, Y.; Ge, C.; Cui, X.; Sun, J.; Fang, J., *J. Am. Chem. Soc.* **2014**, *136*, 226-233.
46. Omata, Y.; Folan, M.; Shaw, M.; Messer, R. L.; Lockwood, P. E.; Hobbs, D.; Bouillaguet, S.; Sano, H.; Lewis, J. B.; Wataha, J. C., *Toxicol. In vitro* **2006**, *20*, 882-890.

47. Nordberg, J.; Zhong, L.; Holmgren, A.; Arnér, E. S., *J. Biol Chem.* **1998**, *273*, 10835-10842.
48. Bhuniya, S.; Lee, M. H.; Jeon, H. M.; Han, J. H.; Lee, J. H.; Park, N.; Maiti, S.; Kang, C.; Kim, J. S., *Chem. Commun.* **2013**, *49*, 7141-7143.
49. Fuson, R. C.; Price, C. C.; Bauman, R. A.; Bullitt, O. H.; Hatchard, W. R.; Maynert, E. W., *J. Org. Chem.* **1946**, *11*, 487-498.
50. Sandalova, T.; Zhong, L.; Lindqvist, Y.; Holmgren, A.; Schneider, G., *Proc. Natl. Acad. Sci.* **2001**, *98*, 9533-9538.
51. Trott, O.; Olson, A. J., *J. Comput. Chem.* **2010**, *31*, 455-461.
52. Pettersen, E. F.; Goddard, T. D.; Huang, C. C.; Couch, G. S.; Greenblatt, D. M.; Meng, E. C.; Ferrin, T. E., *J. Comput. Chem.* **2004**, *25*, 1605-1612.
53. Ghosh, S.; Bhattacherjee, D.; Satpati, P.; Bhabak, K. P., *J. Biomol. Struct. Dyn.* **2021**, 1-12.

Chapter 4

Cysteine –triggered Fluorogenic Prodrugs for the Adjuvant Delivery of Hydrogen Sulfide and the Anti-cancer Compounds

4.1. Introduction

In mammalian cells, a low and sustained level of endogenous H_2S is maintained by the key transferase and lyase family of enzymes.[1,2] Considering the involvement and association of H_2S with several beneficial physiological processes such as anti-inflammation, cardioprotection, protection against oxidative stress, angiogenesis, anti-proliferation etc, several organosulfur compounds were being developed in last 1-2 decades as the exogenous donors of H_2S.[3-5] The release of H_2S from most of the organic donors could be possible in the presence of various stimuli such as ROS, thiols, pH, light and enzymes namely esterase, carbonic anhydrase and nitroreductase.[6-9] While earlier reports were associated with the examples of non-fluorogenic H_2S donors, recent reports highlight the importance of stimuli-responsive turn-on fluorogenic H_2S donors with several examples.[10,11] While the most abundant cellular biothiol is GSH that plays active role in the cellular homeostasis, the essential amino acid Cys and Hcy are also present in the cells however, at relatively lower concentrations. For example, the intracellular concentration of Cys is reported to be around 30–200 μM.[12] Similar to GSH, the proper regulation of the concentration of Cys is also associated with many physiological functions and the dysregulation leads to various disease states. For example, a high level of Cys leads to cardiovascular, Alzheimer's and other diseases.[13,14] Whereas, a low levels of Cys is related to psoriasis, liver damage, growth retardation, neurotoxicity, hematopoietic dysfunction, hair depigmentation etc.[15] Considering the beneficial effects of H_2S, several reports appeared recently towards the development of Cys-triggered fluorogenic donors of H_2S (Figure 4.1). For example, in 2021, Feng and co-workers have reported a coumarin-based isothiocyanate **CM-NCS** that was responsive towards Cys and released H_2S with turn-on fluorescence.[16] The probe was found to be compatible to both in vitro and in vivo applications. In the same year (2021), Zhang and co-workers have reported a phenyl thiocarbamate-based fluorogenic H_2S donor **Pro-S** that released H_2S in the presence of Cys and was compatible to aqueous as well as cellular environments.[17] In 2022, Zhu *et al.* have reported another aromatic isothiocyanate-based Cys-responsive fluorogenic probe **Gol-NCS**. The probe was shown to target golgi body and was capable to sense the oxidative stress in golgi body.[18] In another report, Zhao and co-workers have described the effective sensing of Cys selectively using the hemicyanine-based NIR fluorogenic probe **CyOH-NCS**.[19] A Cys-selective thiocyanate moiety was connected that was able to undergo self-immolative cleavage to release H_2S with turn-on NIR

fluorescence. The probe was highly sensitive and was capable of sensing Cys in the in vitro as well as in vivo conditions.

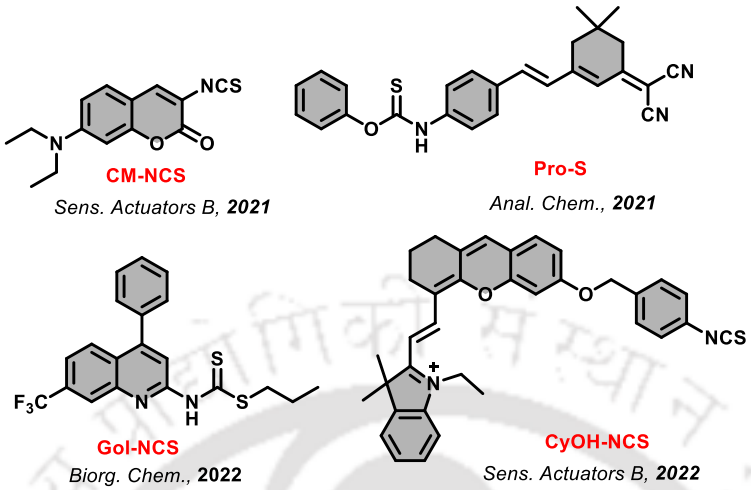

Figure 4.1. Representative examples of the previously reported Cys-responsive turn-on fluorogenic H_2S donors.

4.2. Outline of the chapter

In this chapter, we have developed two turn-on fluorogenic isothiocyanates **NB-ITC** and **AM-ITC** that are responsive towards Cys. Inspired by the anti-cancer and chemopreventive activity of isothiocyanates from cruciferous vegetables, we have synthesized fluorogenic isothiocyanates and evaluated their anti-cancer activities in triple-negative breast cancer cell line (MDA-MB-231). The isothiocyanate **AM-ITC** was developed as a prodrug of the potent anti-cancer compound amonafide. The active fluorogenic drug amonafide was released along with the release of H_2S upon the reaction of **AM-ITC** with Cys. The release of amine (amonafide) was confirmed by UV-Vis, fluorescence, and HPLC experiments. The selective reactivity of **AM-ITC** towards Cys was further confirmed by selectivity studies towards thiol and non-thiol analytes. Furthermore, the release of H_2S from these isothiocyanates was confirmed by nucleophilic-substitution cyclization-based probe **WSP2** and the release of active drug in the cellular environment was evidenced further by the fluorescence imaging experiments.

4.3. Results and Discussion

4.3.1. Synthesis of AM-ITC and NB-ITC

In this chapter, we have synthesized two isothiocyanates namely **NB-ITC** and **AM-ITC** using the commercially available precursor 3-nitro-1,8-naphthalic anhydride **4.1** (Scheme 4.1). An initial reduction of the nitro group in **4.1** with tin(II) chloride dihydrate in absolute

ethanol led to the formation of the corresponding amine **4.2**. Condensation of compound **4.2** with two different amines such as *n*-butylamine and 1,2-dimethylethylenediamine in absolute ethanol produced the imide compounds **4.3** and **4.4**, respectively.[20] The final isothiocyanates **NB-ITC** and **AM-ITC** were synthesized upon the reaction of imides with thiocarbonyl diimidazole in dry DMF at reasonably good yields. All the intermediates as well as the final compounds were characterized using NMR spectroscopic and ESI-MS spectrometric analyses.

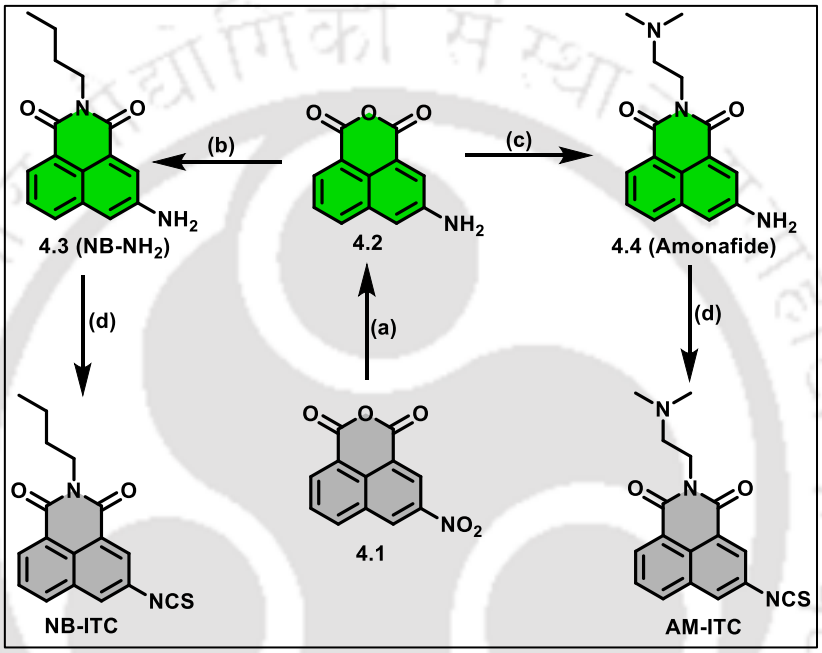

Scheme 4.1. Synthetic scheme to **NB-ITC** and **AM-ITC**. Reagents and conditions. (a) $SnCl_2 \cdot 2H_2O$, Ethanol, 90 °C, 2.5 h; (b) *n*-Butylamine, Ethanol, 90 °C, 2.5 h; (c) *N,N*-Dimethyl-1,2-ethylenediamine, Ethanol, 90 °C, 2.5 h; (d) Thiocarbonyl diimidazole, dry DMF, 0 °C-RT, 24 h.

4.3.2. Absorption and emission studies

The isothiocyanates synthesized in the present study were evaluated for their reactivity towards the major biothiols such as Cys, GSH, DTT and Hcy using UV-Vis spectrophotometric analysis. While no significant alteration in the spectral pattern was observed in the presence of GSH, DTT and Hcy (data not shown), significant changes in the absorption spectra for the reaction of **NB-ITC** and **AM-ITC** with Cys was observed with the intense absorption maxima at 350 nm with a hump at around 385 nm (Figures 4.2A and 4.2B). The spectral pattern of the prodrugs in the presence of Cys resembled well with the absorption spectra of the corresponding free

amine compounds such as NB-NH_2 and amonafide, indicating their formation in the reaction with Cys. The release of free amines from the isothiocyanate-based probes was confirmed further using fluorescence emission studies. While both the isothiocyanates were very weakly fluorescent, intense emissions at around 575-580 nm were observed upon their reactions with Cys. Interestingly, the emission spectra matched well with the emission spectral pattern of the pure and free amines (Figures 4.2C and 4.2D).

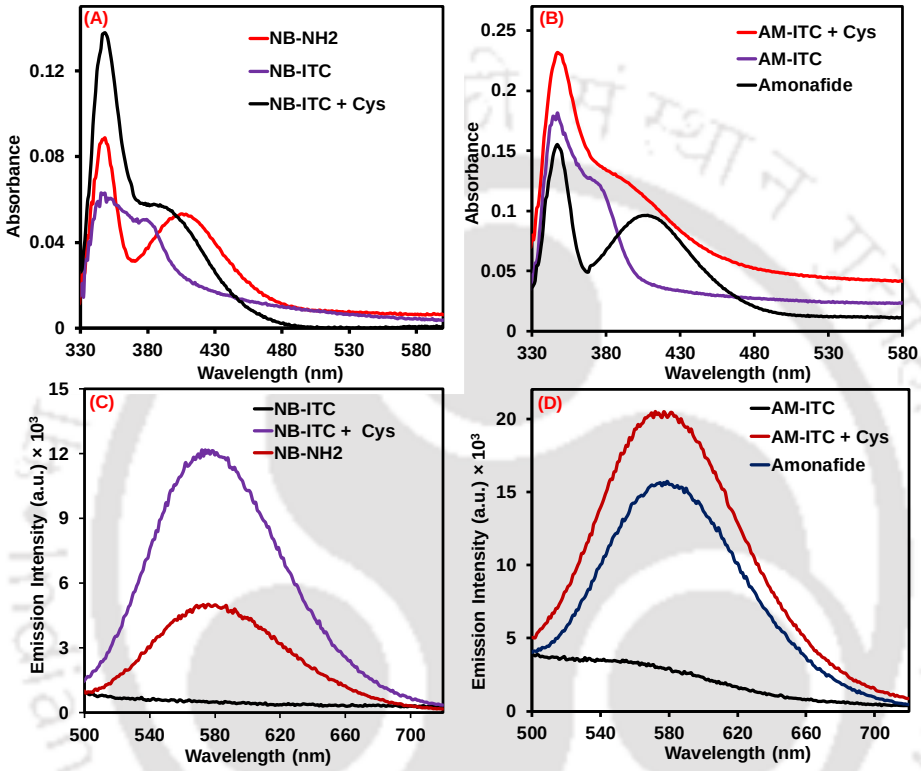

Figure 4.2. Absorption spectra of (A) **NB-ITC** (25.0 μM) and (B) **AM-ITC** (25.0 μM) in the presence and absence of Cys (1.0 mM) along with the spectra of the free fluorophore. Emission spectra of (C) **NB-ITC** (5.0 μM) and (D) **AM-ITC** (5.0 μM) in the presence and absence of Cys (200.0 μM) along with the emission spectra of the released fluorophore. The experiments were carried out in phosphate buffer saline, PBS (20 mM, pH 7.4).

With the initial indication of excitation and emission spectral pattern of both the isothiocyanates in the presence of Cys, the detailed kinetics was studied. The release of free amines such as NB-NH_2 and amonafide from the probes **NB-ITC** and **AM-ITC** (5.0 μM) in the absence and presence of Cys (200.0 μM) was monitored over 60 min to understand the stability and their relative reactivity profiles. As shown in Figure 4.3A, very weak emission intensity was observed for both the probes in the absence of Cys, indicating reasonable stability of the probes over the complete duration. However, a rapid

increase in the emission intensity within initial 10-15 min was observed in the presence of Cys with the subsequent saturation kinetic pattern, indicating the rapid reactivity of the probes towards Cys. Moreover, a significantly higher reactivity of **AM-ITC** as compared to **NB-ITC** was evident from the reasonably higher emission intensity of the reaction of **AM-ITC** with Cys. With the information of higher reactivity of **AM-ITC** towards Cys than **NB-ITC** over 60 min, their relative reactivity towards Cys was studied further at a variable concentration of Cys (0.0-500.0 μM). Interestingly, a significantly higher emission from **AM-ITC** as compared to **NB-ITC** was observed at all concentrations of Cys (Figure 4.3B). While an enhanced emission pattern was observed at lower concentration of Cys, a saturated emission pattern was observed for both the probes at higher concentration of Cys (180-200 μM).

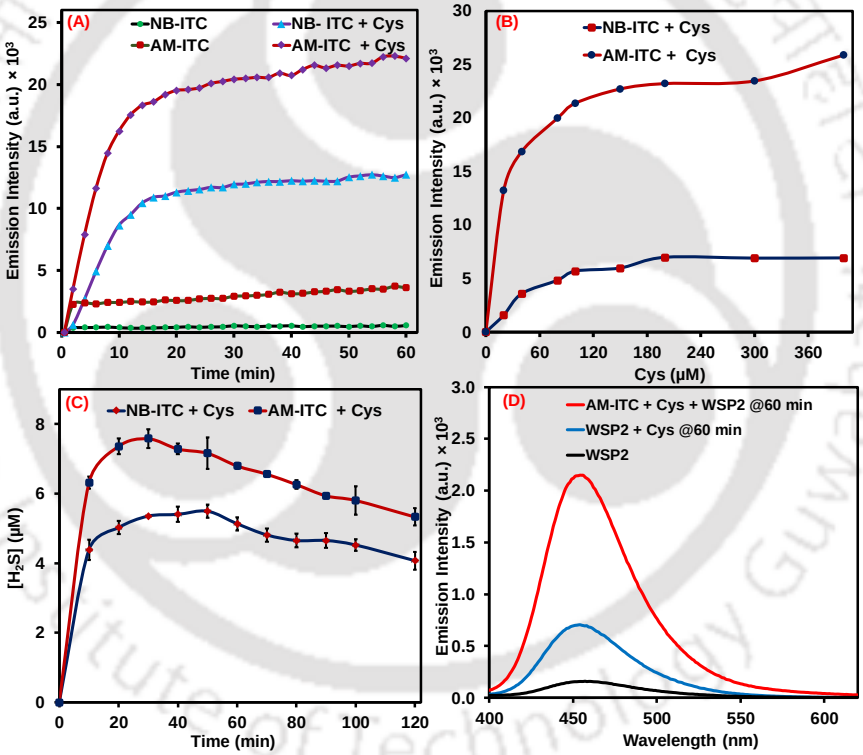

Figure 4.3. (A) Emission spectra of **NB-ITC** (5.0 μM) and **AM-ITC** (5.0 μM) in the absence and presence of Cys (200 μM). (B) Emission spectra of **NB-ITC** (5.0 μM) and **AM-ITC** (5.0 μM) with increasing concentration of Cys (0-400 μM). (C) The H_2S release profile of **NB-ITC** (25.0 μM) and **AM-ITC** (25.0 μM) in the presence of Cys (1.0 mM) over 120 min using MB assay. (D) Emission spectra after 60 min from **WSP2** (25.0 μM) in the presence of Cys (1.0 mM) and **AM-ITC** (25.0 μM) + Cys (1.0 mM).

4.3.3. Measurement of the released H_2S from the probes

After confirming the release of the free amines with intense fluorescence turn-on from the isothiocyanates in the presence of Cys, the release of H_2S from the probes was studied. From the previous literature reports, it is evident that isothiocyanates release H_2S upon their reactions with Cys.[21] Therefore, the release of H_2S from both **NB-ITC** and **AM-ITC** was analyzed and quantified using the conventional MB assay over a period of 120 min. As shown in Figure 4.3C, a sustained release of H_2S was observed from both the probes in the presence of Cys over 120 min. The maximum peak intensity was observed at around 20-30 min and then decreased slightly over a period of 120 min. Moreover, similar to the higher emission intensity from **AM-ITC** than **NB-ITC** in the presence of Cys, the amount of released H_2S from **AM-ITC** was also found to be higher than that of **NB-ITC**. However, as the measurement of the released H_2S using the MB assay is not completely quantitative in nature, H_2S release from **AM-ITC** was further confirmed using the nucleophilic-substitution cyclization-based fluorescent probe **WSP2**. Initially, the background reaction of **WSP2** with Cys was saturated by incubating **WSP2** with Cys for 60 min and the emission intensity was measured using a fluorescence spectrophotometer. Interestingly, a significant enhancement of fluorescence intensity was observed upon the reaction of **WSP2** with the released H_2S from the reaction of **AM-ITC** + Cys as evidenced in Figure 4.3D.

4.3.4. Reaction of AM-ITC with bio-analytes

Considering the higher response from **AM-ITC** than the **NB-ITC** towards Cys with higher emission intensity as well as higher amount of H_2S, this probe was chosen for further detailed studies. Moreover, **AM-ITC**, upon the reaction with Cys produces amonafide, which is reported as a potent anti-cancer compound.[22,23] The selective reactivity of **AM-ITC** towards Cys over the other relevant thiol and non-thiol bio-analytes was validated further by reacting the probe (5.0 μM) with various bio-analytes (200 μM) and by measuring the fluorescence emission intensity. As shown in Figure 4.4A, a much lower emission was observed with most of the bio-analytes. Moreover, very weak emission response was observed in the presence of thiol-based analytes except Cys that exhibited significantly higher emission, indicating the selectivity of **AM-ITC** towards Cys.

4.3.5. Reactivity of AM-ITC at different pH conditions

With the observation that **AM-ITC** showed selectivity towards Cys over other thiol as well as non-thiol bio-analytes, the stability and the reactivity pattern of **AM-ITC** (5.0 μM)

towards Cys (200.0 µM) was studied over a wider range of pH (4-10). As shown in Figure 4.4B, a lower emission profile was observed at pH 4-5 and the emission intensity increased significantly at pH 6 and almost saturated up to pH 10. Additionally, very low emission intensity of the pure **AM-ITC** in the absence of Cys was observed for the entire pH range, indicating good stability of the prodrug over the pH ranges.

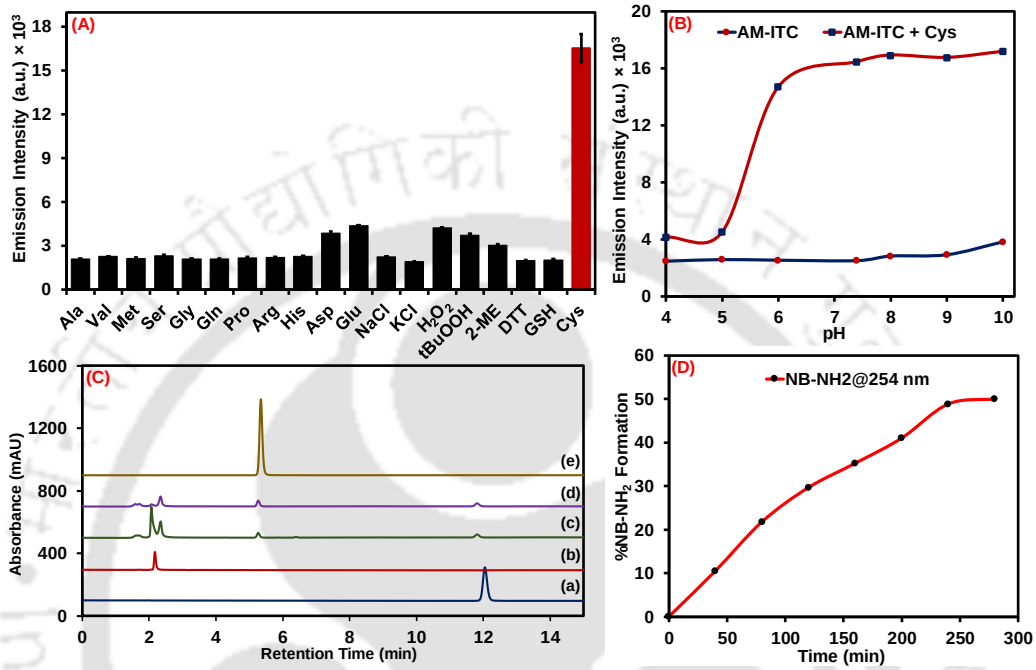

Figure 4.4. (A) The emission intensity of **AM-ITC** (5.0 µM) upon the addition of various thiol and non-thiol bio-analytes (200.0 µM) in PBS (20 mM, pH 7.4). (B) Emission spectra of **AM-ITC** (5.0 µM) in the presence and absence Cys (200 µM) at pH ranges from 4-10. (C) Reverse-phase HPLC chromatogram for the reaction of **NB-ITC** (25.0 µM) with Cys (1250.0 µM). Legends: (a) pure **NB-ITC** @254 nm; (b) Cys @210 nm; (c) **NB-ITC** + Cys @210 nm; (d) **NB-ITC** + Cys @254 nm; (e) **NB-NH$_2$** @254 nm. (D) Percentage of **NB-NH$_2$** formation at 254 nm with the progress of the reaction of **NB-ITC** with Cys over 300 min.

4.3.6. Reaction kinetics of NB-ITC with Cys by HPLC

After confirming the release of fluorophore as well as H_2S from the probes, the kinetics of the reaction of **NB-ITC** (25.0 µM) with Cys (1250.0 µM) was studied and the products were analyzed using reverse-phase HPLC method. The reaction of **NB-ITC** with Cys in the ratio 1:50 generated the fluorophore NB-NH_2 along with a small peak for the intermediate at around 2 min, which could be assigned to intermediate **4.7** as confirmed further by ESI-MS analysis. The percentage

formation of the released fluorophore (NB-NH_2) from the reaction of **NB-ITC** with Cys was monitored and plotted over 300 min (Figure 4.4C and 4.4D).

4.3.7. Mechanistic insights

The mechanistic pathways for the reaction of **NB-ITC** with Cys were evaluated using HPLC and ESI-MS analysis. Treatment of the probe with Cys in 1:50 ratio gives three compounds such as aliphatic cyclic intermediate, aromatic cyclic intermediate, and the corresponding fluorogenic amine compound along with a small amount of the starting material. The formation of these intermediates was further confirmed by ESI-MS analysis. Based on the observation, a plausible mechanism is proposed. The reaction of isothiocyanates with Cys initially results in an unobservable intermediate **4.5**. Once intermediate **4.5** is formed, the primary amine of the Cys residue attacks the thiocarbonyl centre to form the tetrahedral intermediate **4.6**. There can be two possible pathways for the decomposition of intermediate **4.6**. In path A, the released fluorophore **4.3** and the aliphatic cyclic compound **4.7** gets released, whereas in path B, release of aromatic cyclic compound **4.8** and H_2S was proposed (Figure 4.5).

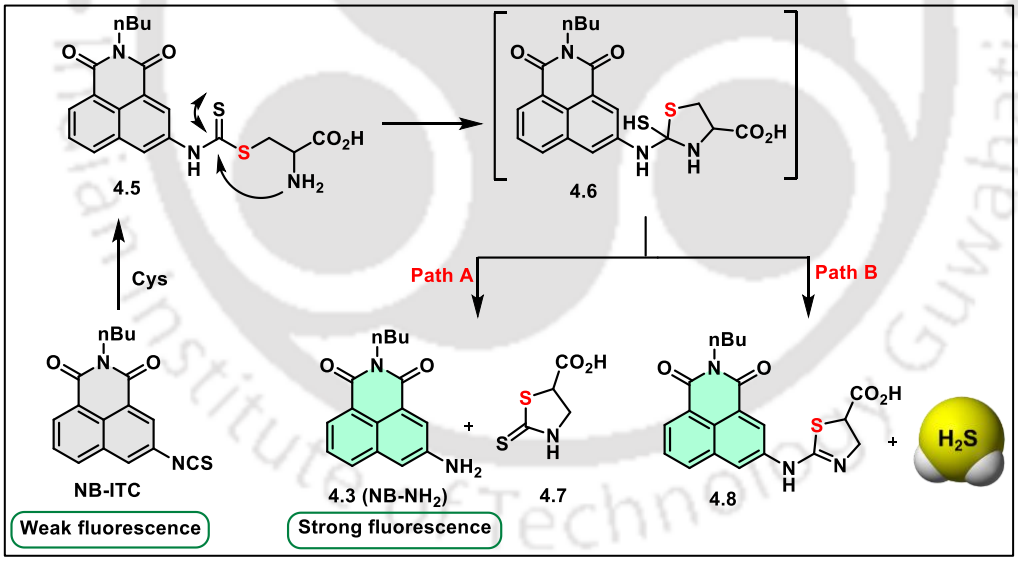

Figure 4.5. Plausible mechanism for the fluorogenic release of H_2S from the reaction of isothiocyanates with Cys.

4.3.8. Anti-proliferative activity

In order to understand the compatibility of synthesized isothiocyanate-based prodrugs and their released compounds in cellular medium, their toxicity profile was studied in a dose-dependent manner (5.0, 10.0, and 25.0 µM) in a representative

breast cancer cells (MDA-MB-231) after an incubation for 48 h. As shown in Figure 4.7A, **NB-ITC** was almost non-toxic at all concentrations, however, the corresponding released amine (NB-NH_2) exhibited moderate anti-proliferative activity under the identical condition. Although, **AM-ITC** exhibited moderate anti-proliferative activity, the corresponding released fluorophore, amonafide, which is a known anti-cancer compound, exhibited very potent anti-proliferative activity. The relatively lower anti-proliferative activity of **AM-ITC** as compared to the free amonafide could be due to the gradual release of amonafide from **AM-ITC** under the cellular medium over time in the presence of the endogenous Cys.

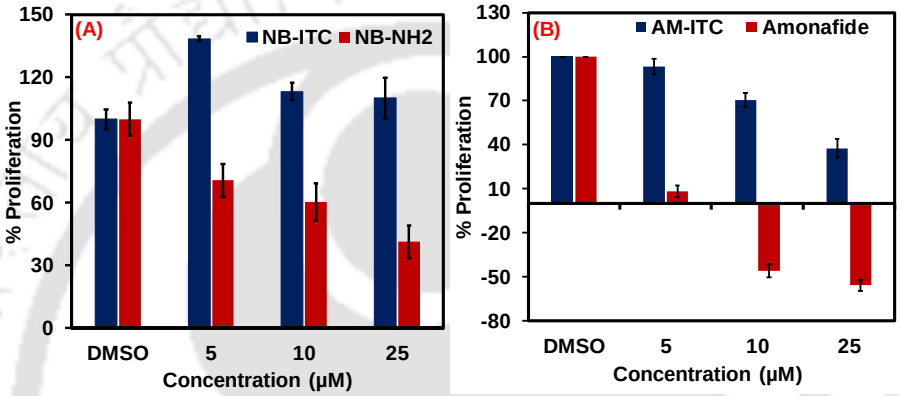

Figure 4.7. The dose-dependent anti-proliferative activity of (A) **NB-ITC** and the released fluorophore NB-NH_2, and (B) **AM-ITC** and the released fluorophore amonafide in MDA-MB-231 cells over 48 h.

4.3.9. Fluorescence microscopic images

To understand the release of the fluorogenic amines in the cellular medium, the fluorescent microscopic experiments were carried out in the cellular medium (MDA-MB-231 cells). The cultured cells were incubated with **AM-ITC** (5.0 μM) and imaging was performed using a fluorescence microscope. Initially, **AM-ITC** was incubated for 30 min in MDA-MB-231 cells and the cells were washed with DPBS. A green fluorescence for **AM-ITC** with a lesser intensity under the green channel indicates the reaction with endogenous Cys to give the fluorescent amine amonafide. The reactivity of **AM-ITC** with endogenous Cys under the cellular experimental condition was validated further by the pre-treatment of cells with thiol quenchers such as NEM (N-ethylmaleimide). Lack of fluorescence emission in the presence of NEM indicates the complete quenching of intracellular thiols. Interestingly, addition of exogenous Cys to the NEM pre-treated cells in the presence of **AM-ITC** showed a significant enhancement of fluorescence emission in the green

channel. These results further confirm the selectivity of isothiocyanates towards Cys (Figure 4.8).

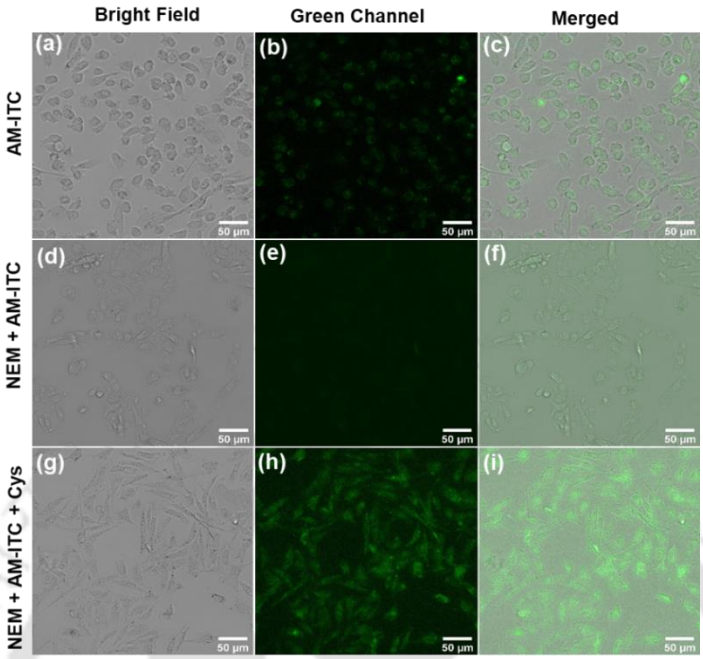

Figure 4.8. (A) Fluorescence microscopic images (bright field, green channel, and merged) in MDA-MB-231 cells. (a-c) **AM-ITC**, (d-f) NEM + **AM-ITC** and (g-i) NEM + **AM-ITC** + Cys. The scale bar represents 50 µm.

4.4. Conclusions

In summary, we describe herein the isothiocyanate-based Cys-triggered turn-on fluorogenic prodrug (**AM-ITC**) of the anti-cancer compound amonafide with the concomitant delivery of H_2S. A representative control probe **NB-ITC** was also designed and studied under the identical condition. The isothiocyanate-based prodrug reacts selectively with Cys over the other biologically relevant thiols and releases the active drug along with H_2S. The adjuvant delivery of the active drug and H_2S was confirmed in the aqueous medium using UV-Vis, fluorescence spectroscopic as well as HPLC analyses. The delivery process was further validated in a representative breast cancer cell line (MDA-MB-231). Interestingly, the prodrug **AM-ITC** was found to be less toxic than the active drug amonafide in the cellular medium, indicating the importance of the bio-analyte-triggered drug uncaging process. The present strategy with the well-known anti-cancer compound amonafide and H_2S would be helpful in amonafide-induced side effects during anti-cancer treatments.

4.5. Experimental section

4.5.1. Materials and method

All the reagents were purchased either from Sigma Aldrich or from reliable local suppliers and used without further purification unless otherwise stated. Thin layer chromatographic (TLC) analyses were carried out on pre-coated silica gel on aluminium sheets and the compounds were visualized by irradiation with UV or fluorescent light. Organic solvents used for column chromatographic separations were distilled before use. The NMR spectra were recorded with a Bruker Ascend^{TM} 400 and 600 MHz NMR Spectrometers. Chemical shifts are cited with respect to Me_4Si as an internal standard. Mass spectra were obtained using Agilent 6520 Accurate-Mass Quadrupole Time-of-Flight (Q-TOF) LC/MS spectrometer. UV-Vis spectra were recorded on Agilent Cary 100 spectrophotometer. Fluorescence emissions were recorded on the Horiba Yvon Fluoromax-4 spectrophotometer.

4.5.2. Synthetic methods

Synthesis of compound 4.2[24]

To a solution of $SnCl_2$ (4.50 g, 20.56 mmol) in conc. hydrochloric acid (3.50 mL, 0.14 mmol) in a double-necked round bottom flask, was added dropwise a suspension of 3-nitro-1,8-naphthalic anhydride **4.1** (1.00 g, 4.11 mmol) in absolute ethanol (2.0 mL) and the resulting suspension was refluxed at 90 ºC for 2 h. The reaction mixture was cooled to room temperature during which the crude product was precipitated as orange solid. The precipitate was filtered off and washed sequentially with ice-cold water, cold ethanol and diethyl ether and dried under vacuum. The crude product as orange solid was used in the next step without purification. R_f = 0.5 (50% ethyl acetate in pet. ether). Yield = 81% (0.71 g). ^{1}H NMR (600 MHz, DMSO-d_6): δ (ppm) = 8.18 (d, J = 8.3 Hz, 1H), 8.13 (d, J = 7.2 Hz, 1H), 8.02 (d, J = 2.3 Hz, 1H), 7.68 (t, J = 7.8 Hz, 1H), 7.52 (d, J = 2.4 Hz, 1H). ^{13}C NMR (150 MHz, DMSO-d_6): δ (ppm) = 160.91, 160.76, 133.29, 132.98, 128.02, 127.52, 123.74, 123.68, 119.50, 118.58, 115.09. ESI-MS: *m/z* calc. for $C_{12}H_7NO_3$ $[M + H]^+$ = 214.0504, obs. 214.0503.

Synthesis of compound 4.3[25]

To a suspension of compound **4.2** (3.00 g, 14.08 mmol) in absolute ethanol (10 mL), *N, N*-dimethyl-1,2-ethylenediamine (2.06 g, 28.16 mmol) was added dropwise. The reaction mixture was refluxed at 90 ºC for 3 h. The progress of the reaction was monitored by TLC analysis. Upon the completion of reaction, the reaction mixture was allowed to cool to room temperature during which a yellow precipitate was observed, which was filtered off,

washed with cold ethanol and pet. ether and dried under vacuum. The residue was purified by basic alumina column chromatography using DCM as eluent to afford the pure product as a yellow fluffy solid. R_f = 0.7 (10% MeOH in DCM, silica TLC). Yield= 63% (2.50 g). ^{1}H NMR (600 MHz, DMSO-d_6): δ (ppm) = δ 8.07 (d, *J* = 7.2 Hz, 1H), 8.03 (d, *J* = 8.2 Hz, 1H), 7.95 (d, *J* = 2.3 Hz, 1H), 7.61 (dd, *J* = 8.4, 7.1 Hz, 1H), 7.28 (d, *J* = 2.3 Hz, 1H), 6.01 (s, 2H), 4.12 (t, *J* = 6.9 Hz, 2H), 2.48 (t, *J* = 6.9 Hz, 2H), 2.19 (s, 6H). ^{13}C NMR (150 MHz, DMSO-d_6): δ (ppm) = 163.7, 163.6, 147.9, 133.5, 131.5, 126.9, 126.9, 125.4, 122.5, 121.8, 121.7, 120.6, 111.7, 56.5, 45.4, 37.5. ESI-MS: *m/z* calc. for $C_{16}H_7N_3O_2$ $[M + H]^+$ = 284.1399, obs. 284.1399.

Synthesis of compound 4.4[25]

To a suspension of compound **4.2** (1.50 g, 7.00 mmol) in absolute ethanol (2.0 mL), *n*-butylamine (0.56 g, 7.70 mmol) was added and refluxed at 90 ºC for 3 h. The progress of the reaction was monitored by TLC analysis. The solution was cooled to room temperature and the precipitate obtained was washed sequentially with ice-cold ethanol and pet. ether. The resulting brown solid was dried under vacuum and purified by silica gel column chromatography using ethyl acetate and pet. ether as eluents to afford the pure product as a yellow solid. R_f = 0.5 (50% ethyl acetate in pet. ether). Yield = 54% (1.02 g). ^{1}H NMR (600 MHz, $CDCl_3$): δ (ppm) = δ 8.62 (d, *J* = 7.3 Hz, 1H), 8.57 (d, *J* = 8.0 Hz, 1H), 8.42 (dt, *J* = 8.4, 1.3 Hz, 1H), 7.77 – 7.71 (m, 1H), 7.46 (d, *J* = 7.9 Hz, 1H), 4.19 – 4.14 (m, 2H), 1.75 – 1.66 (m, 2H), 1.44 (h, *J* = 7.4 Hz, 2H), 0.97 (t, *J* = 7.4 Hz, 3H). ^{13}C NMR (150 MHz, $CDCl_3$): δ (ppm) = 164.6, 164.3, 145.4, 145.3, 133.5, 131.8, 127.6, 127.5, 127.3, 123.7, 122.6, 122.0, 114.0, 40.3, 30.3, 20.5, 14.0. ESI-MS: *m/z* calc. for $C_{16}H_{16}N_2O_2$ $[M + H]^+$ = 269.1290, obs. 269.1293.

Synthesis of NB-ITC

To a solution of compound **4.3** (0.15 g, 0.48 mmol) in dry DMF (1.0 mL) was added triethylamine (0.29 g, 2.89 mmol) at 0 °C under ice-cold condition. The reaction mixture was stirred at 0 °C for 5 min. To the above mixture was added a solution of thiocarbonyl diimidazole (0.17 g, 0.96 mmol) in dry DMF (1.0 mL) dropwise at 0 °C. The reaction was allowed to attain room temperature and then continued for 16 h at room temperature. The progress of the reaction was monitored by TLC analysis. Upon completion, the solvent was evaporated and the crude mixture was purified by silica gel column chromatography. R_f = 0.5 (5% ethyl acetate in pet. ether, silica TLC). Yield = 58% (0.10 g). ^{1}H NMR (600 MHz, $CDCl_3$): δ (ppm) = 8.56 (d, *J* = 7.0 Hz, 1H), 8.37 (t, *J* = 2.3 Hz, 1H), 8.13 (d, *J* = 8.2 Hz, 1H), 7.97 (t, *J* = 1.8 Hz, 1H), 7.78 (t, *J* = 7.7 Hz, 1H), 4.22 – 4.11 (m, 2H), 1.69

(q, *J* = 8.1, 7.6 Hz, 2H), 1.43 (s, *J* = 7.4 Hz, 2H), 0.97 (t, *J* = 7.3 Hz, 3H).^{13}C NMR (150 Hz, $CDCl_3$): δ (ppm) = δ 163.6, 163.0, 139.0, 133.1, 132.1, 131.5, 130.8, 128.7, 128.5, 128.3, 126.4, 124.6, 122.9, 40.5, 30.2, 20.4, 13.9. ESI-MS: *m/z* calc. for $C_{17}H_{14}N_2O_2S$ $[M + H]^+$ = 311.0854, obs. 311.0864.

Synthesis of AM-ITC

To a solution of compound **4.4** (0.25 g, 0.88 mmol) in dry DMF (3.0 mL) was added triethylamine (0.54 g, 5.28 mmol) at 0 °C under ice-cold condition. The reaction mixture was stirred at 0 °C for 5 min. To the above mixture was added a solution of thiocarbonyl diimidazole (0.31 g, 1.76 mmol) in dry DMF (3.0 mL) dropwise at 0 °C. The reaction was allowed to attain room temperature and then continued for 16 h at room temperature. The progress of the reaction was monitored by TLC. Upon completion, the solvent was evaporated and the crude mixture was purified by silica gel column chromatography. R_f = 0.5 (50% ethyl acetate in pet. ether, alumina TLC). Yield = 24% (0.070 g). ^{1}H NMR (600 MHz, $CDCl_3$): δ (ppm) = δ 8.51 (d, *J* = 7.1 Hz, 1H), 8.28 (d, *J* = 2.2 Hz, 1H), 8.12 – 8.04 (m, 1H), 7.91 (d, *J* = 2.1 Hz, 1H), 7.74 (t, *J* = 7.7 Hz, 1H), 4.27 (t, *J* = 6.9 Hz, 2H), 2.61 (t, *J* = 6.9 Hz, 2H), 2.31 (s, 6H). ^{13}C NMR (150 Hz, $CDCl_3$): δ (ppm) = 163.5, 162.9, 139.1, 133.1, 132.0, 131.5, 130.7, 128.6, 128.5, 128.2, 126.3, 124.4, 122.7, 57.0, 45.7, 38.3. ESI-MS: *m/z* calc. for $C_{17}H_{15}N_2O_3S$ $[M + H]^+$ = 326.0963, obs. 326.0971.

4.5.3. UV-Vis and fluorescence spectroscopic studies

All the stock solutions of the biologically relevant analytes were prepared freshly in Milli Q/double distilled water and stock solutions of fluorogenic probes as well as other analytes were prepared freshly in spectroscopy grade DMSO before carrying out the experiments. All the spectroscopic measurements were carried out at room temperatures in buffered medium (PBS buffer 20 mM, pH 7.4). Samples for absorption and emission spectroscopic measurements were taken in quartz cuvettes (1.0 mL). Fluorescence emission spectra were collected with excitation wavelength of 415 nm with a slit width of 5 nm. Time-dependent fluorescence experiments were performed by incubating **AM-ITC** (5.0 µM) or **NB-ITC** (5.0 µM) with suitable analytes (200 µM) over a period of 60 min.

4.5.4. Measurement of H_2S release from AM-ITC

The release of H_2S from **AM-ITC** (5.0 µM) in the presence of Cys (1.0 mM) was monitored by methylene blue assay using UV-Vis spectrophotometer by measuring the absorbance of methylene blue at 670 nm. H_2S is generated by the reaction of **AM-ITC** with Cys in phosphate buffer saline, PBS (20 mM, pH 7.4), and the formation of

methylene blue was monitored at specific time intervals after adding 500 µL of the above solution to 500 µL of methylene blue cocktail [(100 µL of zinc acetate 1% w/v), 200 µL of *N*,*N*-Dimethyl-1,4-phenylenediamine sulfate (20 mM, 7.2 M HCl), 200 µL of Ferric Chloride (30 mM, 1.2 M HCl)] in a 1 mL quartz cuvette. The concentration of H_2S for each sample was calculated against a calibration curve obtained by using the known concentrations of $Na_2S.9H_2O$ without any externally added thiol.

4.5.5. Measurement of H_2S using WSP2 fluorescent probe

The release of H_2S from **AM-ITC** (25.0 µM) in the presence of Cys (1.0 mM) was measured by a nucleophilic-substitution cyclization-based fluorescence probe **WSP2** using a fluorescence spectrophotometer.[29.] Initially, the probe **WSP2** was pre-treated with Cys (1.0 mM) in PBS buffer (20 mM, pH 7.4) and then the emission spectra were recorded to saturate the background reaction with **WSP2**. After that, the aliquot from the reaction of **AM-ITC** (25.0 µM) with Cys (1.0 mM) was added to the above mixture and the emission spectra were recorded after 60 min of incubation to understand the reactivity of **WSP2** with the H_2S generated by the reaction of **AM-ITC** with Cys.

4.5.6. Reaction of bio-analytes with AM-ITC

To understand the reactivity of **AM-ITC** with different analytes, emission profile was monitored using fluorescence spectroscopic studies. The probe **AM-ITC** (5.0 µM) was incubated with different analytes (200 µM) for 15 min. in PBS buffer (20 mM, pH 7.4). The resulting mixture was further incubated for 15 min with the addition of equivalent amount of Cys (200 µM) to the reaction mixture. Excitation was done at 415 nm and the emission was collected in the range 400-740 nm with a slit width of 5 nm.

4.5.7. pH variation studies

The pH variation studies were performed by incubating **AM-ITC** (5.0 µM) with Cys (200.0 µM) at different pH ranges (pH 4 to 10) in PBS (20 mM) and the emission spectrum was measured after 15 min of incubation. The stability of **AM-ITC** was measured under identical conditions without adding any Cys to understand the stability of the probes at different pH ranges.

4.5.8. Measurement of reaction kinetics using HPLC

First, the purity of synthesized probes was analysed using analytical high-performance liquid chromatography (HPLC) Agilent 1220 Infinity II LC system using a reverse-phase C18 column (Luna, 150 × 4.6 mm, 5 µm). HPLC grade acetonitrile and water (Finar Ltd.) were used as mobile phase and the absorbance profile of compounds were detected using a PDA detector at a wavelength of 254 and 350 nm. The stock solutions of the samples

were prepared in HPLC grade acetonitrile and were injected into the system using the autosampler at a flow rate of 1.0 mL min^{-1} using an acetonitrile/water system as a mobile phase (0–10 min: 75% acetonitrile in water; 10–15 min: 95% acetonitrile in water)..

4.5.9. Cell culture

The triple-negative breast cancer (TNBC) cells (MDA-MB-231) were obtained from the National Centre for Cell Science (NCCS), Pune, India. The cells were cultured in DMEM medium (Gibco) supplemented with 10% (v/v) FBS (Gibco) and 1% Pen-Strep (Gibco). Cells were cultured as a monolayer in a humidified incubator at 37 ºC in the presence of a 5% CO_2 level.

4.5.10. Cell viability assay

The synthesized prodrugs **NB-ITC** and **AM-ITC** were screened for their anti-proliferative activities using the conventional MTT assay in a triple negative breast cancer cell line. MDA-MB-231 cells were seeded in 96-well culture plates at a density of 2 ×10^4 cells/100 mL per well and treated with the freshly prepared test compounds **AM-ITC** (5.0, 10.0, and 25.0 µM) and **NB-ITC** (5.0, 10.0, and 25.0 µM) for 0 h (control) and 48 h (experimental), respectively. At the end of the treatment period, 10 mL of 5 mg/mL of MTT was added to the plate (control) and incubated for 4 h. Following the 4 h incubation, the reagent from the plate was removed and the purple formazan crystals were dissolved using 100 µL of DMSO (Avra Synthesis Pvt Ltd) and the absorbance at 570 nm was measured using a microplate reader (Thermo Scientific™ Multiskan™ GO microplate reader). In the experimental set, a similar MTT treatment protocol was followed only after 48 h. The mean ΔOD values were calculated by the subtraction of mean OD values of 0 h plate (control) from the mean OD values of identical wells at 48 h plate (experimental) and the percentage proliferation was calculated keeping the mean ΔOD of untreated control as 100%.

4.5.11. Fluorescence microscopic studies

MDA-MB-231 cells were cultured in high glucose DMEM medium supplemented with 10% (v/v) fetal bovine serum (FBS) and 1% penicillin/streptomycin at 37 °C under 5% CO_2 atmosphere. Cells were then plated (2.0 × 10^4 cells per plate) in 35 mm cell culture Petri dishes containing 2.0 mL of DMEM and incubated at 37 °C under 5% CO_2 for 24 h. The confluent cells were washed with DPBS and finally incubated with the prodrugs (5.0 µM). After washing the cells with DPBS (3 times), cellular morphology was carefully observed and imaged using Bio-Rad ZOE™ fluorescent cell imager under a bright field and suitable fluorescent emission filters.

4.6. References

1. Predmore, B. L.; Lefer, D. J.; Gojon, G., *Antioxid. Redox Signaling* **2012**, *17*, 119.
2. Stipanuk, M. H.; Ueki, I., *Inherited Metab. Dis.* **2011**, *34*, 17-32.
3. Li, L.; Bhatia, M.; Zhu, Y. Z.; Zhu, Y. C.; Ramnath, R. D.; Wang, Z. J.; Anuar, F. B.; Whiteman, M.; Salto-Tellez, M.; Moore, P. K., *FASEB J.* **2005**, *19*, 1196-1198.
4. Eto, K.; Asada, T.; Arima, K.; Makifuchi, T.; Kimura, H., *Biochem. Biophys. Res. Commun.* **2002**, *293*, 1485-1488.
5. Wallace, J. L.; Vong, L.; McKnight, W.; Dicay, M.; Martin, G. R., *Gastroenterology* **2009**, *137*, 569-578.e561.
6. Zhao, Y.; Wang, H.; Xian, M. *J. Am. Chem. Soc.* **2011**, *133*, 15.
7. Zheng, Y.; Yu, B.; Ji, K.; Pan, Z.; Chittavong, V.; Wang, B., *Angew. Chem. Int. Ed.* **2016**, *55*, 4514-4518.
8. Zhao, Y.; Biggs, T. D.; Xian, M., *Chem. Commun.* **2014**, *50*, 11788.
9. Shukla, P.; Khodade, V. S.; SharathChandra, M.; Chauhan, P.; Mishra, S.; Siddaramappa, S.; Pradeep, B. E.; Singh, A.; Chakrapani, H., *Chem. Sci.* **2017**, *8*, 4967-4972.
10. Zhao, Y.; Cerda, M. M.; Pluth, M. D., *Chem. Sci.* **2019**, *10*, 1873-1878.
11. Hu, Y.; Li, X.; Fang, Y.; Shi, W.; Li, X.; Chen, W.; Xian, M.; Ma, H., *Chem. Sci.* **2019**, *10*, 7690-7694.
12. Chao, J.; Zhao, J.; Jia, J.; Zhang, Y.; Huo, F.; Yin, C., *Spectrochim. Acta - A: Mol. Biomol. Spectrosc.* **2021**, *263*, 120173.
13. Bai, Y.; Wu, M.-X.; Ma, Q.-J.; Wang, C.-Y.; Sun, J.-G.; Tian, M.-J.; Li, J.-S., *New J. Chem.* **2019**, *43*, 14763-14771.
14. Huang, S.; Ma, J.; Yi, Y.; Li, M.; Cai, P.; Wu, N., *Org. Biomol. Chem.* **2022**, *20*, 4081-4085.
15. Abid, M.; Aadil, R. M., *Food Sci. Nutr.* **2020**, *8*, 4696-4707.
16. Hong, J.; Feng, G., *Sens. Actuators B Chem.* **2021**, *326*, 129016.
17. Zhao, X.; Ning, L.; Zhou, X.; Song, Z.; Zhang, J.; Guan, F.; Yang, X.-F., *Anal. Chem.* **2021**, *93*, 4894-4901.
18. Zhu, H.; Liu, C.; Rong, X.; Zhang, Y.; Su, M.; Wang, X.; Liu, M.; Zhang, X.; Sheng, W.; Zhu, B., *Bioorg. Chem.* **2022**, *122*, 105741.
19. Zhang, M.; Wang, S.; Fu, Y.; Meng, M.; Jin, H.; Zhao, W., *Sens. Actuators B: Chem.* **2022**, *366*, 132013.

20. Braña, M. F.; Cacho, M.; García, M. A.; de Pascual-Teresa, B.; Ramos, A.; Domínguez, M. T.; Pozuelo, J. M.; Abradelo, C.; Rey-Stolle, M. F.; Yuste, M.; Báñez-Coronel, M.; Lacal, J. C., *J. Med. Chem.* **2004**, *47*, 1391-1399.
21. Lin, Y.; Yang, X.; Lu, Y.; Liang, D.; Huang, D., *Org. Lett.* **2019**, *21*, 5977-5980.
22. Walunj, D.; Thankarajan, E.; Prasad, C.; Tuchinsky, H.; Baldan, S.; Sherman, M. Y.; Patsenker, L.; Gellerman, G., *Eur. J. Med. Chem.* **2021**, *225*, 113811.
23. Kornek, G.; Raderer, M.; Depisch, D.; Haider, K.; Fazeny, B.; Dittrich, C.; Scheithauer, W., *Eur. J. Cancer* **1994**, *30*, 398-400.
24. Botz, A.; Chenavier, Y.; Pécaut, J.; Delangle, P.; Gateau, C., *Tetrahedron Lett.* **2018**, *59*, 2550-2553.
25. Yue, L.; Tang, Y.; Huang, H.; Song, W.; Lin, W., *Sens. Actuators B Chem.* **2021**, *344*, 130245.

Thesis Overview and Future Perspectives

The present thesis entitled "***Stimuli-responsive Turn-on Fluorogenic Donors of Hydrogen Sulfide (H_2S) and the Prodrugs of Anti-cancer Compounds***" describes the development of fluorogenic donors of H_2S using organotrisulfide, organopolysulfide, and isothiocyanates that are triggered by bioanalytes such as biothiols (Cys, GSH) and antioxidant enzymes (TrxR). Initially, the probes are in the fluorescence-*off* state, however, upon the reaction with bioanalytes, the fluorescence gets turned-*on*. The release of the fluorophore and H_2S from these donors were confirmed by spectrophotometric methods.

Several non-fluorogenic organic donors of H_2S have been developed over the last few years for the sustained release of H_2S in aqueous and cellular media as the inorganic salts such as Na_2S or NaHS (instantaneous sources) are not suitable for the cellular applications. However, real-time monitoring of H_2S release in living cells is a big challenge using the currently available detection techniques. While the conventional methylene blue (MB) assay for estimating H_2S utilizes highly acidic conditions, the commonly used ion-sensitive electrodes (ISEs) and amperometric microsensors work in alkaline and acidic/neutral media, respectively. These are therefore not feasible in cellular medium. Although recent reports highlight numerous reaction-based fluorescent sensors of H_2S suitable in the cellular medium, many of them interfere with cell-abundant biothiols with false fluorescent signals for H_2S. Therefore, at present, the real-time detection of intracellular release of H_2S is not feasible with both non-fluorescent organic donors as well as with turn-on fluorescent sensors of H_2S. Inspired by these observations, we have developed thiol-reactive organotrisulfide-based self-immolative fluorogenic donors of H_2S (**UTS-1** and **UTS-2**) compatible in both aqueous and cellular media. The biothiol-reactive organotrisulfide-based self-immolative fluorogenic donors of H_2S were rationally designed for the efficient intracellular delivery of H_2S and further to lysosome with a concomitant turn-on fluorescence. Upon activation by thiols, they release H_2S in a controlled manner with a concomitant release of the fluorophore for the real-time monitoring of the H_2S release profile. The probe **UTS-2** was designed for the targeted delivery of H_2S to an important intracellular organelle such as lysosome (acidic pH), containing many bio-molecules and hydrolytic enzymes. However, the main drawback of

our designed probe was that the chosen fluorophore absorbs in the UV region with high energetic blue emission, which might be harmful to the cells (Chapter 2).

In chapter 3, we have reported an antioxidant enzyme TrxR-triggered fluorogenic donors of H_2S compatible in aqueous as well as cellular media. The design of TrxR-responsive organopolysulfide-based self-immolative turn-on fluorogenic donor of H_2S (**DCI-PS**) was reported. The corresponding disulfide analogue (**DCI-DS**) was synthesized for monitoring the turn-on fluorogenic processes without the donation of H_2S. Upon activation, **DCI-PS** released H_2S in a sustained manner with a concomitant fluorescence emission in the NIR region for the real-time monitoring of the H_2S release profile. In order to understand the active participation of the selenoproteins TrxR, fluorescence emission experiments were performed using the cell lysate of a representative breast cancer cells (MDA-MB-231). Interestingly, while a higher fluorescence enhancement was observed in the presence of cell lysate, the emission intensity decreased gradually in the presence of reported small-molecule inhibitors of TrxR such as ebselen, 2,4-dinitrochlorobenzene (DNCB) and triphenylphosphinegold(I) chloride.

In chapter 4, we have synthesized two isothiocyanate-based prodrugs **AM-ITC** and **NB-ITC** that are responsive toward Cys to release H_2S as well as amine compounds that showed anti-cancer activities. The prodrug **AM-ITC** reacts with Cys to give the anti-cancer compound amonafide, H_2S, and other by-products. The release of fluorophore and H_2S from these prodrugs was confirmed using spectroscopic studies in the presence of Cys under physiological conditions. These isothiocyanates display satisfactory results in aqueous solution as well as in cellular medium. **AM-ITC** showed selectivity towards Cys as compared to other thiols such as GSH, DTT, and Hcy in PBS buffer (20 mM, pH 7.4). Initially, the prodrug is weakly fluorescent due to perturbation of fluorescence by the PET process, however, upon reaction with cysteine, there is an enhancement of fluorescence intensity. Furthermore, anti-cancer activity of the prodrug and the released active anti-cancer compounds were validated further by the cellular cytotoxicity assay (MTT assay) in MDA-MB-231 cells.

In summary, we have developed polysulfides and isothiocyanate-based H_2S donors. These donors are initially in the fluorescence-off state, however, upon the reaction with bioanalytes, they release the fluorophore along with H_2S and the fluorescence gets turned-on. Although the amount of H_2S release is less because H_2S is a highly volatile gas and it

is highly recommended to do these experiments inside the glove box. However, further investigations, as listed below, may be considered as important future perspectives of the present thesis.

1) To evaluate the potencies of polar trisulfides as compared to non-polar trisulfides in organ-specific cells. This study warrants future investigations into the effects of H_2S in various applications.

2) The selective synthesis of polar trisulfides could be planned based on the feedback of the above studies.

3) Adjuvant delivery of H_2S released from polysulfides with commercial drugs associated with the H_2S-deficiency could be considered to understand the protective effects of H_2S towards the diseases.

4) The effect of sulfane sulfur in various disease models such as diabetes, inflammation, etc could be studied in the future from the synthesized compounds.

List of Publications and Presentations

Publications

1. **S. K. Mahato**, D. Bhattacherjee, P. Barman and K. P. Bhabak*, "Thioredoxin reductase-triggered fluorogenic donor of hydrogen sulfide: a model study with a symmetrical organopolysulfide probe with turn-on near-infrared fluorescent emission" *J. Mater. Chem. B*, 2022, **10**, 2183-2193.

2. K. Banerjee, D. Bhattacherjee, **S. K. Mahato**, A. Sufian, K. P. Bhabak*, "Benzimidazole- and Imidazole-Fused Selenazolium and Selenazinium Selenocyanates: Ionic Organoselenium Compounds with Efficient Peroxide Scavenging Activities" *Inorg. Chem.*, 2021, **60**, 12984-12999.

3. **S. K. Mahato**, D. Bhattacherjee, and K. P. Bhabak*, "The biothiol-triggered organotrisulfide-based self-immolative fluorogenic donors of hydrogen sulfide enable lysosomal trafficking" *Chem. Commun*., 2020, **56**, 7769-7772

4. D. Bhattacherjee, A. Sufian, **S. K. Mahato**, S. Begum, K. Banerjee, S. De, H. K. Srivastava*, K. P. Bhabak*, "Trisulfides over disulfides: highly selective synthetic strategies, anti-proliferative activities and sustained H_2S release profiles" *Chem. Commun*., 2019, **55**, 13534-13537.

Poster Presentations

1. Presented a poster in **National Organic Symposium Trust** (**XVI-J-NOST**), held at Indian Institute of Science, Bangalore, India during Oct 31 – Nov 1, **2020**.
2. Presented a poster in **Research Conclave**, held at Indian Institute of Technology Guwahati, India during Jan 20 – 23, **2022**.
3. Presented a poster at the **28th National Symposium in Chemistry** (**CRSI-NSC-28**) held during Mar 25-27, **2022** at IIT Guwahati.
4. Presented a poster at the **North-East Research Conclave** (**NERC**) held during May 20-22, **2022** at IIT Guwahati.

Supplementary data for Chapter 2

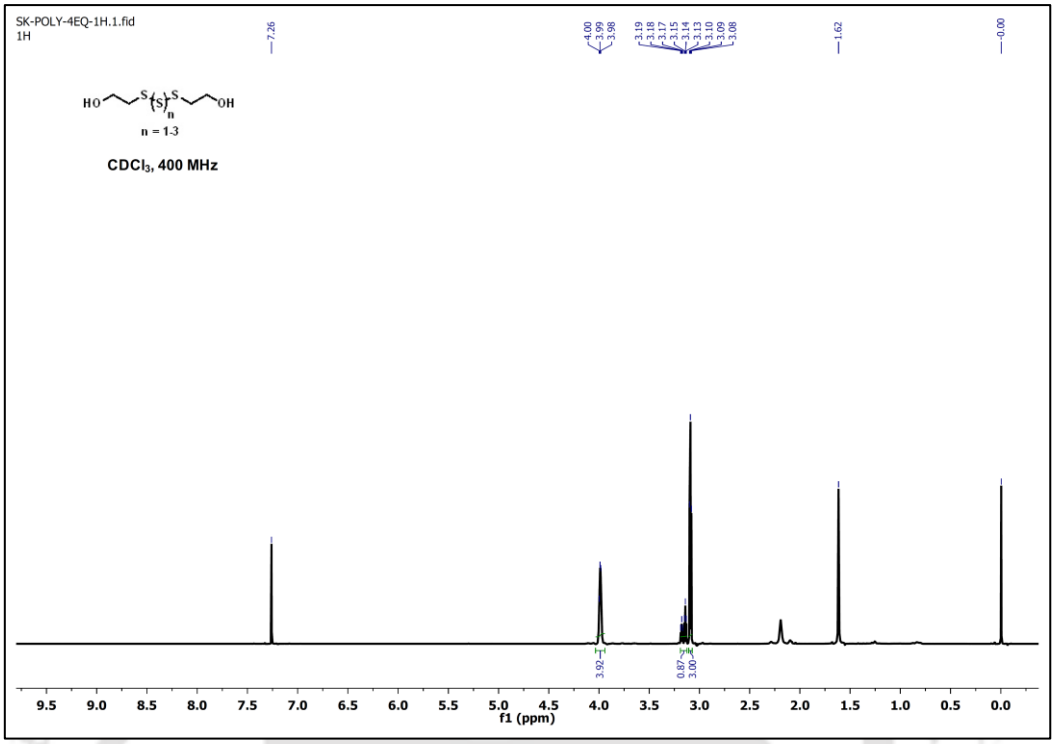

Figure A3.1. ^{1}H NMR spectrum ($CDCl_3$, 400 MHz) of compounds **2.4-2.6**.

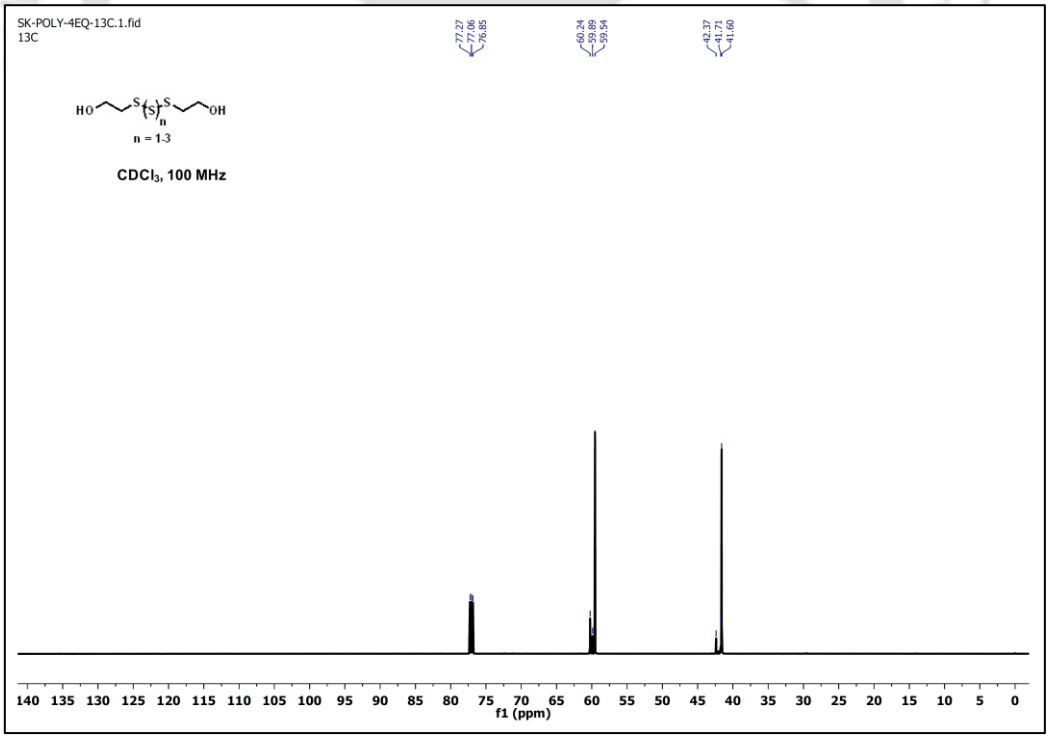

Figure A3.2. ^{13}C NMR spectrum ($CDCl_3$, 100 MHz) of compounds **2.4-2.6**.

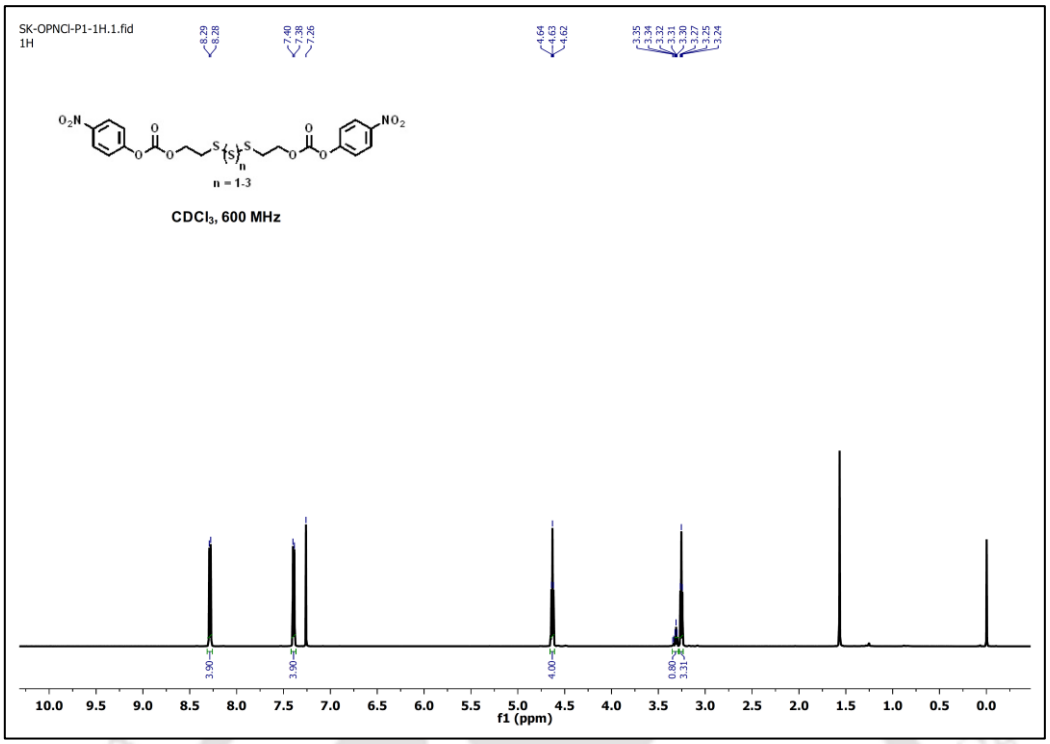

Figure A3.3. ^{1}H NMR spectrum ($CDCl_3$, 600 MHz) of compounds **2.7-2.9**.

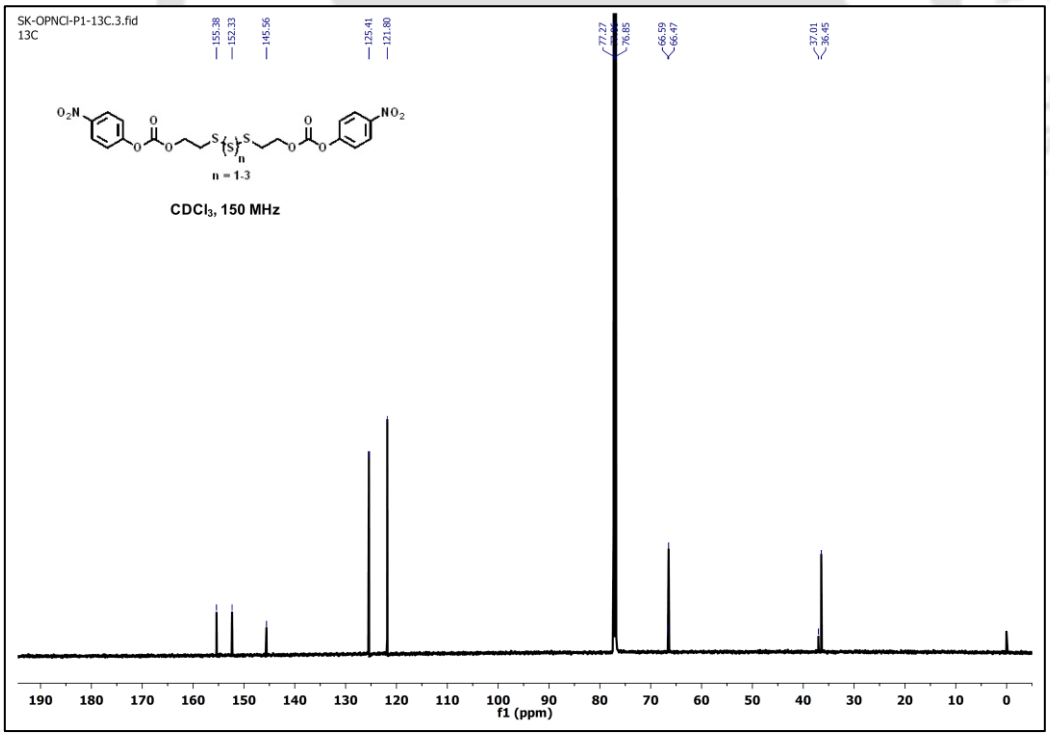

Figure A3.4. ^{13}C NMR spectrum ($CDCl_3$, 150 MHz) of compounds **2.7-2.9**.

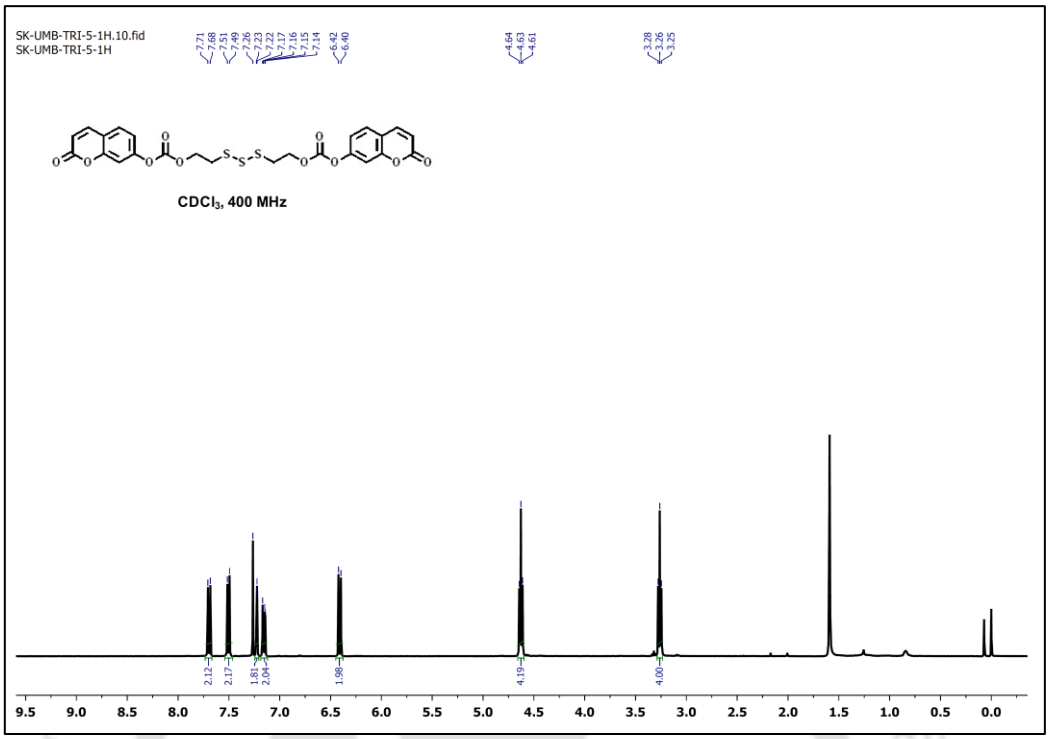

Figure A3.5. ^{1}H NMR spectrum ($CDCl_3$, 400 MHz) of **UTS-1**

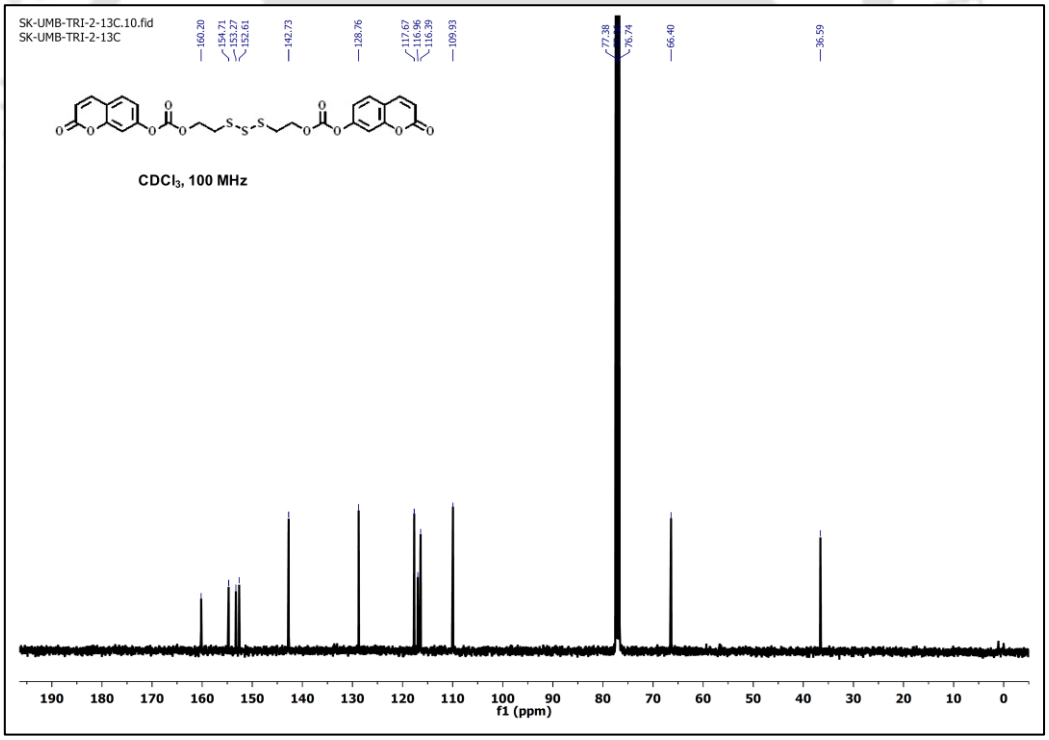

Figure A3.6. ^{13}C NMR spectrum ($CDCl_3$, 100 MHz) of **UTS-1**

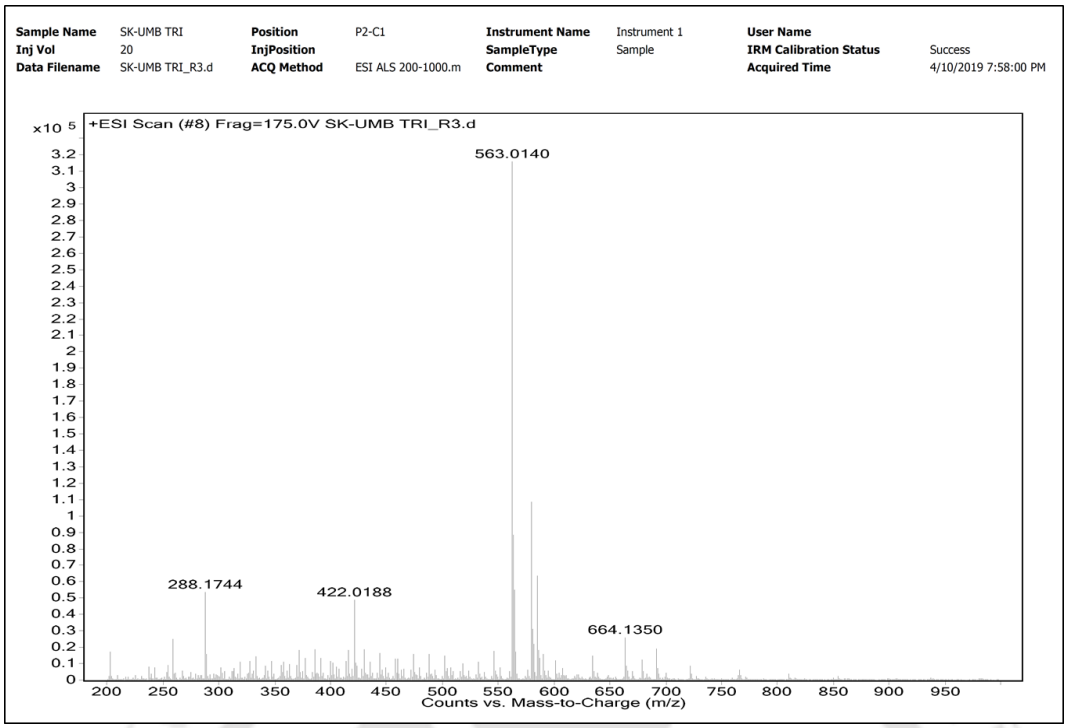

Figure A3.7. ESI-MS (+ve) spectrum of **UTS -1**. ESI-MS *m/z* calcd. for $C_{24}H_{18}O_{10}S_3$ $[M+H]^+$ = 563.0140, obs. 563.0140.

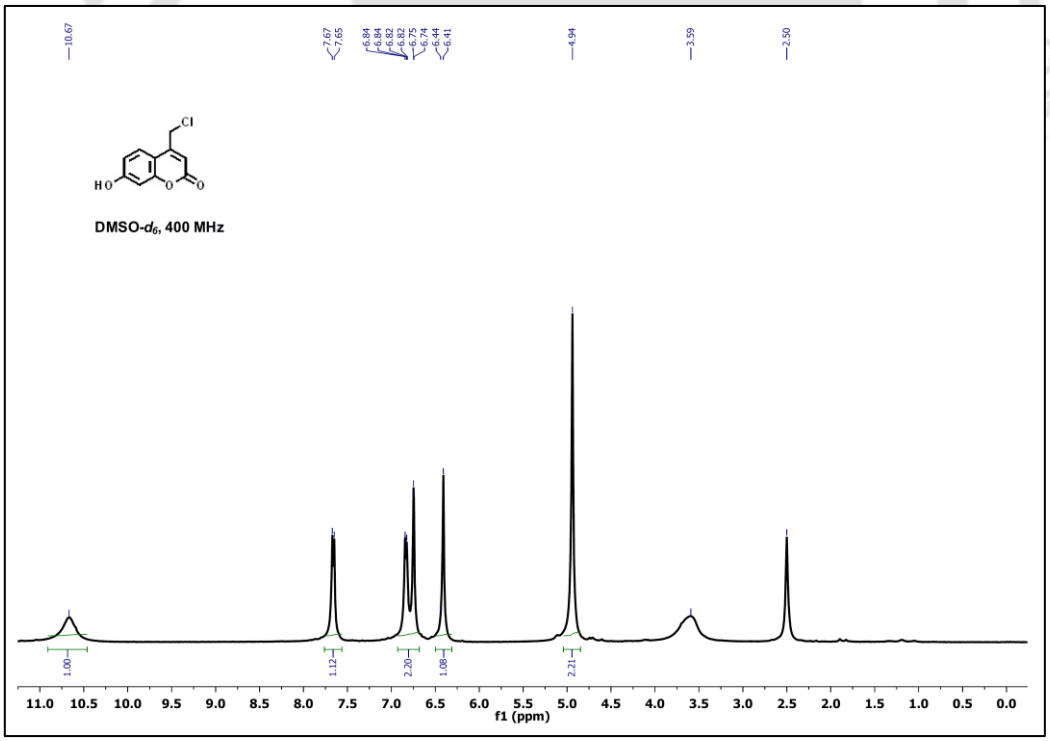

Figure A3.8. ^{1}H NMR spectrum (DMSO-d_6, 400 MHz) of compound **2.13**.

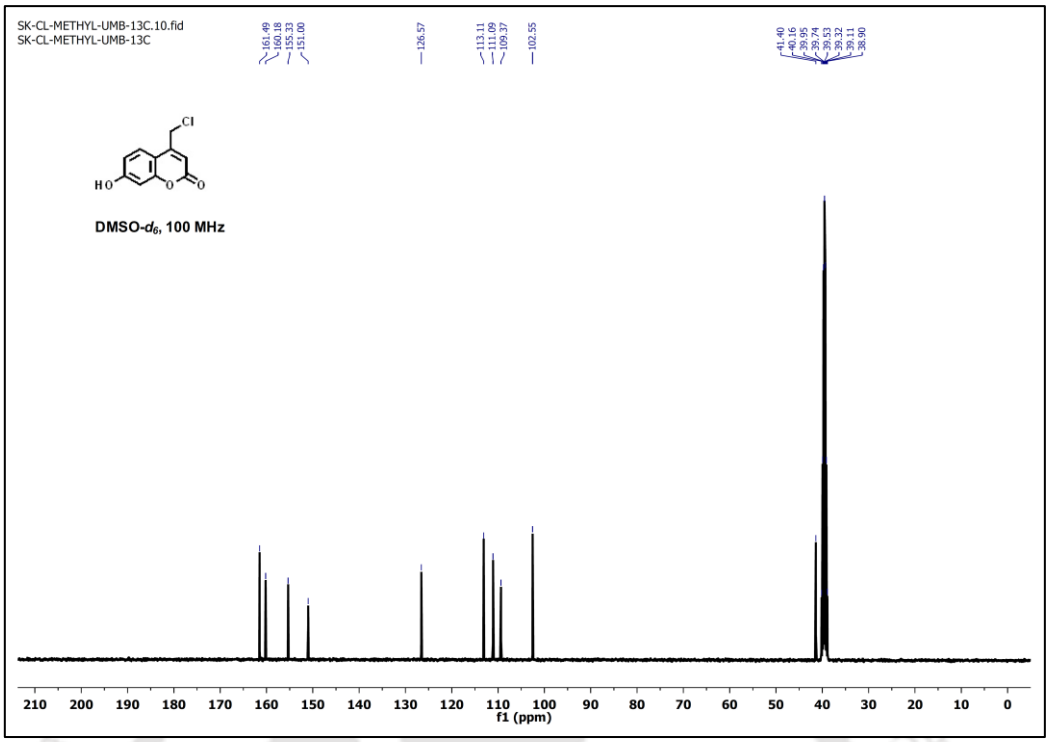

Figure A3.9. ^{13}C NMR spectrum (DMSO-d_6, 100 MHz) of compound **2.13**.

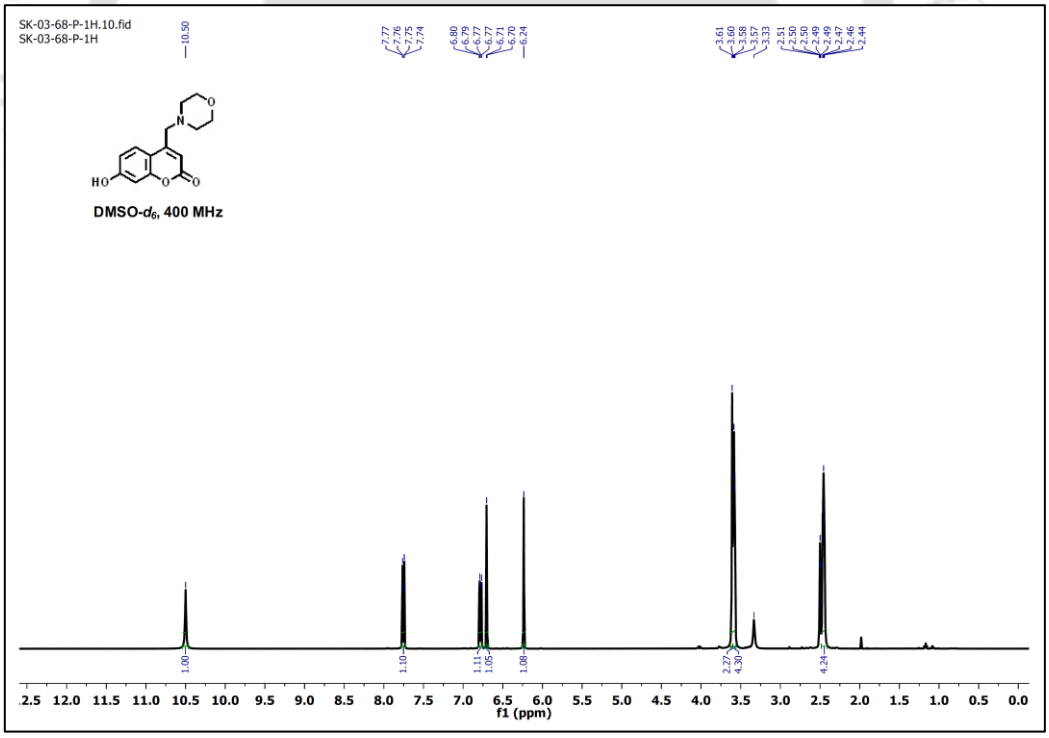

Figure A3.10. ^{1}H NMR spectrum (DMSO-d_6, 400 MHz) of compound **2.1b**.

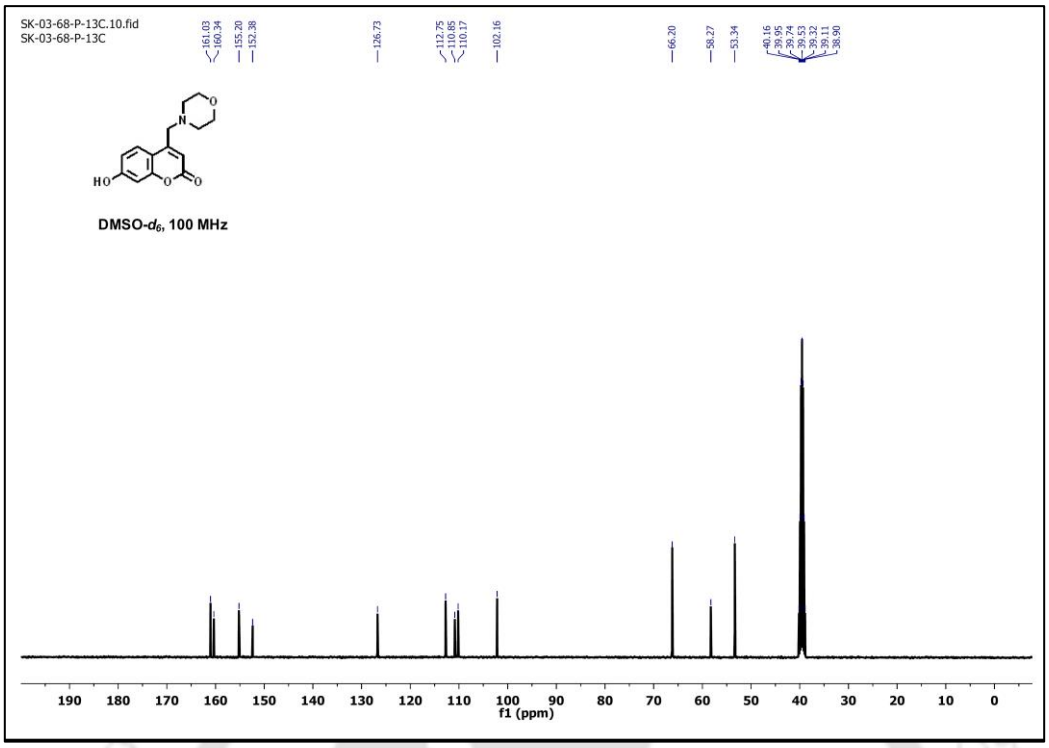

Figure A3.11. ^{13}C NMR spectrum (DMSO-d_6, 100 MHz) of compound **2.1b**.

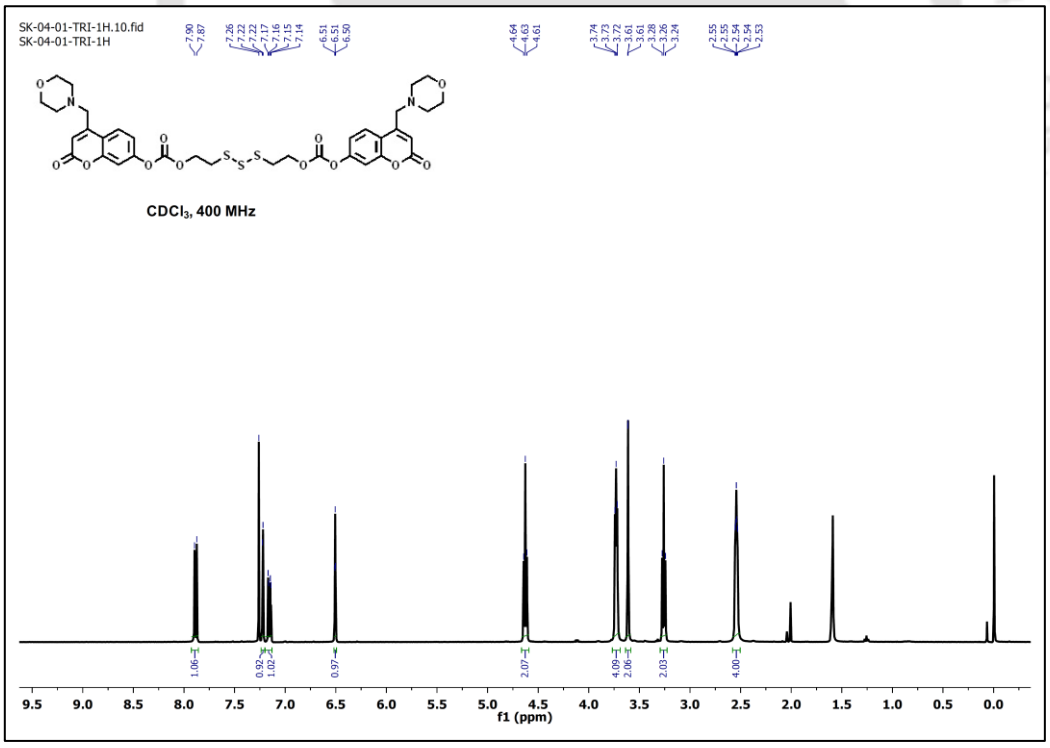

Figure A3.12. ^{1}H NMR spectrum ($CDCl_3$, 400 MHz) of **UTS-2**

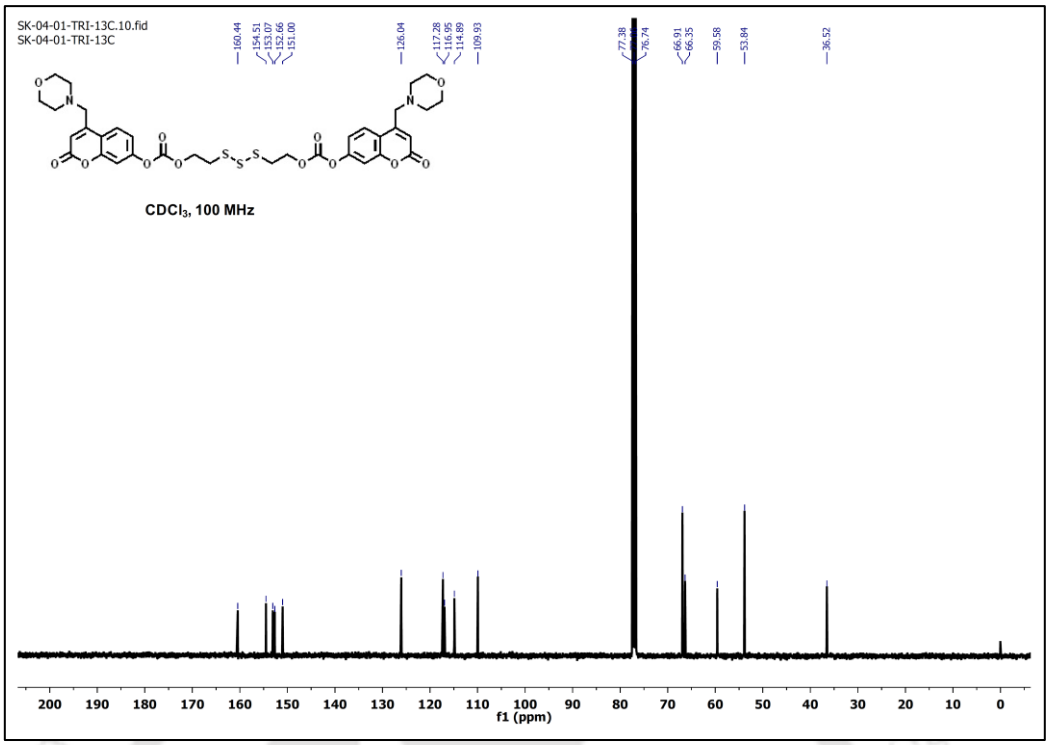

Figure A3.13. ^{13}C NMR spectrum ($CDCl_3$, 100 MHz) of **UTS-2**

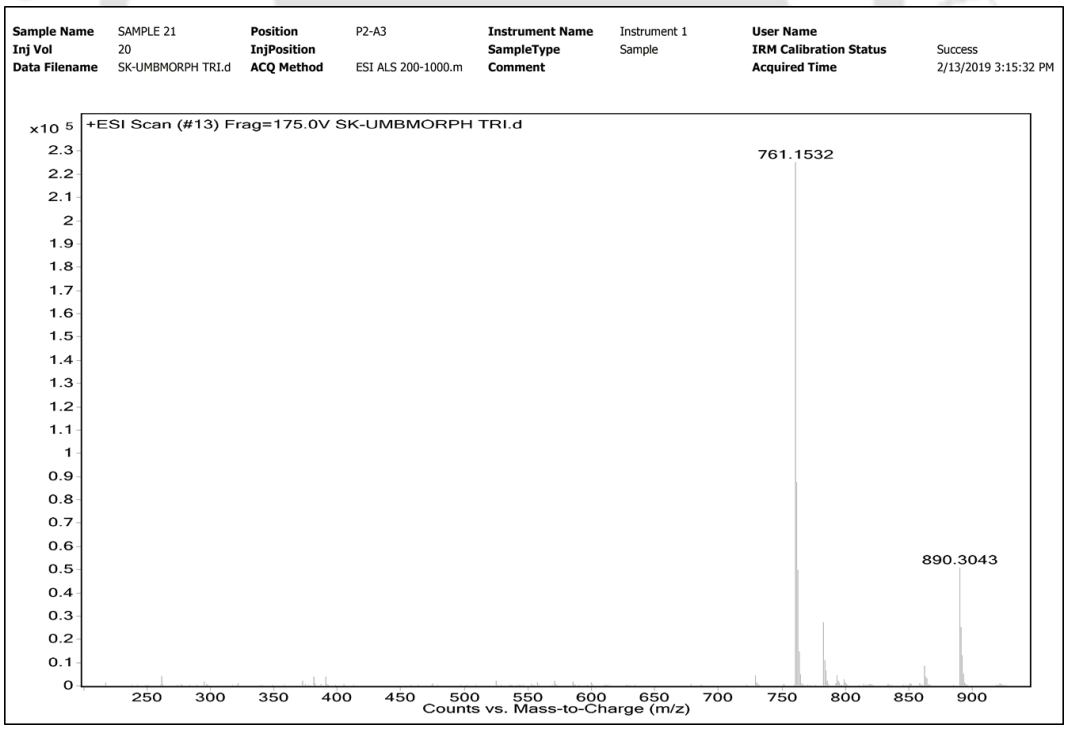

Figure A3.14. ESI-MS (+ve) spectrum of **UTS-2**. ESI-MS (+ve) *m/z* calcd. for $[C_{34}H_{36}N_2O_{12}S_3]$ $[M+H]^+$ = 761.1509, obs. 761.1532.

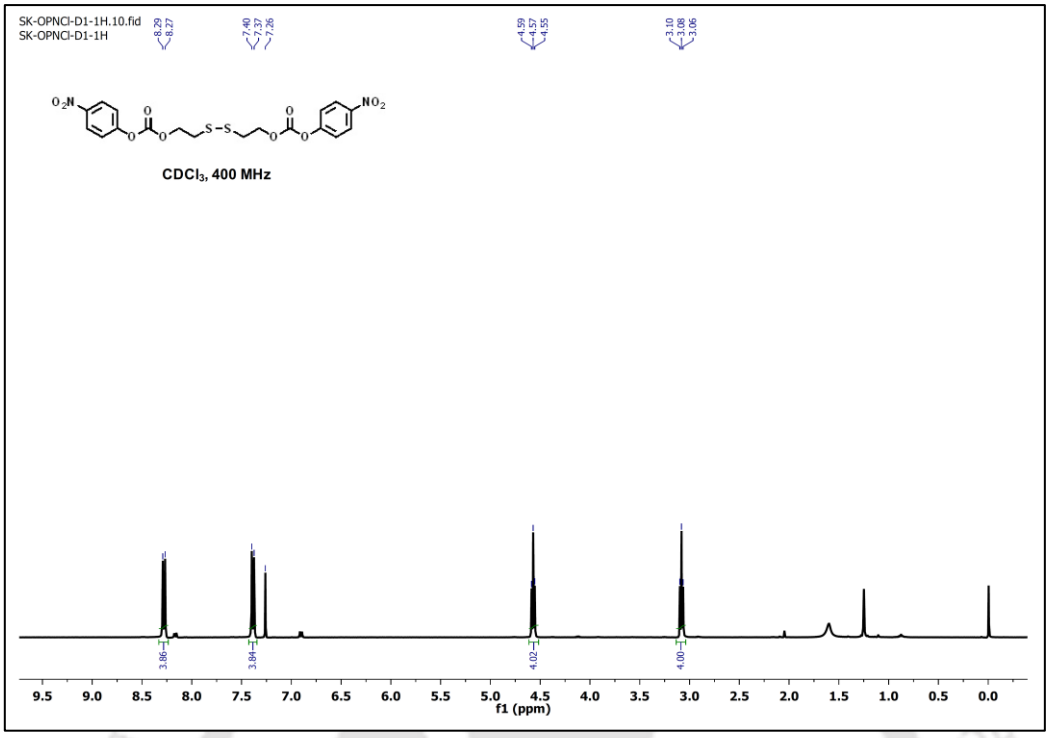

Figure A3.15. ^{1}H NMR spectrum ($CDCl_3$, 400 MHz) of compound **2.17**.

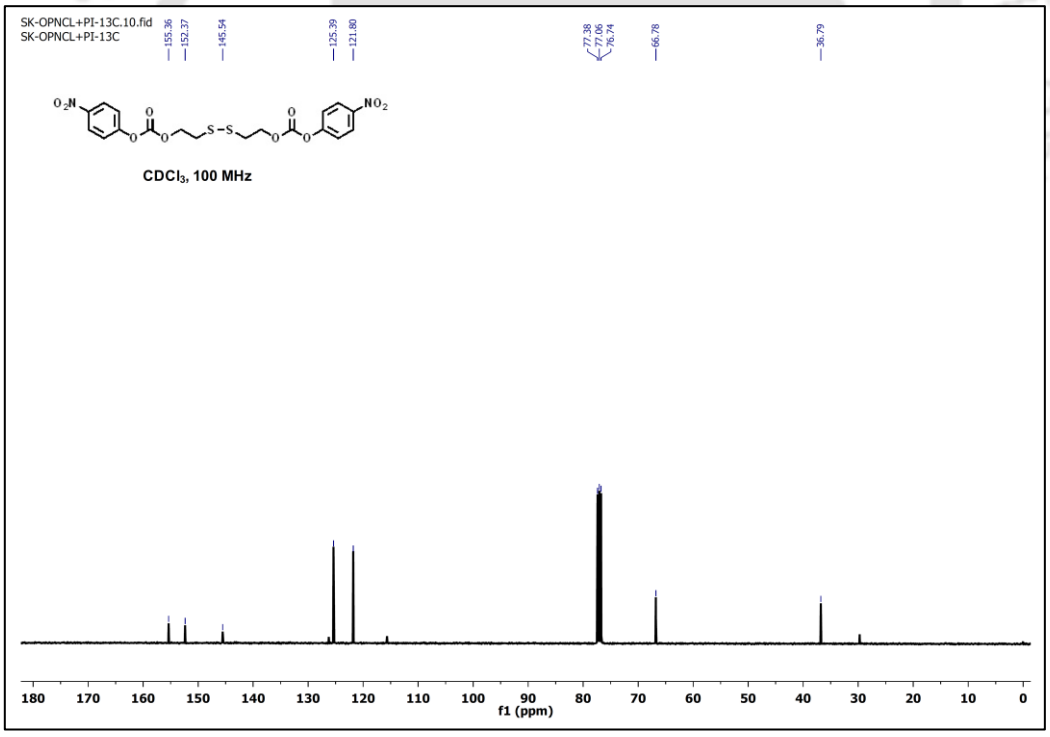

Figure A3.16. ^{13}C NMR spectrum ($CDCl_3$, 100 MHz) of compound **2.17**.

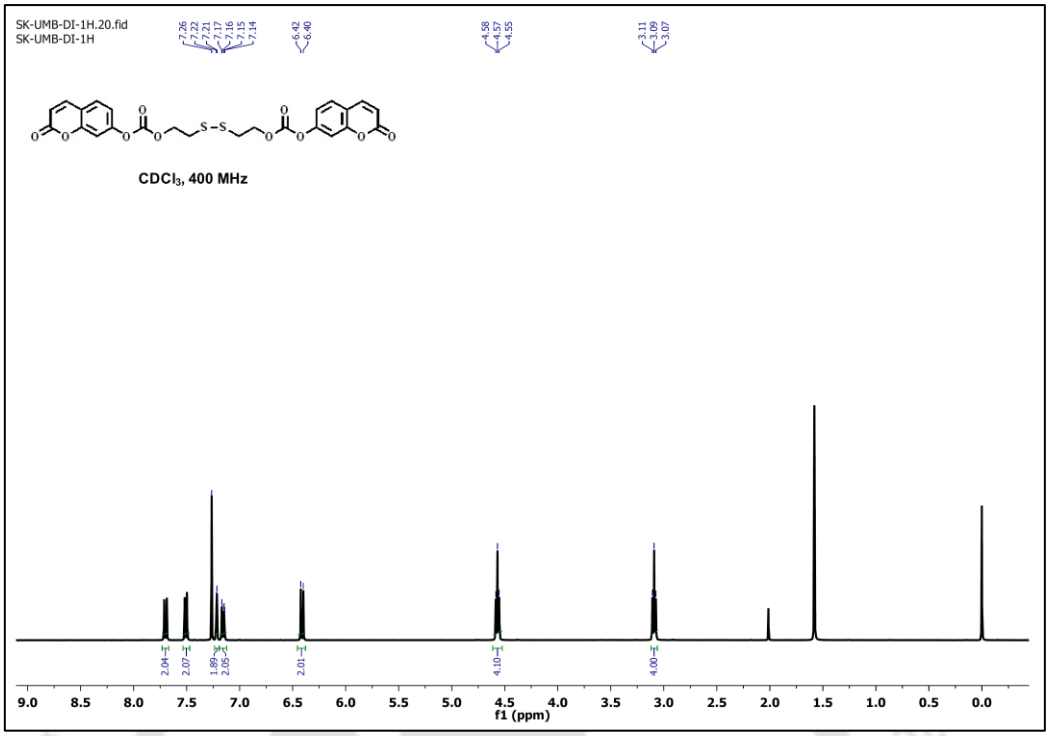

Figure A3.17. ^{1}H NMR spectrum ($CDCl_3$, 400 MHz) of **UDS-1**.

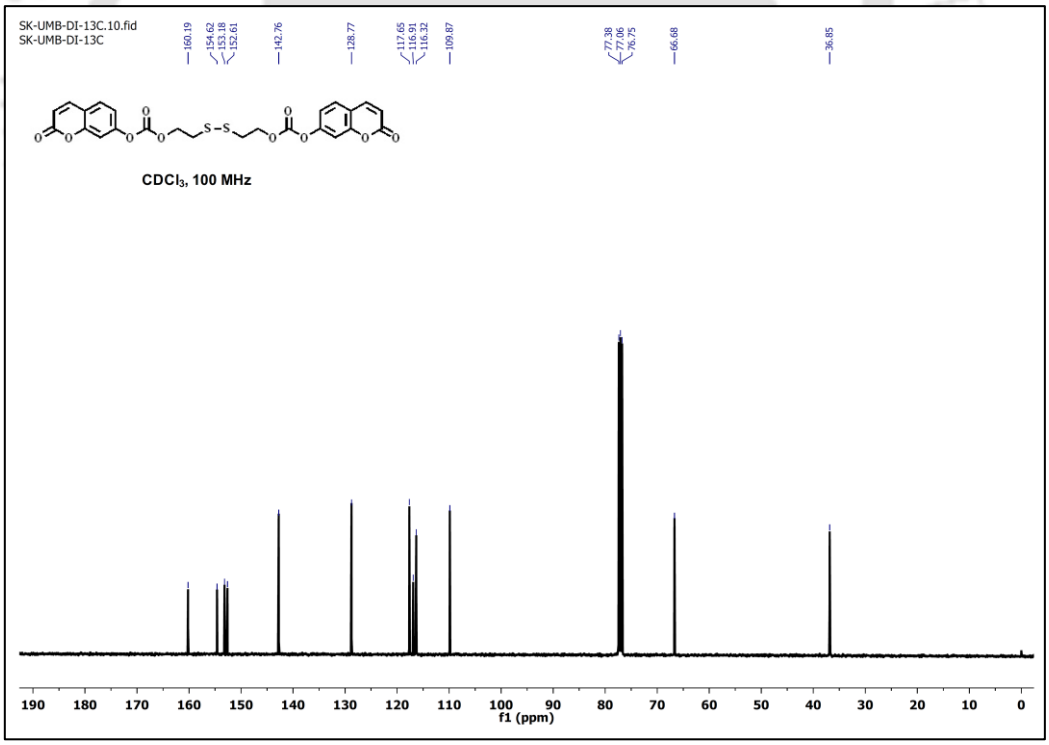

Figure A3.18. ^{13}C NMR spectrum ($CDCl_3$, 100 MHz) of **UDS-1**.

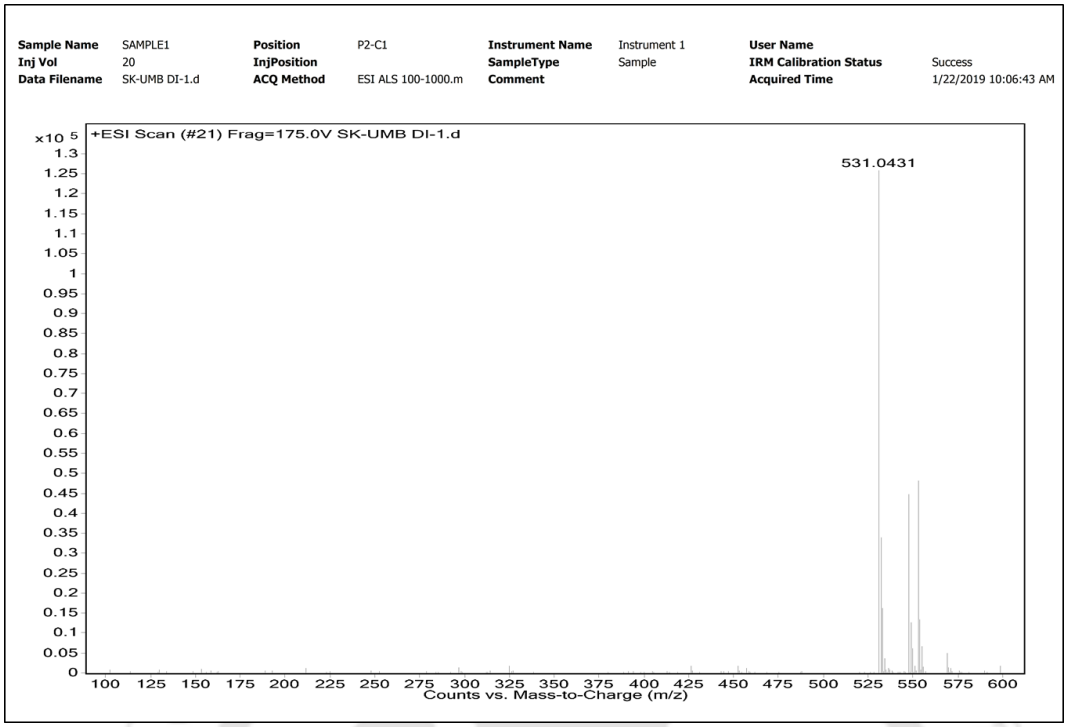

Figure A3.19. ESI-MS (+ve) spectrum of **UDS-1**. ESI-MS *m/z* calcd. for $C_{24}H_{18}O_{10}S_2$ $[M+H]^+$ = 531.0420, obs. 531.0431.

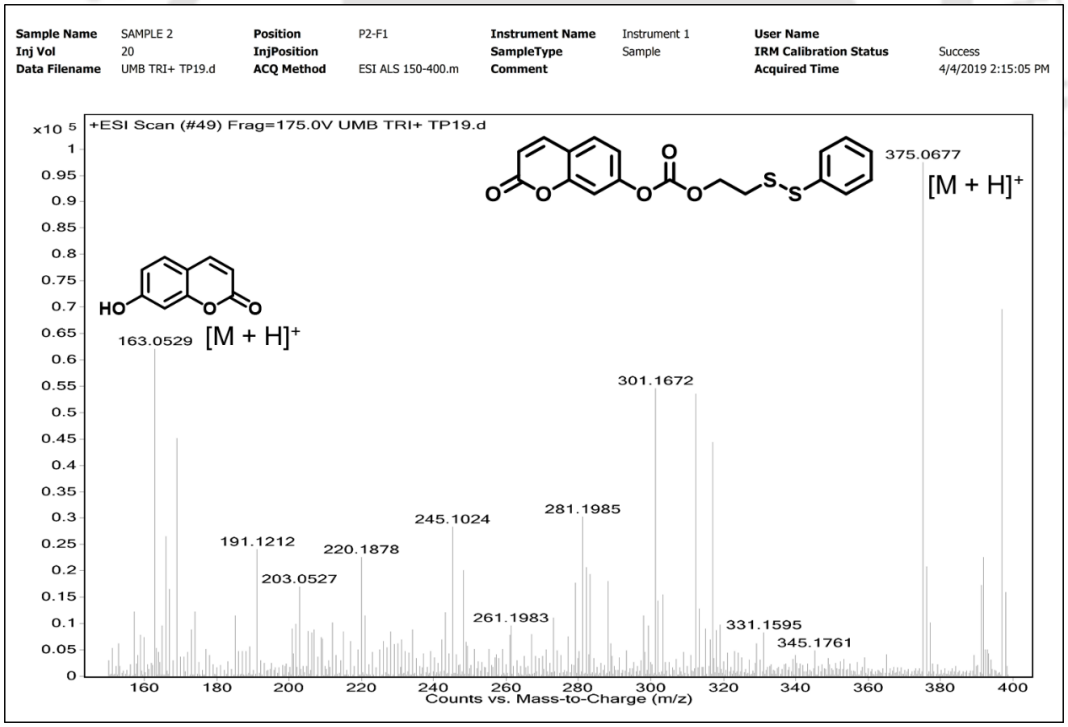

Figure A3.20. ESI-MS spectrum of the reaction mixture upon the reaction of **UTS-1** with 7.0 equiv of PhSH in acetonitrile. The released umbelliferone **2.1a** and the key mixed disulfide intermediate **2.21** could be identified under mass analysis condition. ESI-MS (+ve) *m/z* calcd. for compound **2.1a** $C_9H_6O_3$ $[M+H]^+$ = 163.0395, obs. 163.0529, *m/z* calcd. for compound **2.21** $C_{18}H_{14}O_5S_2$ $[M+H]^+$ = 375.0361, obs. 375.0677.

Supplementary data for Chapter 3

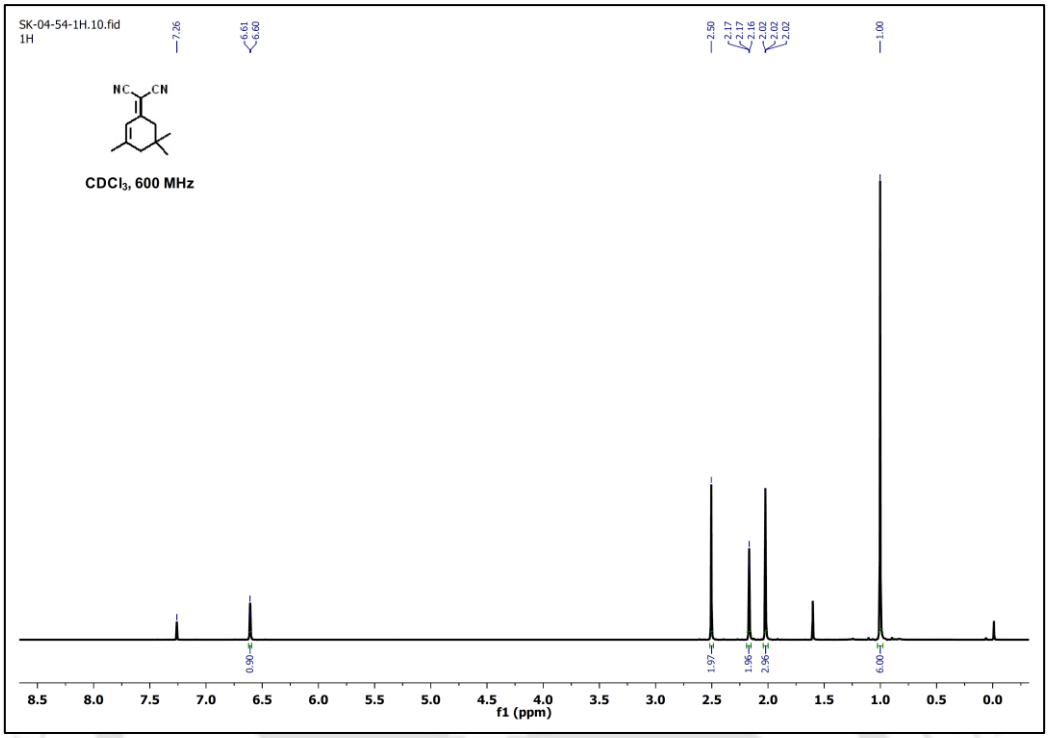

Figure A4.1. ^{1}H NMR spectrum ($CDCl_3$, 600 MHz) of compound **3.2**.

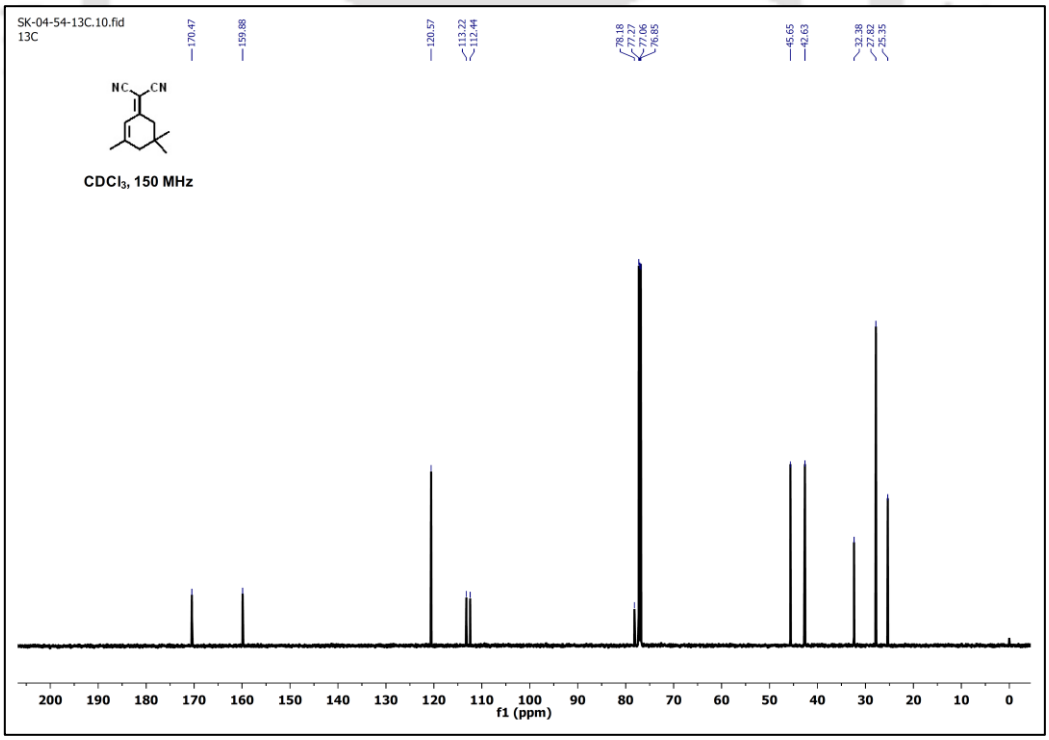

Figure A4.2. ^{13}C NMR spectrum ($CDCl_3$, 150 MHz) of compound **3.2**.

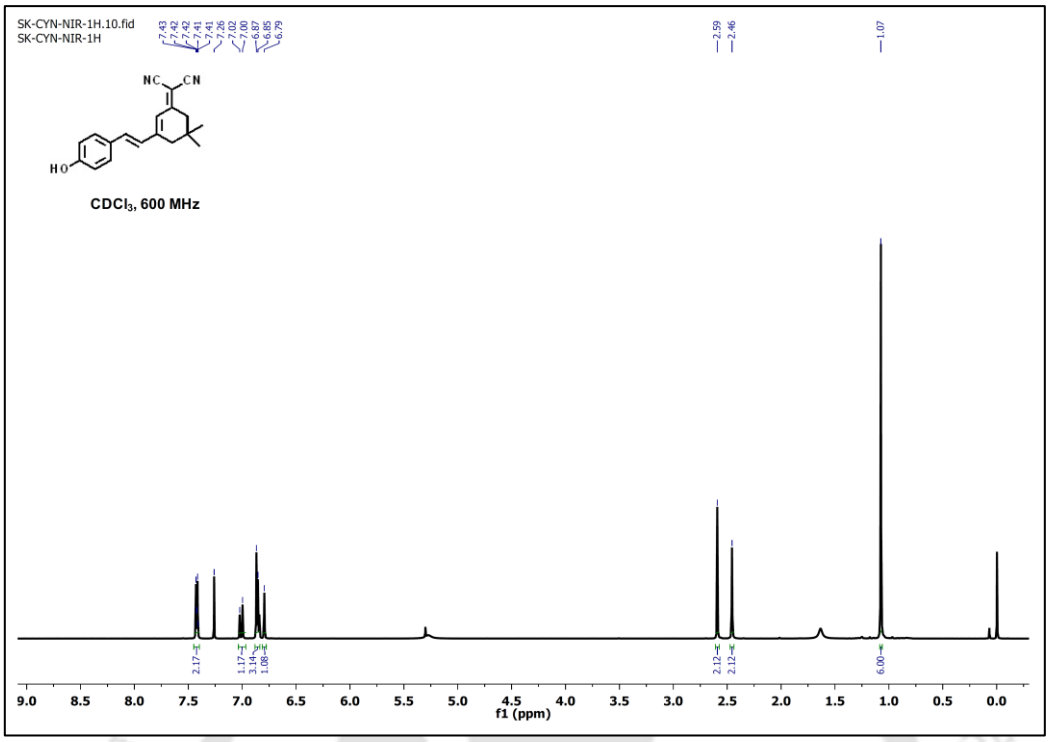

Figure A4.3. ^{1}H NMR spectrum ($CDCl_3$, 600 MHz) of **DCI-OH**.

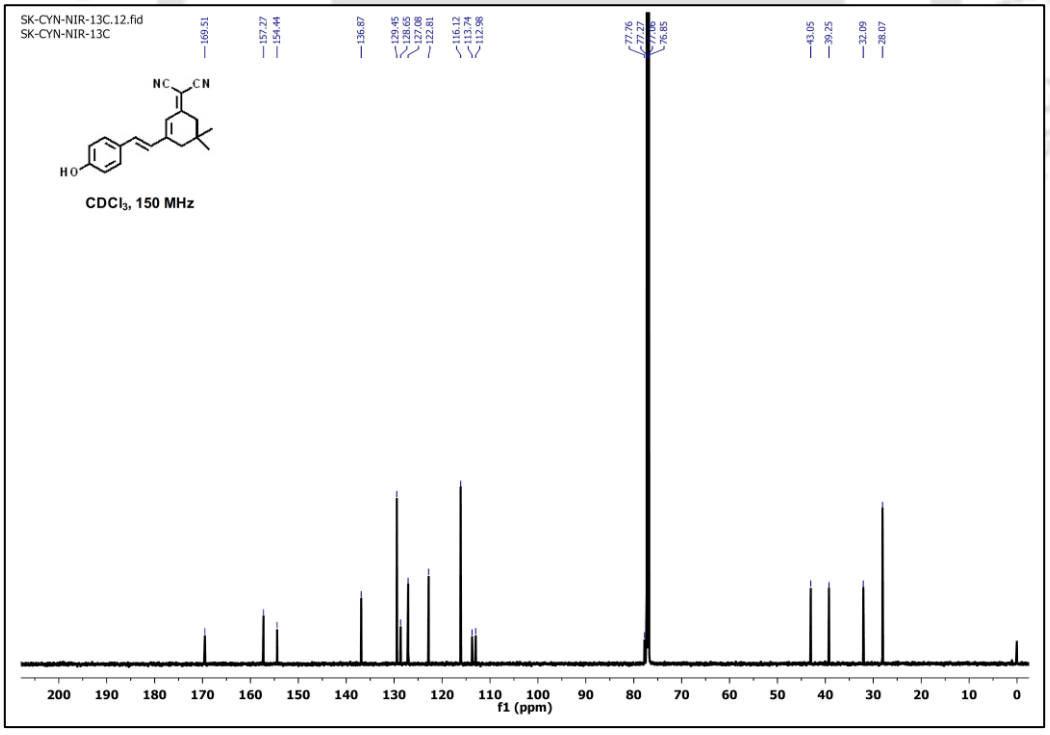

Figure A4.4. ^{13}C NMR spectrum ($CDCl_3$, 150 MHz) of **DCI-OH**.

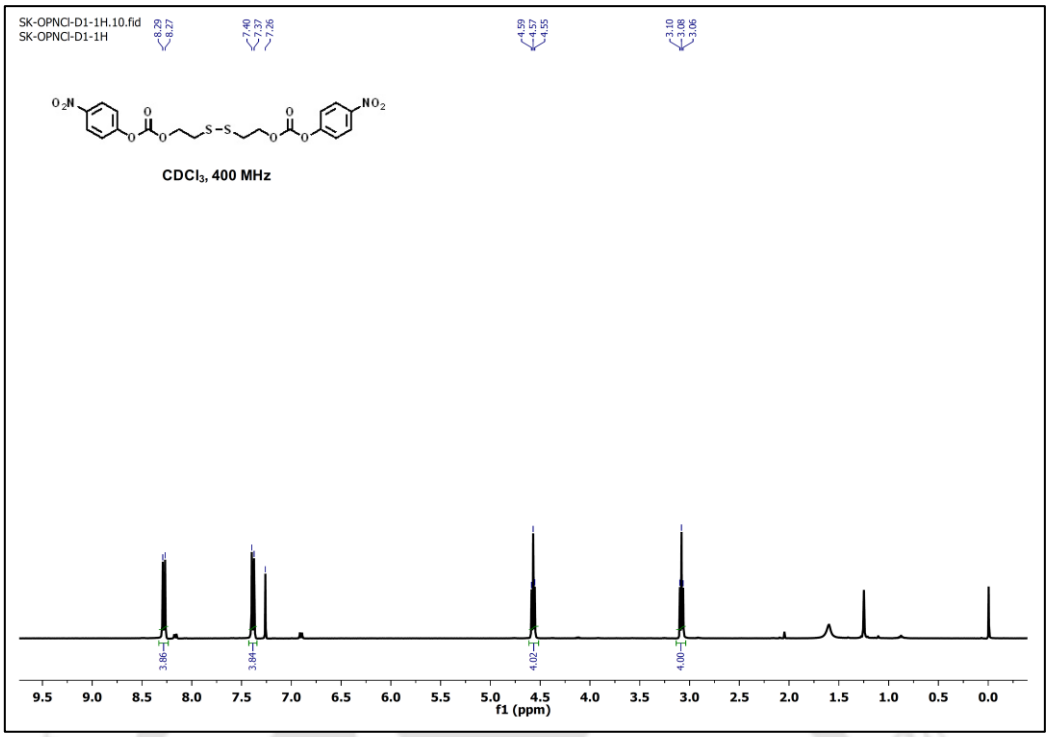

Figure A4.5. ^{1}H NMR spectrum ($CDCl_3$, 400 MHz) of compound **2.17**.

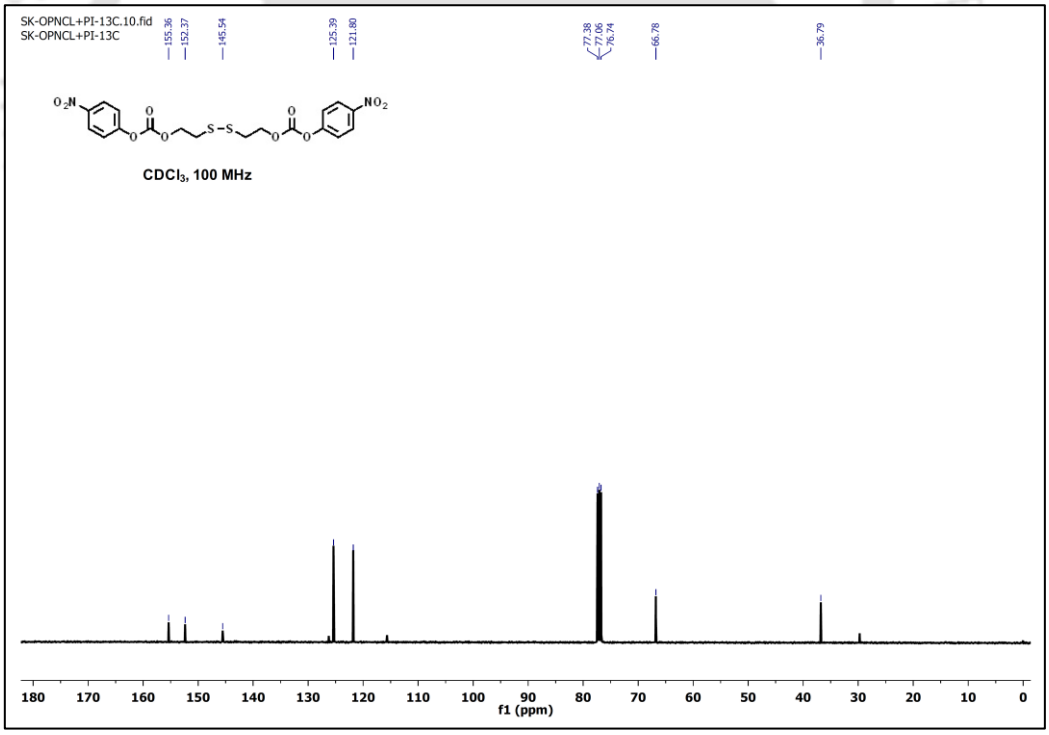

Figure A4.6. ^{13}C NMR spectrum ($CDCl_3$, 100 MHz) of compound **2.17**.

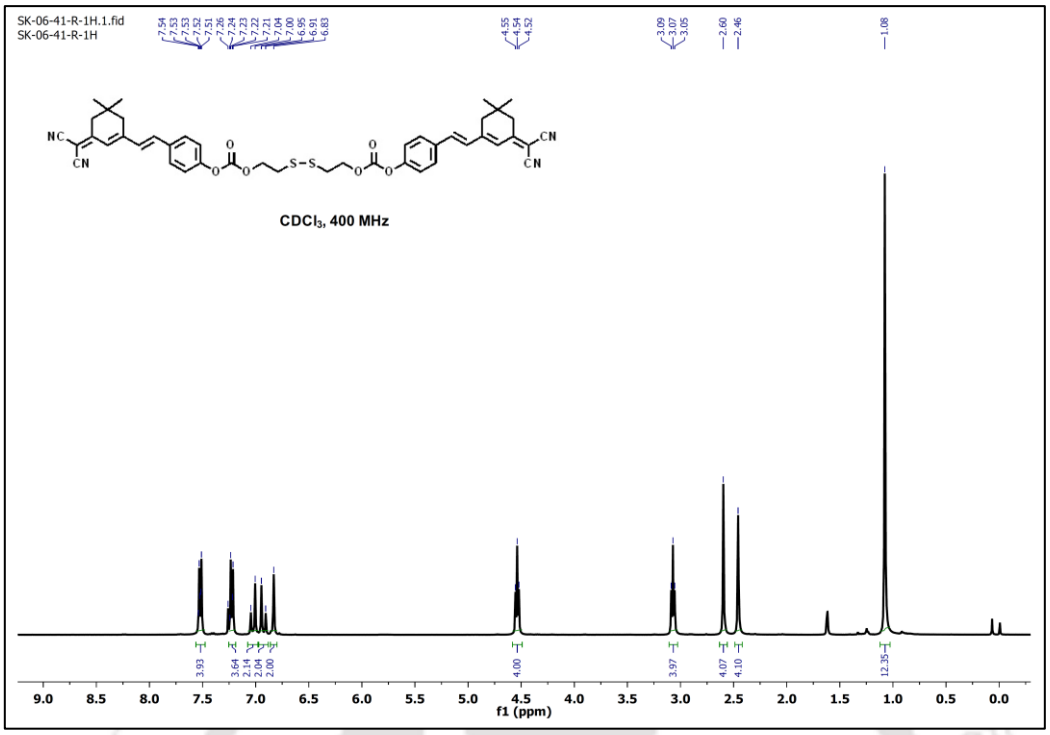

Figure A4.7. ^{1}H NMR spectrum ($CDCl_3$, 400 MHz) of **DCI-DS**.

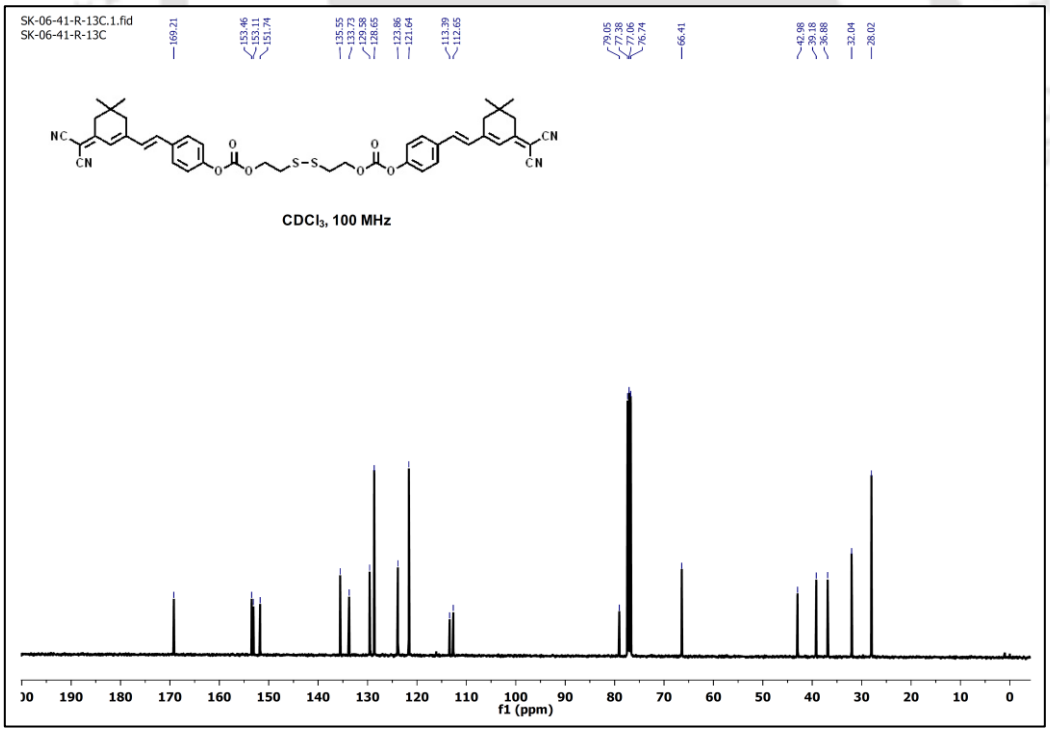

Figure A4.8. ^{13}C NMR spectrum ($CDCl_3$, 100 MHz) of **DCI-DS**.

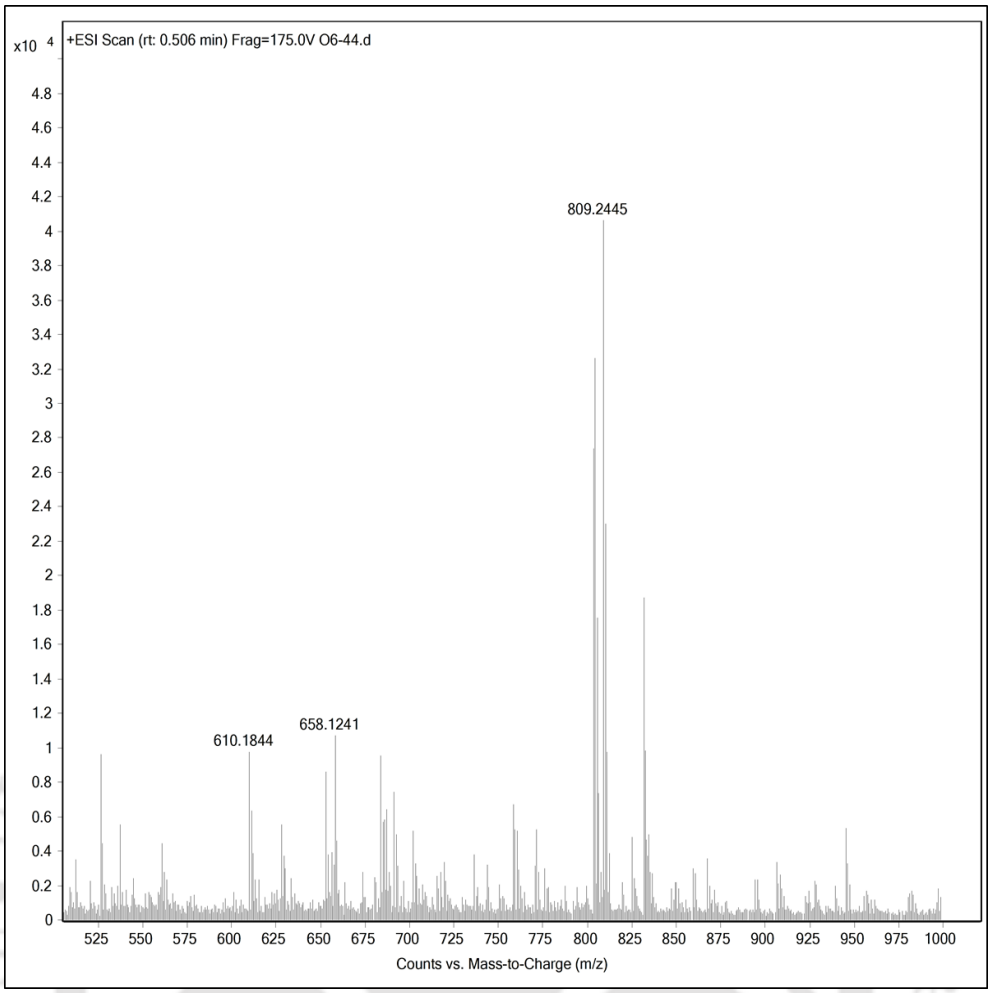

Figure A4.9. ESI-MS (+ ve) spectrum of **DCI-DS**. ESI-MS : *m/z* calcd. for $C_{44}H_{46}N_5O_6S_2$ $[M + Na]^+$ = 809.2443, obs. 809.2449.

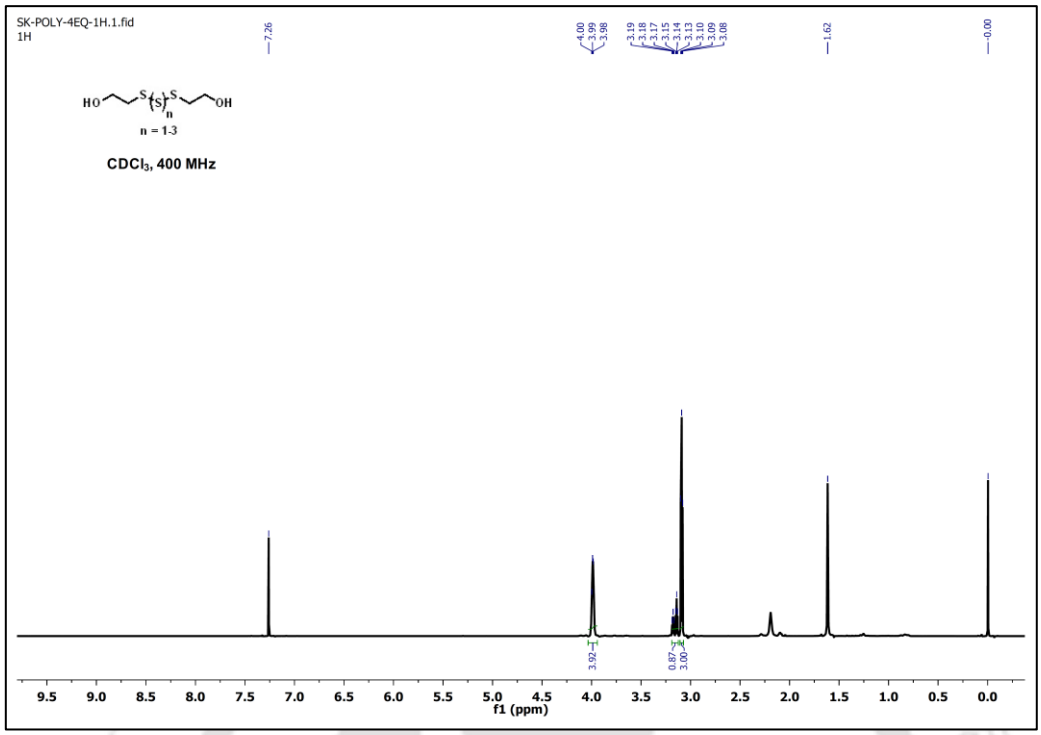

Figure A4.10. ^{1}H NMR spectrum ($CDCl_3$, 400 MHz) of compounds **2.4-2.6**.

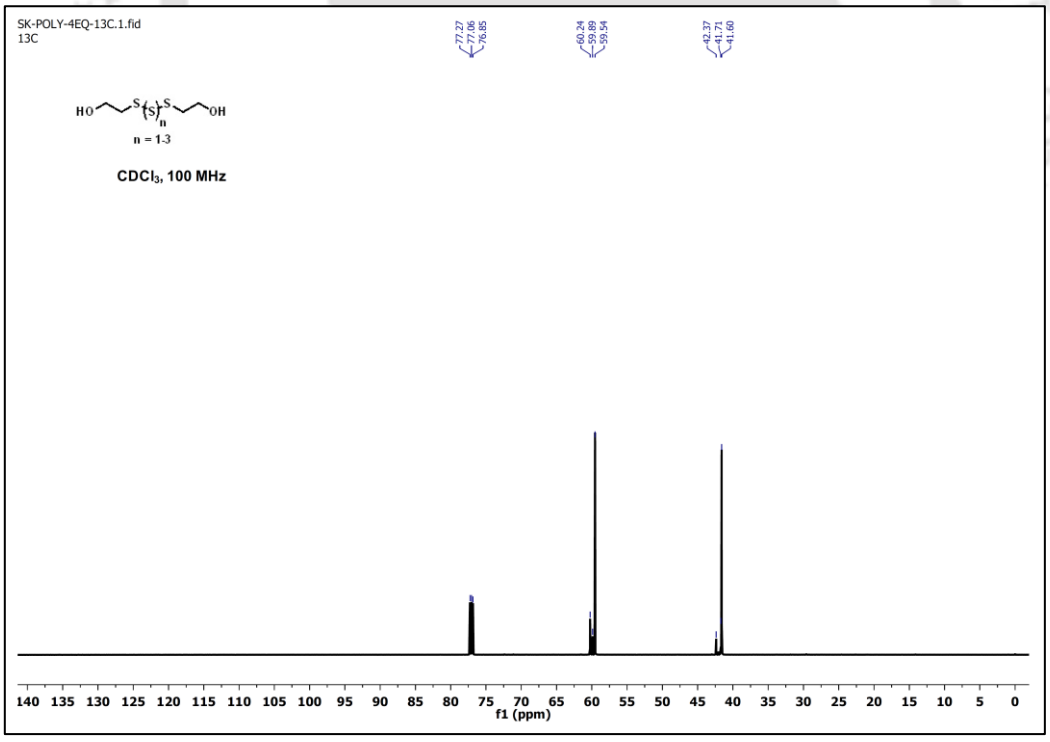

Figure A4.11. ^{13}C NMR spectrum ($CDCl_3$, 100 MHz) of compounds **2.4-2.6**.

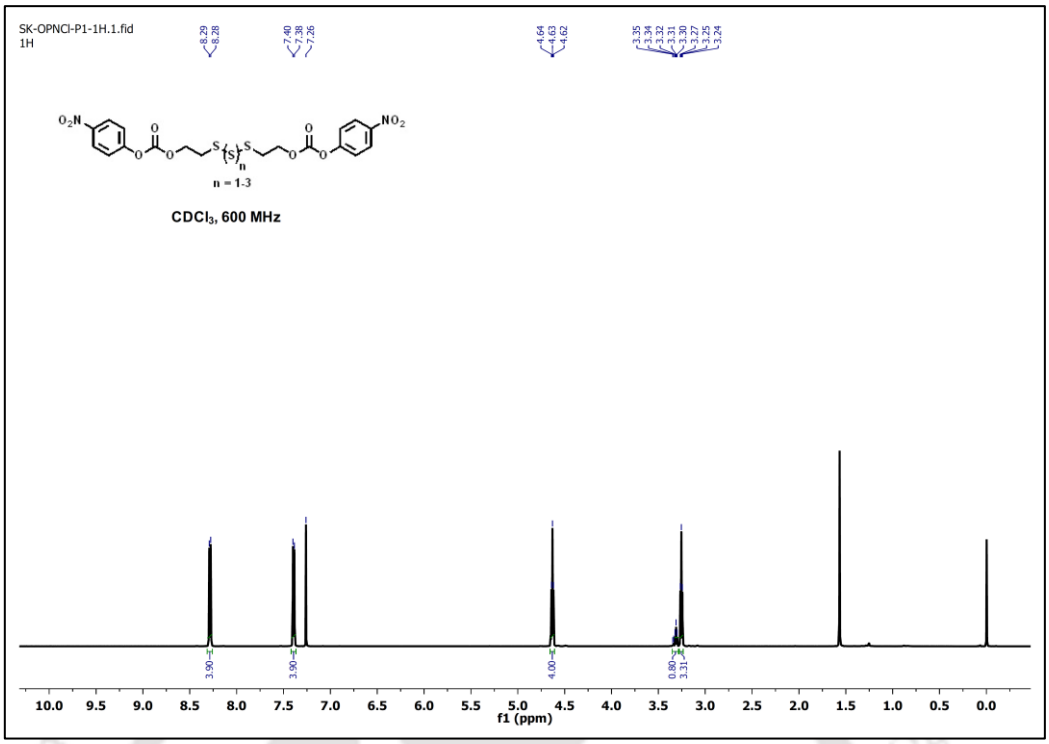

Figure A4.12. ^{1}H NMR spectrum ($CDCl_3$, 600 MHz) of compounds **2.7-2.9**.

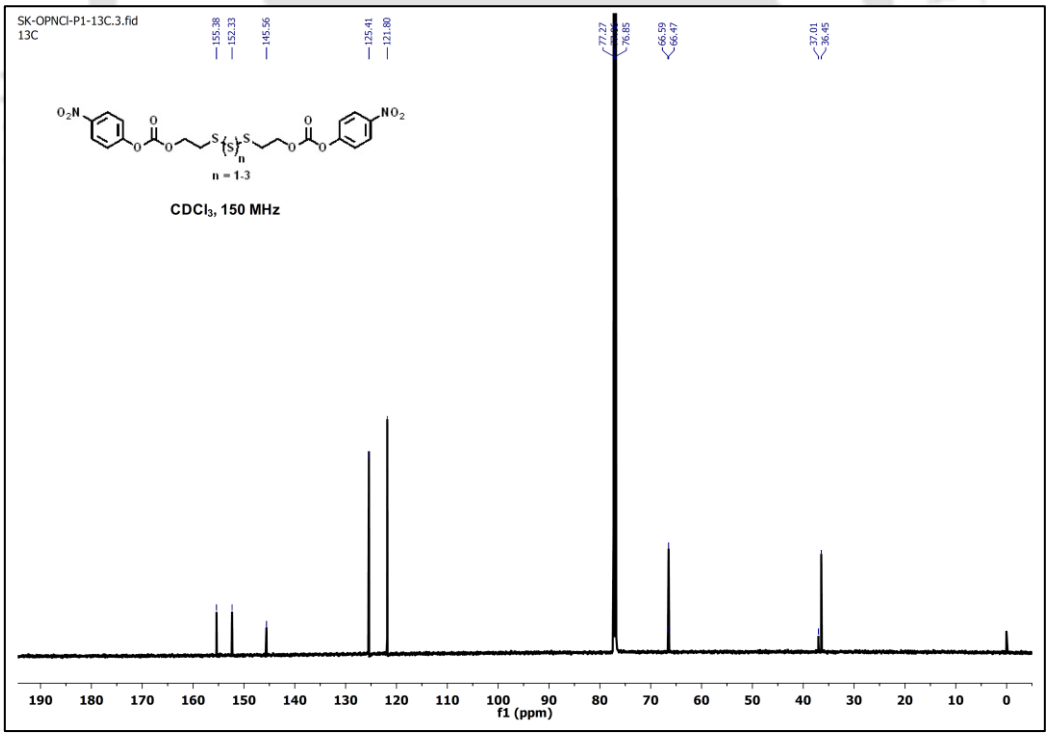

Figure A4.13. ^{13}C NMR spectrum ($CDCl_3$, 150 MHz) of compounds **2.7-2.9**.

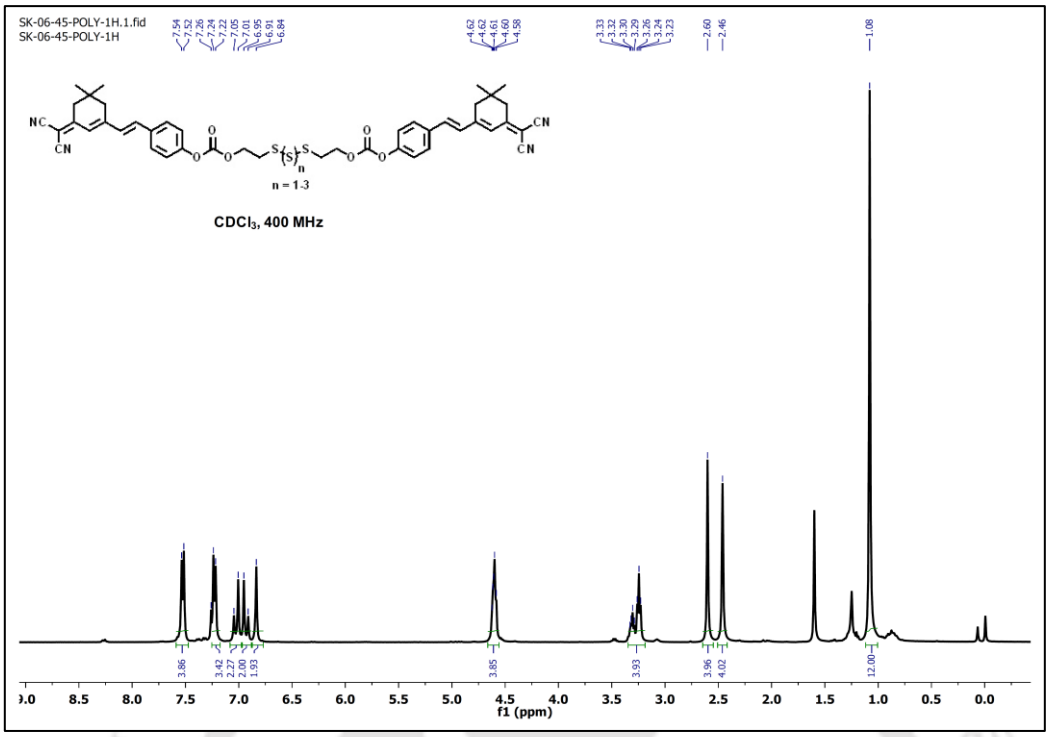

Figure A4.14. ^{1}H NMR spectrum ($CDCl_3$, 400 MHz) of **DCI-PS**.

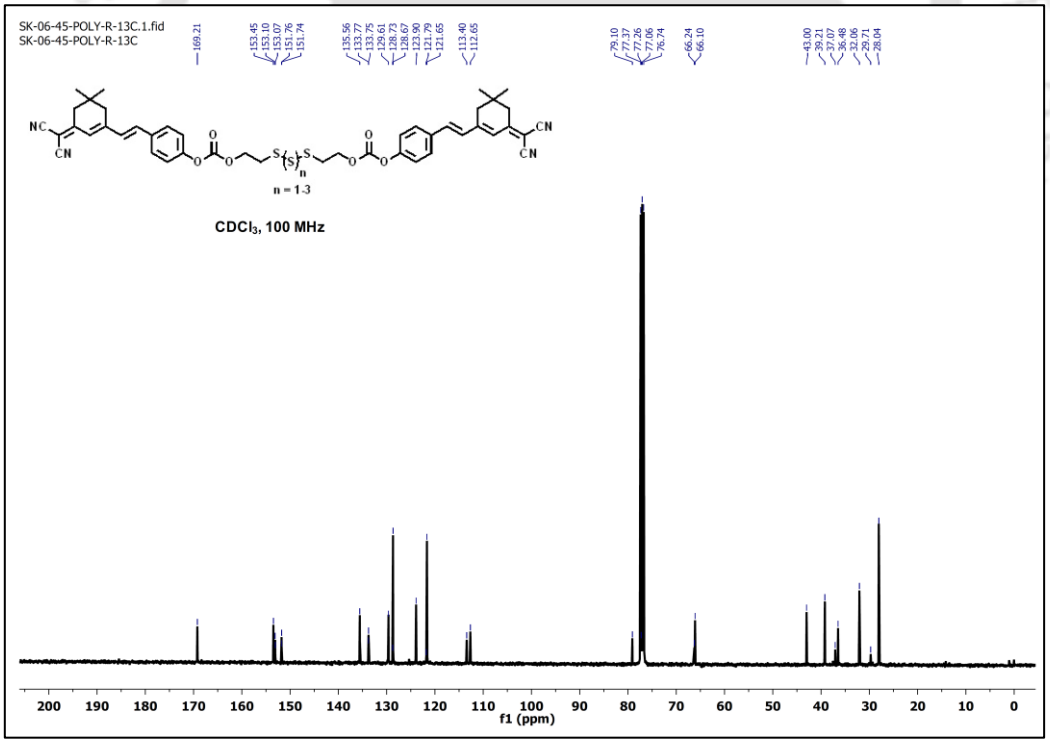

Figure A4.15. ^{13}C NMR spectrum ($CDCl_3$, 100 MHz) of **DCI-PS**.

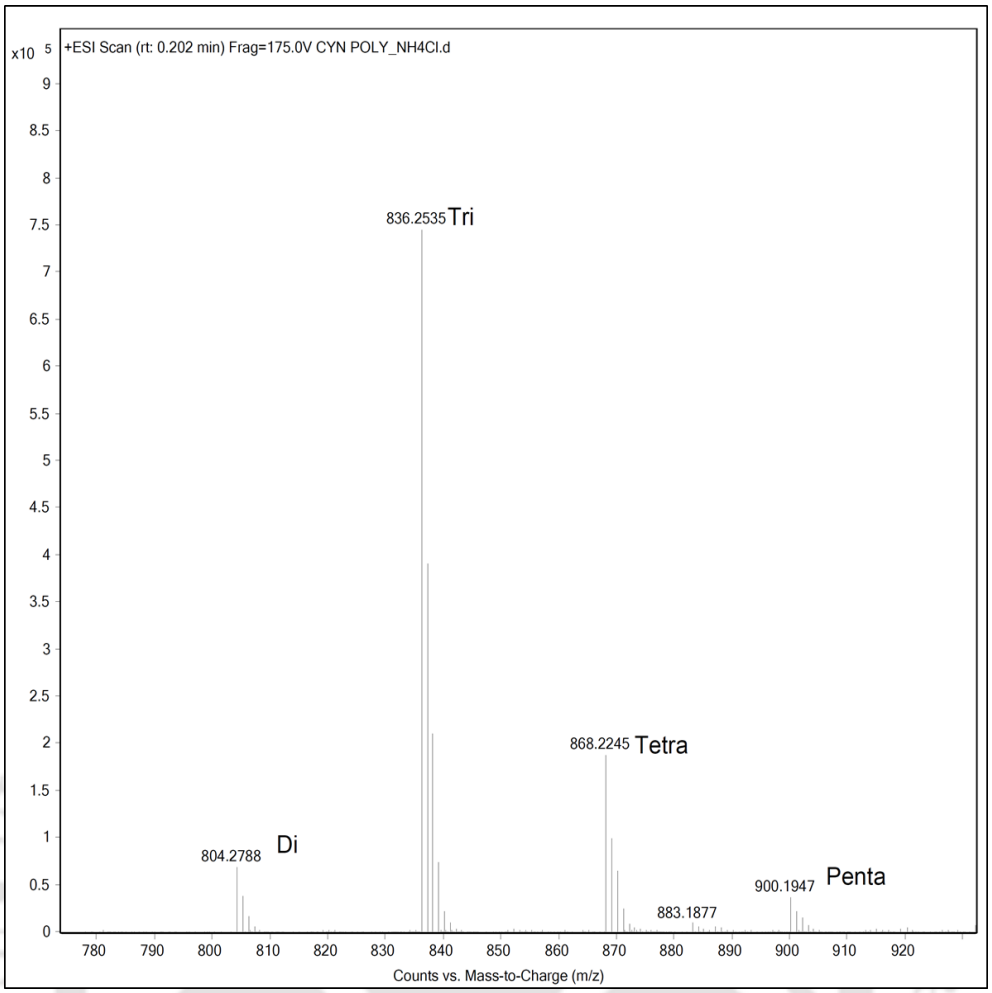

Figure A4.16. Zoomed ESI-MS (+ve) spectrum of **DCI-PS** showing disulfide, trisulfide, tetrasulfide and pentasulfide forms of **DCI-PS**. ESI-MS *m/z* calcd. for $C_{44}H_{46}N_5O_6S_3$ $[M + NH_4]^+$: 836.2610, obs. 836.2535, *m/z* calcd. for $C_{44}H_{46}N_5O_6S_4$ $[M + NH_4]^+$: 868.2331, obs. 868.2245, *m/z* calcd. for $C_{44}H_{46}N_5O_6S_5$ $[M + NH_4]^+$: 900.2052, obs. 900.1947.

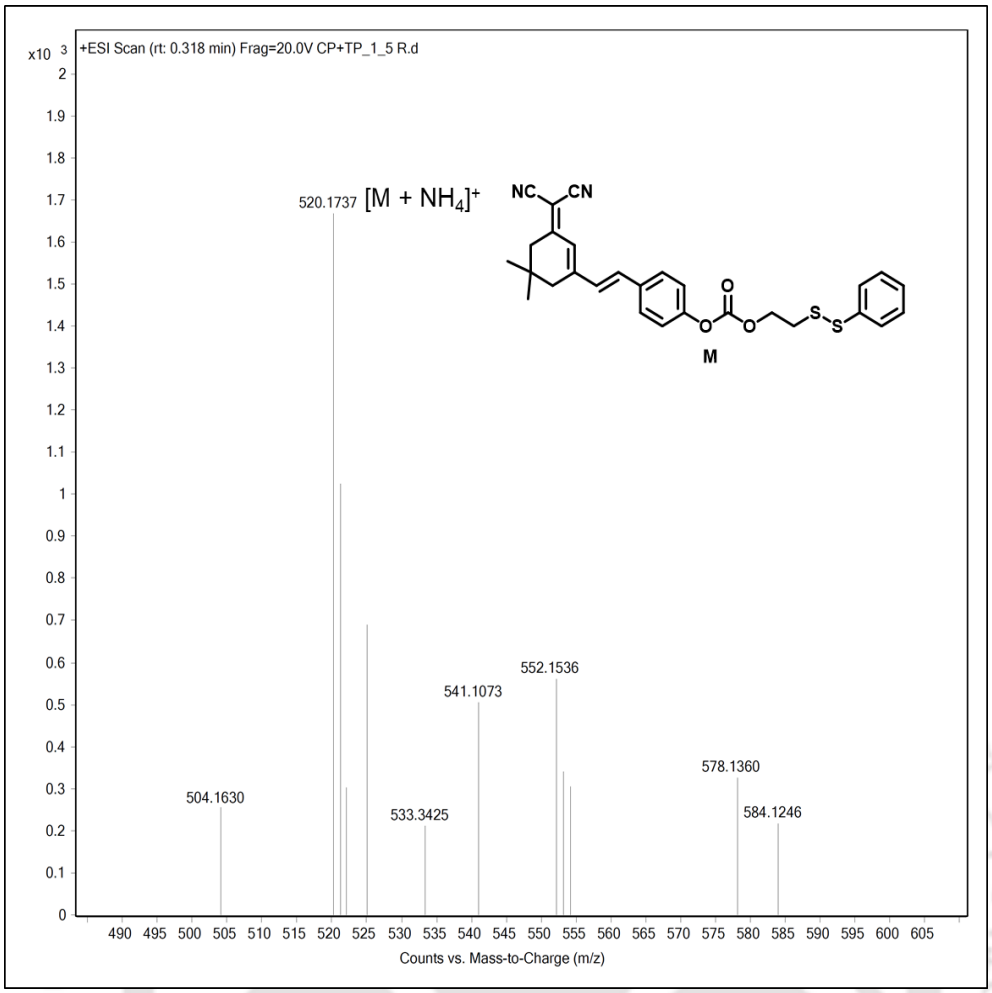

Figure A4.17. ESI-MS (+ve) spectrum of the reaction mixture of **DCI-DS** and PhSH (1:5) in acetonitrile, representing the formation of intermediate **3.4**. ESI-MS *m/z* calcd. for $[M + NH_4]^+$ = 520.1729, obs. 520.1850.

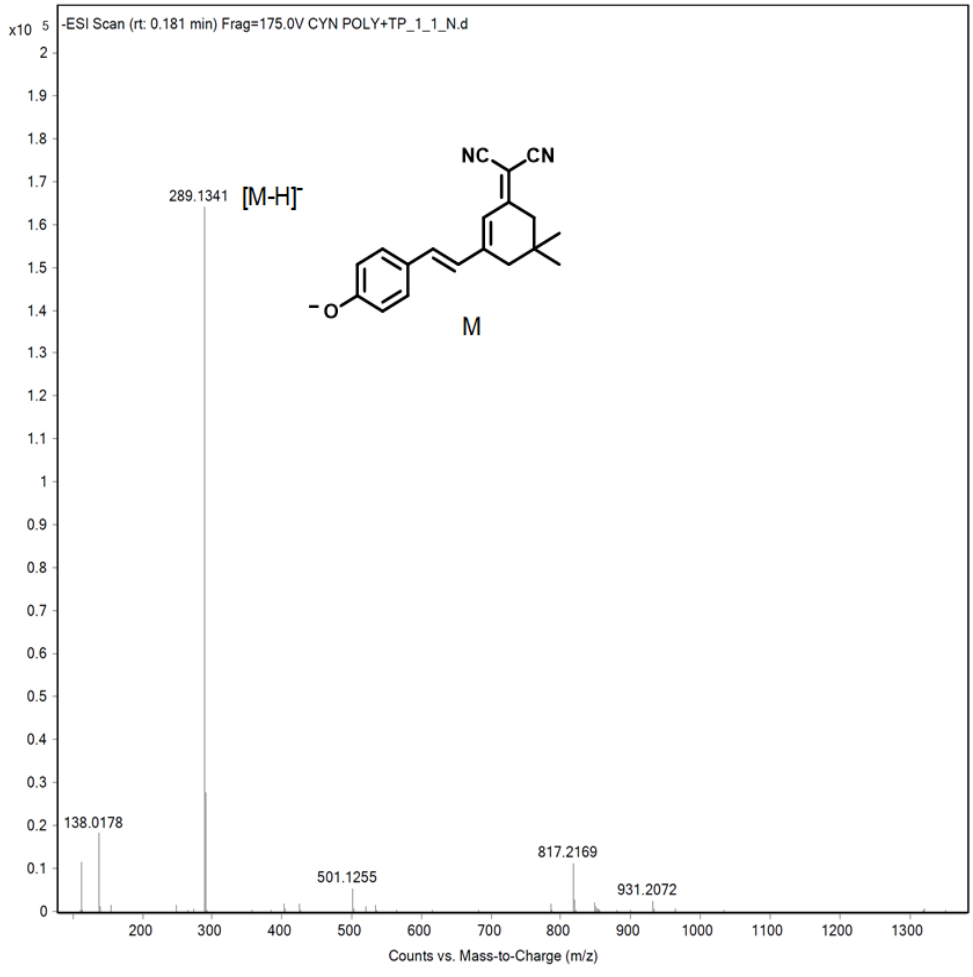

Figure **A4.18**. ESI-MS (-ve) spectrum of the reaction mixture of **DCI-PS** and **PhSH** (1:5) in acetonitrile. The formation of the released fluorophore **DCI-OH** was detected under the mass spectrometric condition. ESI-MS (-ve) calcd. for $C_{19}H_{18}N_2O$ $[M - H]^-$ = 289.1346, obs. 289.134.

Supplementary data for Chapter 4

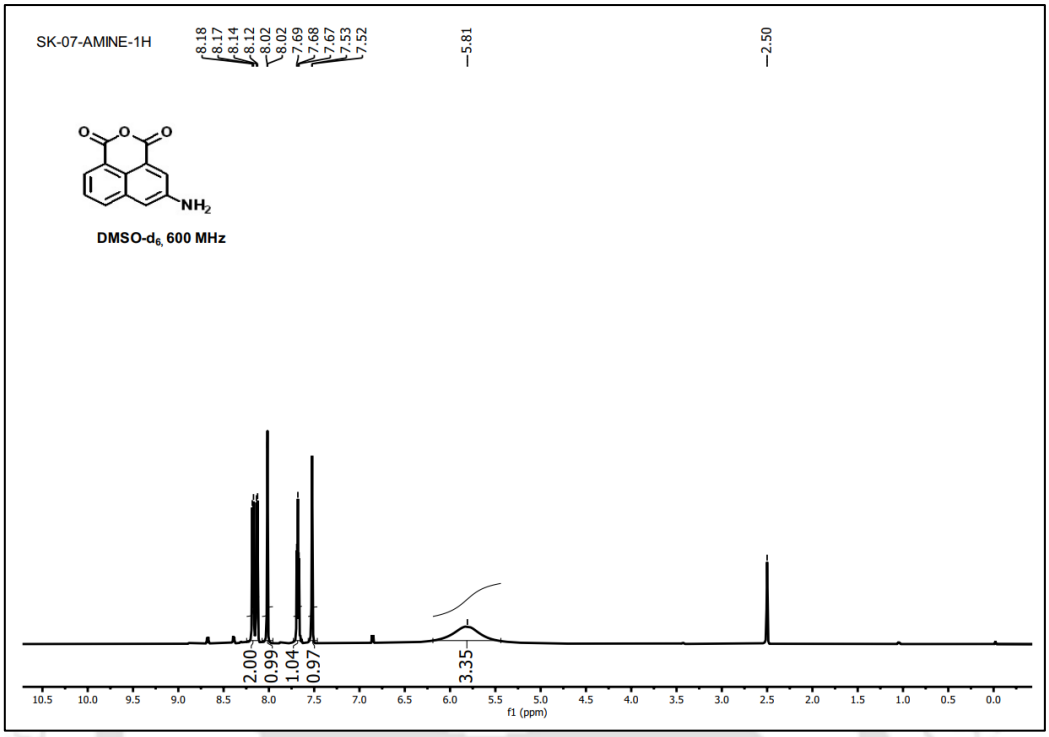

Figure A5.1. ^{1}H NMR spectrum (DMSO-d_6, 600 MHz) of compound **4.2**.

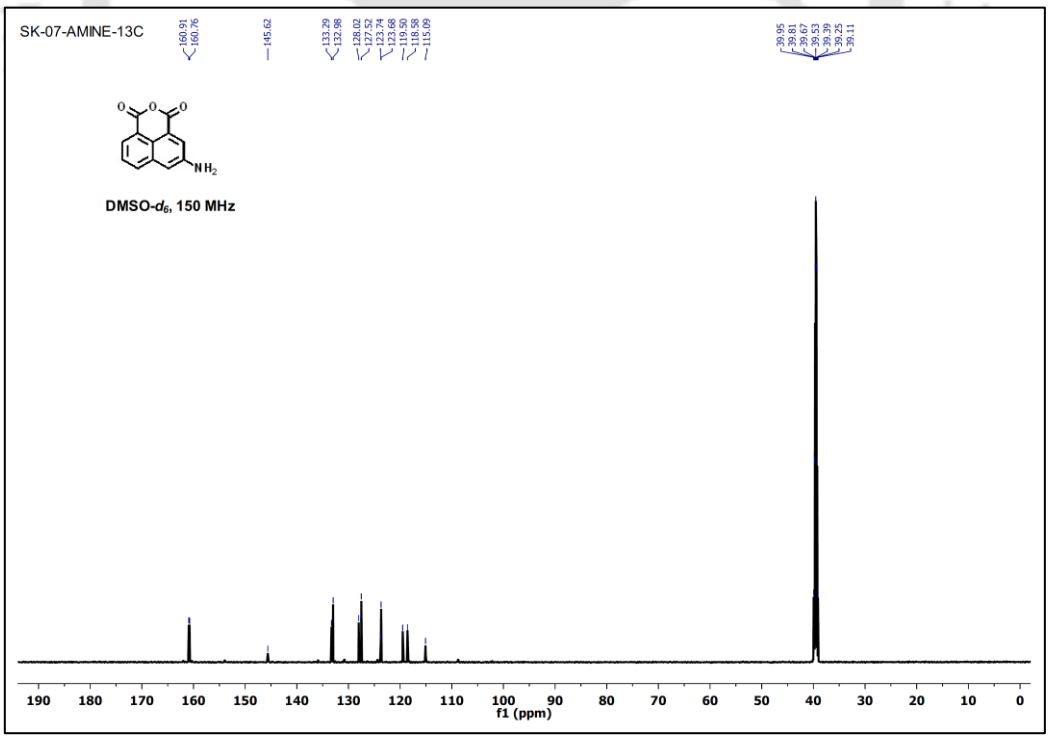

Figure A5.2. ^{13}C NMR spectrum (DMSO-d_6, 150 MHz) of compound **4.2**.

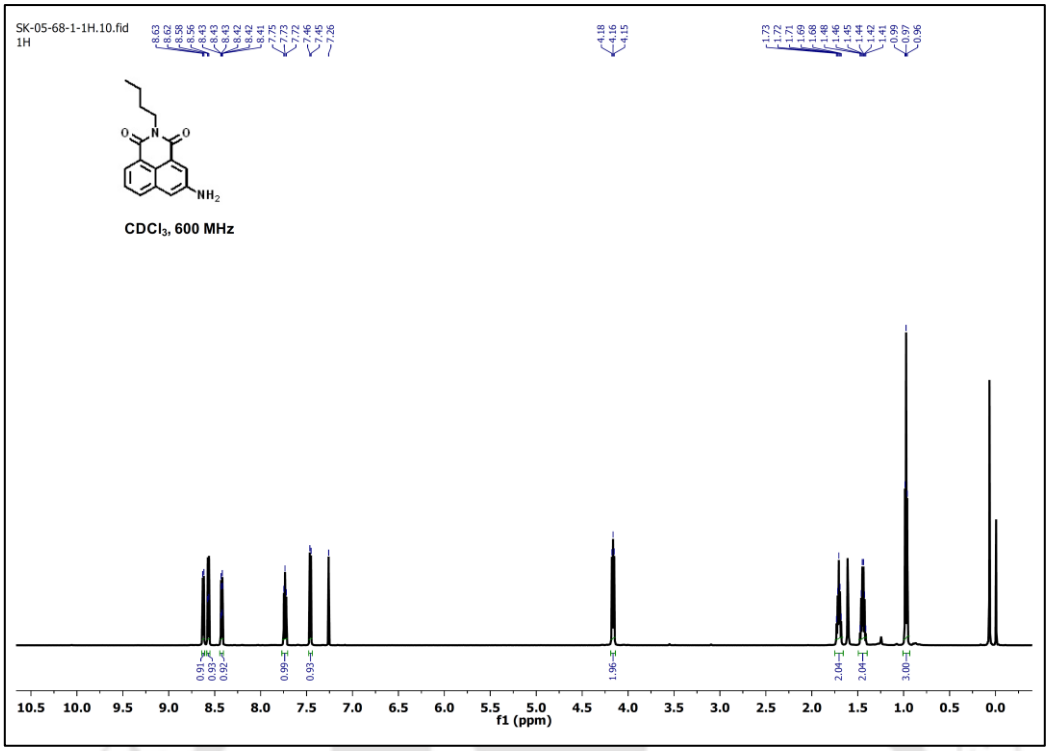

Figure A5.3. ^{1}H NMR spectrum ($CDCl_3$, 600 MHz) of compound **4.3**.

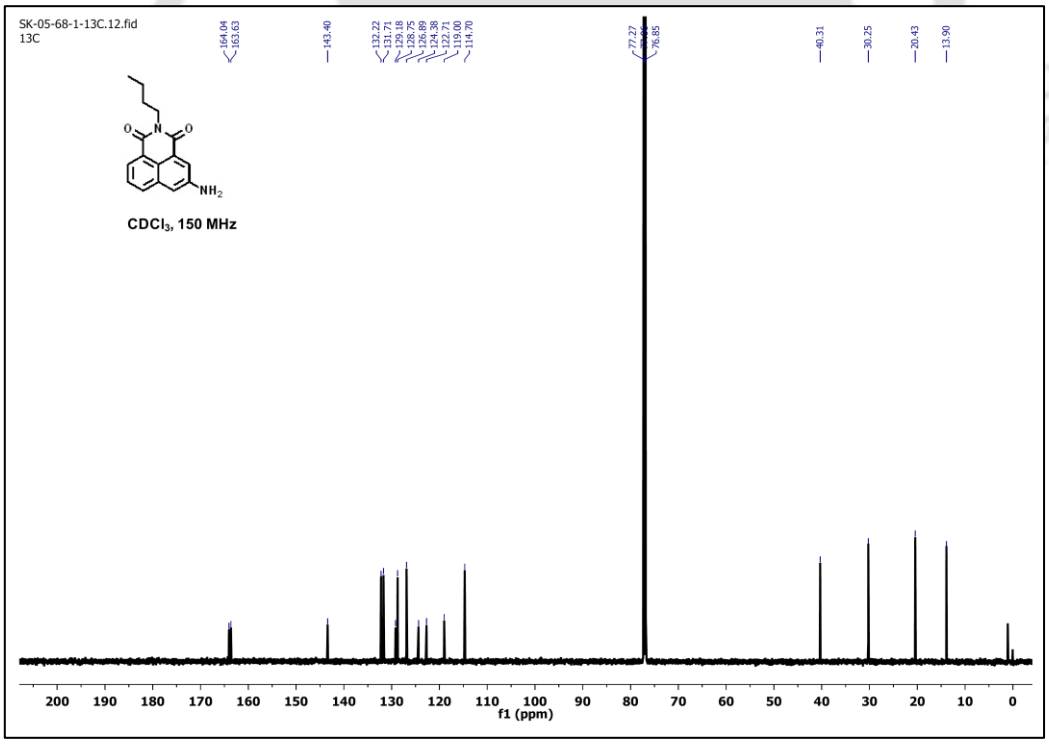

Figure A5.4. ^{1}H NMR spectrum ($CDCl_3$, 150 MHz) of compound **4.3**.

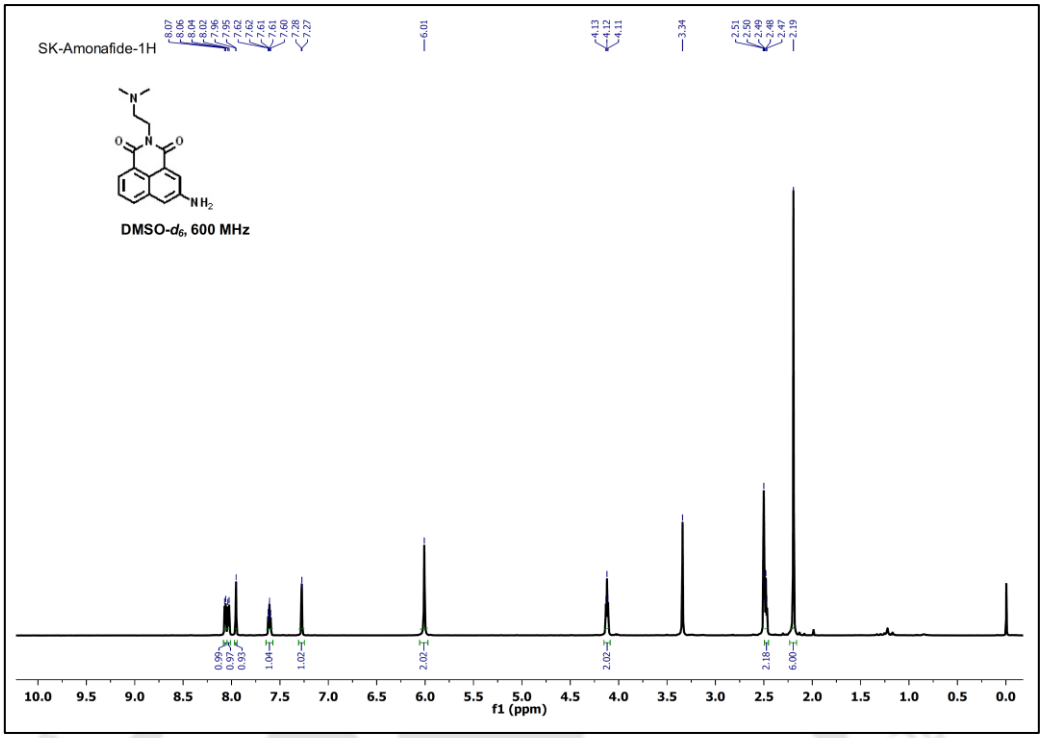

Figure A5.5. ^{1}H NMR spectrum (DMSO-d_6, 600 MHz) of compound **4.4**.

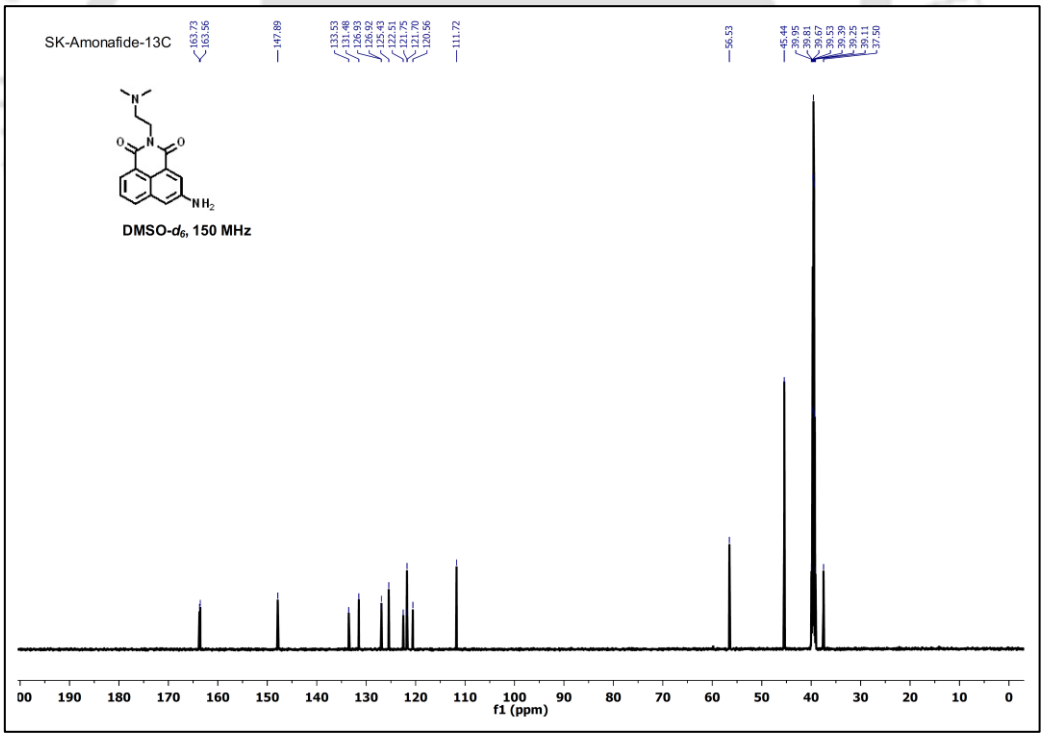

Figure A5.6. ^{13}C NMR spectrum (DMSO-d_6, 150 MHz) of compound **4.4**.

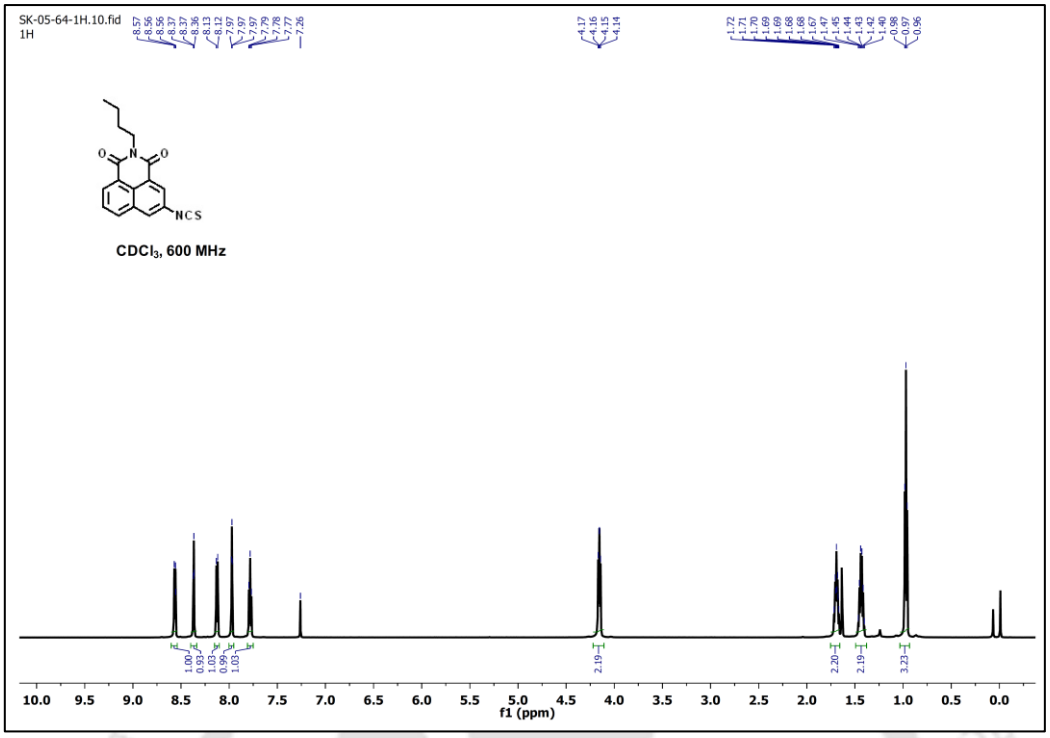

Figure A5.7. ^{1}H NMR spectrum ($CDCl_3$, 600 MHz) of **NB-ITC**.

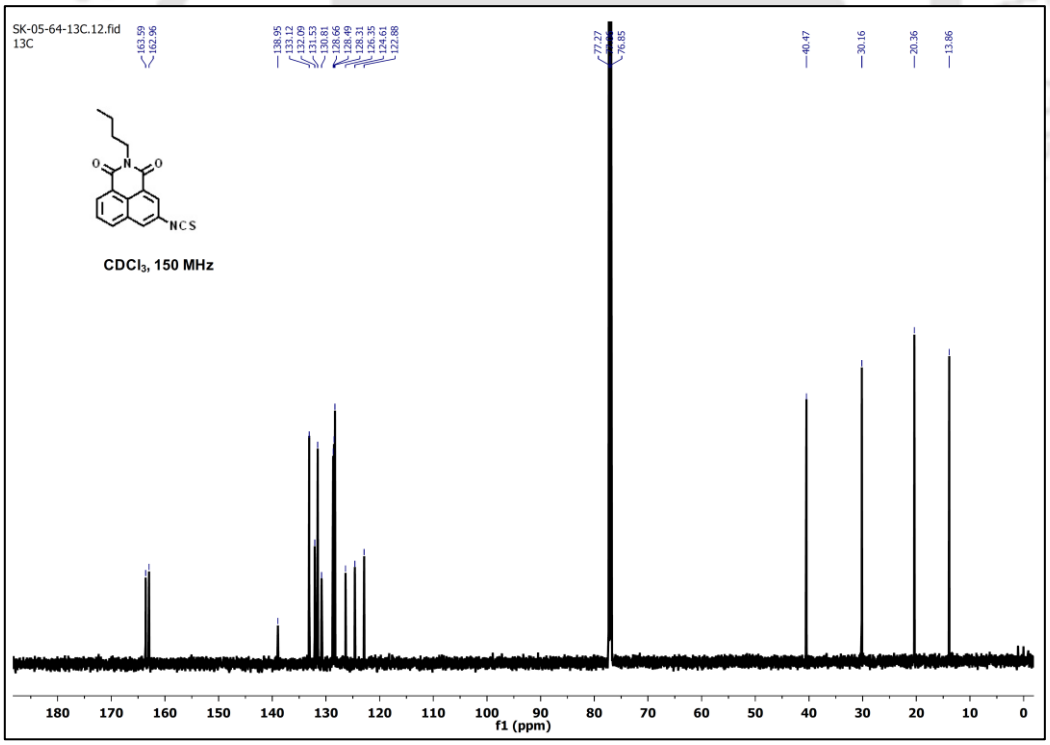

Figure A5.8. ^{13}C NMR spectrum ($CDCl_3$, 150 MHz) of **NB-ITC**.

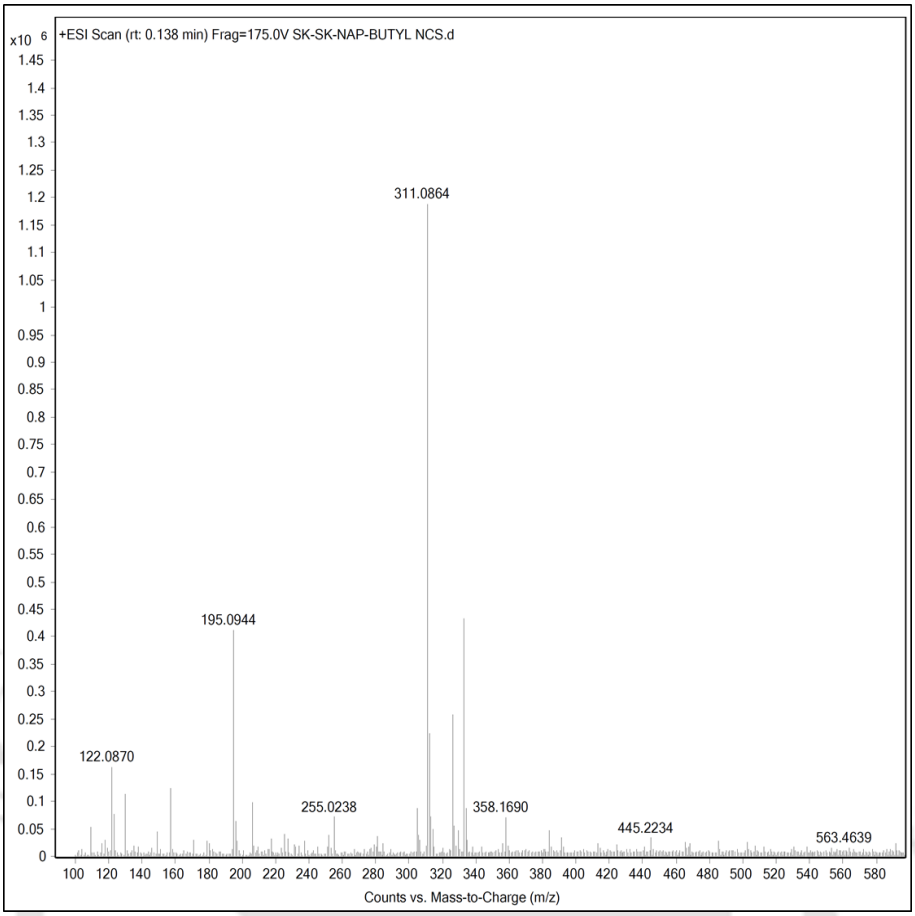

Figure A5.9. ESI-MS (+ve) spectrum of **NB-ITC**. ESI-MS: *m/z* calcd. for $C_{17}H_{14}N_2O_2S$ $[M + H]^+$ = 311.0854, obs. 311.0864.

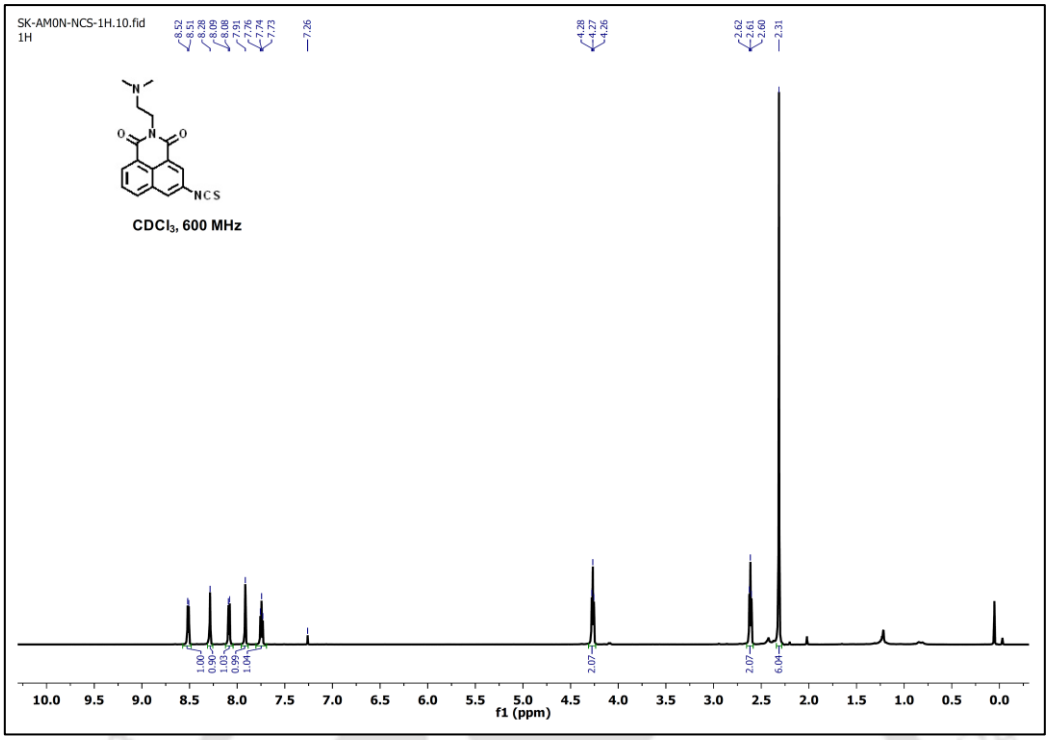

Figure A5.10. ^{1}H NMR spectrum ($CDCl_3$, 600 MHz) of **AM-ITC**.

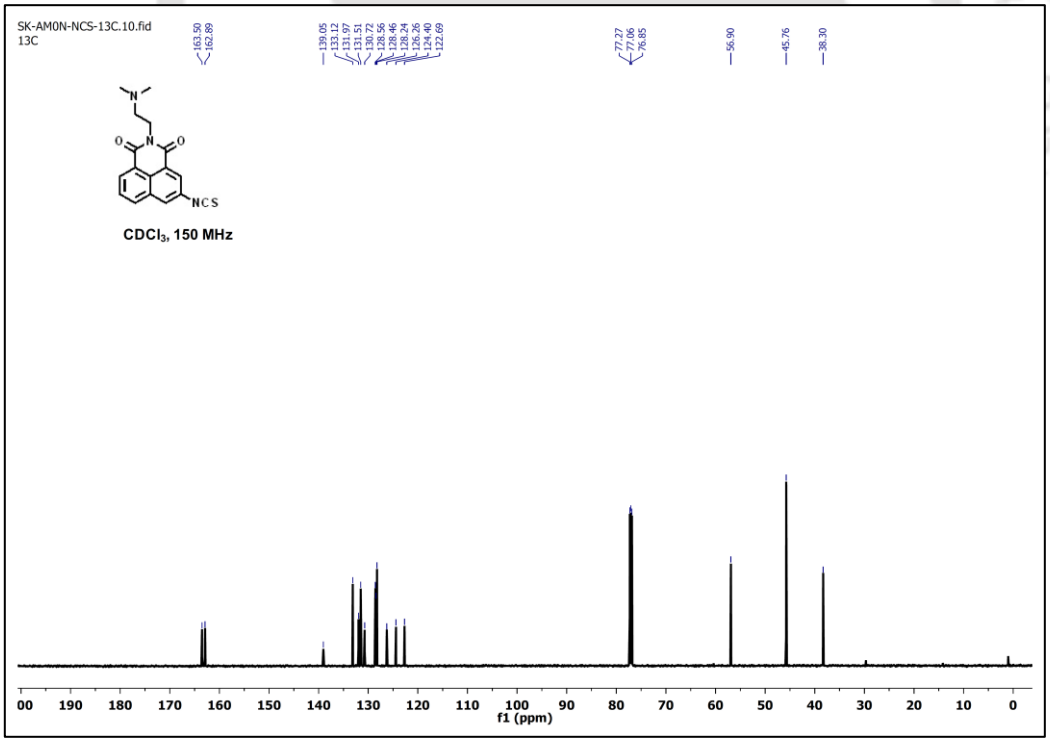

Figure A5.11. ^{13}C NMR spectrum ($CDCl_3$, 150 MHz) of **AM-ITC**.

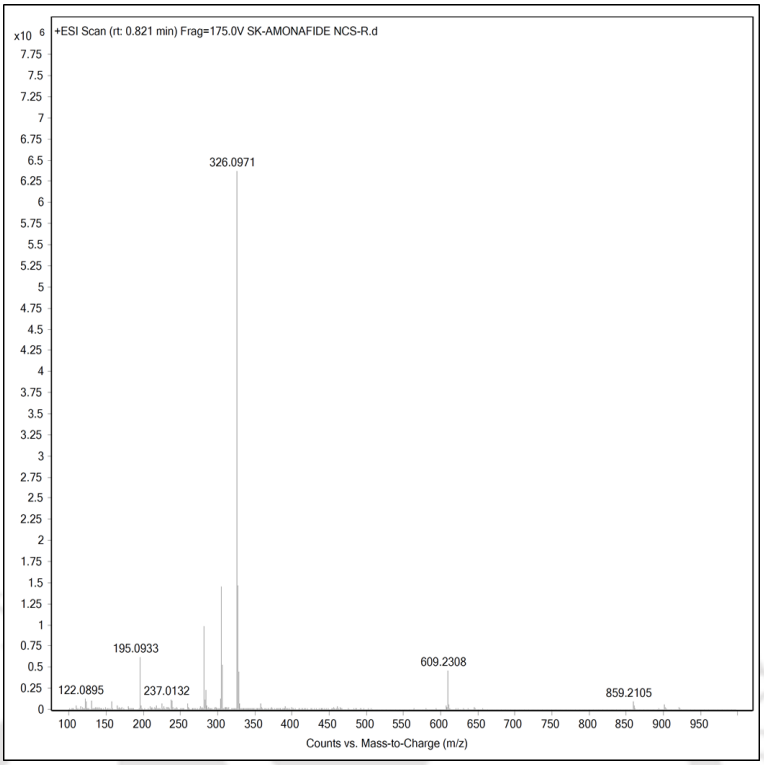

Figure A5.12. ESI-MS (+ve) spectrum of **AM-ITC**. ESI-MS: *m/z* calcd. for $C_{17}H_{16}N_3O_2S$ $[M + H]^+$ = 311.0854, obs. 311.0864.

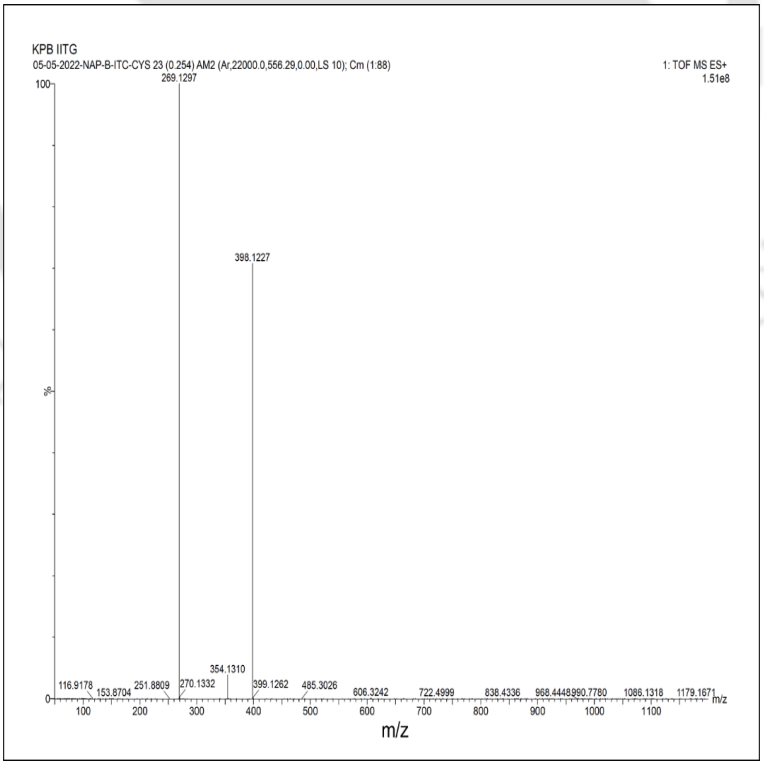

Figure A5.13. ESI-MS (+ve) spectrum for the reaction of **NB-ITC** with Cys in acetonitrile. The released compound **NAB** was observed under mass spectrometric conditions. ESI-MS (+ve) *m/z* calcd. for $C_{16}H_{16}N_2O_2$ $[M+H]^+$ = 269.1290, obs. 269.1297.

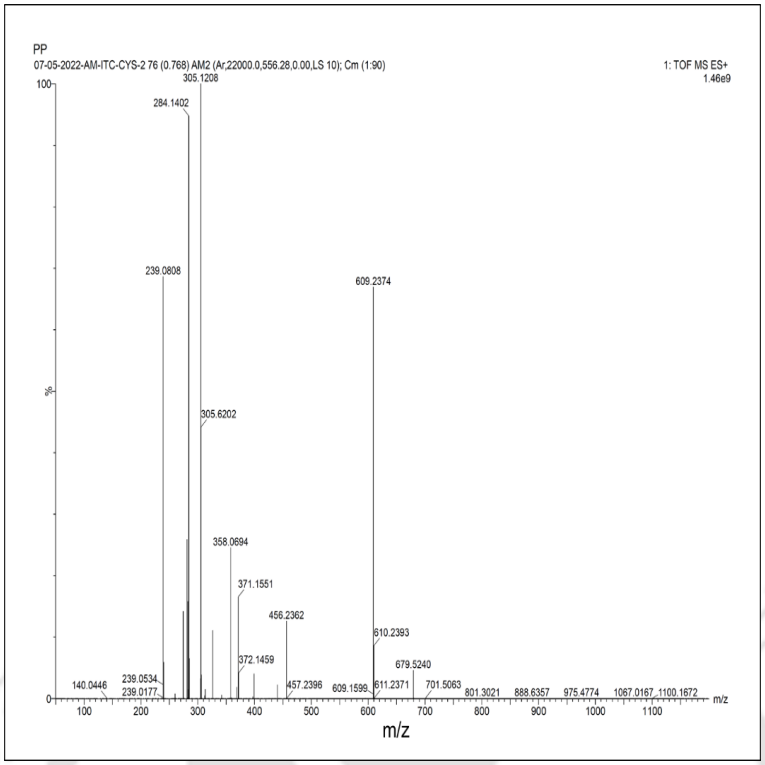

Figure A5.14. ESI-MS (+ve) spectrum for the reaction of **AM-ITC** with cysteine in acetonitrile. The released compound **amonafide** mass was observed under mass spectrometric conditions. ESI-MS (+ve) *m/z* calcd. for $C_{16}H_{17}N_3O_2$ $[M+H]^+$ = 284.1399, obs. 284.1402.